5-2008

Temperature Characterization of the Ultracapacitor Serial Resistance using a Constant Voltage Source

Curtis W. Miller
University of Tennessee - Knoxville

To the Graduate Council:

I am submitting herewith a thesis written by Curtis W. Miller entitled "Temperature Characterization of the Ultracapacitor Serial Resistance using a Constant Voltage Source." I have examined the final electronic copy of this thesis for form and content and recommend that it be accepted in partial fulfillment of the requirements for the degree of Master of Science, with a major in Electrical Engineering.

Leon Tolbert, Major Professor

We have read this thesis and recommend its acceptance:

Jack Lawler, Syed Kamrul Islam

Accepted for the Council:
Dixie L. Thompson

Vice Provost and Dean of the Graduate School

(Original signatures are on file with official student records.)

To the Graduate Council:

I am submitting herewith a thesis written by Curtis W. Miller entitled "Temperature Characterization of the Ultracapacitor Serial Resistance using a Constant Voltage Source." I have examined the final electronic copy of this thesis for form and content and recommend that it be accepted in partial fulfillment of the requirements for the Master of Science, with a major in Electrical Engineering.

_____
Leon Tolbert, Major Professor

We have read this thesis
and recommend its acceptance:

_____
Jack Lawler

_____
Syed Kamrul Islam

Accepted for the Council:

_____
Carolyn R. Hodges, Vice Provost and
Dean of the Graduate School

(Original signatures are on file with official student records.)

Temperature Characterization of the Ultracapacitor Serial Resistance using a Constant Voltage Source

A Thesis

Presented for the

Master of Science

The University of Tennessee, Knoxville

Curtis W. Miller

May 2008

Dedication

This thesis is dedicated to my parents, Carlos and Edie Miller, for their continued support of my life's endeavors. Without their encouragement and support, the dream of achieving a Masters would not have been possible. To my brother, for all the encouragement and talks we have shared throughout my schooling despite our brotherly differences. To my cousins and good friends, I want to thank them for sending their wishes and support.

Acknowledgments

I would like to thank my advisor, Dr. Leon Tolbert, for never giving up hope on me. His guidance, tolerance, and support have helped me through the Master's program. His knowledge and work ethic have been the standards I strive to meet in my professional career.

In addition, I would like to thank Dr. Jack Lawler for taking the first chance on me. Without his help and acceptance, the journey would have never begun. For the guidance and mentoring of a small town Midwestern during the beginning years, I am forever in your debt.

I would like to thank Dr. Syed Islam for not only being a committee member but for being a good friend and instructor. Helping with assignments or the simple chats in the hallway between classes will always be remembered.

Lastly, I would like to thank PEERMC personnel for the opportunity to work, perform my research, and being a part of their lives. The knowledge and friendships shared will never be forgotten.

Abstract

This thesis examines the temperature effects on an ultracapacitor's equivalent series resistance using a constant voltage source. Previous research has focused on developing models using constant current source. However, as the ultracapacitor technology develops, allowing for the expansion of these devices into new power applications, it is important to understand how ultracapacitors will perform in various temperatures and charging and discharging methods. By predicting the ultracapacitor behavior, systems can be optimized for efficiency and minimize internal circuit losses.

For this thesis, Matlab was used to plot the experimental data and to provide best fit curves with their respective coefficients to allow for resistance measurements for one RC time constant to be performed. The research presented in this thesis shows the ultracapacitor's series resistance was more dependent on change in current than temperature variations. The resistance was did show a minor dependence on temperature, however it was insignificant compared to the change in current levels. The analysis of the resistance values allowed for the development of a resistance equation that accounted for the variations in current and temperature. These resistive equations were compared to the calculated resistance measurements. Sufficient agreement was shown between the developed resistance equations and the calculated resistance values.

Table of Contents

List of Figures

List of Tables

Chapter 1.

This chapter will provide an introduction to the ultracapacitor. A brief discussion on the advantages and disadvantages will be provided. A brief chapter outline of this thesis is provided at the end of the chapter.

1.1 Introduction

The design of the automobile propulsion system is going through a major evolution, perhaps the biggest since its invention. The center of this change focuses on electrifying the power train of the automobile. In a world that is expressing growing concerns for the environment and conservation of natural resources, the development of hybrid electric vehicles (HEVs) has taken an accelerated pace. Another factor that has contributed to the acceleration of HEVs is energy supplies. In the U.S., modes of transportation consume two-thirds of the petroleum [1]. As economies of other developing countries mature, the automotive population is expected to be five times larger by mid-century, growing from 700 million to 2.5 billion [1, 2]. With petroleum being a finite resource, where will the oil come from? Where will the emissions be dispersed? The automobile companies have reduced the emission of greenhouse gases, but due to the growth in the automotive population, air pollution continues to increase. The answers to these gloomy questions compel us to make every effort for sustainable road transportation.

A decade ago, the only examples of HEVs were in laboratories or university shops competing in design competitions. With the help of initiatives and many years of

Table 1.1Characteristics of BEV, HEV and FCEV [2]

Types of EVs	Battery EVs	Hybrid EVs	Fuel Cell EVs
Propulsion	Electric motor drives	Electric motor drives Internal Combustion Engine	Electric motor drives
Energy system	Battery Ultracapacitor	Battery Ultracapacitor ICE generating unit	Fuel cells Ultracapacitors
Energy source and infrastructure	Electric grid charging facilities	Gasoline station Electric grid charging stations (optional)	Hydrogen Methanol or gasoline Ethanol
Characteristics	Zero emissions Independence on crude oils 100-200 km short range High initial cost Commercially available	Very Low emissions Long driving range Dependence on crude oil Complex Commercially available	Zero emission or ultra low emission High energy efficiency Independence on crude oils Satisfied driving range High cost now Under development
Major issues	Battery and battery management High performance propulsion Charging facilities	Managing multiple energy sources Dependent on driving cycle Battery sizing and management	Fuel cell cost Fuel processor Fueling system

development, HEV technology is maturing and commercially available. Today there are more than 500,000 commercial HEVs on the roads.

Hybrid electric vehicles have reduced emissions, but until a total electric vehicle (EV) is developed will there be zero emissions and no dependence on fossil fuels. This decade, researchers with the FreedomCAR initiative sponsored by the U.S. Department of Energy are developing battery EV (BEV) and fuel cell EV (FCEV). Table 1.1 shows a few characteristics of BEV, HEV, and FCEV.

Battery EVs have had limited acceptance in the marketplace. Driving range, performance, battery lifetime, and weight of the batteries are the major issues it must overcome. Fuel Cell EVs have obstacles which need to be solved before fuel cells will be a commodity in the marketplace. Warming time during starting and poor regenerative capability are two issues that need to be solved. Another important concern is the decrease in output voltage as the load demand increases.

Double layer chemical capacitors can help solve the drawbacks associated with BEVs and FCEVs. These capacitors have established colloquial names as supercapacitors, ultracapacitors, gold capacitors, power capacitors or double-layer capacitors. In this thesis, the term ultracapacitor will be used.

Electrolyte conductivity is one of the most important ultracapacitor properties which are temperature dependent. The effective series resistance, ESR, and the capacitance will vary with temperature due to the thermal variations of the electrolyte ionic conductivity and carbon conductivity. The presence of a significant ESR restricts the charge and discharge rates at a given voltage difference. Therefore, studying the evolution of the ESR and capacitance with temperature fluctuations is important in

determining the power dissipation and optimizing the system to achieve the highest efficiency.

1.2 Advantages of Ultracapacitors

There are two fundamentally different ways to store electrical energy; indirectly as potential chemical energy or directly as an electrostatic way [3]. Indirect storage requires an Faradaic oxidation and reduction of electrochemically active agents. In a Faradaic process, the electron transfer produces a chemical or oxidation state change in the electroactive material based on Faraday's Law. An example of an Faradaic process is a battery.

Direct electrical storage is achieved electrostatically. This process is achieved by positive and negative charges residing on two plates separated by a vacuum or molecular dielectric. This is a non-Faradaic process. An example of a non-Faradaic process is a capacitor.

Chemical conversions in a battery, usually in the form of phase changes, take place at the anode and cathode. These phase changes result in a depletion of chemical electrode reagents, thus hindering the life cycle of battery cells. Depending on the type of battery, the life cycle can vary between one thousand to several thousand charge/discharge cycles. By contrast, ultracapacitors have no chemical and phase change associated with the charge/discharge cycles; thus providing virtually unlimited cyclability (>100,000 charge/discharge cycles). Ultracapacitors have a significantly longer lifetime than batteries.

In the automotive industry, ultracapacitors have several key benefits. First, the

high power density of ultracapacitors can be used to reduce the weight and size of the power source. In driving conditions, short duration events that require substantial power but little energy occur frequently. Ultracapacitors can be sized for this peak power requirement, thus allowing the main power source to be smaller. Low internal impedance makes ultracapacitors proficient for supplying peak power during transients, such as during acceleration. During regenerative braking, more power can be recovered into the ultracapacitor than in a battery, thereby increasing the overall system efficiency. Ultracapacitors allow regenerative braking even when the batteries are fully charged [4]. Because the fast transients experienced by the batteries are lessened, the discharge depth of the batteries should be reduced, thereby increasing battery life expectancy. A recent comparison of ultracapacitors and batteries in electrical vehicle applications showed that the capacitor had an efficiency advantage over that of nickel metal hydride batteries, 92% to 85% respectively [5].

Ultracapacitors have a state of charge indication. The potential difference of the ultracapacitor is directly proportional to charge on the capacitor. When charging or discharging, the voltage across the terminals gives an indication to the amount of charge on the capacitor. On a battery, the potential difference remains constant as long as the two phases are in equilibrium [3]. Therefore, a state of charge indication for batteries is more complex and not straightforward. Figure 1.1 shows the difference between capacitors and batteries.

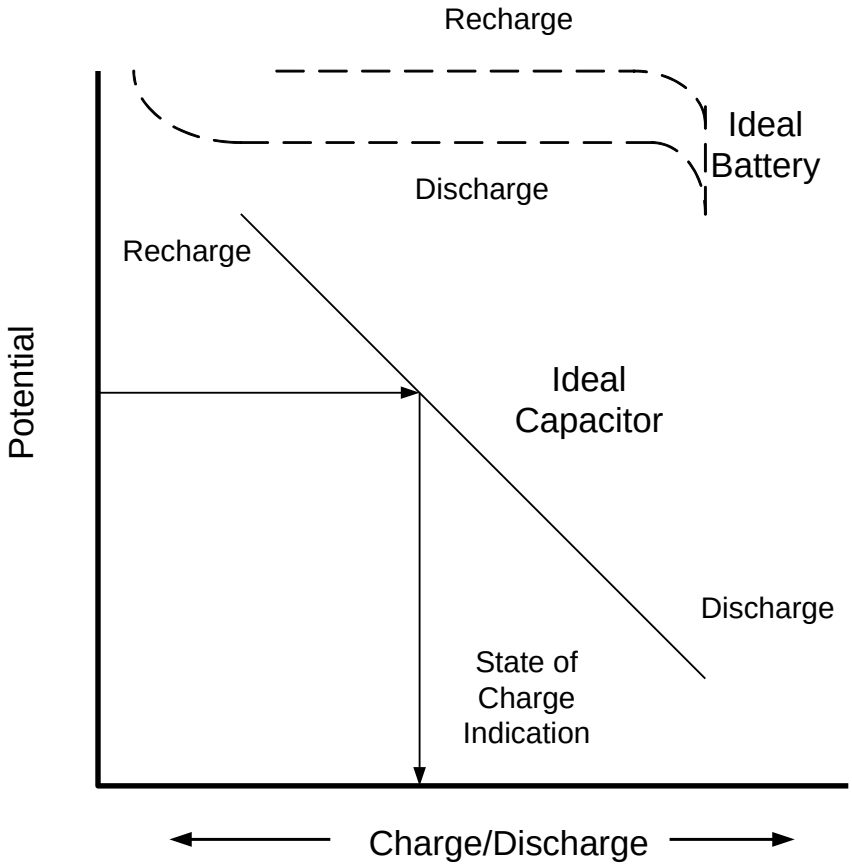

Figure 1.1 Difference of charge and discharge between a capacitor and battery [3].

1.3 Disadvantages of Ultracapacitors

Ultracapacitors are not without their shortcomings. The capacitors do not have the energy density of a battery. Ultracapacitors have approximately one-tenth the energy density of batteries. Only when the energy density of the capacitor is equal to a battery will the capacitor totally replace the battery. The second disadvantage of ultracapacitors is its low operating voltage. Presently, the maximum voltages attainable are around 3.5 volts per cell. This requires several cells to be connected in series to reach the desired voltage levels. Recalling that the equivalent capacitance of series connected capacitors is the reciprocal of the sum the individual capacitors; thereby, decreasing the overall capacitance. Placing capacitors in parallel is needed to offset this effect. By having capacitors in series and parallel branches creates design complications. These complications include wiring, control schemes, and monitoring. Having multiple branches introduces additional ohmic losses via the wire or copper bus bars that connect the capacitors together; this adds extra heat and decreases the overall efficiency of the system. Due to the low internal impedance, the capacitors will need to be matched. This will help prevent overcharging or discharging of the capacitors near the end each branch. Ensuring each capacitor receives the same applied voltage and current becomes more complicated.

The performance and lifetime of an ultracapacitor are temperature dependent. In automotive applications, this is very important. One major factor that is temperature dependent is electrolyte conductivity. The electrolyte conductivity is inversely proportional to the temperature change. The conductivity depends principally on the viscosity of the solvent and the degree of dissociation of the electrolyte at a given salt

concentration [3]. This determines the solution component of the ESR. The second factor is the actual capacitance of the ultracapacitor. The capacitance is dependent on two factors. First is the temperature dependence of the dielectric constant of the solvent. Generally, it will decrease with an increase in temperature [3]. The second is the effective thickness of the double layer. The interphasal fluid tends to expand as the temperature increases causing the effective average thickness of the compact part of the double layer to increase, decreasing the capacitance [3].

Self-discharge of ultracapacitors is dependent on the significant heat of activation. The electrochemical kinetics of these processes can have a wide range that can create substantial differences in self-discharge rates over a temperature range. Because this is an intrinsic aspect of chemical and electrochemical rate processes, little can be done to offset the temperature effects [3].

1.5 Outline of the Thesis

The objective of this study is to develop necessary modeling and simulation tools for evaluating the temperature dependence of ESR in a constant voltage charge and discharge cycle.

Chapter 2 provides a brief overview of the first ultracapacitor structure models. Then a discussion of the various equivalent circuit models will be presented.

Chapter 3 provides experimental results and a brief discussion of the differences.

Chapter 4 discusses the system modeling approach. This is followed by the results of system simulations.

Chapter 5 provides conclusions and an overall summary of work.

Chapter 2.

The previous chapter briefly discussed the advantages and disadvantages of ultracapacitors. This chapter will provide a review of the structure and equivalent circuits for an ultracapacitor that has been simulated to model the complex behavior of ultracapacitors in various environmental conditions.

2.1 Ultracapacitor Interface Models

A common capacitor consists of a dielectric separating two conducting plates. In many applications, aluminum foil is used for the plates and air, ceramic, paper or mica is used as the dielectric. The charge, *q*, for this capacitor is proportional to the applied voltage, *v*, and known capacitance, *C*.

$$q = vC \qquad (2.1)$$

The capacitance is dependent on the physical characteristics of the capacitor. In parallel plate capacitors, capacitance is proportional to the surface area of each plate, *A*, permittivity of the dielectric material, ε, and indirectly to the distance between the plates, *d*.

$$C = \frac{\varepsilon * A}{d} \qquad (2.2)$$

To make this case apply to the general capacitor case, three inferences can be made:

1. The larger surface area on the plates, the larger the capacitance.
2. The smaller the distance separating the plates, the greater the capacitance.

3. The higher the permittivity, the higher the capacitance.

Despite the substantial differences in construction and structure of the parallel plate capacitors and ultracapacitors, the above general inferences will apply.

Ultracapacitors use an electrode-solution interface that behaves similar to a capacitor. For a voltage potential, a charge on the metal electrode, q_m, and in the solution, q_s will exist. Depending on the excess or deficiency of electrons, the charge on the metal will be positive or negative. These electrons reside in a very thin layer on the metal surface. The solution charge is determined by the cations or anions in the vicinity of the electrode surface [4]. At all times,

$$q_m = -q_s \qquad (2.3)$$

applies to one metal surface; in actual experiments, both metal electrodes would have to be considered. A two electrode, two interface system in a single capacitor cell is shown in Figure 2.1. However, the interaction between conducting phases is not this straightforward. Due to the coulombic interaction between the metal and electrolyte, the situation is more complicated [4].

Consider a charged metal sphere of macroscopic size, surrounded by a layer of uncharged electrolyte with a thickness of a few millimeters. This is surrounded by a vacuum. Figure 2.2 depicts a cross-section view. A charge on the metal, q_m, resides on the surface creating an excess cation concentration near the electrode in the solution. Recalling Gauss's law which states the net charge, q, inside a Gaussian surface is given by the integral of the electric field over the surface;

$$q = \varepsilon_0 \oint E \cdot ds \qquad (2.4)$$

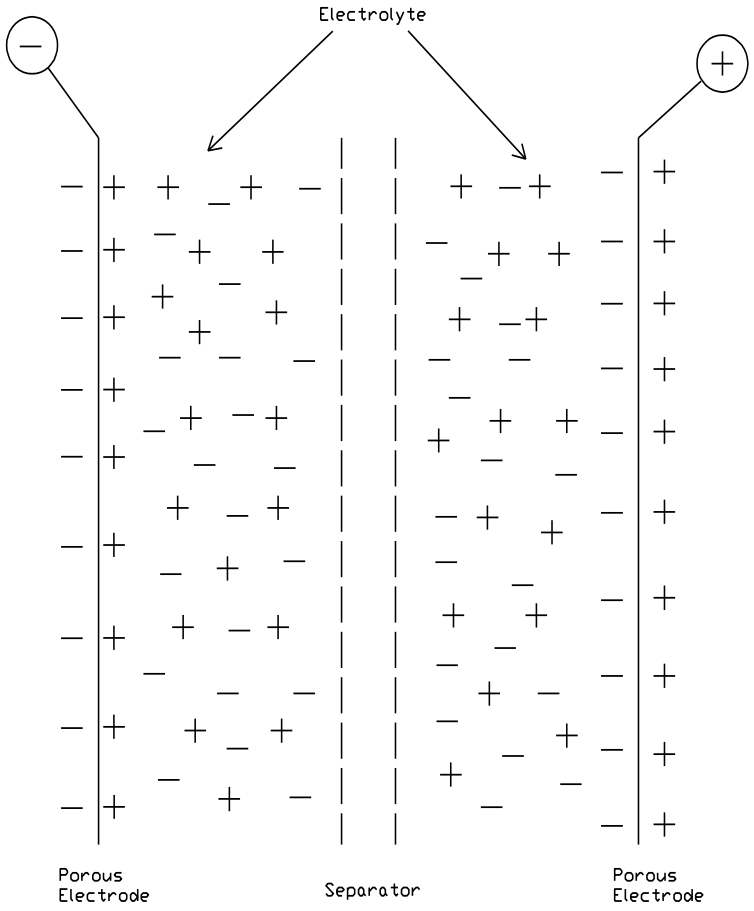

Figure 2.1 Single cell of an ultracapacitor showing the two electrodes. [3]

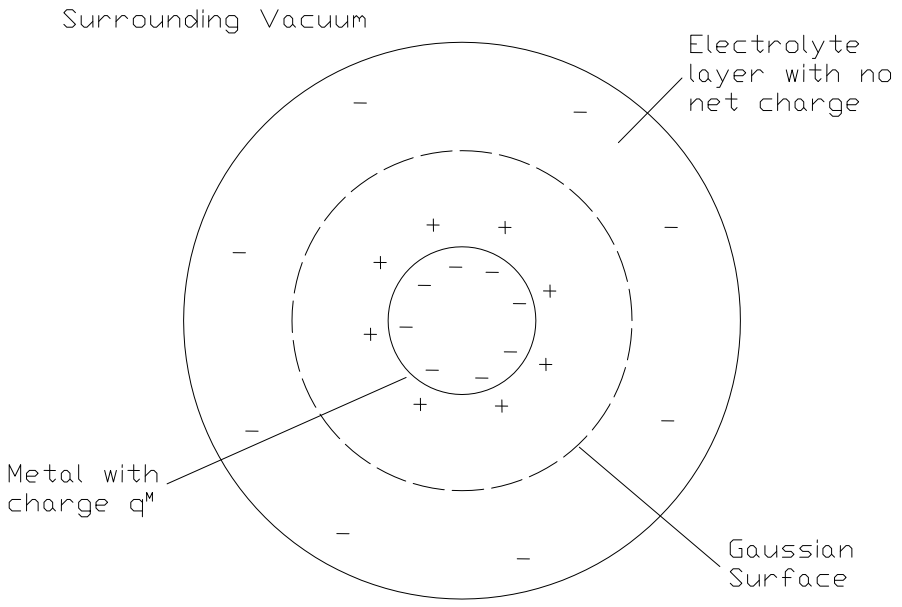

Figure 2.2 Cross-sectional interaction view between a metal sphere surrounded by electrolyte layer. [4]

where ε_0 the electric constant or permittivity of free space, dS is an infinitesimal vector that is normal to the surface and E is the electric field strength vector [4]. Now consider the Gaussian surface in Figure 2.2. If no current is flowing, then *E* at every point is zero and the net enclosed charge is zero. Placing the Gaussian surface on the fringes of the surface region where the metal and solution meet, one could reach the same conclusion as previously stated. Thus, the positive charge in the solution exactly compensates the excess metal charge and resides at the metal-solution interface. Moving the Gaussian surface beyond the electrolyte layer, the enclosed charged still must remain zero. However, the net charge of the system has a charge of q_m; thereby, a $-q_m$ charge must reside on the outer surface of the electrolyte [4]. This conclusion applies to any Gaussian surface; thus the conjecture is the excess charge actually resides on the surface of the conducting phase [4].

Recalling from electrostatics, the work done to bring a unit positive test charge from an infinite distance to a given distance from the center is independent on the path. A plot of potential vs. distance from the center of this assembly is shown in Figure 2.3. Since the E is zero within the electrolyte and metal, no work is required to move the charge through the electrolyte; therefore, the potential is constant.

Helmholtz was the first to think about charge separation at interfaces. His idea consisted of two array layers of opposite charge separated by a distance of molecular order. Figure 2.4 shows the Helmholtz model. Later researchers realized there were two flaws with the Helmholtz model. First, it became apparent that the ions on the solution side of the double layer would not remain in a static compact array but be subject to the effects of thermal fluctuation according to the Boltzmann principle [3]. Second, the

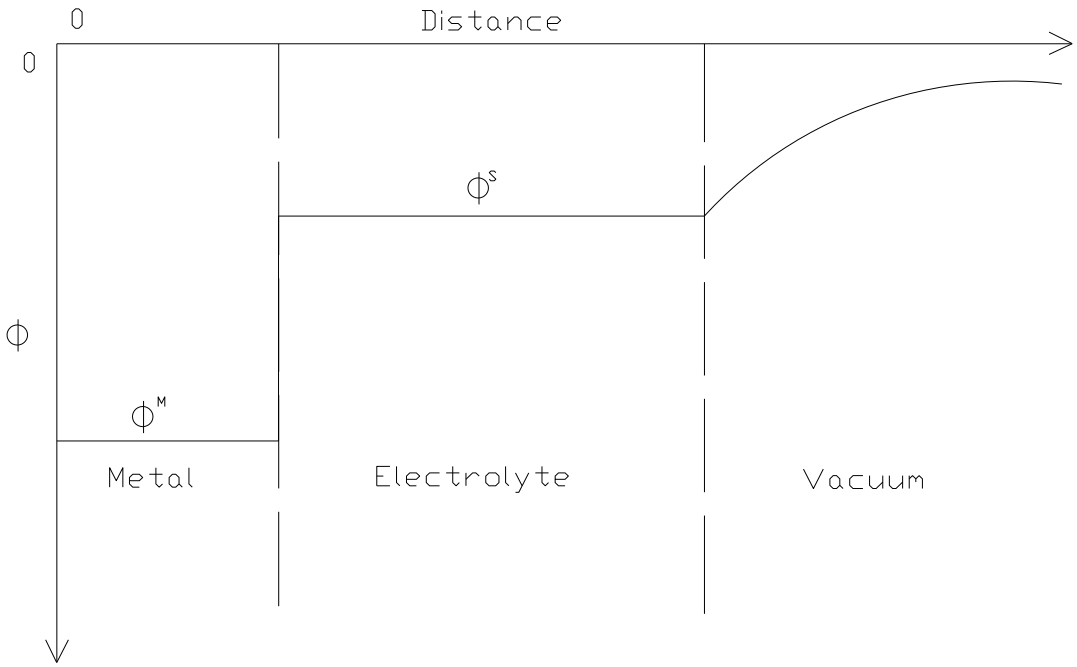

Figure 2.3 Potential profile through system in Figure 2.2. [4]

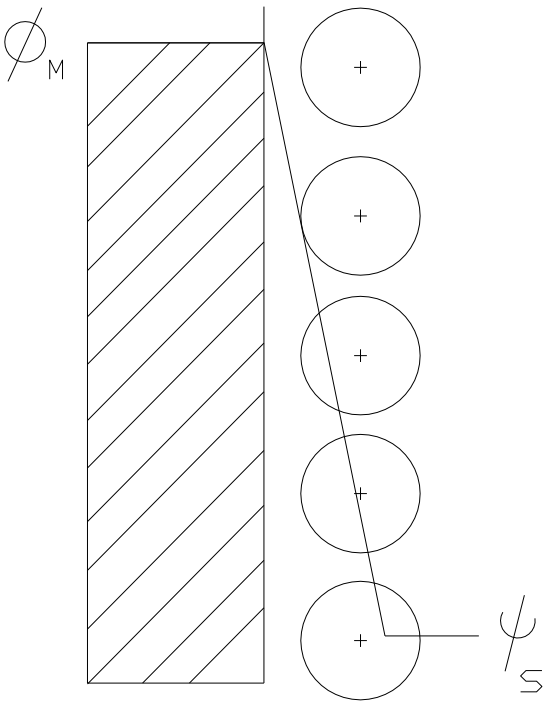

Figure 2.4 Helmholz model. [3]

structure is equivalent to a parallel-plate capacitor. The relationship between the charge density, σ , and voltage drop, *V*, between the plates is:

$$\sigma = \frac{\varepsilon * \varepsilon_0}{d} V \qquad (2.5)$$

In this equation, ε is the dielectric constant of the medium, ε_0 is the permittivity of free space and *d* is the interplate spacing. The differential capacitance is:

$$\frac{\partial \sigma}{\partial V} = C_d = \frac{\varepsilon * \varepsilon_0}{d} \qquad (2.6)$$

This equation predicts the differential capacitance to be constant. However, variations in the differential capacitance with potential and concentration suggest that either the dielectric constant of the medium or the interplate spacing depends on these variables. [4] Hence, a more sophisticated model is needed.

With the charge of the electrode confined to the surface, the same is not totally true on the solution side. At low concentrations of electrolyte, it may require a significant thickness of solution to accumulate the excess charge needed to counterbalance charge density on the metal, σ^M [4]. Gouy-Chapman theory introduced a mathematical model based on combined application of the Boltzmann's energy distribution equation and Poisson's equation. This model introduces a diffuse layer of charge in the solution [4]. The greatest concentration of excess charge would be adjacent to the electrode, while lesser concentrations would be found at greater distances [4]. Thus, an average distance, *d*, is used in the above equation and will be dependent on potential and electrolyte concentration. With a highly charged electrode, the diffuse layer should become more compact and C_d should rise [4]. However, the serious problem with

Gouy-Chapman theory is the overestimation of the double-layer capacitance. The theory predicts the V-shape capacitance function for the observed behavior in NaF at low concentrations and potentials not too far from the potential of zero charge, PZC. However, in actual systems, a flattening in capacitance at more extreme potentials occurs and the PZC valley disappears completely at high electrolyte concentrations [4]. Despite the theory's elements of truth, the failures within the Gouy-Chapman theory are significant and reflect major defects.

In the Gouy-Chapman theory, the ions are not restricted with respect to the location of the solution phase. The theory considers ions as point charges that can approach the surface boundary arbitrarily close, thereby at high polarization, the effective separation distance between the metallic and solution phase can decrease to zero [4]. This is not realistic. In 1924, Stern developed modifications to overcome the serious problems in the Gouy-Chapman theory.

Ions have a finite size and cannot approach the surface any closer than the ionic radius. The layer closest to the electrode, the inner layer, contains solvent molecules and other species which are said to be specifically absorbed. The loci for these electrical centers reside in the inner Helmholtz plane, IHP, at a distance x_1. The total charge density for this inner layer is σ^i. If the ions remained solvated, the thickness of the primary solution sheath would have to be added to the ionic radius. For solvated ions, the loci of centers reside at a distance, $x_{2,}$ and this layer is called the outer Helmholtz plane, OHP. The interaction of the solvated ions with the metal surface involves long range electrostatic forces; therefore, there interaction is independent of the chemical properties of the ions. These are said to be nonspecifically adsorbed. Due to thermal agitation in

the solution, the nonspecifically adsorbed ions are distributed throughout a three dimensional region called the diffuse layer. The diffuse layer extends from the OHP into the bulk of the solution. The charge density in the diffuse layer is σ^d. [4] The total charge density on the solution side of the double layer is, σ^s:

$$\sigma^s = \sigma^i + \sigma^d = -\sigma^M \qquad (2.7)$$

Figure 2.5 depicts the proposed model where anions are specifically absorbed. In the Stern modification, there is a capacitance associated with each "layer". The capacitance associated with the charge held at the OHP and independent of potential is C_H [4]. The diffuse layer charge, C_D, will vary with electrolyte concentration and potential. In systems near the PZC and low electrolyte concentration, one can expect C_D to vary in a V-shape fashion. At large electrolyte concentrations or large polarizations in dilute media, C_D becomes so large that the contribution to the overall capacitance is negligible. [4] The composite capacitance, C_d, is the related to C_H and C_D by the following equation:

$$\frac{1}{C_d} = \frac{1}{C_H} + \frac{1}{C_D} \qquad (2.8)$$

The derivation for Equation 2.8 is derived in [4]. The variation in C_d shows that the composite capacitance has a complex behavior and will be governed by the smaller of the two terms. Figure 2.6 illustrates the expected behavior of C_d according to Stern's modifications The three models previously discussed only consider long-range electrostatic effects as the basis for the excess charge on the solution side. One must consider the influence of charged or uncharged particles that are absorbed by chemical reactions at the surface of the electrode. Also, these theories neglect the effects of ion

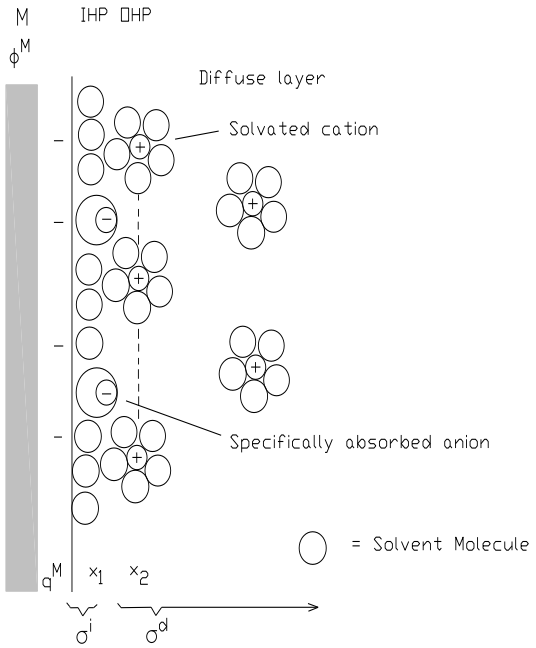

Figure 2.5 Proposed model of the double-layer region under conditions where anions are specifically adsorbed. [4]

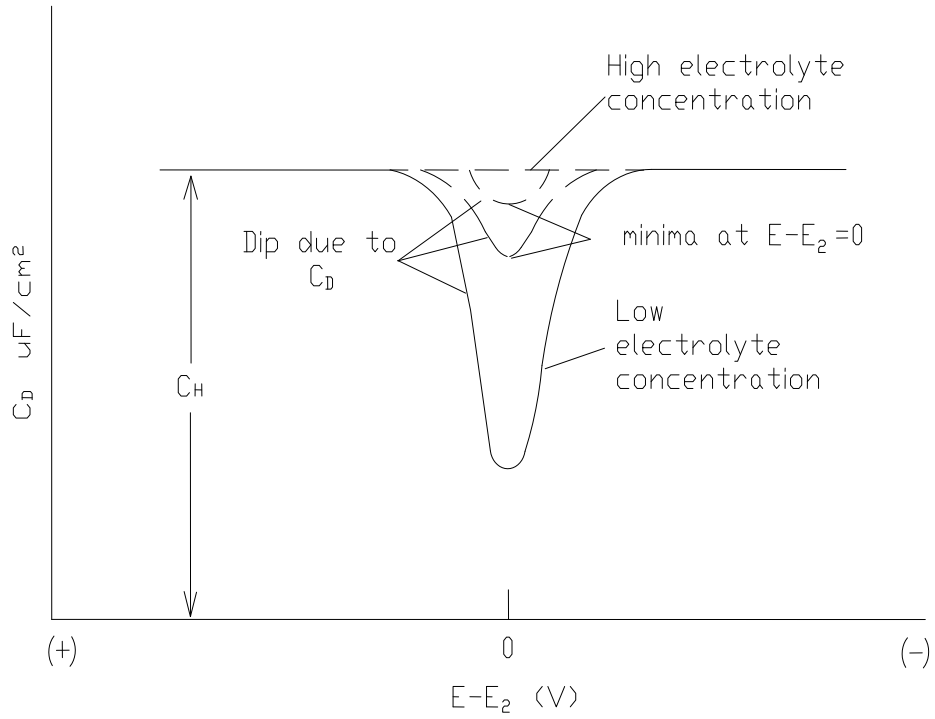

Figure 2.6 Expected behavior of Cd as electrolyte concentration changes. [4]

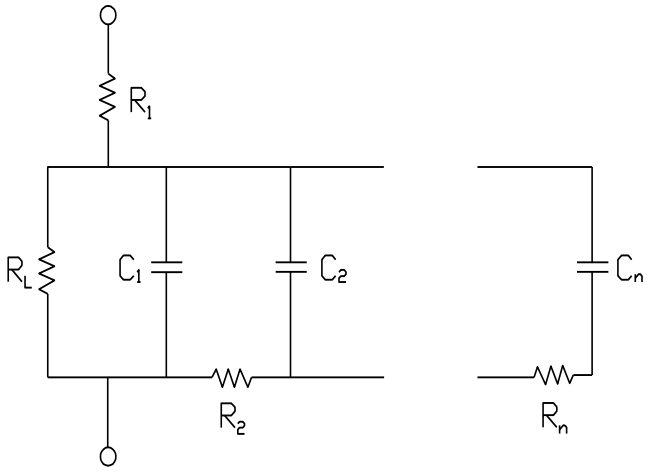

Figure 2.7 Ladder Circuit Equivalent Model [7]

pairing and strong nonspecific interactions of the ions with the electrode surface charge. The study of these effects is beyond the scope of this thesis and can be found in detail in [4] and [3].

2.2 Ladder Circuit Model

In the previous section, the general models for the metal-solution interface were presented. In this section, the ladder circuit model will be presented as an overall model for ultracapacitor behavior.

The ladder circuit developed in [7] investigates the ladder model in slow discharge and pulse load applications. The circuit diagram for the ladder model is shown in Figure 2.7.

In [7], the ladder model was used because of its success in modeling nickel/carbon fiber electrodes in ultracapacitors. The parameters in the circuit model

were determined using ac impedance methods. AC impedance measurements are frequently used to determine the characteristics of batteries and other electrical devices. A small Alitude sinusoidal voltage is applied to the ultracapacitor and the resulting sinusoidal current is measured. The magnitude and phase of the impedance are calculated from the voltage and current. [7] Superimposing the sinusoidal voltage on a dc bias level allows a small signal model to be studied as a function of dc bias level. DC bias levels of 0 V, 0.5 V, 1 V, 1.5 V, 2 V and 2.5 V were recorded. The frequency range from 1 Hz to 10 kHz was used.

The ac impedance data was input to a computer model that was developed at the University of Twente in the Netherlands. The program utilizes nonlinear least squares fitting techniques to ascertain circuit parameters. However, R_L, was fixed at 3500 Ω in determining the other ladder parameters. R_L, which models the leakage current in ultracapacitors, typically has values that are significantly larger than the internal resistance or series resistance. This means the leakage current for ultracapacitors is typically on the order of hours for self discharge.

In [7], the classical equivalent and ladder circuit in slow discharge and pulse load applications are compared using PSPICE. The leakage current, i_L, was neglected because the length of the tests was less than 100 seconds. For the slow discharge tests, the ultracapacitor was charged to a specified initial voltage, 2.5 volts, using the circuit shown in Figure 2.8 R_A and R_B can be adjusted to provide the desired current levels. Once charged, R_A was removed and R_B set to a known value. The switch, a MOSFET, was closed and at the moment of closure, the change in current and voltage was measured. This measurement is utilized to calculate a value for the ESR, equivalent series

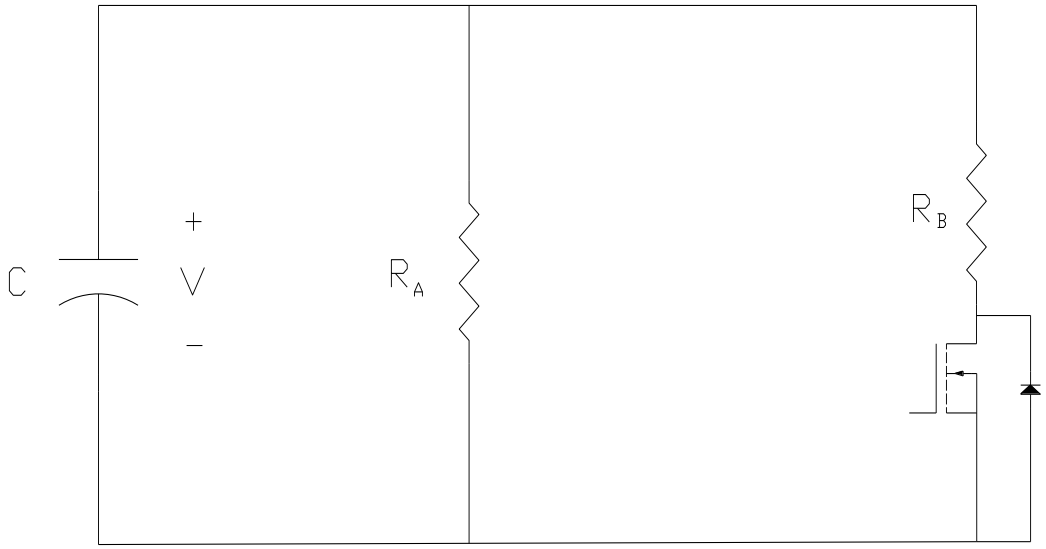

Figure 2.8 Test Circuit [7]

resistance. The contact resistance in the circuit is included in the ESR value. It is assumed the capacitance is the manufacture's rated value. The circuit parameters for the various ladder circuits are shown in Table 2.1. The plots of the actual capacitor voltage, the classical equivalent circuit simulation results, and the ladder circuits were plotted. The initial drop was accurately predicted in all the models. However, during the slow discharge test, the classical equivalent circuit begins to drift apart from the actual response at 2 Volts. The ladder circuits predict a lower capacitor voltage throughout the discharge test. As the number of ladder circuits or RC branches increases from one to five, the actual voltage does become closer to the simulated voltage. [7]

Each of the model simulations had the same initial current. However, the current waveforms predicted higher than measured current data. The ladder current decayed

Table 2.1 Parameters of the Ladder Circuits [7]

	R_L (Ω)	R_1(Ω)	C_1(F)	R_2(Ω)	C_2(F)	R_3(Ω)	C_3(F)	R_4(Ω)	C_4(F)	R_5(Ω)	C_5(F)
L1	3500	.079	38.8								
L2	3500	.07	6.65	.055	33.72						
L3	3500	.06	.007	.021	14.7	.095	27				
L4	3500	.058	.036	.018	5.9	.029	21.4	.28	16		
L5	3500	.058	.028	.016	2.71	.016	13.5	.069	19.2	.96	8.9

faster than the classical equivalent model. However, the actual current was approaching the classical equivalent model which showed a higher ending current than the ladder model. [7]

For the pulse test, the capacitor was initially charged to 2.5 volts, the MOSFET was gated using a 250 Hz pulse waveform, R_A and R_B was measured as 61.1233 ohms and .877 ohms [7]. The voltage waveform for each ladder model, classical equivalent model, and actual data were plotted together. All the models predicted a lower voltage than what was actually observed. When compared together, the ladder model L1 provided the closest response to the actual voltage data. However, the classical equivalent model very closely matches the actual current waveform.

In [7], the ladder model looked at slow discharge and pulse load testing for an

ultracapacitor. To determine the model parameters, ac impedance tests were used at six different bias levels to create five RC branches, L1 through L5. These models along with the classical equivalent model were constructed using PSPICE to determine model behavior. From the analysis between the models and actual test data, the classic equivalent model provided a suitable representation for the voltage waveform for an ultracapacitor in slow discharge application. For the pulse application, both the classical equivalent and L1 ladder circuit predicted approximately the same voltage drop as measured in laboratory [7]. Higher order ladder circuits are needed to study details in the voltage and current waveforms.

2.3 Impedance Spectroscopy Modeling

Simple RC circuits can not accurately describe the voltage behavior and energy efficiency of ultracapacitors during dynamic current profiles. With the technological advances of ultracapacitors in the power industry, the inability to accurately measure these variables can be significant in the various applications. In a vehicle application, the voltage and temperature of the ultracapacitor will change noticeably. Impedance spectroscopy provides a unique tool for the analysis of ultracapacitors under dynamic conditions. Provided frequency ranges can extend into the millihertz or microhertz region, precision measurements can be made without the limitations of nonlinearities or long relaxation times.

In [9] an EIS meter from the Institute for Power Electronics and Electrical Drives was used to measure the complex impedance of the ultracapacitor. The EIS meter is capable of measuring impedances at frequencies between 6 kHz-10μHz with high

accuracy. To accomplish the impedance measurements, small ac current flows through the capacitor and the ac voltage response is measured. While the impedance measurements are taken, the ultracapacitor is at a constant dc potential; no superimposed dc current is supplied to the ultracapacitor. During normal operations in a vehicle application, the voltage and temperature of the ultracapacitor can change therefore, four different voltages, 0.6 V, 1.2 V, 1.8 V, and 2.4 V, and six different temperatures, -30^{o}C, -10^{o}C, 5^{o}C, 20^{o}C, 35^{o}C and 50^{o}C, were recorded.

N interleaved RC circuits should lead to satisfying results; however, 2N parameters would be required in the calculation. Since there is a strong influence of each parameter on the other, it would nearly impossible to determine all the parameters. A possible solution is shown in the Figure 2.9. The ultracapacitor is modeled with an inductor, L, series resistor, R_i, and a complex pore impedance, Z_p. The pore impedance is responsible for the -45^{o} slope and approaches an ideal capacitor at low frequencies. Although the behavior of inductor is not interesting for an ultracapcitor application, the model retains an inductor to avoid errors in the intermediate frequency range. This error could influence the estimation of R_i.

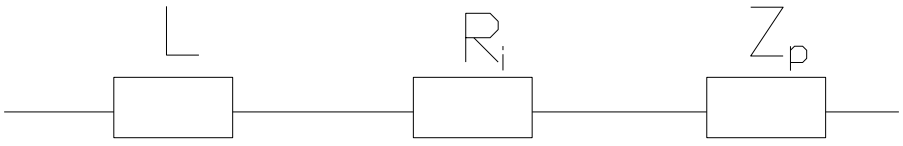

Figure 2.9 Equivalent circuit for impedance spectroscopy modeling. [9]

In [9], equation 1 gives the mathematical expression for $Z_p(j\omega)$. The real part of the impedance increases with decreasing frequency and the full capacitance is available at dc conditions. The expression contains two independent parameters, C and τ, and along with R_i and L, four parameters are needed for the determination of the model. Aside from the inductance, the remaining three parameters are temperature dependent and not constant over the range of operation voltages. A large number of impedance measurements have been performed to determine R_i, C, and τ. The results are placed into lookup tables which have been implemented into the Simulink model. Figure 4 in [9] shows an exAle of these lookup tables.

To model the results in Matlab/Simulink, the frequency domain model needs to be transformed into the time domain. Section 4 in [9] provides an appropriate method to determine the inverse transform of $Z_p(j\omega)$. Comparisons of equations 2 through 5 and mathematical operations are used to determine coefficients of the model parameters allowing new RC circuits that can be integrated into the software tools for the circuit or system simulation. It should restated the parameters for the RC circuits are derived from two experimental parameters, C and τ. [9] For a given current profile, the model is designed to provide precise voltage response and estimation of power dissipation. Figure 2.10 represents a block diagram of the simulation model. [9]

The current profile used provides a highly dynamic load profile at the beginning with deeper discharge and charge periods occurring at the end. The current profile is shown in Figure 7 of [9]. Differences between the measured and modeled voltages are in nearly perfect agreement. This can be verified by Figure 8 in [9]. During the deeper discharge and charge period, the maximum deviation between the measured and

calculated capacitor voltage was 25 mV.

The energy efficiency was another important aspect investigated. To experimentally determine the efficiency, the ultracapacitor was partially charged and discharged with a constant dc current whose amplitude varied. Multiple charge/discharge cycles took place at various amplitudes; the last three cycles which started and finished at the same internal capacitor conditions were used for the efficiency calculation. The deviations between the measured and calculated efficiency values never exceeded 0.5%. Since the self-discharge characteristics are neglected, systematic variations were discovered in the model. The work for the model is focused on dynamic modeling and the necessary insertion the self discharge mechanism would be required to improve the accuracy.

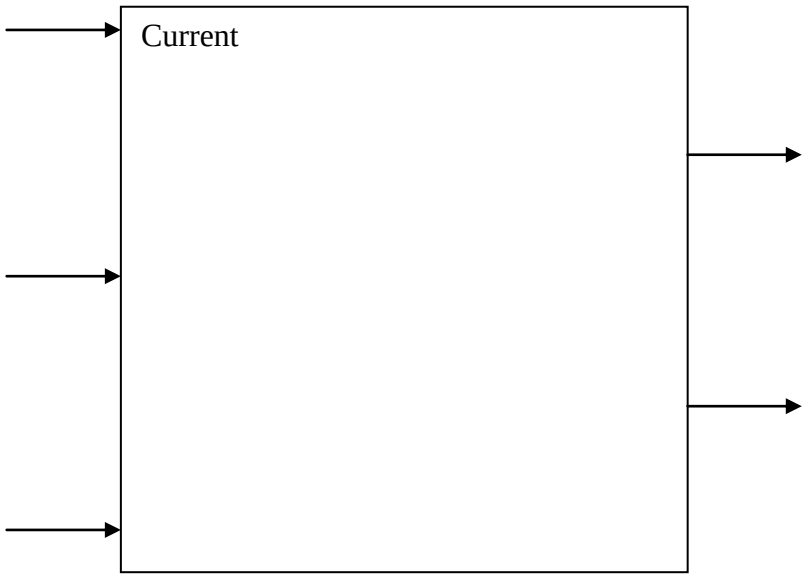

Figure 2.10 Block Diagram of Ultracapacitor [9]

2.4 Parallel Circuit Model

In [10] and [11], a different model was proposed to describe the terminal behavior of ultracapacitors. A simple RC circuit did not correctly predict the nonlinear rise and fall of the ultracapacitor voltage before and after a charge or discharge. This is shown in Figure 1 in [11]. Due to the leveling off of the voltage level after a discharge, the change cannot be due to an internal resistance. Instead, internal charge redistribution between the internal capacitances is theorized [11].

Before an equivalent circuit structure had been formulated, two model requirements were established. First, the model should be simple and describe the terminal behavior over a 30-minute range with sufficient accuracy. Second, the parameters of the model should be based upon measurements at the terminals of the ultracapacitor.

Three physics aspects provided additional insight in the determination of the circuit model. The first physics factor was based on the electrochemistry of the interface between two materials in different phases. The double-layer capacitance is modeled by a large number of parallel resistive capacitive branches with different time constants [10, 11] . The second factor looks at the interfacial tension in the double layer. It can be expected that the capacitance of the device depends on the potential difference. In the practical range, the differential capacitance measured experimentally varies linearly with the capacitor voltage [11]. The final factor addresses the ultracapacitor's self discharge characteristics. For pulse applications, an inductor may be added; however, measurements show the inductance to be small enough, in the nano-Henry range, that it can be neglected for most applications.

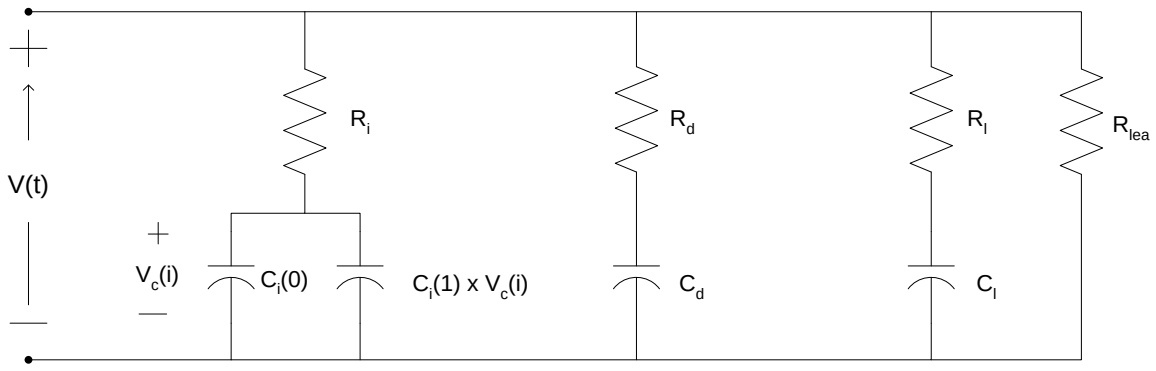

Figure 2.11 Proposed parallel circuit model [10, 11].

With the aforementioned ultracapacitor requirements considered, a model consisting of three RC branches that provide three different time constants that factor in the different charge transfers is proposed. Figure 2.11 shows the proposed model.

The first branch dominates the immediate behavior of the ultracapacitor. For this model, this branch describes the ultracapacitor behavior in the time range of seconds. The elements in this branch are R_i, $C_i(0)$ and $C_i(1)$. Also, the branch contains the voltage dependent differential capacitor, C_{diff} which will be discussed later. The second branch consists of elements R_d and C_d. This branch dominates the ultracapacitor behavior in the minute range. Finally, the third branch, referred to as the long branch, consists of R_l and C_l. This branch determines the behavior for times longer than ten minutes. R_{lea} is the leakeage resistance. [11]

The basic charge for a capacitor in Equation 2.1 does not apply to voltage dependent capacitance. A beneficial definition for describing differential capacitance is

$$C_{diff}(V) = \frac{dQ}{dV}\Big|_{V'} \tag{2.9}$$

In Eq. 2.9, dQ is an incremental change in charge at a certain voltage, V' which produces an incremental voltage change [11]. In this model, the differential capacitor is composed of a fixed capacitance, $C_i(0)$, and a voltage dependent capacitor, $C_i(1)$:

$$C_{diff}(V) = C_i(0) + C_i(1) * V \tag{2.10}$$

To verify the differential capacitance model, small amounts of charge at various voltages were injected with the resulting change in voltage measured. The results are shown in Figure 3 in [11]. The results provide confirmation that the change in the differential capacitance can be approximated by a linear function of the voltage. The consequence the nonlinear behavior of the first branch is more energy per voltage increment is stored at a higher voltage than a constant linear capacitor. The stored energy in the first branch of the capacitor is:

$$E = \frac{1}{2} C_i(0) * V^2 + \frac{1}{3} C_i(1) * V^3 \tag{2.11}$$

This is derived by assuming a constant charge current and using Eqs. 2.9 and 2.10.

In order to determine the model parameters, conditioning of the ultracapacitor or several weeks of self discharge is required. This process ensures all model equivalent capacitances have zero voltage and any internal charge distribution has ceased; meaning the initial storage charge is known. Also, a precisely timed and controlled current source is needed to regulate the amount of charge supplied to the ultracapacitor. The charge current reaches a set value within 20 milliseconds after being turned on; meaning a constant current is used in the experiment to determine the ultracapacitor parameters. The charge current is approximately five percent of the specified short circuit current. The short circuit current is the rated voltage divided by the manufacture's specified inner resistance. When the

terminal voltage reaches the rated value, the current is removed [11].

The assumption that the three equivalent branches have distinct time constants was used in determining the model parameters. This philosophy allows each branch to be observed independently. The immediate or first branch is responsible for the fast controlled charging process. Once the external charging has ceased, the first branch capacitors contain all the charge. After a short delay, stored charge redistributes to the second branch without affecting the third branch. Once equalization between the first and second branches is accomplished, charge begins to distribute to the third leg [11].

The in-depth calculations for determining each model parameter is provided in [11]. To develop an equivalent circuit model, these parameter calculations were performed on a 470 F and 1500 F ultracapacitor. For model verification, the 470 F equivalent circuit model was simulated using various charge cycles. The simulation results were compared with measurements from the 470 F ultracapacitor which was subjected to the same charge cycle. In [11], Figure 6 shows the model verification results. In Figure 6, the simulation and measurements are in good agreement except for low operating voltages and times beyond 30 minutes. At voltages less than one volt or 45% of the rated voltage, the difference between the simulation and measurements increases. The assumption that only the first or immediate branch capacitors are voltage dependent creates the error. In reality, all the capacitors in the model are voltage dependent. Due to the model neglecting the RC time constants that model ultracapacitor behavior in the hours or days, the model agreement in these time spans creates the inaccuracy [11].

The behavior of the ultracapacitor was explored to test the charge redistribution

theory. Using the equivalent ultracapacitor model, if the immediate branch is discharged to zero volts, the terminal voltage will be 0.93 V or 41% of the rated voltage within 30 minutes [11]. The actual measured voltage was 1.09 V or 47.4% [11]. If the ultracapacitor was quickly charged to 2.3 V, at the end of the 30 minutes, the terminal voltage lowers to 1.6 V or 70%. The immediate charge that can be recovered is 60% of the initial charge supplied to the immediate branch. The charge is not lost, merely redistributed to the slower reacting branch; therefore the charge cannot be recovered quickly [11].

For voltages above 40% of rated terminal voltages and within the specified time period, the model is shown to predict the behavior of the ultracapacitor accurately. By comparing the terminal behavior of the ultracapacitor against the equivalent model, both support the initial theory of charge redistribution to the various RC branches. The error at low voltages and extended time constants is due to the assumptions made to keep the model and parameters' identification simple.

2.5 Serial Resistance and Capacitance Variations with Temperature

In [11], the model does not account for temperature variations in the resistive or capacitive elements in the equivalent ultracapacitor model.

The circuit model consists of two equivalent branches with two distinct time constants. The circuit parameters for the two branches were determined in the same manner as described in [11] or Section 2.4. The experimental circuit consists of a unidirectional current serial chopper composed of a MOSFET power switch. In order to evacuate accumulated energy in the high power inductance, a fast recovery diode to act

as a free wheel diode was used. The ultracapacitors were placed in a temperature controlled climatic room that can vary between -40°C and 50°C. The acquisition system was controlled through Labview software that processed the output thermocouple signals and the various current and voltage sensors. The study uses 2700 and 3700 F capacitors with activated carbon electrodes and organic electrolyte. The experimental results were used to determine the circuit parameters [5].

The determination of the ESR as a temperature dependent function was difficult due to exact dimensions of the double layer thickness and section; therefore, the establishment of an empirical law using experimental results was suggested. Using Section 3 in [5] to determine the serial resistance, the results showing the variations as a function of temperature are shown in Figure 5 of [5]. The series resistance varies by approximately 50% when the temperature is increased from -25°C to 25°C. Therefore, negative temperatures show higher power dissipation than positive temperatures causing the efficiency to decrease. [5]

The correlation between the empirical values for series resistance and temperature is approximated using the quadratic equation:

$$R_1(T) = aT^3 + bT^2 + cT + e \qquad (2.12)$$

where *a*, *b*, *c* and *e* are experimentally determined constants. Figure 5 in [5] shows the change in the serial resistance with respect to temperature.

Figure 4 of [5] shows approximately a 9-second difference in charging time between T = 25°C and T = -25°C. The discrepancy is the result of two different effects. The first effect is the result of the varying series resistance. If the series resistance changes, the RC time constant will increase or decrease. The voltage is described using

the following equation:

$$V(t) = R_1 * I_{ch} + V_c(t) \tag{2.13}$$

$V_c(t)$ represents the voltage that depends only on the ultracapacitor capacitance aspect and is directly proportional to the ultracapacitor charge time, Δt, at a constant current and for a given capacitance. For a given charge voltage, the series resistance, R_1, increases with a decrease in temperature, the result is a decrease in $V(t)$ and ultimately a shorter charging time [5].

The second effect is a result of the variation of the total capacitance with temperature variations. The ultracapacitor global capacitance depends on the electrolyte dielectric constant and on the thickness of the double-layer both of which are temperature dependent; it is difficult to provide an analytical relationship between the capacitor and temperature. The variation of these parameters leads to a variation of the ultracapacitor's capacitance as a function of temperature. The variations of C_0 and C_v were determined using the method describe in Section 2 of [5]. The values of C_0 and C_v for a 3700 F, 2.5 V ultracapacitor have been measured for different temperatures and are shown in Table 2.2. The variations of C_0 and C_v are less important than the series resistance, R_1. The capacitance variations, approximately 21% and 17%, are considerable less than the 50% of the series resistance. Figure 6 of [5] shows the relationship between C_0 and C_v plotted against temperature. Figure 6 shows a negative correlation between C_0 and C_v; meaning as the temperature decreases, C_0 decreases whereas C_v has a slight increase. The variation of the global capacitance is principally dependent on C_0; thereby C_0 is a parameter which is not completely disregarded. Polynomial equations, Eq. 2.14 and Eq. 2.15 show the equation format with a_i and b_i determined from the fitted curves of C_0 and C_v. [5]

Table 2.2 Parameter Values for 3700 F, 2.5 V Ultracapacitor [5]

	T= -35°C	T= -15°C	T= 0°C	T= 25°C
C_0 (F)	1979	2186	2255	2399
C_v(F/V)	672	638	611	553

$$C_0(T) = a_3T^3 + a_2T^2 + a_1T + a_0 \quad (2.14)$$

$$C_v(T) = b_3T^3 + b_2T^2 + b_1T + b_0 \quad (2.15)$$

The variables, R_1, C_0, and C_v that account for the temperature variations, was implemented in Saber and Spice software. Figure 7a in [5] shows the results for the 3700 F ultracapacitor with a 145 A current charge and T= -35°C. In [5], Figure 7b provides the results of the 2700 F with 95 A current charge and T= 35°C. Both curves, simulation and experimental, agree well with only small differences between the two. The interpolation of the experimental curve by a polynomial law is the cause for the discrepancy. In practice, the small error can be neglected. The temperature-based equivalent circuit can describe the behavior of the ultracapacitor.

2.6 Chapter Summary

This chapter provided an overview of the past and current models used to estimate

the behavior of the ultracapacitor. In section 2.1, an overview of the first pioneers to study the charge interaction at the metal-solution boundary was provided to show the need to study the variations in the ultracapacitor's terminal behavior. In addition, early researchers provided an explanation why an ultracapacitor cannot be viewed as classical capacitor but rather a complex circuit.

Sections 2.2 through 2.5 provide an overview for present ultracapacitor models used today. The models described in each section consist of multiple RC circuits to predict the terminal behavior of the ultracapacitor. The model parameters were determined using two methods: constant current or impedance spectroscopy.

Chapter 3.

Chapter 3 provides the circuit configuration that was assembled to gather the experimental data of charging and discharging ultracapacitors. This chapter contains screen captures from the oscilloscope, Matlab plots of the data, and best fit curves of the data to help analyze the observed behavior.

3.1 Experimental Circuit Configuration

The test circuit constructed to obtain the Maxwell 450, 900, and 1800 F ultracapacitors test results utilized a parallel circuit configuration that consisted of a charging circuit and a discharge circuit. Figure 3.1 shows the test circuit configuration.

Two Leach F0219 contactors were used as switches to isolate the charge and

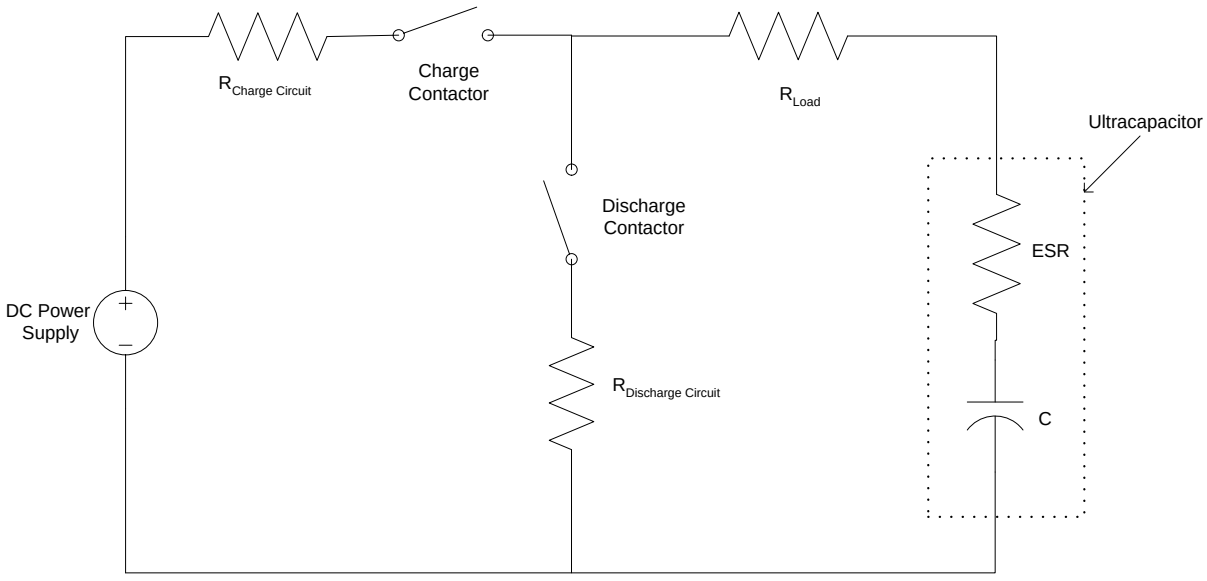

Figure 3.1 Ultracapacitor test circuit diagram.

Table 3.1 Load Resistor Values

Manufacturer (Ω)	Measured (mΩ)
0.1	94.8
0.1	94
0.6	616
0.6	613
0.6	614
0.8	760
0.8	756

discharge circuits. The contactors use a 24 V solenoid to energize and close the normally open contactor. To accomplish the different test current levels, several power resistors were placed in parallel. The resistors are Ohmite 300 W resistors with a tolerance of ±10%. Two 0.1 Ω resistors, model C300KR10, three 0.63 Ω, model C300KR63, and two 0.8 Ω, model E300KR80, resistors were used for the resistive load in this thesis. To accurately measure the actual resistance of each resistor and charge and discharge circuit resistances, an AEMC Micro ohmmeter model 5600 was used. Table 3.1 lists the resistance values from both the manufacturer and the measured resistance values using the ohmmeter.

The charge circuit resistance was measured at the power source voltage terminals, points A and B in Figure 3.2. The load resistors and ultracapacitor were removed from

the circuit by shorting their respective terminal leads together. The charge circuit contactor remained in the circuit and was closed to include its internal resistance. Figure 3.2 provides the location of load resistors and ultracapacitor. The charge circuit resistance was measured three times and an average taken.

The discharge circuit was measured at the ultracapacitor terminals, points A and B in Figure 3.3. The load terminals were shorted together and the discharge circuit contactor closed to account for its internal resistance. The discharge circuit was measured three times and an average recorded. The average measured charge and discharge circuit resistance was 7.7 mΩ and 0.56 mΩ, respectively.

The ultracapacitor voltage measurements were made at a terminal block located outside the environmental chamber. With the ultracapacitor inside the environmental chamber, the use of a terminal block was necessary due to the lack of a long oscilloscope

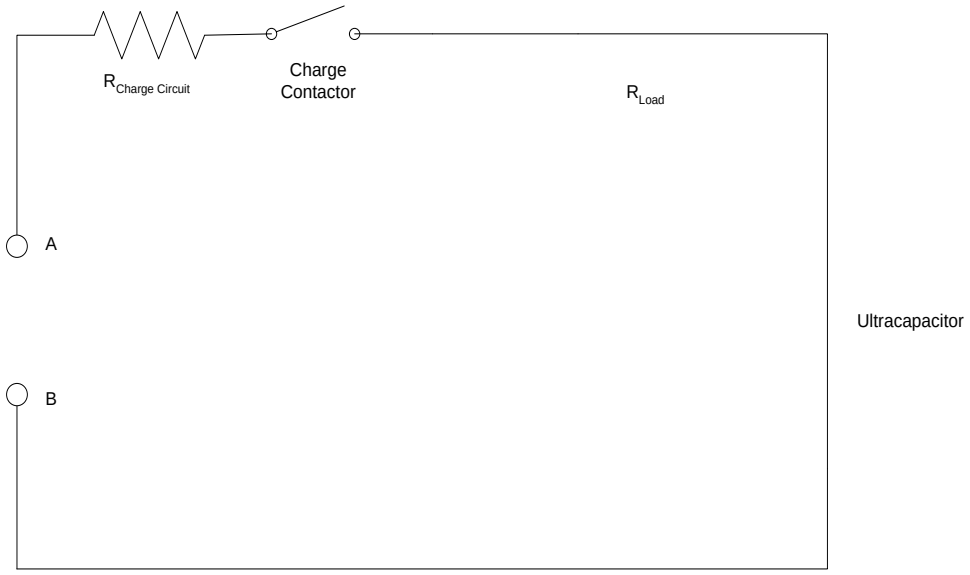

Figure 3.2 Charge Circuit Resistance Diagram

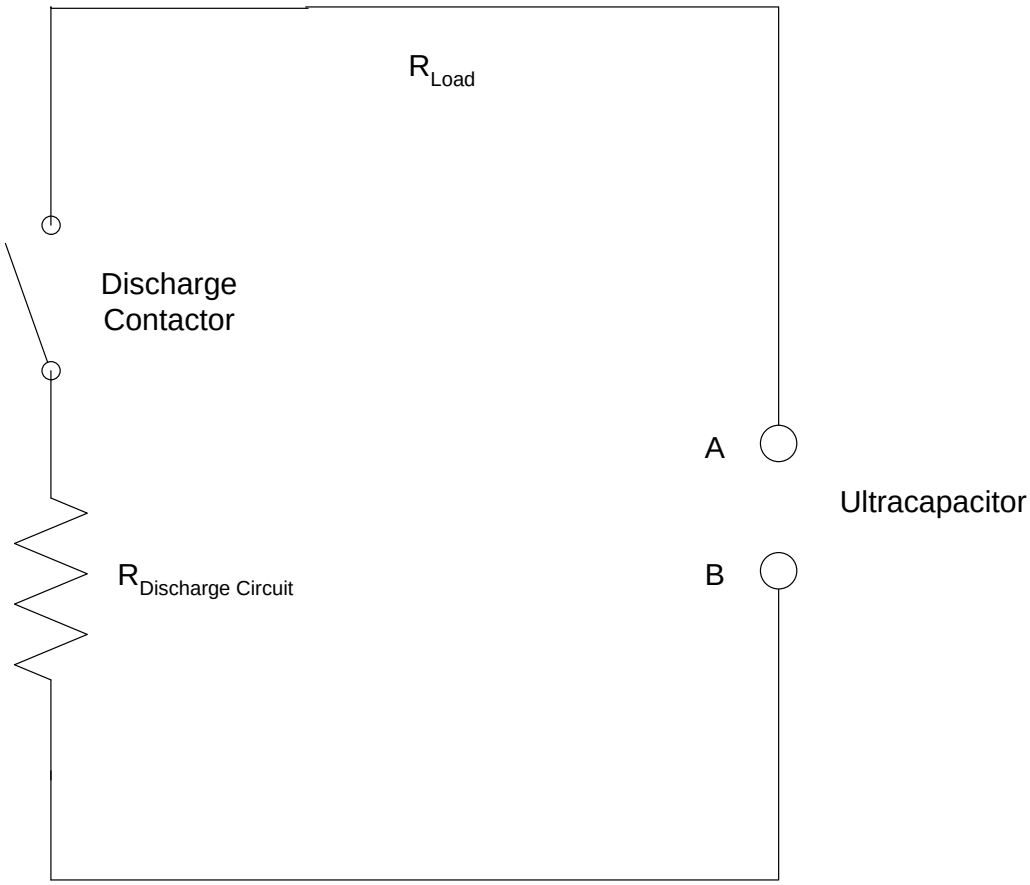

Figure 3.3 Discharge Circuit Resistance Diagram

voltage lead length. The voltage leads were attached at the positive and negative voltage terminals of the ultracapacitor. The voltage wires were passed through a side access hole of the environmental chamber to the terminal strip. The oscilloscope voltage probes were attached at the terminal strip.

The current probe was attached between the ultracapacitor and load resistors. The orientation is such that power or current flow into the capacitor was positive. The current probe was placed as close to the ultracapacitor without being placed inside the environmental chamber. In Figure 3.4, the environmental chamber shows the location of the current probe. The current probe, A6304XI, was attached to a Tektronix AM503B current amplifier. The current amplifier was attached to the oscilloscope using a BNC connector. The current amplifier was adjusted to provide a 10 mV deflection on the oscilloscope when 20 A passed through the current probe. Before each current measurement, verification of a zero dc current measurement was observed on the oscilloscope. If a dc offset was present, the current probe was zeroed before the next experiment proceeded.

The data was collected using a Yokogawa DL750 data recorder. After an ultracapacitor was charged or discharged, a screen capture and comma separated variable (CSV) file was saved to a removable media storage device. After completion of the file saving, the experiment continued to the next element.

The environmental chamber, ESPEC ESX-3CA, was utilized to provide necessary control of the temperature. However, the ultracapacitor's environment may be at the desired temperature but the ultracapacitor itself may not be at the correct temperature. To ensure the ultracapacitor was at the desired temperature, a thermocouple surrounded

by insulation was attached to the center of the ultracapacitor. Thermal grease was used to provide a good heat transfer between the ultracapacitor and thermocouple. The ultracapacitor detail in Figure 3.4 provides a graphical representation. When the thermocouple displayed a temperature reading of $\pm 0.5^{o}$C of the desired temperature, the experiment proceeded.

3.2 Data Scaling for Experimental Comparison

Before comparison of the temperature effects on the series resistance can be determined, the data needed to be scaled to provide accurate comparisons. As stated in Section 3.1, a *.csv file was saved using the Yokogawa DL750 data recorder. In order to interrupt the *.csv data, a Matlab program was written to import and multiply the data by the appropriate scale factor. The current values in the *.csv files need to be multiplied by the current amplifier scale factor while the voltage is a direct measurement. After the current and voltage scale factors are adjusted, the voltage and current are multiplied together to provide the power graph. Figure 3.5 shows an example of the Matlab graphs. All the Matlab graphs can be viewed in Appendix A at the end of this thesis.
The Matlab program provides the opportunity of placing more than one voltage, current, or power plots together to determine patterns and differences. Figure 3.6 provides a plot of the *.csv data for the 900 F ultracapacitor 25 A charge at the following temperatures: -25 ^{o}C, 0 ^{o}C, 25 ^{o}C, and 50 ^{o}C.

Before the graph is beneficial, two corrections need to be made. First, the graph shows various start times for each experiment. In order to provide a more accurate

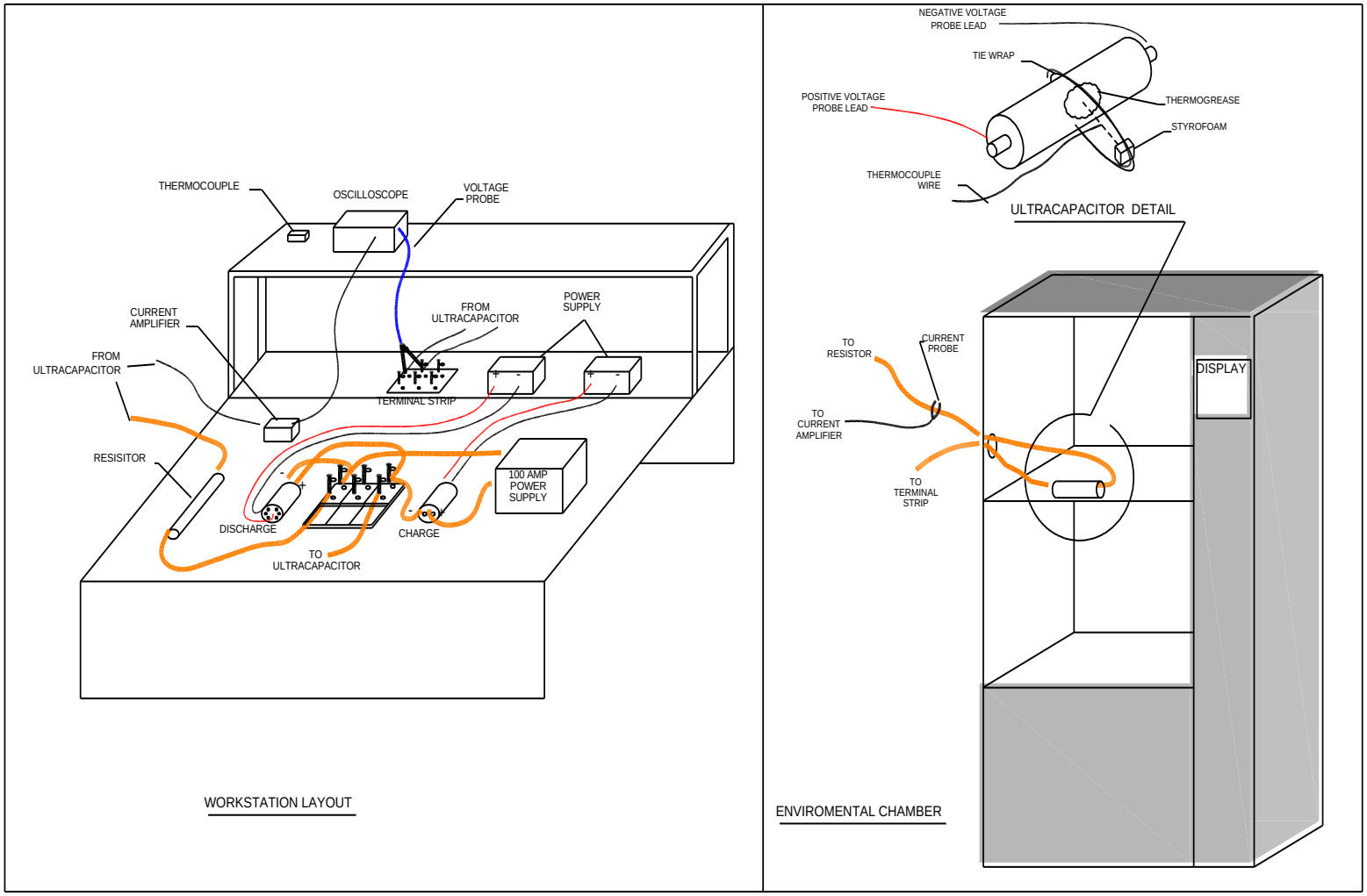

Figure 3.4 Experimental connections for ultracapacitor testing.

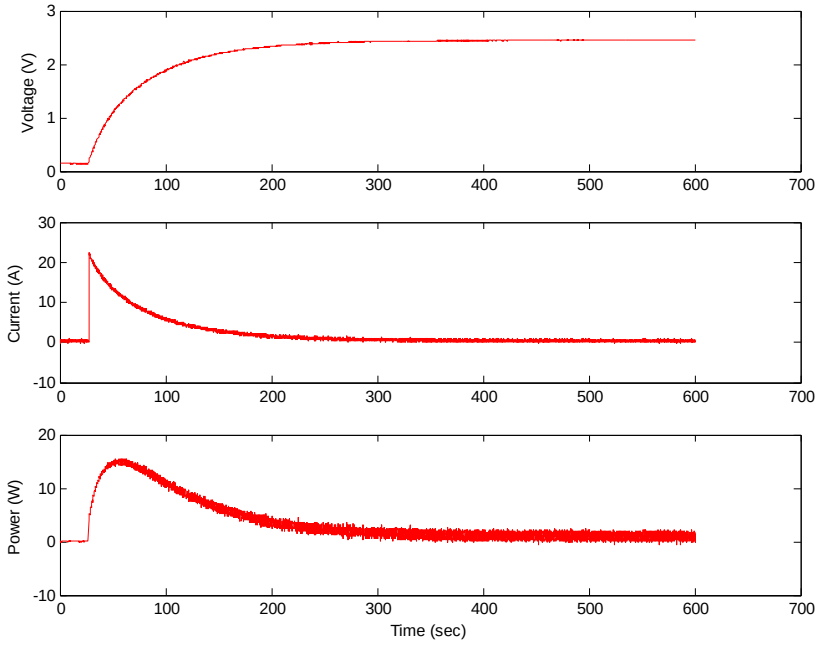

Figure 3.5 Matlab graphs for 450 F ultracapacitor at 25 A charge, T= 25oC.

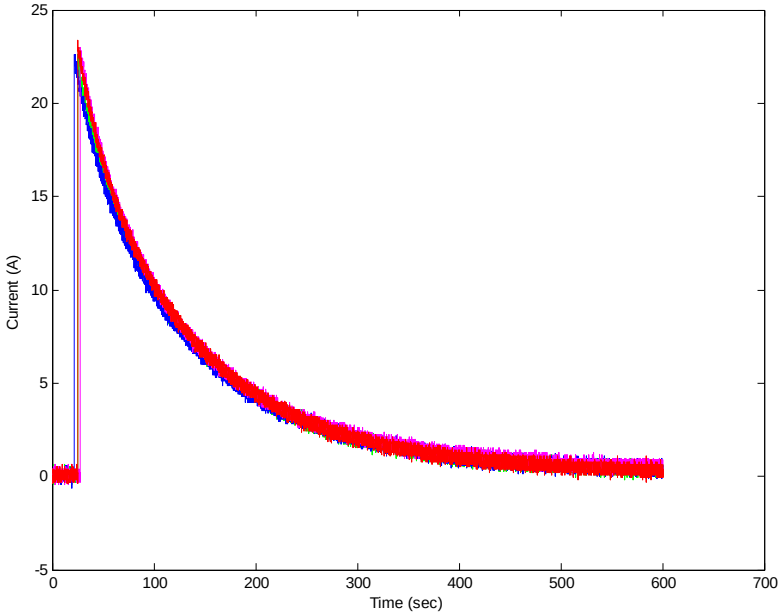

Figure 3.6 900 F ultracapacitor 25 A charge current at various temperatures (-25 ^{o}C, 0 ^{o}C, 25 ^{o}C, and 50 ^{o}C)

comparison, the start times for the various temperatures need to correlate. The exact start times for each experiment were found for each temperature curve. The necessary subtraction of time was determined and incorporated in the time vector. The start time for every best fit curve was time shifted to provide an experimental start time of zero seconds. Second, the noise from the data file makes a comparison of two pieces of data that overlay hard to distinguish. Therefore, Matlab's curve fitting toolbox was used to determine a best fit curve with a 99% confidence level for each voltage, current, and power curve. Figure 3.7 shows an example of a best fit.

Using best fit curves eliminates the noise at the low current and voltage levels by averaging the values. However, the best fit curve does not match the data perfectly and introduces errors in the resistance parameter calculations. The best fit curves with the necessary time correction were used to determine and evaluate differences in the ultracapacitor's parameters.

3.3 Experimental Results

The experimental results are shown in the following section. Due to the same effects of the temperature on all three ultracapacitors, it was necessary to eliminate repeated graphs. The graphs included will show overall characteristics to demonstrate the resistance differences caused by the temperature variations.

Figure 3.8 and 3.9 show the charge and discharge voltages for the three different size ultracapacitors using a 25 A charging current. Within each group, there are four

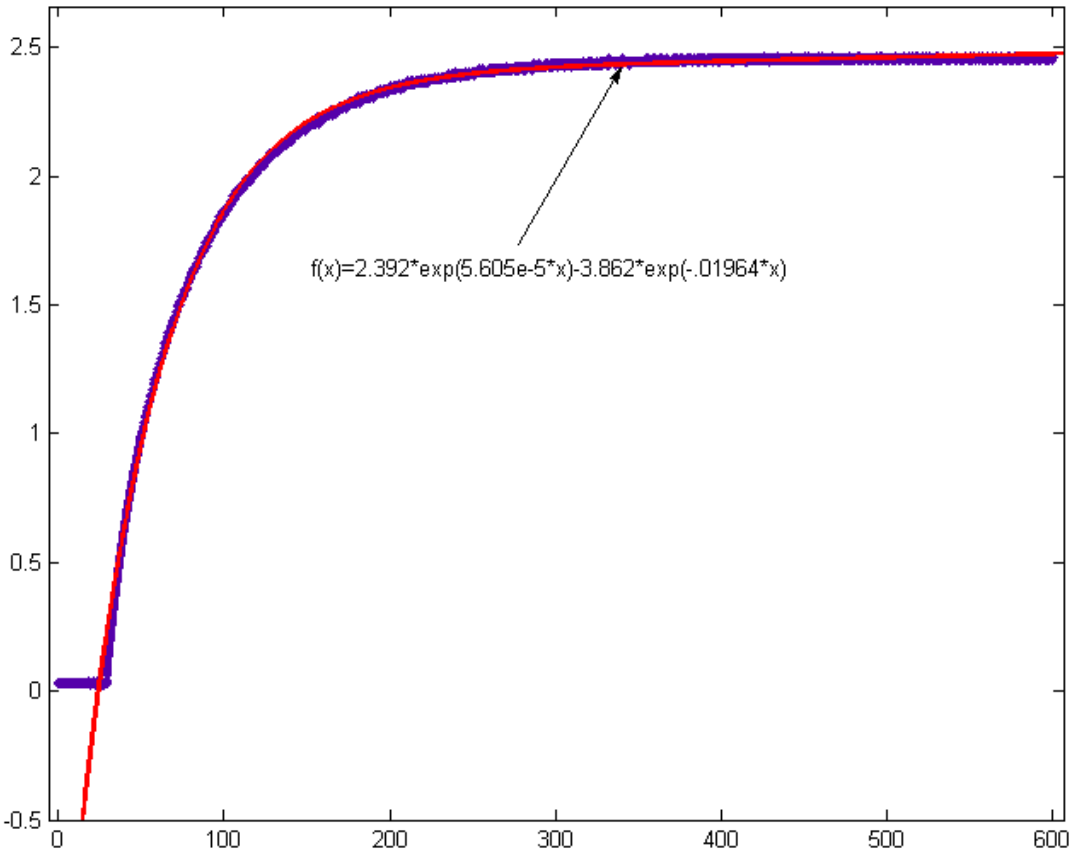

Figure 3.7 Best fit curve for ultracapacitor data.

different lines that vary in color. The color difference represents the different test temperatures, -25 ^{o}C (red), 0 ^{o}C (green), 25 ^{o}C (blue) and 50 ^{o}C (magenta). Looking at Figure 3.8, the temperature effects are more pronounced on the charge voltage for the1800 F group. The graph shows a lower beginning voltage for the lower temperatures. However, as the voltage and time increase, the ending voltages for the lower temperatures are higher than those for the higher temperatures. In Figure 3.8, it appears the lower temperature curves cross the higher temperature curves at the knee of voltage curve.

Figure 3.9 shows the current graphs using a 25 A current charge for the three various ultracapacitors. The currents appear to experience the same effects as the voltage; however, less pronounced. For each group, the ending current is higher for the 50 ^{o}C than the -25^{o} C temperature. The lower temperature best fit current crosses the higher temperature's best fit current curves at the knee of the current curve which is similar to the 25 A. The 900 F ultracapacitor currents appear to be more susceptible to the temperature effects than the 450 or 1800 F groups.

Figure 3.10 shows the discharge voltage profiles of the different size ultracapacitors. The discharge voltage experiences similar temperature effects as the charge voltage. The lower and higher voltages appear to reverse positions near the knee of the voltage curves. However, the temperature effects are more noticeable at the start and end of the discharge. In the 450 F group, the 50^{o}C temperature has a higher slope than the -25^{o}C temperature. At the end of the discharge cycle, the -25^{o}C voltage is slightly higher than the 50^{o}C voltage. For the 900 F group, the effects are opposite that of the 450 F group. At the initial discharge, the 1800 F appears to experience less

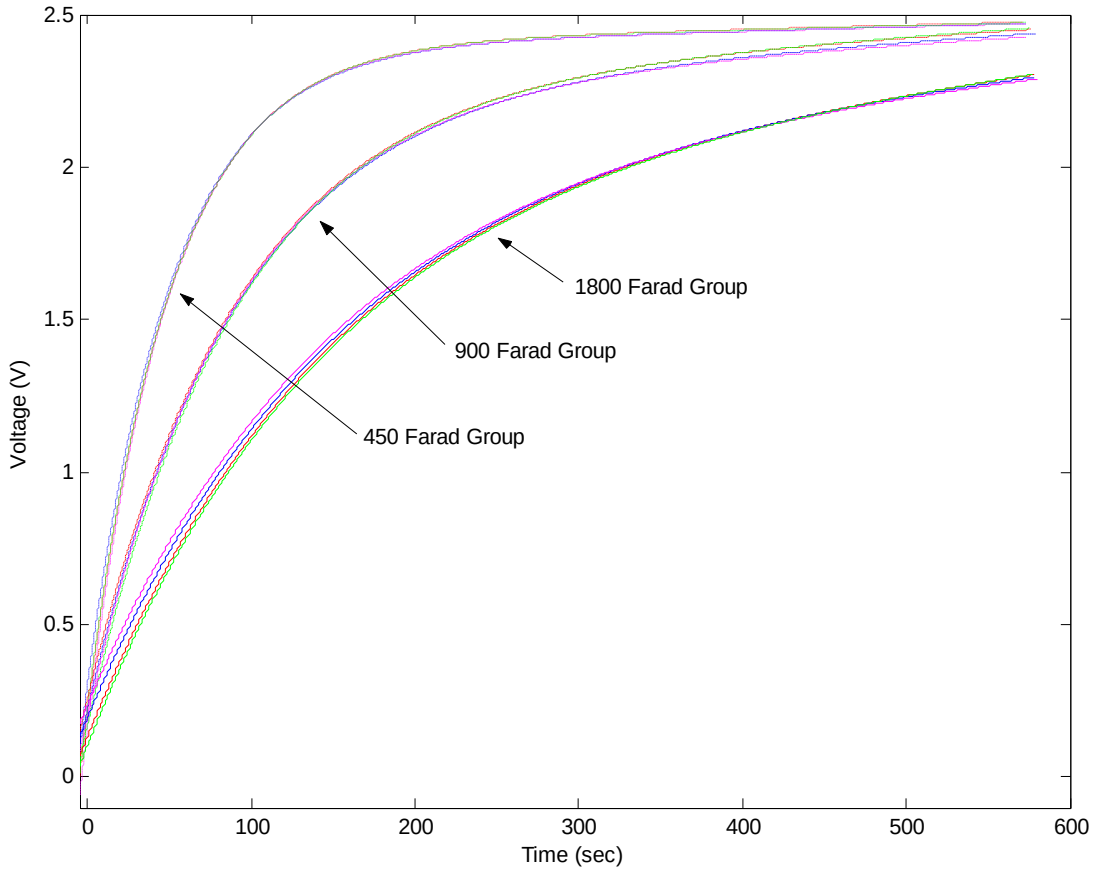

Figure 3.8 Charge voltage plots using a 25 A charge current for the various ultracapacitors.

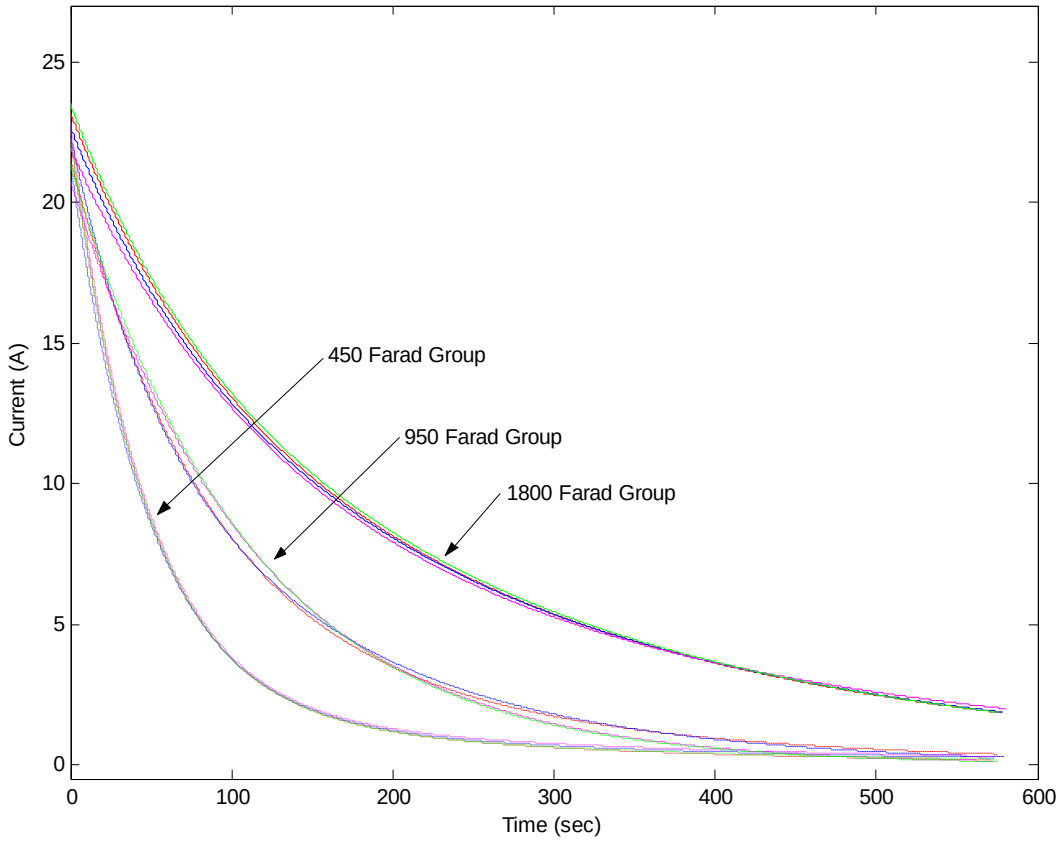

Figure 3.9 Charge current plots using a 25 A charge current for the various ultracapacitors.

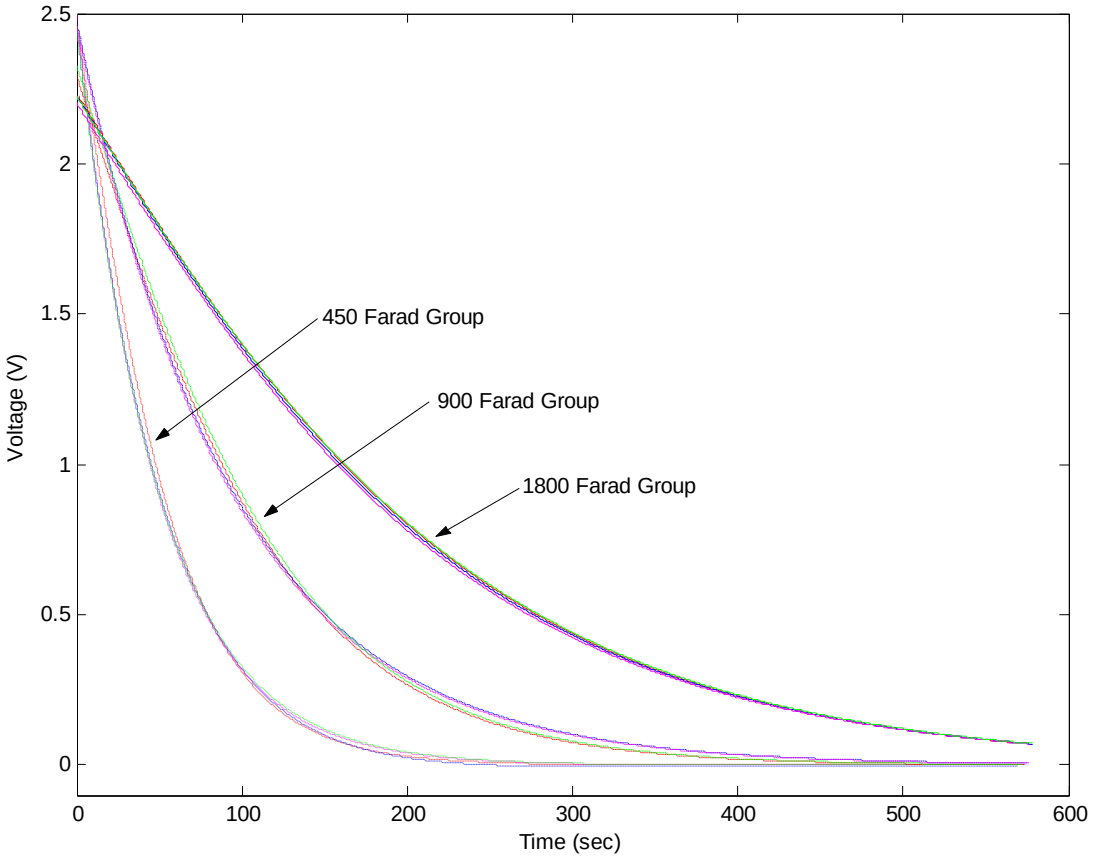

Figure 3.10 Discharge voltage plots using a 25 A discharge current for various ultracapacitors.

temperature effects than the 450 or 900 F groups.

Figure 3.11 shows differences in the 25 A discharge currents for the three ultracapacitors. The 900 F current group experiences the greatest variations caused by the temperature variations. At the end of the discharge cycle, the current levels are higher for the lower temperatures. In each ultracapacitor's group, the lower and higher temperature curves cross near the knee.

Figure 3.12 displays the charge voltage graphs using a 50 A charge current. The 1800 F group shows the greatest temperature dependence. Unlike the 50^{o}C curve in the 25 A graph (Figure 3.6), the 50 A, 50^{o}C curve does not cross the lower temperatures at the knee of the temperature curves.

Figure 3.13 shows the current profiles for all three ultracapacitors using a 50 A charging current. The 450 F group has a large temperature variation around 100 seconds. In the 900 F group, separation of the current curves can be seen around 230 seconds. At the end of the discharge period, the 900 F ultracapacitor 50^{o}C curve shows a higher residual current level than the lower temperatures.

Figure 3.14 provides a graph showing the differences the temperature effects have on the three ultracapacitor's terminal voltage using a 50 A discharge current. According to the different temperature curves, the 1800 F ultracapacitor is still the most dependent on temperature variations. Unlike the 25 A discharge current graphs, the higher temperatures' voltage curves do not cross the lower temperature voltage curves at the knee in the current curves.

Figure 3.15 show the 50 A discharge current results. The discharge current graph

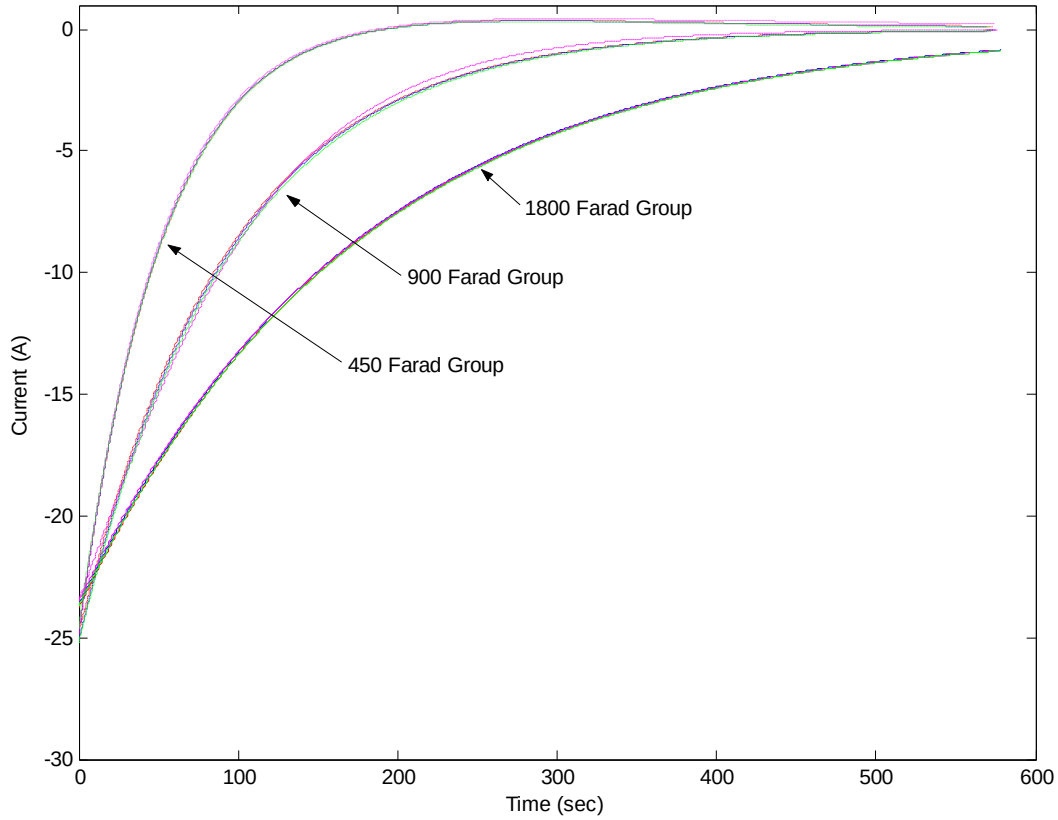

Figure 3.11 Discharge current plots using a 25 A discharge current for the various ultracapacitors.

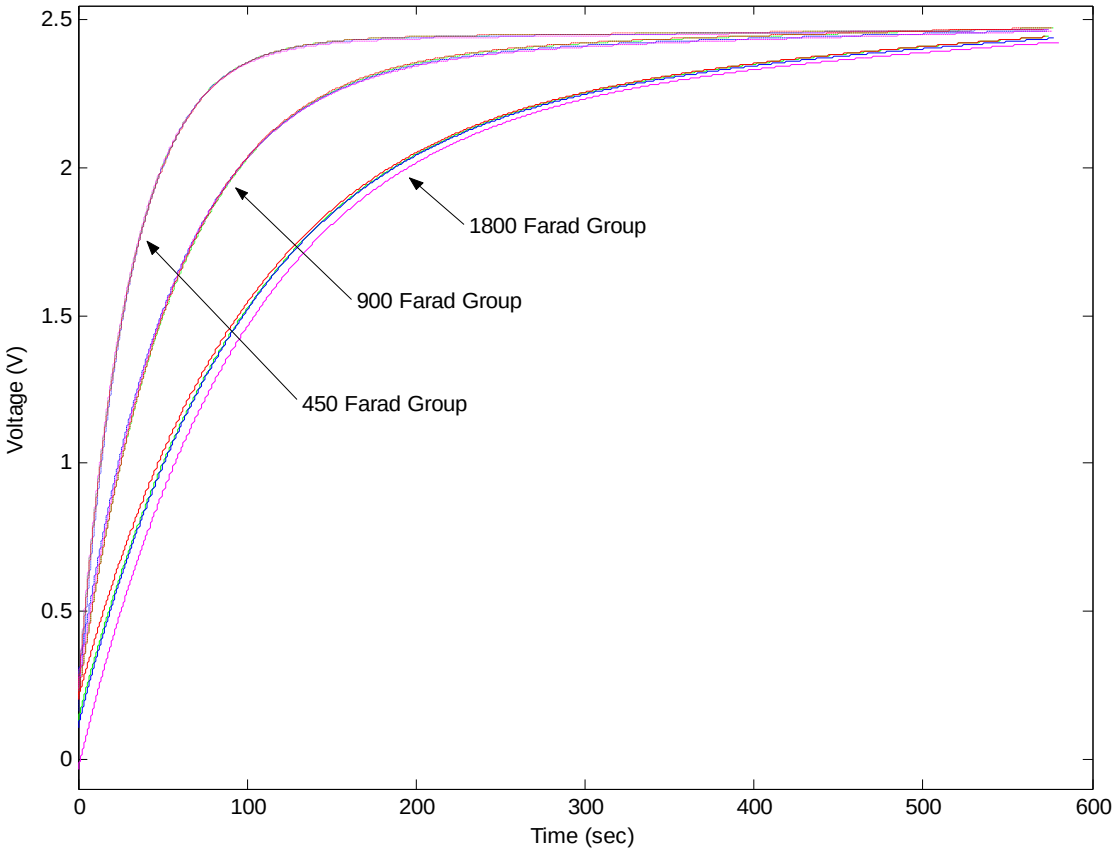

Figure 3.12 Charge voltage plots using a 50 A charge current for the various ultracapacitors.

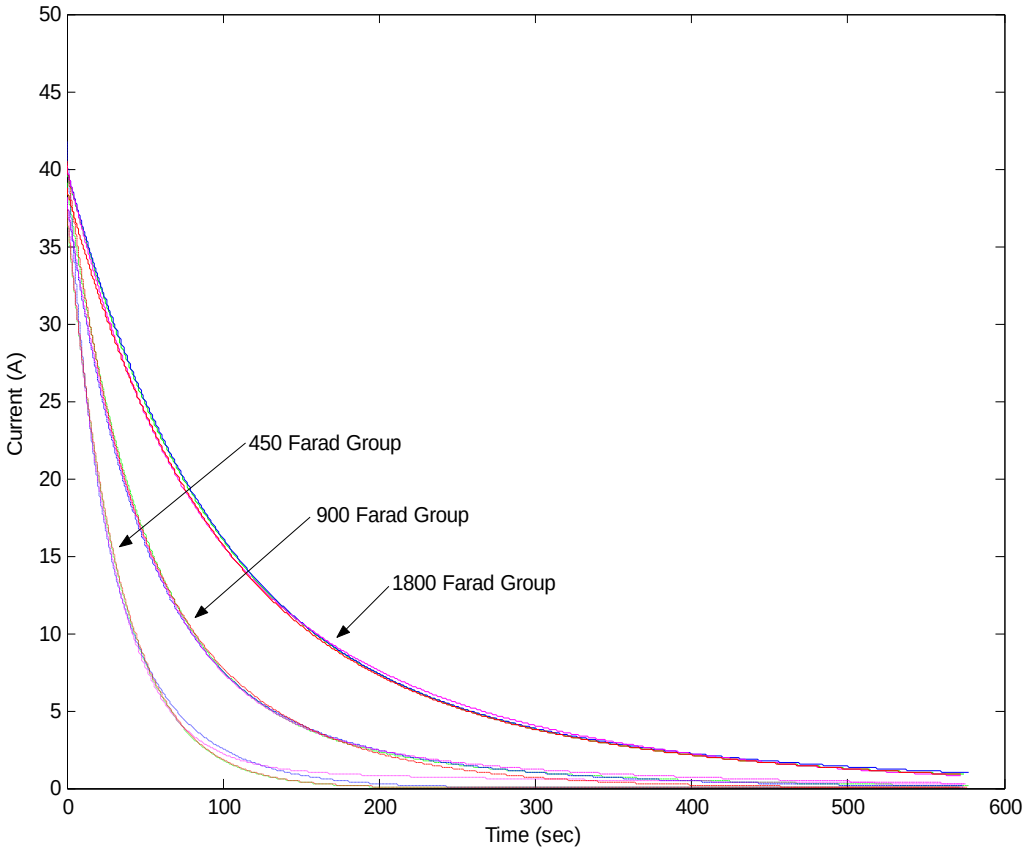

Figure 3.13 Charge current plots using a 50 A charge current for the various ultracapacitors.

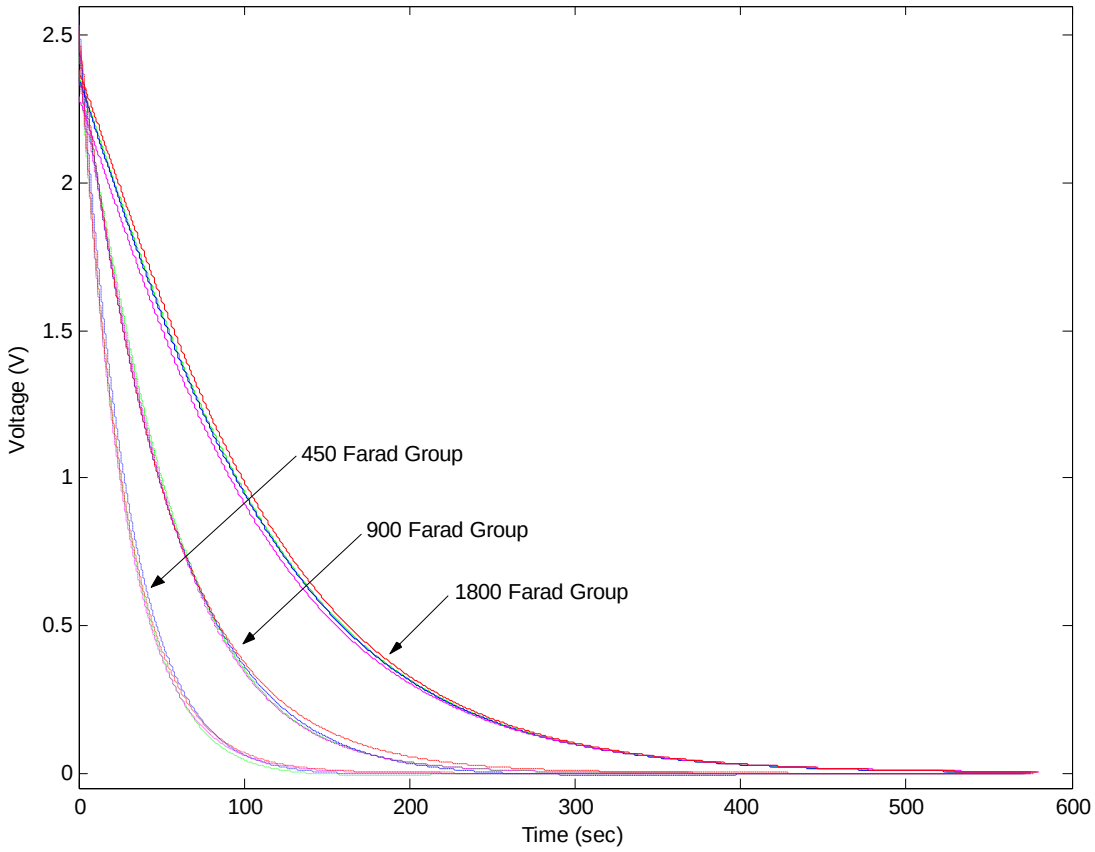

Figure 3.14 Discharge voltage plots using a 50 A discharge current for various ultracapacitors.

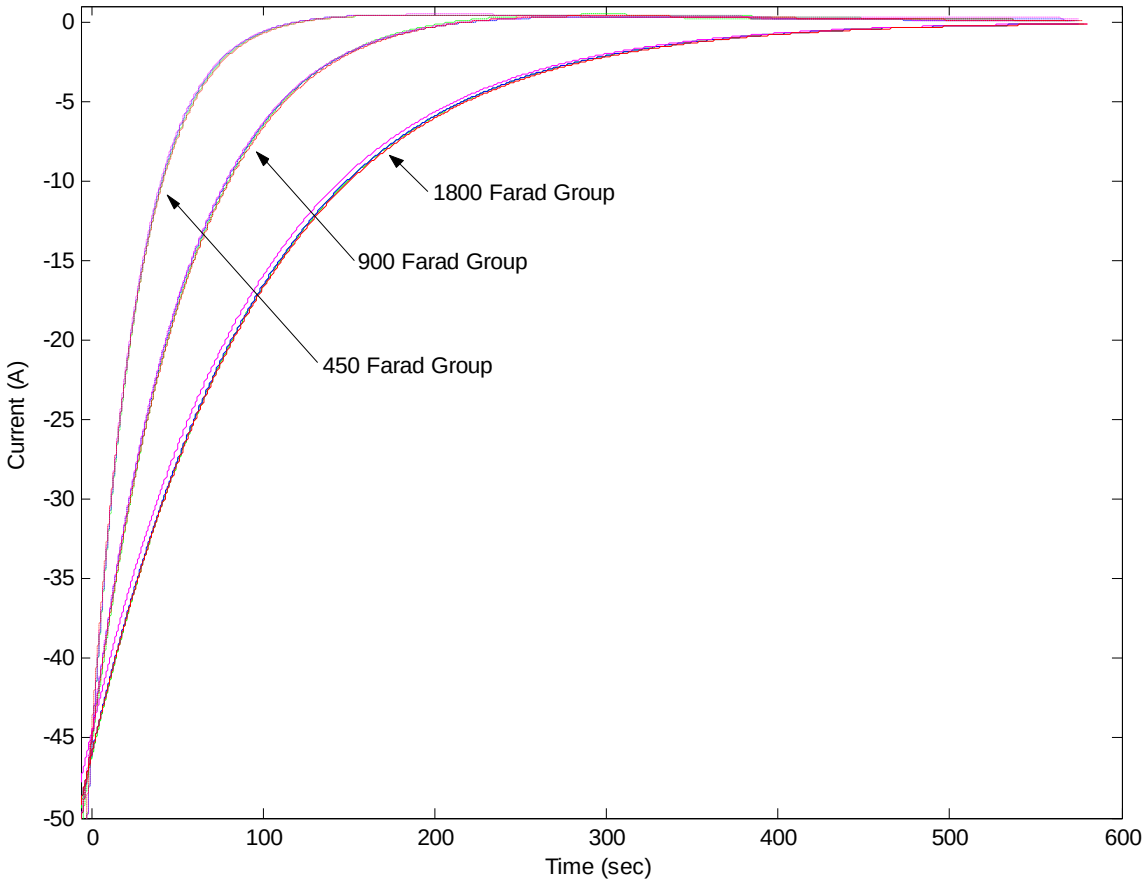

Figure 3.15 Discharge current plots using a 50 A discharge current for various ultracapacitors.

shows the lower temperatures have higher discharge current levels than the higher temperature current curves. There is no crossing at the knee of the current curves like the 25 A charge and discharge current graphs. The 1800 F capacitor continues to show the strongest dependence on variations in the temperature.

Figure 3.16 displays the various ultracapacitors' charge voltage profile using a 60 A charge current. The 1800 F ultracapacitor continues to show the greatest temperature effects. However, the greatest temperature effects are limited to the end of the 1800 F charge voltage curves. The higher temperatures, 25^{o}C and 50^{o}C, best fit curves have lower voltages at the end of the charge cycle than the lower temperature, -25^{o}C and 0^{o}C, best fit curves.

Figure 3.17 is the 60 A charge current results. The results show a wide current variation starting at the knee of the curve in the 450 F group. In the 450 F group, the two higher temperatures appear to approach the same value while the lower temperatures approach a different value that is lower than the higher temperature at the end of the experiment. For all the groups, the initial slope for the 25^{o}C appears to be the lowest.

Figure 3.18 shows the discharge voltage profile using a 60 A discharge current. The 1800 F displays the greatest deviation at the knee of the voltage curve. At the 1800F knee, two distinct voltages values appear to be approached; one for the higher temperatures and one for the lower temperatures. The 900 F 25^{o}C shows a large variation at the knee as well. Since the 25^{o}C curve does not experience this deviation before or after the knee, experiment best fit curve estimation is suspected to be the cause for the

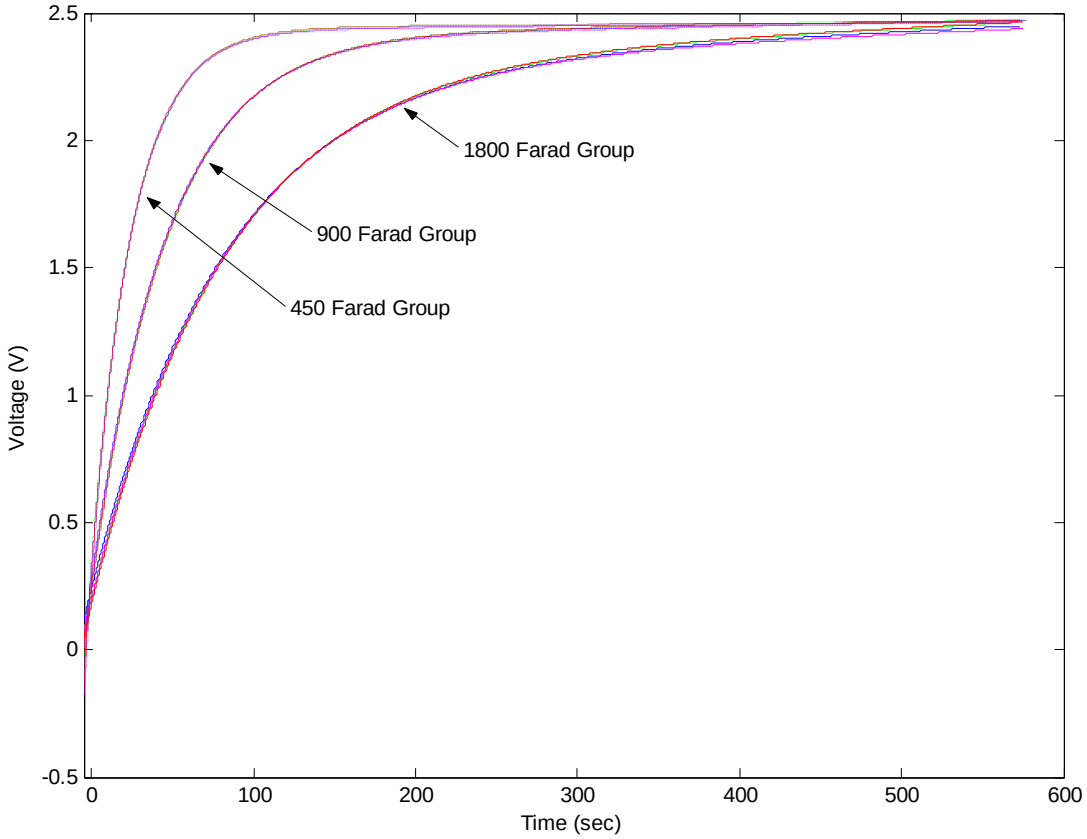

Figure 3.16 Charge voltage plots using a 60 A charge current for various ultracapacitors.

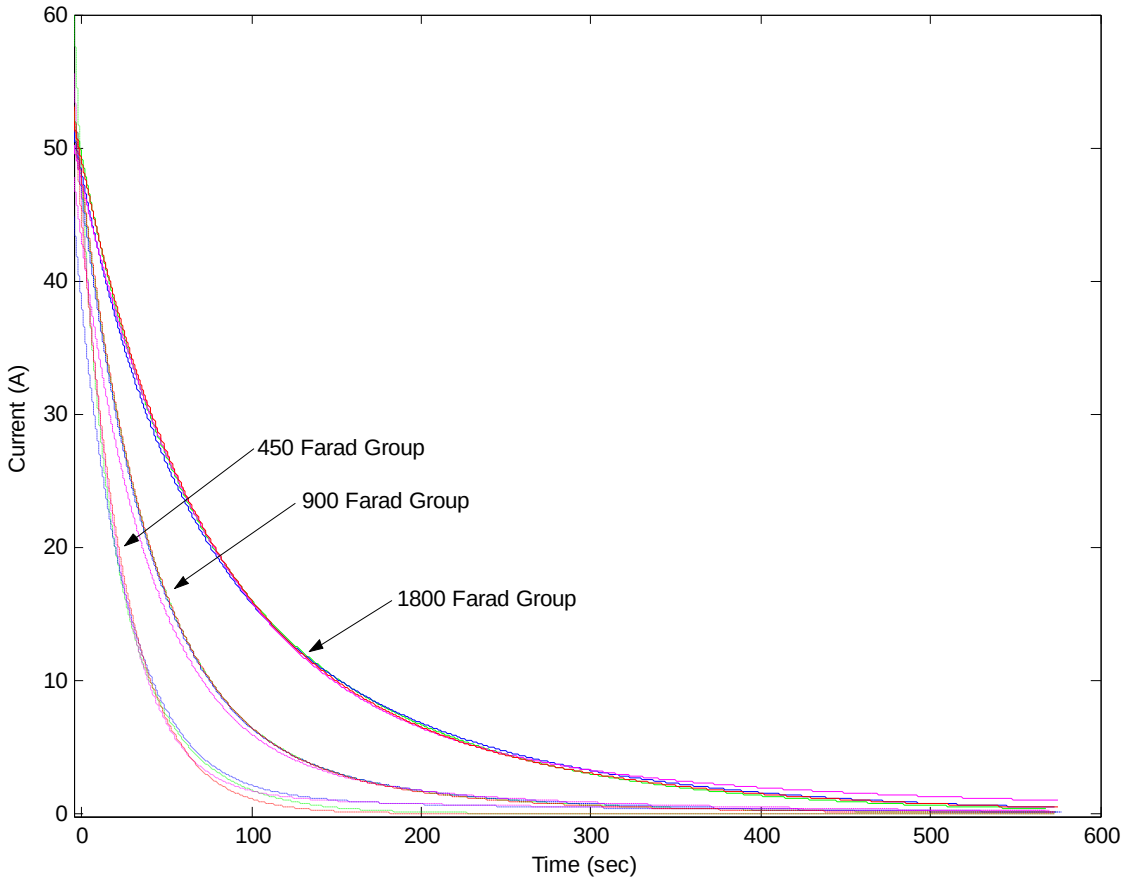

Figure 3.17 Charge current plots using a 60 A charge current for various ultracapacitors.

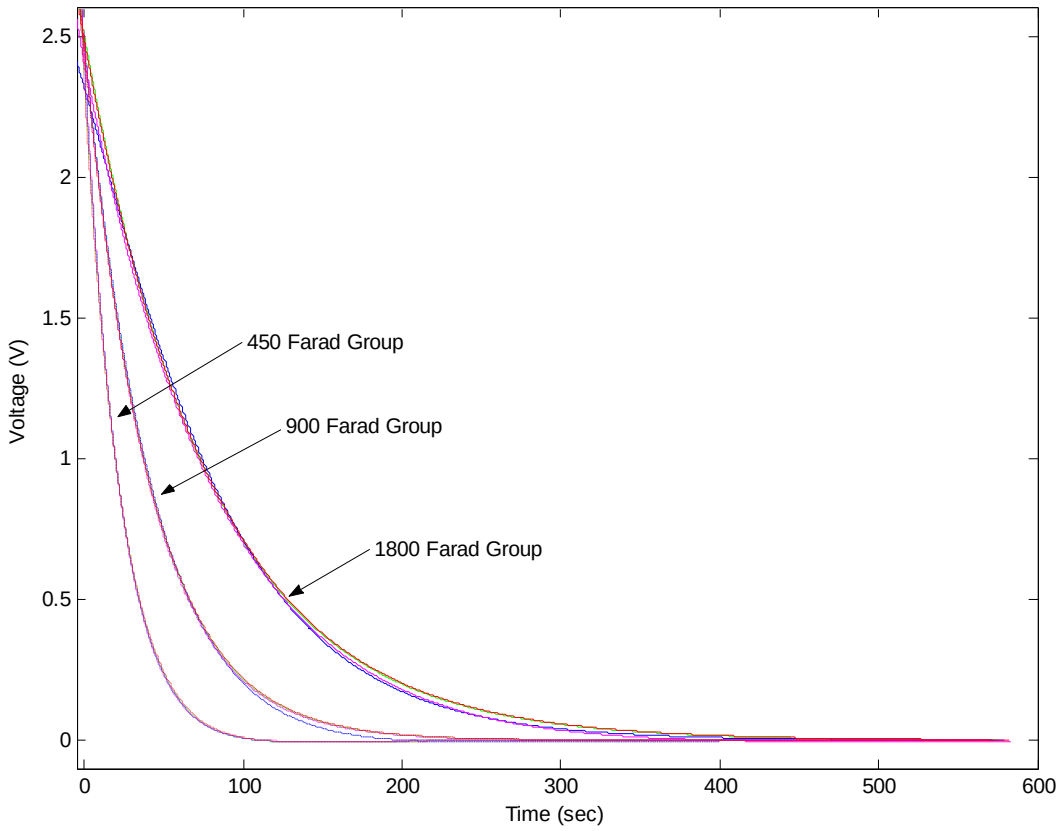

Figure 3.18 Discharge voltage plots using a 60 A discharge current for the various ultracapacitors.

temperature best fit curves. Figure 3.19 displays the discharge current profiles using a 60 A current. The temperature variations are less than the 60 A charge currents. The lower temperatures have a higher ending current value than the higher temperatures. The 1800 F group shows the most dependence on the temperature variations.

Figures 3.8 through 3.19 show the best fit curves for all the temperature and current values tested. The first noticeable difference is the three separate, distinct curves present within each graph, 450, 900, and 1800 F groups. The difference between the curves is a result of the RC time constant associated with a single resistor and capacitor circuit. The time constant, τ, is the product of the resistance and capacitance. If the resistance remains constant, an increase in capacitance will result in an increase of time it takes the capacitor to reach its rated voltage value. If the resistance remains constant, a decrease in capacitance will decrease the time required to charge the capacitor. The reversal is accurate for adjusting the resistance and capacitor remaining constant. Figure 3.20 provides an exAle of the capacitance remaining constant but the resistance changing. Figure 3.20 shows the 900 F ultracapacitor with all three different groups, 25, 50, and 60 current levels shown. As the resistance decreases, the current rises resulting in the decrease in time to reach zero. The initial slope increases with a decrease in resistance levels. In addition, Figure 3.20 shows the four different temperatures studied at each current level.

If the resistance and capacitance values were temperature independent, the voltage and current best fit curves would overlay one another. The difference in the voltage can be attributed to the combination of two things: the resistance and variation of

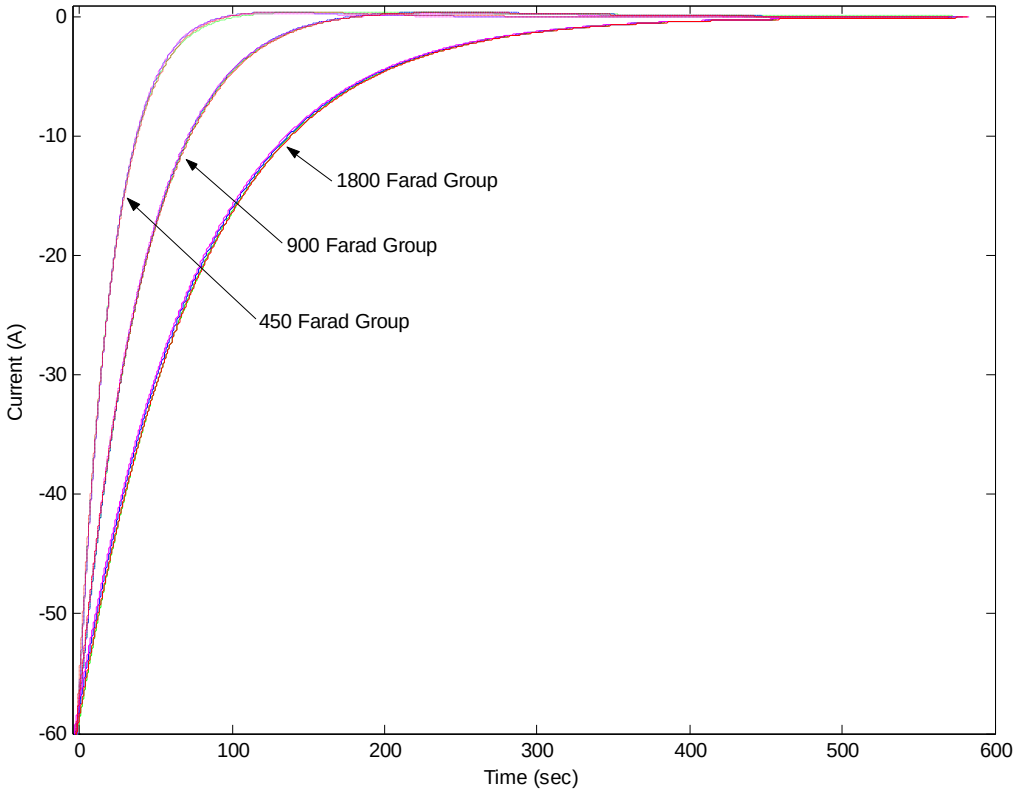

Figure 3.19 Discharge current plots using a 60 A discharge current for various ultracapacitors.

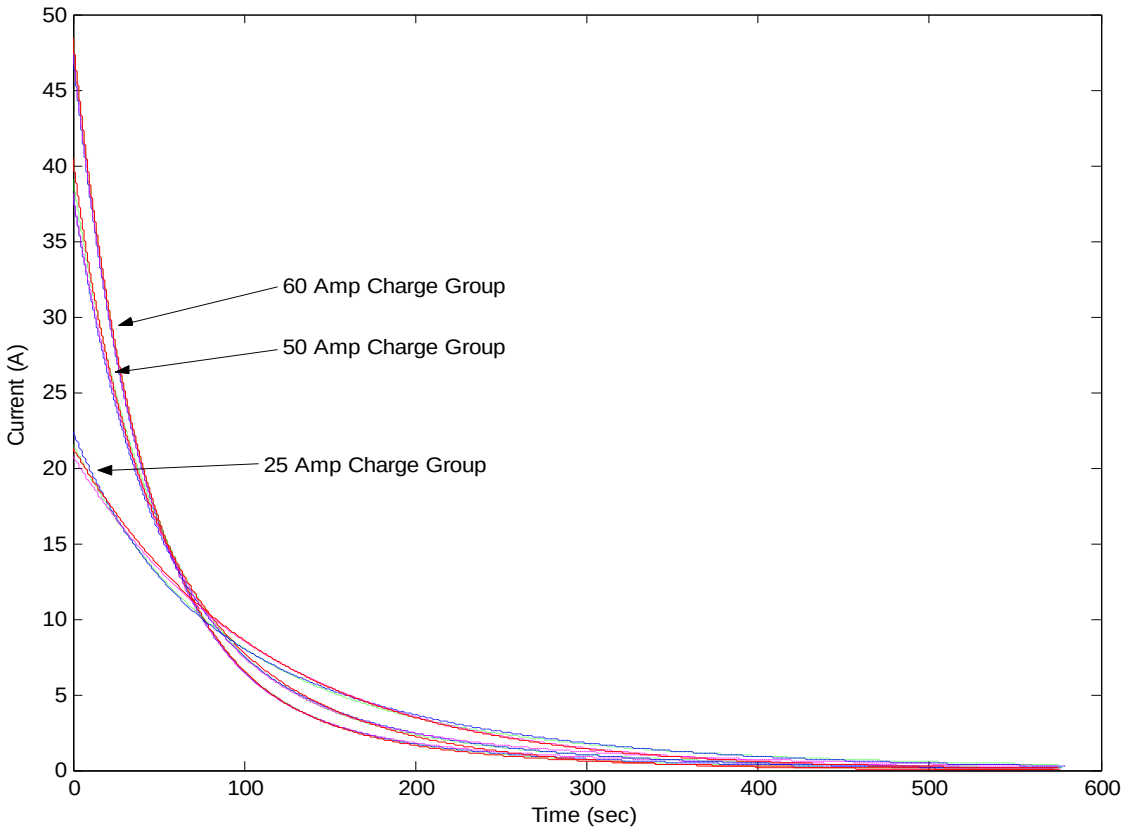

Figure 3.20 900 F Charge Currents and Temperatures.

capacitance levels. The ultracapacitor is assumed to be composed of two RC circuits each with its own distinct time constant. At the beginning of each experiment, the differences in voltage or current best fit curves are hypothesized to be dominated by the equivalent series resistance variations caused by the fluctuations in temperature. If the resistance is high, there is less current flowing through the ultracapacitor. For voltages within one time constant, the high resistance effects on the voltage curve causing the terminal voltage to be lower during the charging cycles. During the discharge voltage cycles, the high resistance results voltage is higher at the experiment's initial state. This observation is supported by the above figures. Another explanation is developed using

$$V(t) = R_1 * I_{ch} + V_c(t) \qquad (3.1)$$

This equation was explained in section 2.5. If $V_c(t)$ is a voltage dependent capacitance that utilizes the charging time, at small times, less than one τ, it is proposed the first term dominates the equation. Within one τ, the variation of R_1 causes the different voltage levels in the experiment because it controls the variation in the dominant term.

Figure 3.6 and 3.7 show the lower and higher temperatures crossing near the knee in each ultracapacitor's group. This crossing is suggests a second RC circuit that has a voltage dependent capacitance. A simple resistance variation would lead to best fit curves which are parallel to one another throughout the entire experimental time.

A voltage dependent capacitance is theorized because the temperature crossing occurs at approximately the same location. Equation 3.1 provides a voltage equation that can be used to describe the ultracapacitor voltage. From the equation, $V_c(t)$ is a voltage dependent capacitor that depends on the charging time, Δt. As Δt grows, $V_c(t)$ becomes

larger thus changing the second RC time constant. As a result, at larger time constants, the second RC circuit plays a more important role than the first RC circuit. This conclusion is supported by [5] and [11]. Despite the discussion concerning the temperature variations within each current level, the experimental results shown little temperature dependent effects on the resistance.

Chapter 4.

Chapter 4 proposes a new ultracapacitor model that considers the ESR variations caused by changes in temperature. The model resistance parameters were developed using a constant voltage charge method.

4.1 Circuit Model

As stated previously, the ultracapacitor can be modeled using RC circuits to predict the ultracapacitor's terminal behavior. A portion of the proposed thesis model was developed using the [11] model as a guide. The second RC branch in the [11] was eliminated due to its associated long time constant. The first RC branch in the [11] model uses a capacitance that composes a constant capacitor and a voltage dependent capacitor. If the time window being examined is not significantly long, the voltage dependent capacitor should have minimal effect on the total capacitance in the first RC branch.

In [5], it was shown that the ESR variations are affected by the changes in environmental temperature hence; this aspect was incorporated into this thesis model. Figure 4.1 provides a circuit representation of the model.

The proposed model utilizes the best fit curves that were described in Chapter 3 to analyze the equivalent series resistance, ESR, variations for four different environmental temperatures, -25^{o}C, 0^{o}C, 25^{o}C, and 50^{o}C and three different current levels, 25 A, 50 A, and 60 A. In Figure 4.1, if the terminal voltage of the ultracapacitor is constant, then the

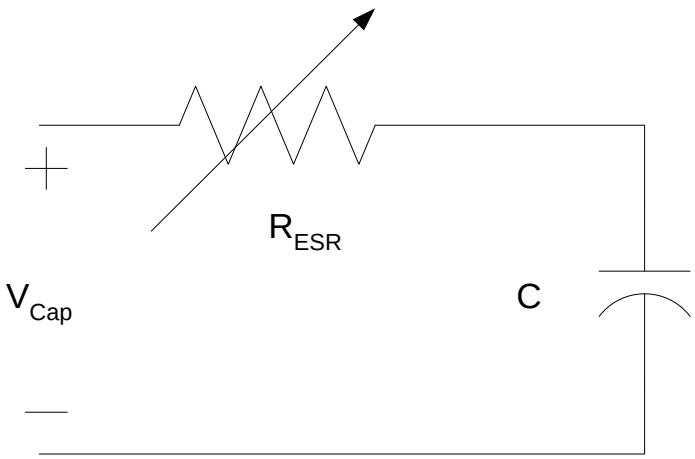

Figure 4.1 Ultracapacitor equivalent circuit model.

voltage across the resistance and capacitor must equal the terminal voltage.

$$V_{Cap} = V_{ESR} + V_C \tag{4.1}$$

Substituting Ohms's Law, V= IR for V_{ESR}, equation 4.1 becomes:

$$V_{Cap} = I_{ESR} * R_{ESR} + V_C \tag{4.2}$$

Initially V_c is discharged and at zero potential. At the initial start of charging, the voltage across the resistance, thus the current through the resistor, dominates the equation. If the resistance changes, according to Ohm's Law, the current has to change to maintain the same voltage.

4.2 Resistance Calculations

To determine the resistance values of the circuit model, the Matlab best fit curve equations were used. The best fit equations supplied by Matlab had the general format of

$$ae^{bx} + ce^{dx} \tag{4.3}$$

Appendix B contains the tables listing the values for each coefficient. A comparison between the each exponential term and the best fit curve was made to determine which exponential term was associated with the appropriate section of the best fit curve. Once the correct exponential term was determined, the exponential term was set to the RC time constant

$$ae^{bx} = RC \tag{4.4}$$

In Equation 4.4, *R* is the equivalent series resistance; *C* is the manufacture suggested capacitance; *b* is the time constant. It is assumed that the variance in capacitance will not be sufficient to affect the test results, thereby, the capacitance was held constant. The coefficient *a* in Eq. 4.4 is proposed to be used by Matlab to ensure the correct zero intercept and the best fit curve match the data. Therefore, the constant, *a*, can be divided out of the equation. Equation 4.5 provides the final equation used to calculate the resistance for each scenario.

$$R = \frac{1}{a}\left(\frac{1}{C}ae^{bx}\right) \tag{4.5}$$

Tables 4.1, 4.2, and 4.3 show the calculated resistance using Eq. 4.5.

Once the calculation to determine the resistance values was completed, the tables were plotted in Excel to determine the temperature dependance on the equilavent series resistance. Figure 4.2 shows the plot of the Table 4.1 data. The remaining figures for the 900 and 1800 F ultracapacitor are in Appendix C.

In Figure 4.2, the resistance at each current level does not vary significantly over

Table 4.1 450 F Resistance Measurements

Temperature	25 Amp (mΩ)	50 Amp (mΩ)	60 Amp (mΩ)
-25°C	2.1792	2.1514	2.1368
0°C	2.179	2.151	2.1368
25°C	2.179	2.1498	2.1361
50°C	2.178	2.1498	2.134

Table 4.2 900 F Resistance Measurements

Temperature	25 A (mΩ)	50 A (mΩ)	60 A (mΩ)
-25°C	1.0988	1.0916	1.0875
0°C	1.0989	1.0916	1.0875
25°C	1.0986	1.0917	1.0874
50°C	1.0984	1.0914	1.0871

Table 4.3 1800 F Resistance Measurements

Temperature	25 A (mΩ)	50 A (mΩ)	60 A (mΩ)
-25°C	.55943	.54992	.54881
0°C	.55939	.54982	.54883
25°C	.55932	.54977	.54884
50°C	.55929	.54975	.54872

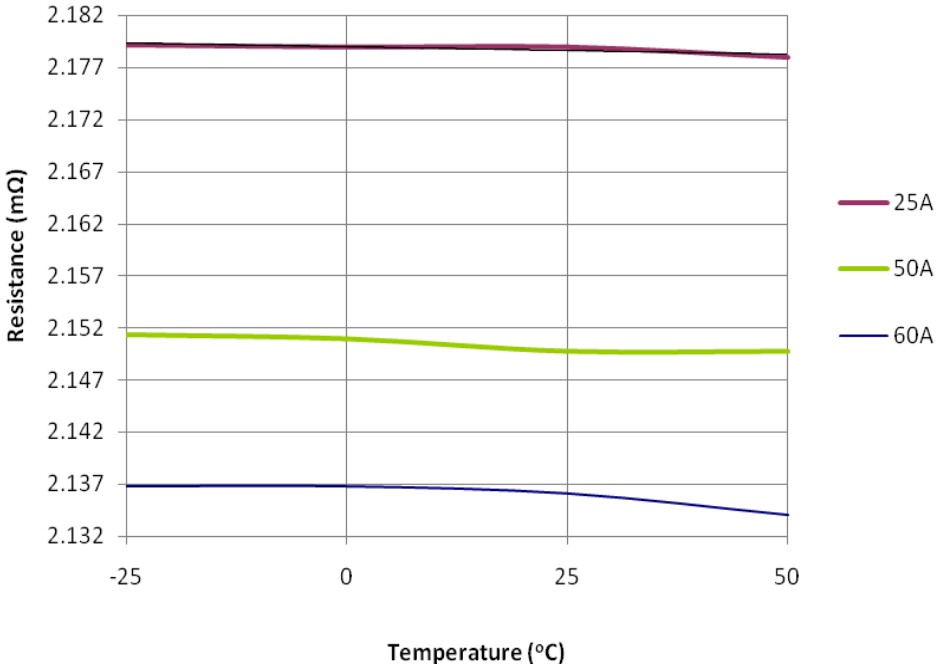

Figure 4.2 450 F ultracapcitor resistance vs. temperature.

the temperature range. The resistance changes are more noticeable between the current levels. The graphs for the 900 and 1800 F ultracapacitor can be found in Appendix C. In Excel, the resistances versus current level were plotted for further investigation. Figure 4.3 provides the plot for the 450 F ultracapacitor. Figure 4.3 shows the resistance values plotted versus the tested current values. The different colors are used to differentiate between the four tested temperatures, -25 ^{o}C, 0 ^{o}C, 25 ^{o}C, and 50 ^{o}C. Figure 4.3 shows a linear relationship between the resistance values and current. The linear relationship is explained by Ohms law. The voltage being applied to the ultracapacitor was constant; therefore, to maintain the same constant voltage, the resistance must decrease if the current increases. Appendix C contains the 900 and 1800 F graph results. To determine an accurate average resistance equation which will represent the resistance variations created by the different current levels, a reference point was established measure the current deviation amount. The 25 A resistance values were established as the baseline. For each temperature category, T= -25^{o}C, 0^{o}C, 25^{o}C and 50^{o}C, the 25 A resistance value was subtracted from corresponding 50 A and 60 A resistance values. Equation 4.6 and 4.7 provides the equation to calculate the difference between the two current levels.

$$\Delta R_1 = R_{25} - R_{50} \tag{4.6}$$

$$\Delta R_2 = R_{25} - R_{60} \tag{4.7}$$

There were four ΔR_1 and ΔR_2 values, one for each temperature value; -25 ^{o}C, 0 ^{o}C, 25 ^{o}C, and 50 ^{o}C. The arithmetic mean was found for R_1 and R_2 and plotted with the reference, 25 A, being zero. Figure 4.4 provides the plot of the 450 F ultracapacitor average resistance difference with respect to the different current levels.

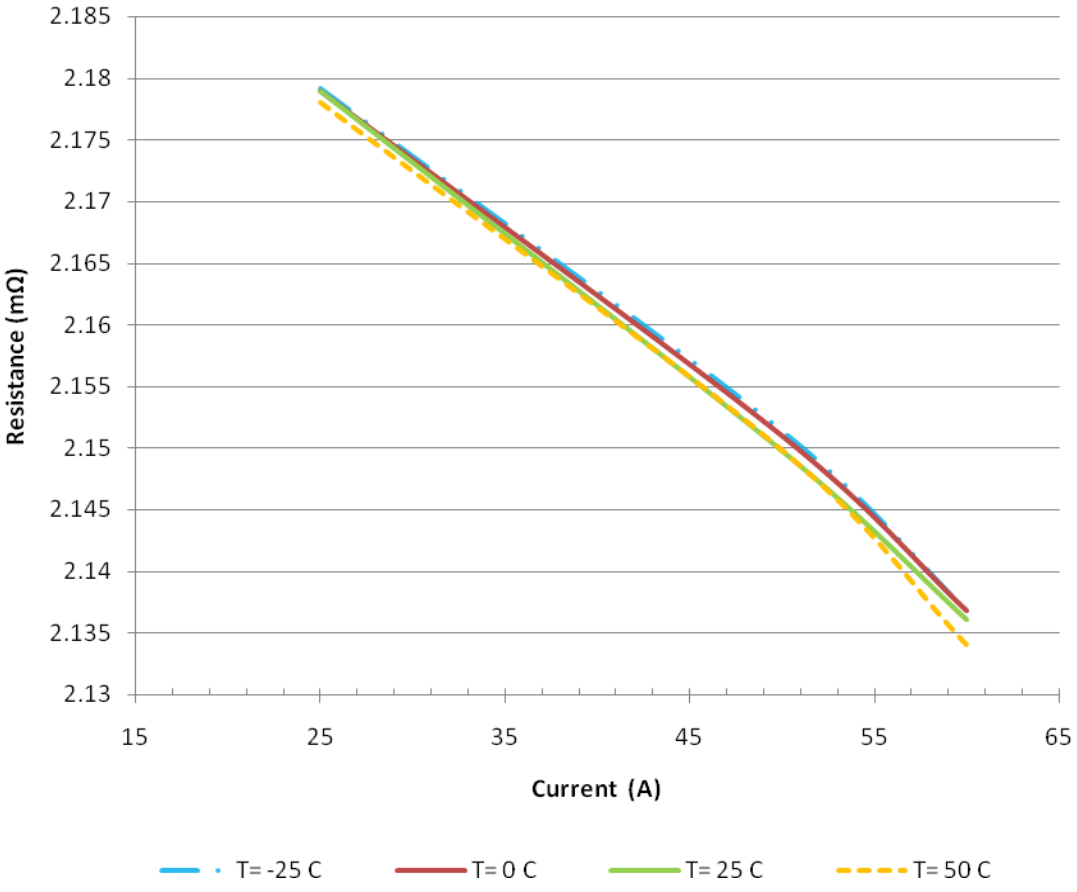

Figure 4.3 450 F ultracapcitor resistance vs current.

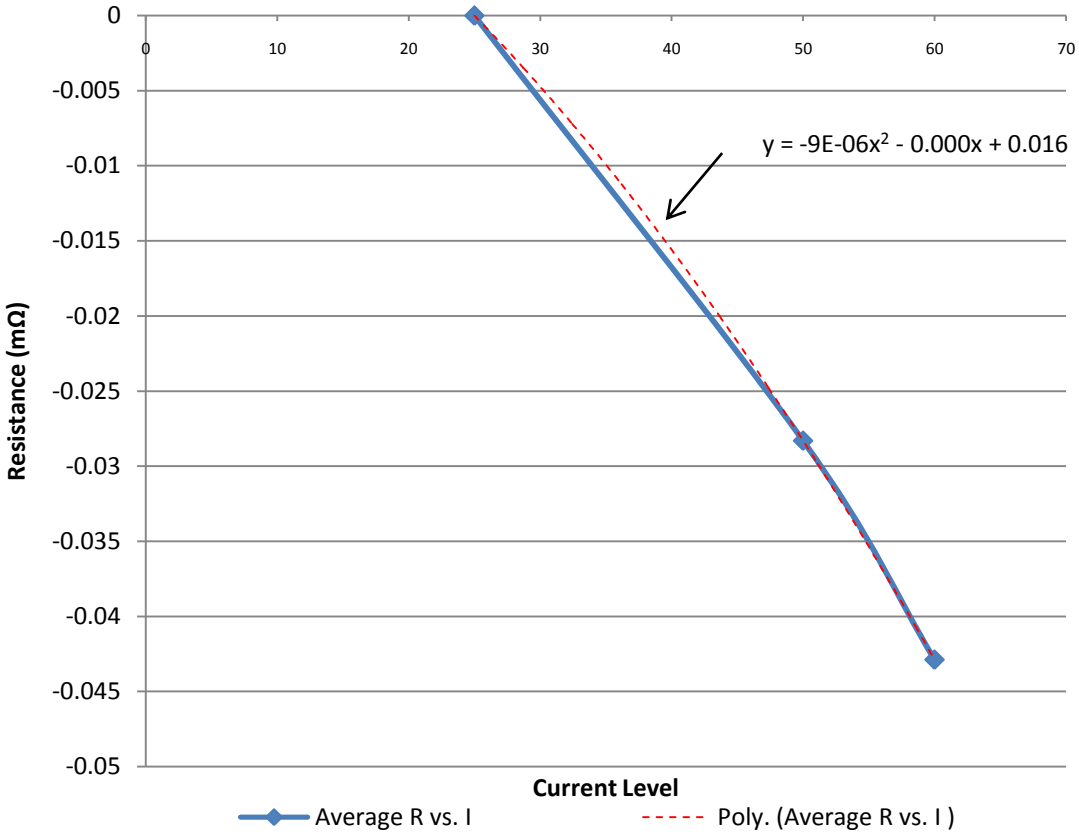

Figure 4.4 450 F average resistance difference vs. current (25 A is reference).

A polynomial equation was used instead of the linear equation for the best fit equation because the polynomial matched every current value on the graph. The linear equation missed the 50 A current point and did not account for the slight curve between the 50 and 60 A current points. For the 450 F ultracapacitor, Eq. 4.8 provides the best fit equation for the estimated resistance value as a result of the different current levels. Equation 4.8 was calculated by using the tread line function in Excel.

$$R_i = -9e^{-6}i^2 - .0004i + .0167 \tag{4.8}$$

Upon completion, the temperature effects on the resistance were investigated. For the temperature effect studies, the temperature 0^{o}C was used as the reference point. For each current level, the resistance value at 0^{o}C was subtracted from three remaining resistance values. Equations 4.9 through 4.11 shows the equations used to calculate the differences between the two temperatures.

$$\Delta R_3 = R_{0^oC} - R_{-25^oC} \tag{4.9}$$

$$\Delta R_4 = R_{0^oC} - R_{25^oC} \tag{4.10}$$

$$\Delta R_5 = R_{0^oC} - R_{50^oC} \tag{4.11}$$

After the temperature differences were calculated, the arithmetic mean was determined for each temperature. The arithmetic mean was plotted using Excel. Figure 4.5 shows the results for 450 F ultracapacitor. Above 0^{o}C, it is interesting to note the exponential decrease in the average resistance value as the temperature increases. Below 0^{o}C, the average resistance has a more linear increase. From Figure 4.5, the resistance varies significantly more above 0^{o}C than at temperature below 0^{o}C. It is possible that the

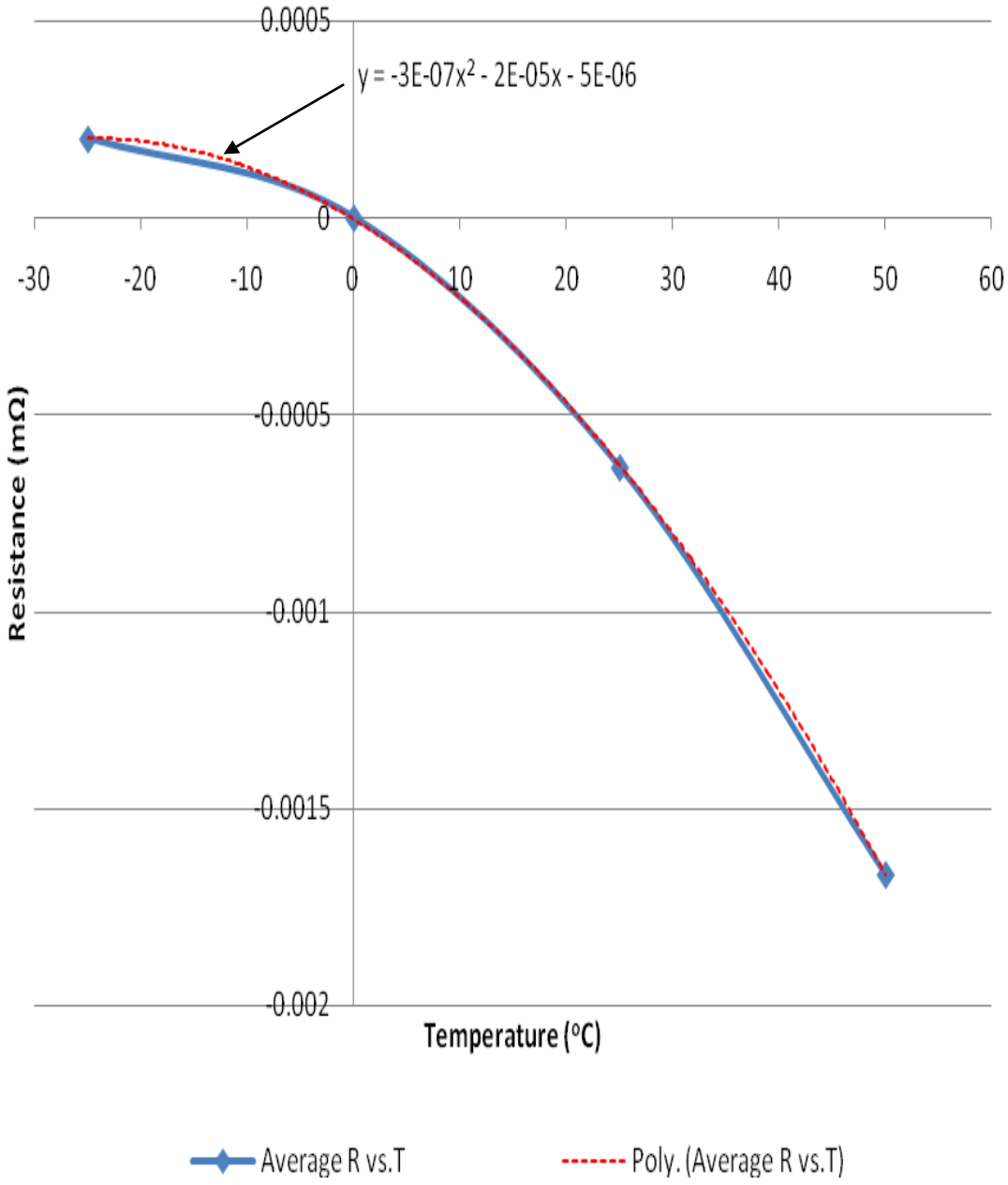

Figure 4.5 450 F average resistance difference vs. temperature (0oC is reference)

exponential decrease is sufficient to create the observed curve between the 50 and 60 A data points in Figure 4.4.

The 450 F ultracapacitor resistance equation with respect to temperature is given by equation 4.11

$$R_T = -3e^{-7}T^2 - 2e^{-5}T - 5e^{-6} \tag{4.11}$$

Before combining equations 4.8 and 4.11 can be completed, the reference point constant needs to be added to the equation. The reference point is the experimental value that was zero during the current and temperature portions. The experimental point for the 450 F ultracapacitor was the 25 A T= 0^{o}C resistance measurement, 2.179 mΩ. Combining equations 4.8 and 4.11 along with the constant 2.179 mΩ will provide a resistance equation that will account for the temperature and current effects on the 450 F ultracapacitor.

$$R_{450}(m\Omega) = -3e^{-7}T^2 - 2e^{-5}T - 5e^{-6} - 9e^{-6}i^2 - .0004i + .0167 + 2.179 \tag{4.12}$$

Combining like terms, equation 4.13 provides the final 450 F ultracapcitor equation.

$$R_{450}(m\Omega) = -3e^{-7}T^2 - 2e^{-5}T - 9e^{-6}i^2 - .0004i + 2.195695 \tag{4.13}$$

Equation 4.14 provides the resistance equation for the 900 F ultracapacitor.

$$R_{900}(m\Omega) = -1.2e^{-7}T^2 - 1.4e^{-6}T - 3.1538e^{-4}i + 1.10696 \tag{4.14}$$

Equation 4.15 provides the resistance equation for the 1800 F ultracapacitor.

$$R_{1800}(m\Omega) = -7e^{-9}T^2 - 2e^{-6}T - 3e^{-4}i + .566993 \tag{4.15}$$

In Equation 4.12 through 4.15, *T* represents the temperature in degrees Centigrade and *i* is the current in A. Using equations 4.13 through 4.15, resistance values were calculated and compared to the calculated resistance obtained from the best fit curve coefficients.

Tables 4.4 through 4.6 show the resistance comparisons for the 450 F ultracapacitors. The 900 and 1800 F results are in Appendix C.

4.3 Chapter Summary

For the short time constants focused on in this thesis, the results from the resistance graphs show changes in the current have greater affects on the resistance than variations in temperature. This result is further confirmed by the coefficients on the temperature terms in equations 4.13 through 4.15. Ohms law supports the linear relationship observed in the resistance versus current and average resistance versus current graphs.

Despite having little effect on the resistance value, the observed average resistance versus temperature plots does show some temperature dependence. The 450 and 900 F ultracapacitors show the resistance experiences an exponential decline as the

Table 4.4 450 F 25 A Resistance Comparison

Temperature	Best Fit Curve	Eq. 4.13	Difference
-25°C	2.1792	2.165993	-0.01321
0°C	2.179	2.161618	-0.01738
25°C	2.179	2.145993	-0.03301
50°C	2.178	2.119118	-0.05888

Table 4.5 450 F 50 A Resistance Comparison

Temperature	Best Fit Curve	Eq. 4.13	Difference
-25°C	2.1514	2.16493	0.01353
0°C	2.151	2.160555	0.009555
25°C	2.1498	2.14493	-0.00487
50°C	2.1498	2.118055	-0.03174

Table 4.6 450 F 60 A Resistance Comparison

Temperature	Best Fit Curve	Eq. 4.13	Difference
-25°C	2.1368	2.1644	0.0276
0°C	2.1368	2.160025	0.023225
25°C	2.1361	2.1444	0.0083
50°C	2.134	2.117525	-0.01647

temperature increases. The 1800 F ultracapacitor shows more linear decay with the increase in temperature. .

The observed ultracapacitor resistance changes will have little effect the total circuit resistance. However, the efficiency of the ultracapacitor will decrease as the temperature increases. The decrease in resistance will allow power dissipation across the equivalent series resistor to increase. Thus, as the temperature increases, the efficiency of the ultracapacitor decreases. In addition, the heat created by the additional current flow will need to be factored into the cooling of the device. If Equation 4.13 provided an accurate resistance value for all temperatures and currents, the 450 F ultracapacitor would see a power dissipation increase of approximately 320 W across the resistor component from a 25 A at T= -25^{o}C operating condition to a 400 A T=60^{o}C condition. Understanding the ultracapacitors behavior in all charging methods will provide application and circuit design engineers the knowledge needed to optimize circuit parameters and account for thermal variations.

Chapter 5.

Chapter 5 provides a summary of this thesis and recommendations for future work in this area.

5.1 Summary

The prime motivation for this thesis was to discover the temperature effects on the equivalent series resistance using a constant voltage instead of the preferred constant current method. As the ultracapacitor technology develops, the use of these devices will broaden in the power industry. As a result, different applications may require various methods of charging or discharging the ultracapacitor. Thus, the temperature effects experienced using a constant voltage source needed to be evaluated.

The early chapters of this thesis provided relevant background information concerning the interface structure and previous developed circuit models. The interface model discussion provided insight to the complex internal behavior displayed at the ultracapacitor's terminals. It provided an argument for the use of complex circuits to model the ultracapacitor's behavior. In addition, Chapter 2 discussed several ultracapacitor circuit models that have been developed to predict the terminal behavior. These models used two basic methods to develop model parameters, constant current and impedance spectroscopy. Of the ultracapacitor models discussed in Chapter 2, one model discussed the temperature effects on the equivalent series resistance. The results of this temperature model showed the ESR variations were significant over a range of temperatures. The consequence of the resistance variation was a decrease of efficiency

and the need for additional thermal management considerations.

The experimental results were shown in the latter chapters of this thesis. Matlab was used to provide a best fit curve and their respective coefficients. The resulting graphs show temperature had little effect on the overall circuit voltage or current over the temperature range of -25^{o}C to 50^{o}C. However, using the best fit coefficients, equivalent series resistance values were calculated for each temperature and current difference. The calculated resistance values show the ESR was affected by the temperature and current variations. Current affected the ESR more than the temperature, and Ohm's Law was proposed to account for the variations.

Along with the previously developed ultracapacitor models, a unique equivalent circuit model are not available that describes every aspect of the ultracapacitor's terminal behavior. The assumption that an equivalent circuit which provides an accurate data set represents an accurate physical model is not possible. The physical model should be tested and a single element altered. The results of this alteration should be studied to see if the change was expected.

Empirical models should be regarded less than physical models. Empirical models allow the addition of elements to create an accurate data fit. However, the addition of such elements may present little relevance to the studied behavior. Therefore, empirical models should contain minimal elements and conclusions drawn should be regarded with little weight.

5.2 Future Work

The first suggestion is to determine the temperature effects on the capacitance. In this thesis, the capacitance was assumed to remain constant. However, it was discussed in Chapter 1 that the capacitance will vary with temperature. The determination of the temperature effects will allow for a complete single branch RC model. The model will more accurately depict the ultracapacitor's response for short duration charge and discharge cycles.

The second suggestion for future research begins with increasing the current and temperature range. The increase of current will provide two benefits. First, the model used in this thesis consisted of multiple RC circuits. Branches that were based on the slow response of the ultracapacitor were removed. Increasing the current will decrease the effects of these additional RC circuits, allowing for a more accurate resistance measurement. In addition, the increase in current will allow for a more complete examination of the resistance variations as a result of the current. In addition to increasing the current, extending the temperature range will allow for better analysis of the resistance changes as a result of the temperature. In [5], the resistance as a function of temperature was generally linear for the temperature ranges in this thesis. Extending the temperature range will allow the researcher to observe if an increase of resistance dependence will develop. The increase in current and temperature will allow the researcher better observation of the increase of power dissipation. The addition of experimental values will allow a better understanding of the electrolyte ionic conductivity properties. Finally, the aforementioned suggestions will allow a model that will increase

the models accuracy and operational range.

Next, determine the parameters of the additional RC circuit. The experimental results in Chapter 3 show a second RC circuit. The effects of the second RC circuit are observed to take effect several time constants into the charge or discharge cycle. The development of a complete ultracapacitor model will provide terminal behavior for several minutes. In addition, it is possible for the additional RC circuits to affect the initial terminal behavior of the ultracapacitor. The effects of the additional RC circuits would be incorporated into the model thus increasing the accuracy of the model.

Finally, a comparison between the constant current and constant voltage resistance values should be evaluated. Is the equivalent series resistance value the same using both charging methods? Will the constant voltage model provide an accurate model in a constant current scenario? If the models are incompatible, determine if a correlation between constant current and constant voltage resistance measurements exists. The answers are valuable in determining circuit design, implementation, and performance in which the ultracapacitor's application is intended.

List of References

References

[1] Strattan, Robert D. "The electrifying future of the hybrid automobile." *IEEE Potentials*, vol. 23, no. 3, pp. 4-7, August/September 2004.

[2] Chan, C.C and Wong, Y.S. "Electric Vehicles Charge Forward." *IEEE Power & Energy*, vol. 2, no. 6, pp. 25-33, November/December 2004.

[3] Conway, Ben. *Electrochemical Supercapacitors Scientific Fundamentals and Technological Applications.* New York: Plenum Publishers, 1999.

[4] Bard, Allen J and Faulkner Larry R., eds. *Electrochemical Methods Fundamentals and Applications*. Massachusetts: John Wiley & Sons Inc.

[5] Bouquain, D. et.al. "Experimental study of supercapacitor serial resistance and capacitance variations with temperature." *Journal of Power Sources*. pp. 86-93, 2003.

[6] Nelms, R. M. and Spyker, R. L., "Classical Equivalent Circuit Parameters for a Double-Layer Capacitor." *IEEE Transactions on Aerospace and Electronic Systems*, vol. 36, no. 3, pp. 829-836, July 2000.

[7] Cahela, D. R. et.al. "Modeling Double-Layer Capacitor Behavior Using Ladder Circuits," *IEEE Transactions on Aerospace and Electronic Systems*, vol. 39, no. 2, pp. 430-438, April 2003.

[8] Buller, Stephan et.al. "A frequency-domain approach to dynamical modeling of Electrochemical power sources." *Electrochimica Acta*. pp. 2347-2356, 2002.

[9] Buller, Stephan et.al. "Modeling the Dynamic Behavior of Supercapacitors Using Impedance Spectroscopy." *IEEE Transactions on Industry Applications*, vol. 38, no. 6, pp.1622-1626, November/December 2002.

[10] Bonert, R. and Zubieta, L. "Measurement Techniques for the Evaluation of Double-Layer Power Capacitors." *IEEE Industry Applications Society Annual Meeting*. New Orleans, Louisiana, October 5-9, 1997, pp. 1097-1100.

[11] Bonert, Richard and Zubieta, Luis. "Characterization of Double-Layer Capacitors for Power Electronics Applications." *IEEE Transactions on Industry Applications*, vol. 36, no. 1, pp. 199-205, January/February 2000.

Appendices

Appendix A

This Appendix contains screen captures from the oscilloscope and the Matlab plots of the data.

A1. 450 F Ultracapacitor Experiment Results

The results for the 450 F are shown in this section. The results are broken into three sub-categories that are based on the current charge and discharge levels. Within each current level, there are four temperatures: -25^{o}C, 0^{o}C, 25^{o}C and 50^{o}C. After each oscilloscope screen capture is the corresponding Matlab plots of the data.

A1.1 450 F 25 A Results

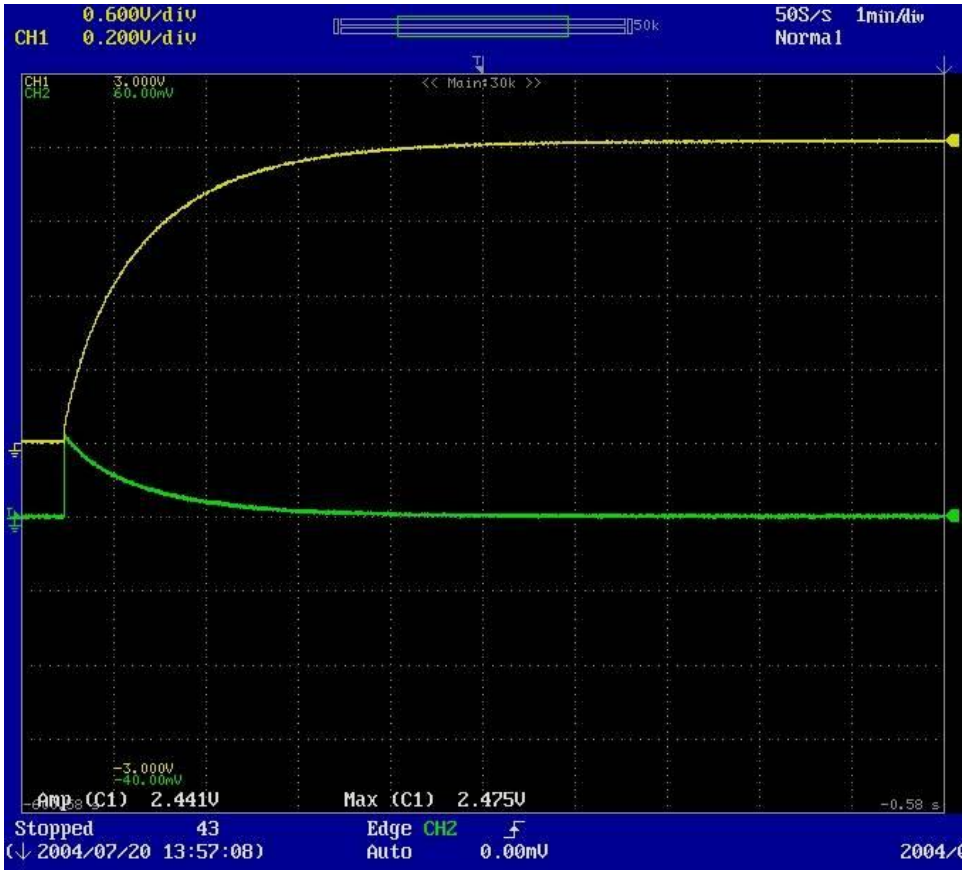

Figure A1.1-1: Oscilloscope Screen Capture of 25 A Charge Cycle at T= -25°C (Timescale: 1 min/div)

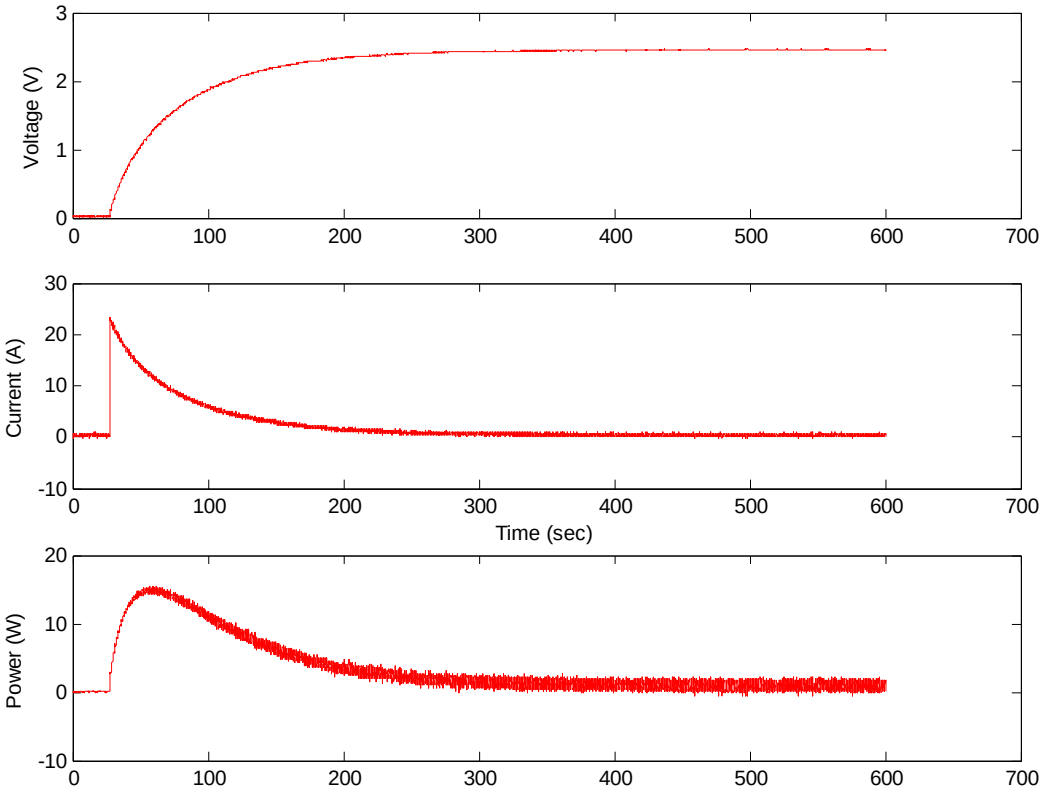

Figure A1.1-2: Plotted Matlab Data of 25 A Charge Cycle at T= -25^{o}C

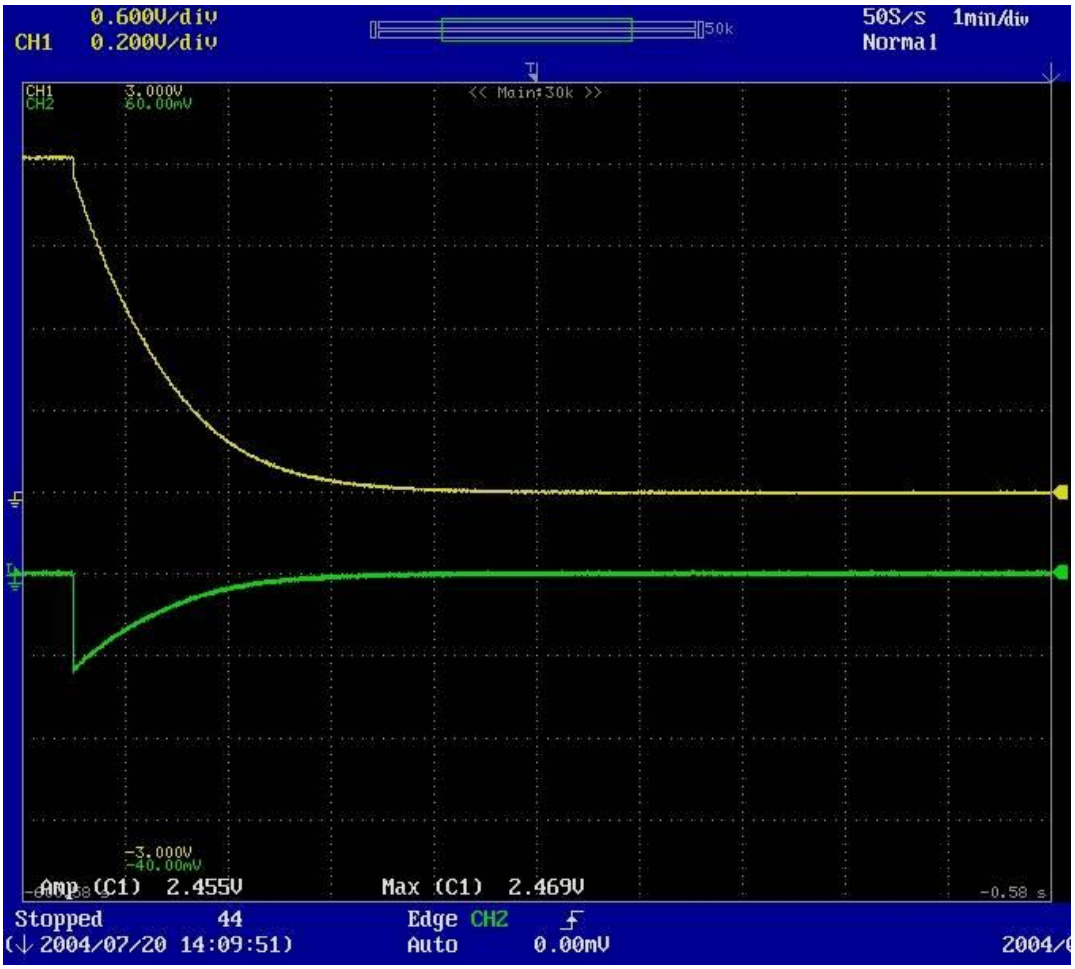

Figure A1.1-3: Oscilloscope Screen Capture of 25 A Discharge Cycle at T= -25°C (Timescale: 1 min/div)

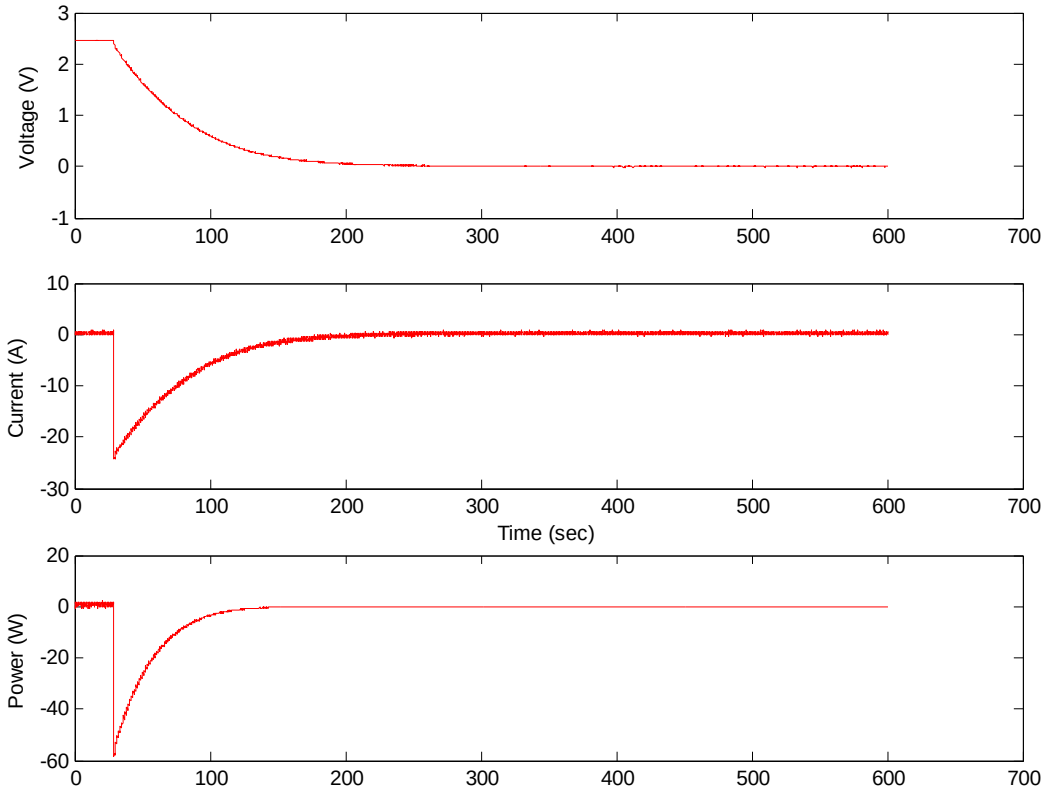

Figure A1.1-4: Plotted Matlab Data of 25 A Discharge Cycle at T= -25^{o}C

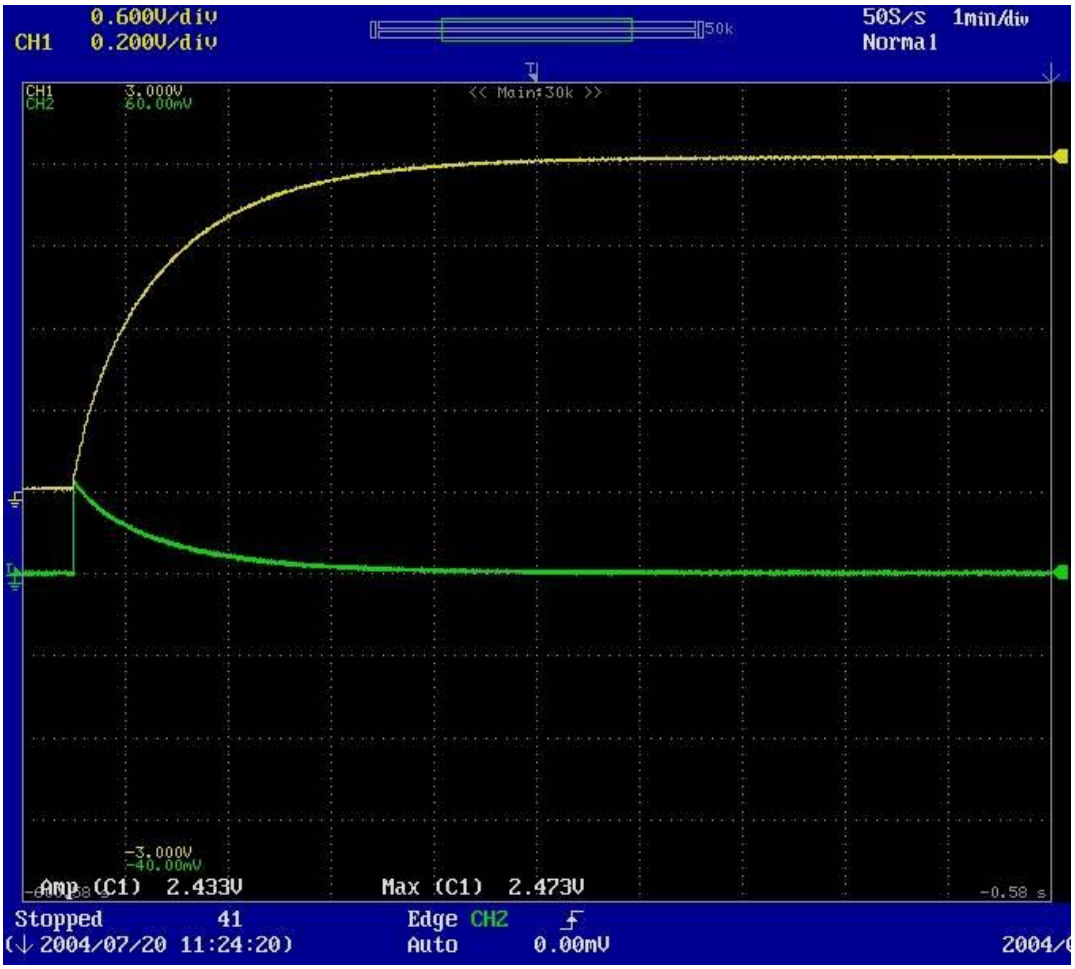

Figure A1.1-5: Oscilloscope Screen Capture of 25 A Charge Cycle at T=0°C (Timescale: 1 min/div)

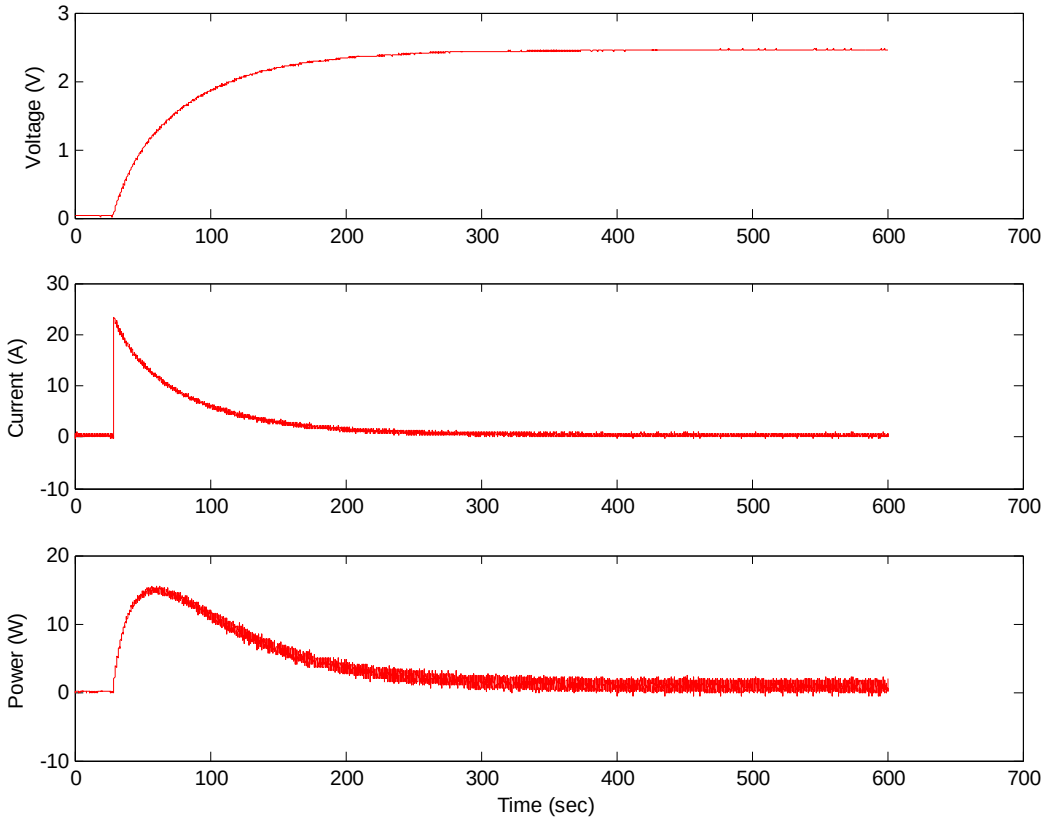

Figure A1.1-6: Plotted Matlab Data of 25 A Charge Cycle at T=0^{o}C

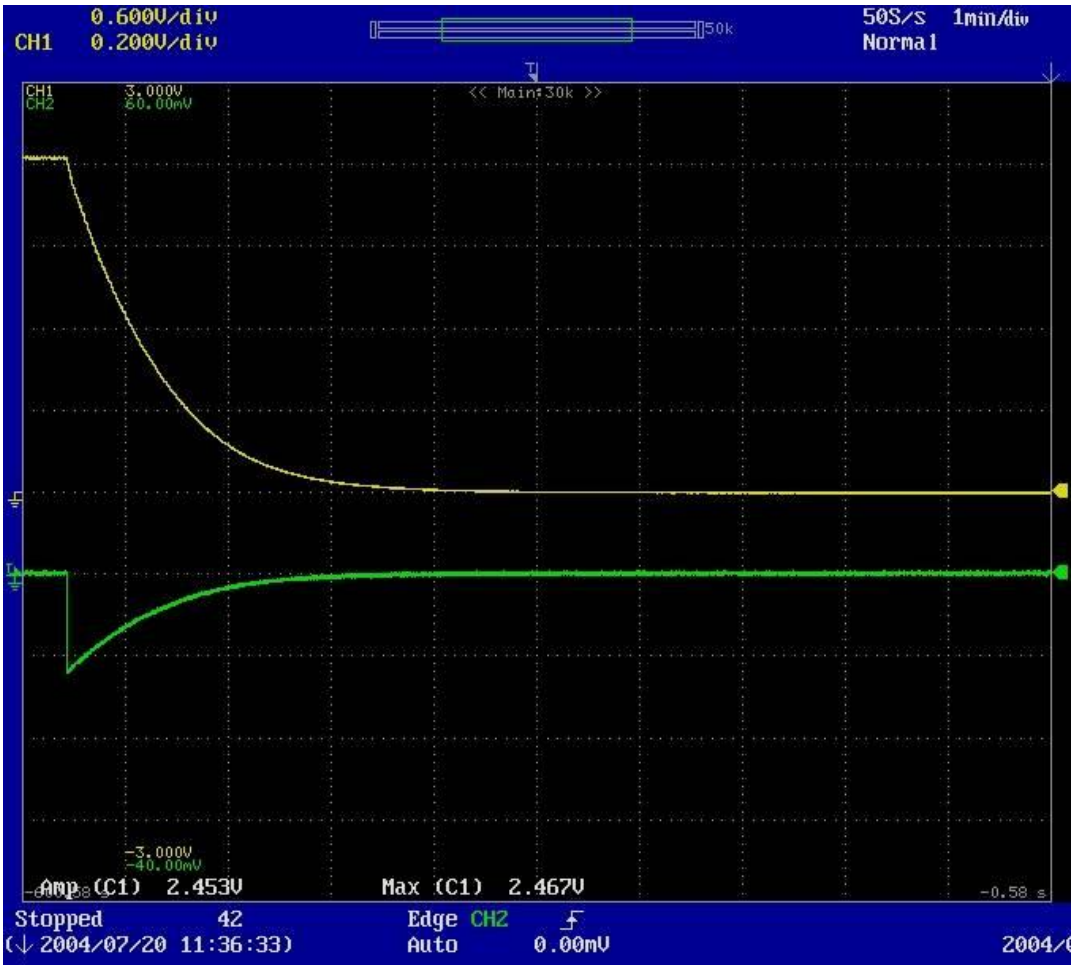

Figure A1.1-7: Oscilloscope Screen Capture of 25 A Discharge Cycle at T=0°C (Timescale: 1 min/div)

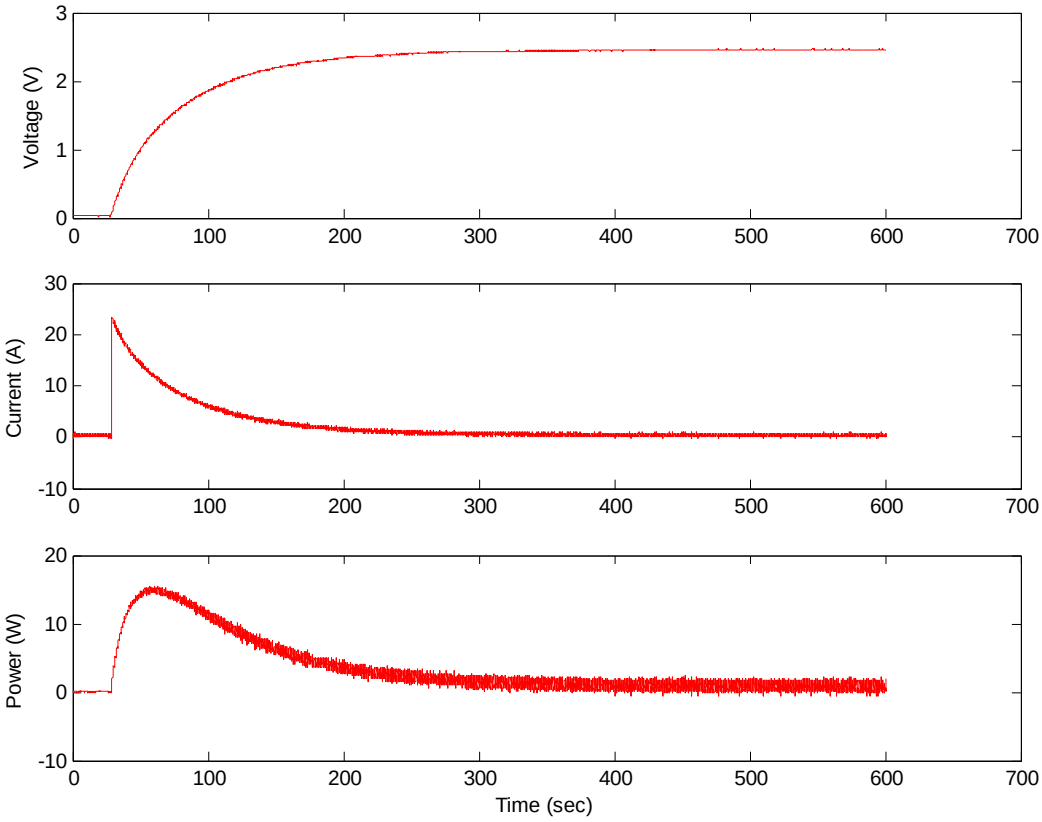

Figure A1.1-8: Plotted Matlab Data of 25 A Discharge Cycle at T=0^{o}C

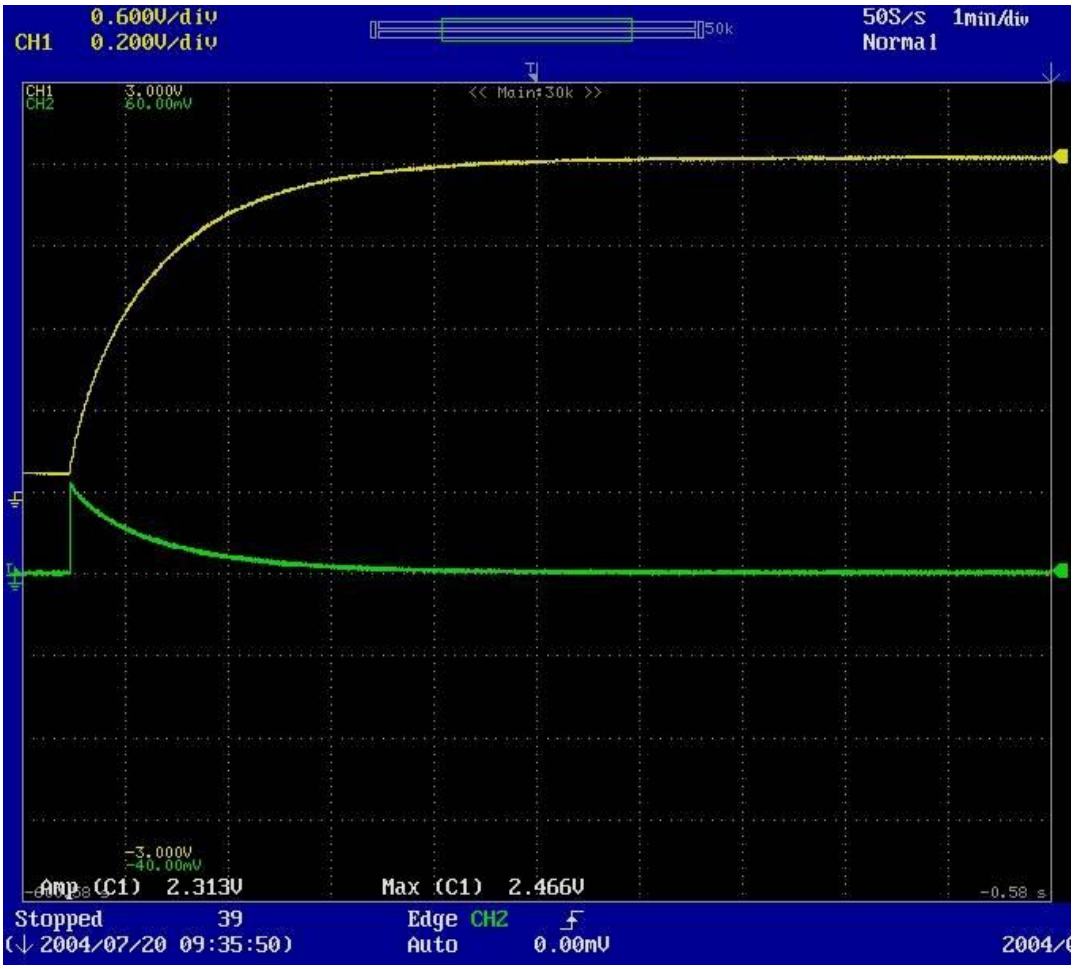

Figure A1.1-9: Oscilloscope Screen Capture of 25 A Charge Cycle at T=25°C (Timescale: 1 min/div)

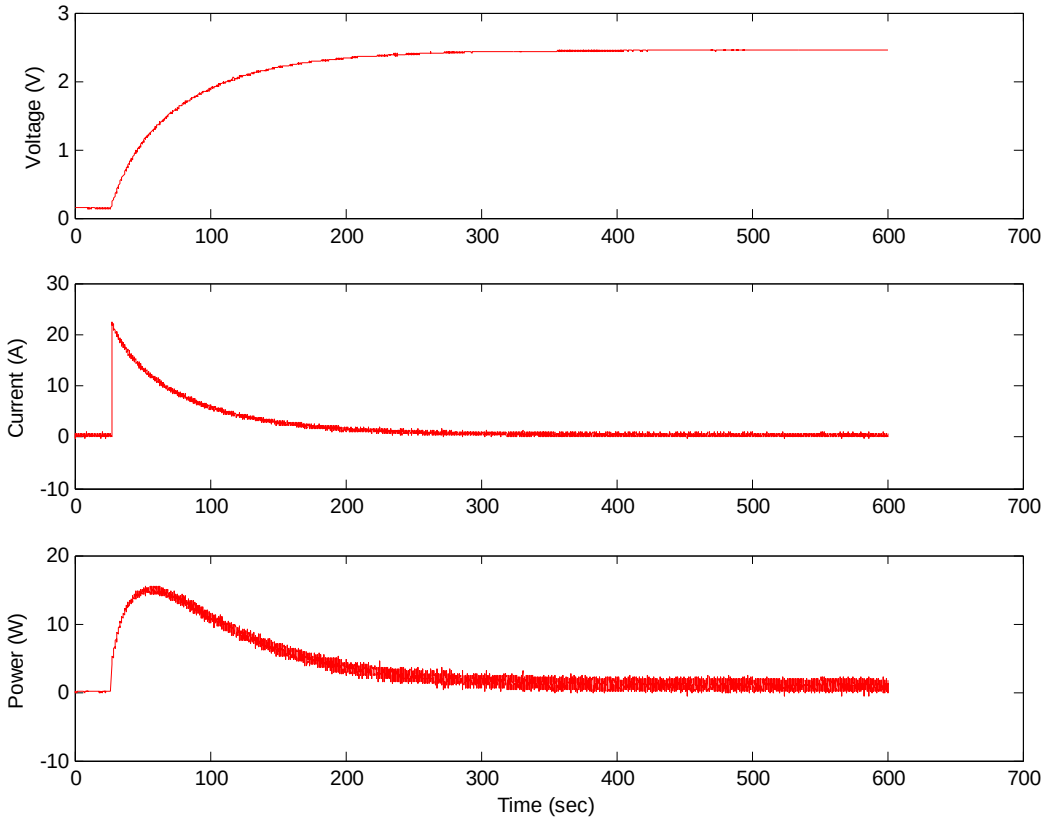

Figure A1.1-10: Plotted Matlab Data of 25 A Charge Cycle at T=25°C

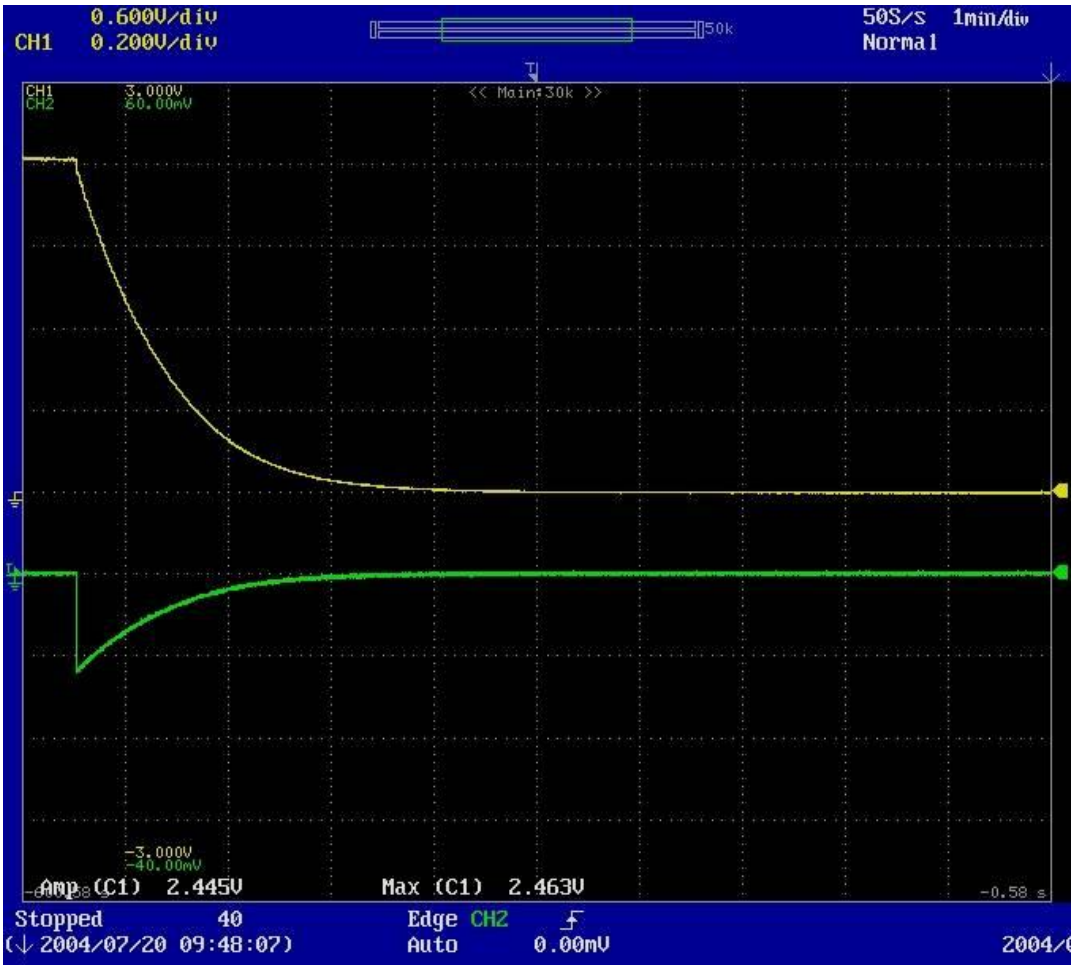

Figure A1.1-11: Oscilloscope Screen Capture of 25 A Discharge Cycle at T=25°C (Timescale: 1 min/div)

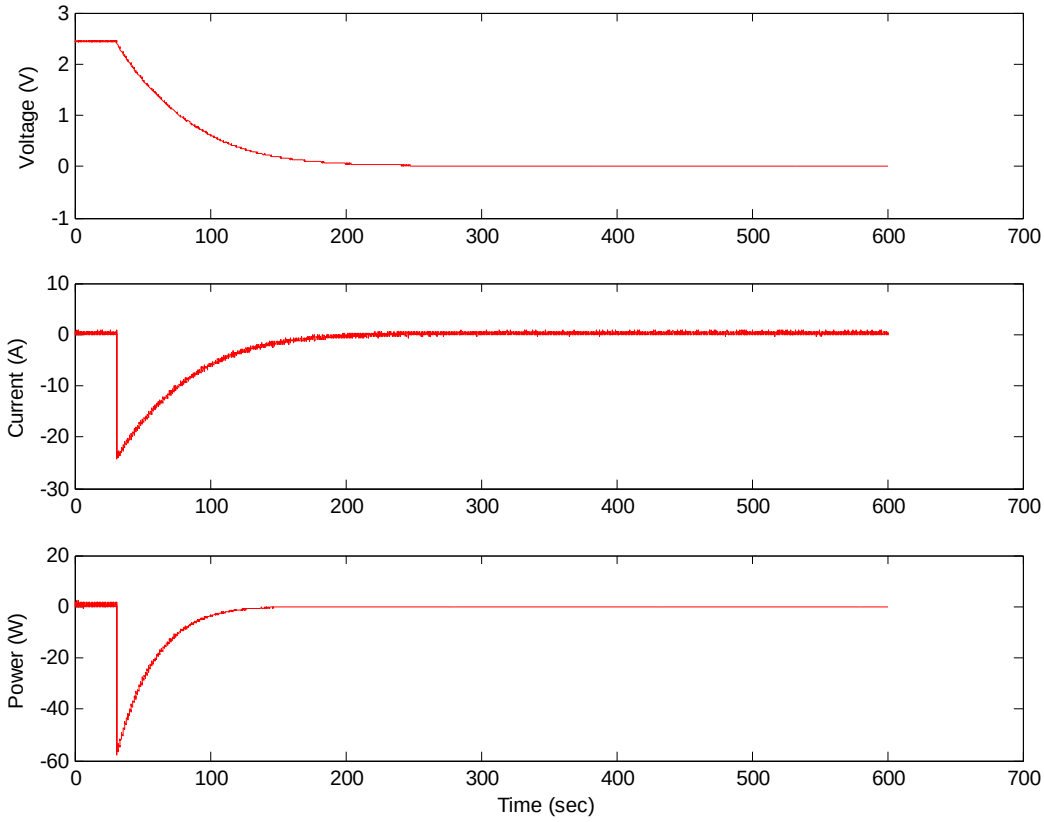

Figure A1.1-12: Plotted Matlab Data of 25 A Charge Cycle at T=25°C

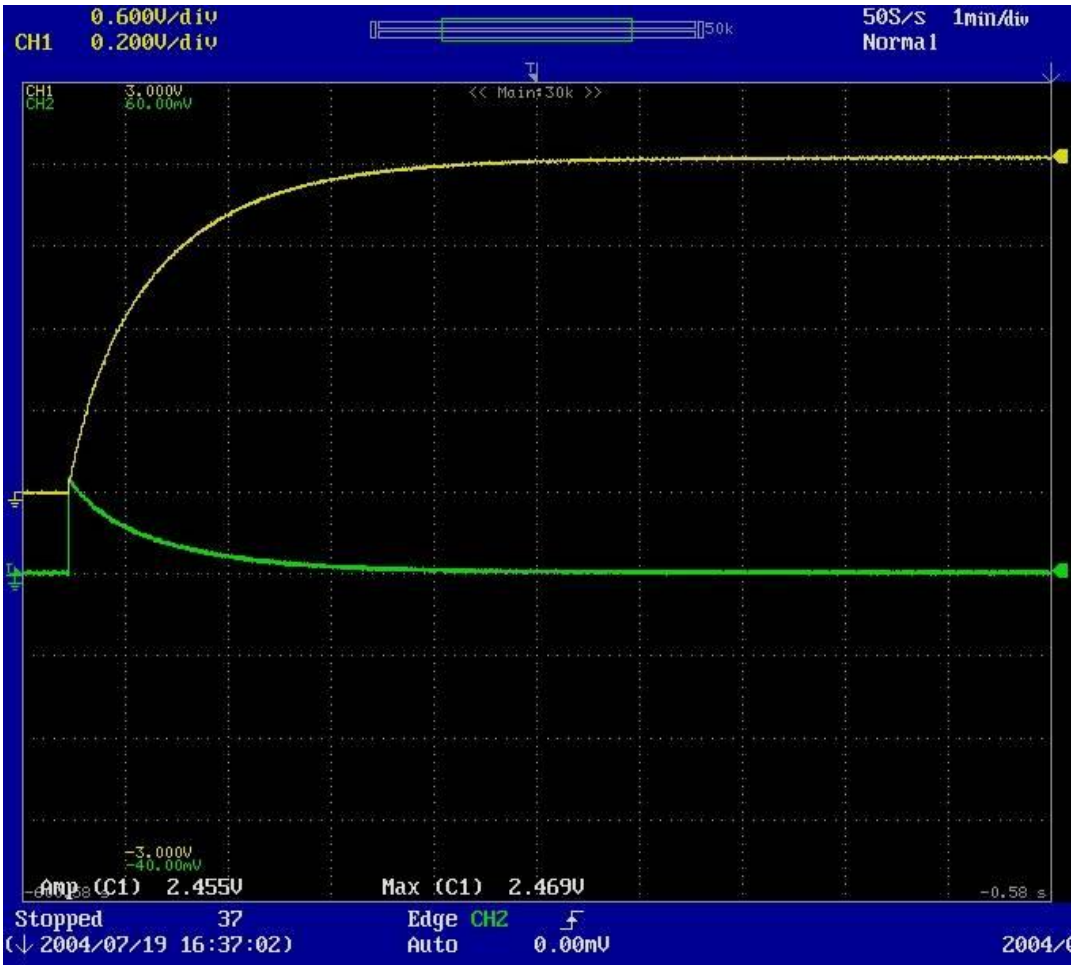

Figure A1.1-13: Oscilloscope Screen Capture of 25 A Charge Cycle at T=50°C (Timescale: 1 min/div)

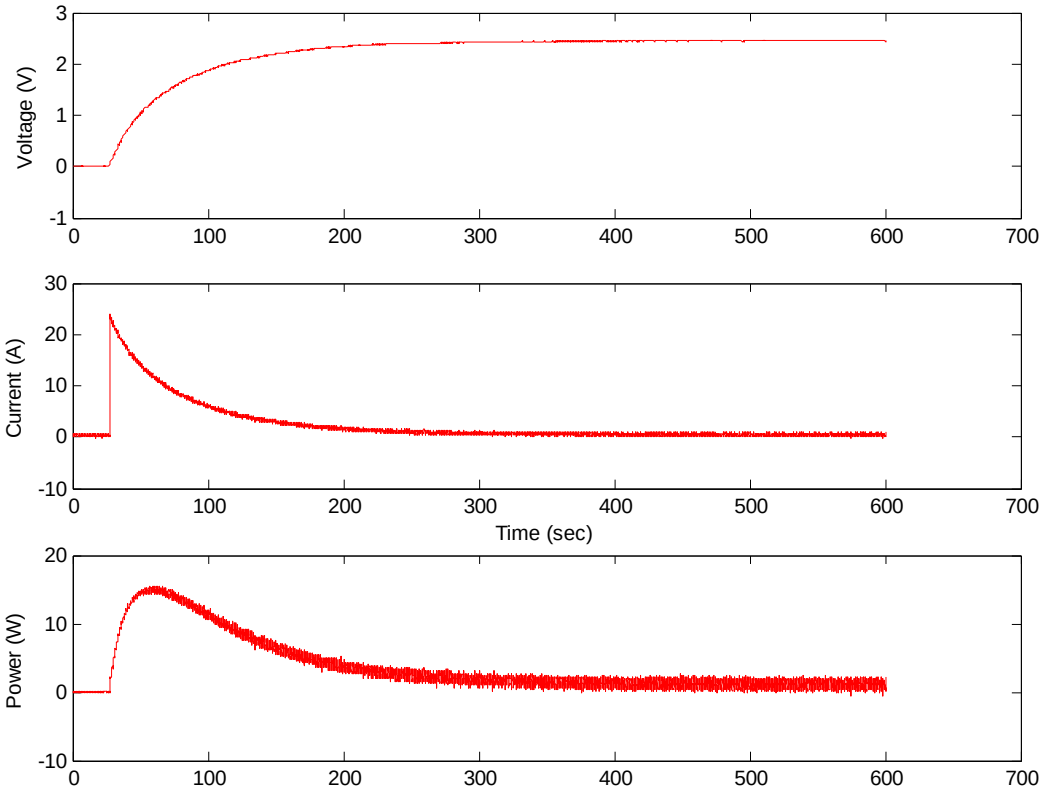

Figure A1.1-14: Plotted Matlab Data of 25 A Charge Cycle at T=50^{o}C

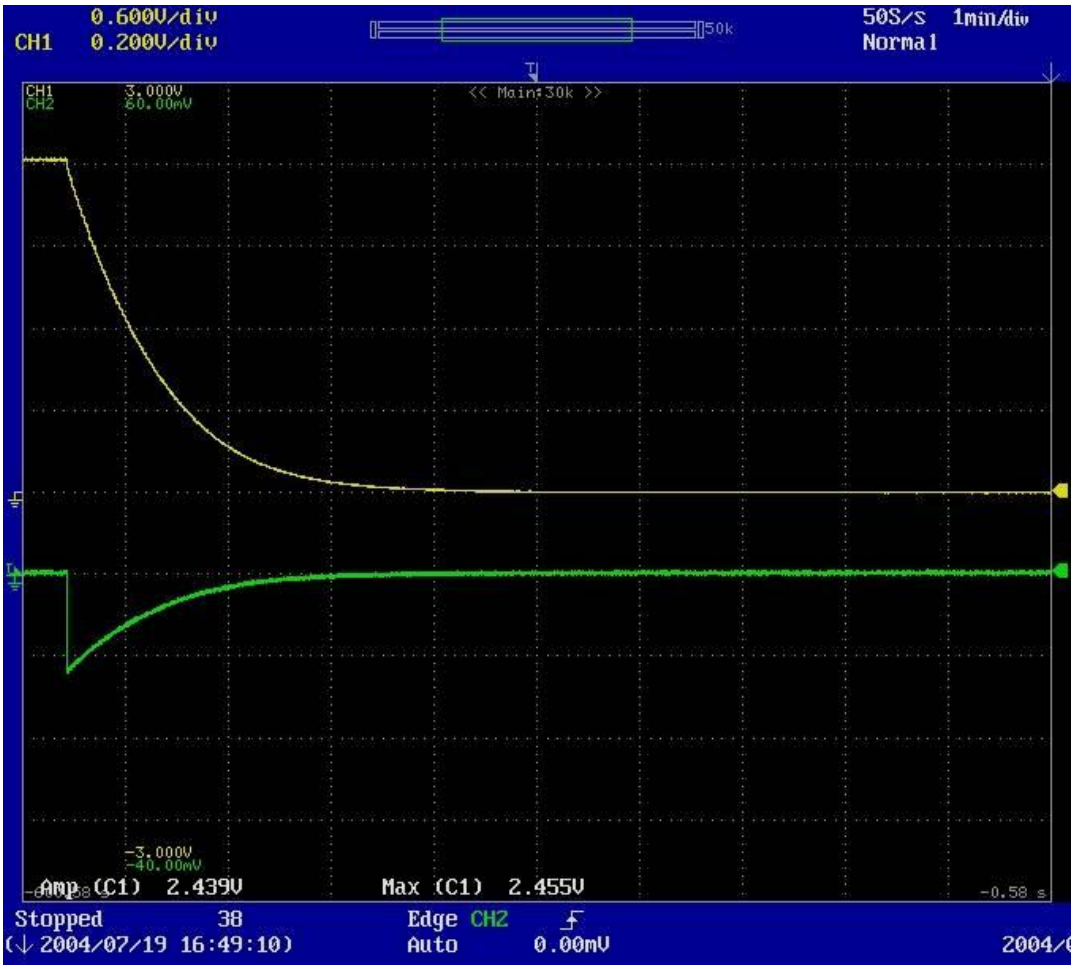

Figure A1.1-15: Oscilloscope Screen Capture of 25 A Discharge Cycle at T=50°C (Timescale: 1 min/div)

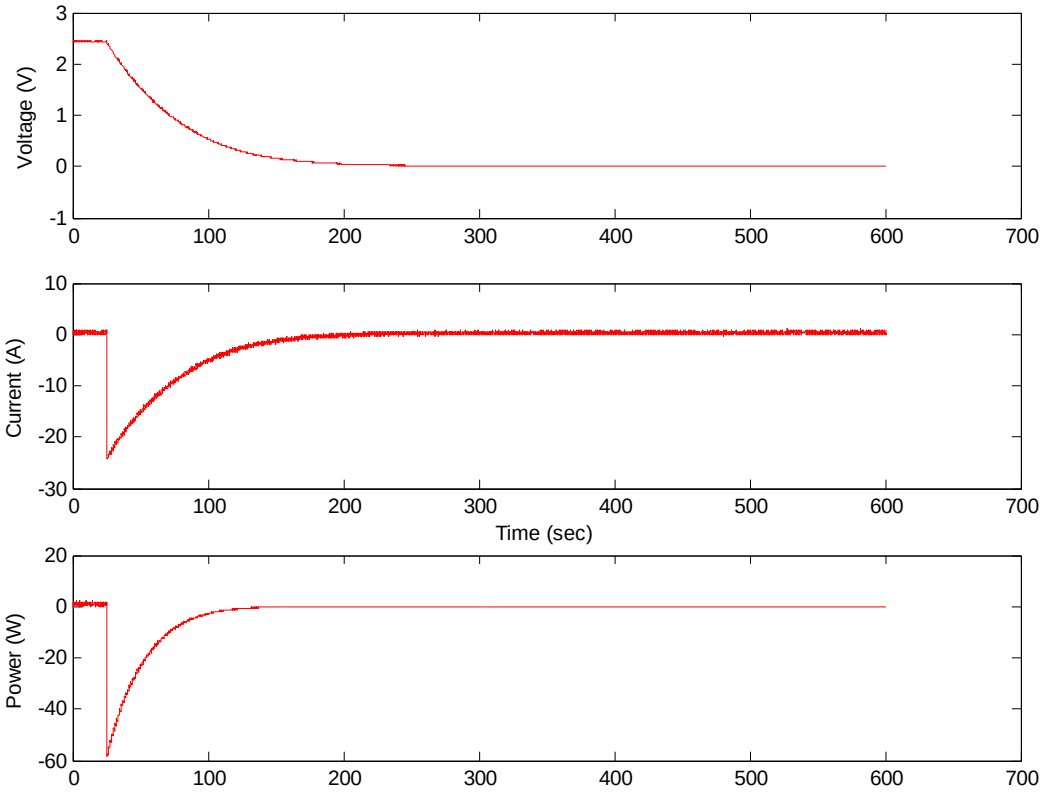

Figure A1.1-16: Plotted Matlab Data of 25 A Discharge Cycle at T=50^{o}C

A1.2 450 F 50 A Results

Figure A1.2-1: Oscilloscope Screen Capture of 50 A Charge Cycle at T= -25°C (Timescale: 1 min/div)

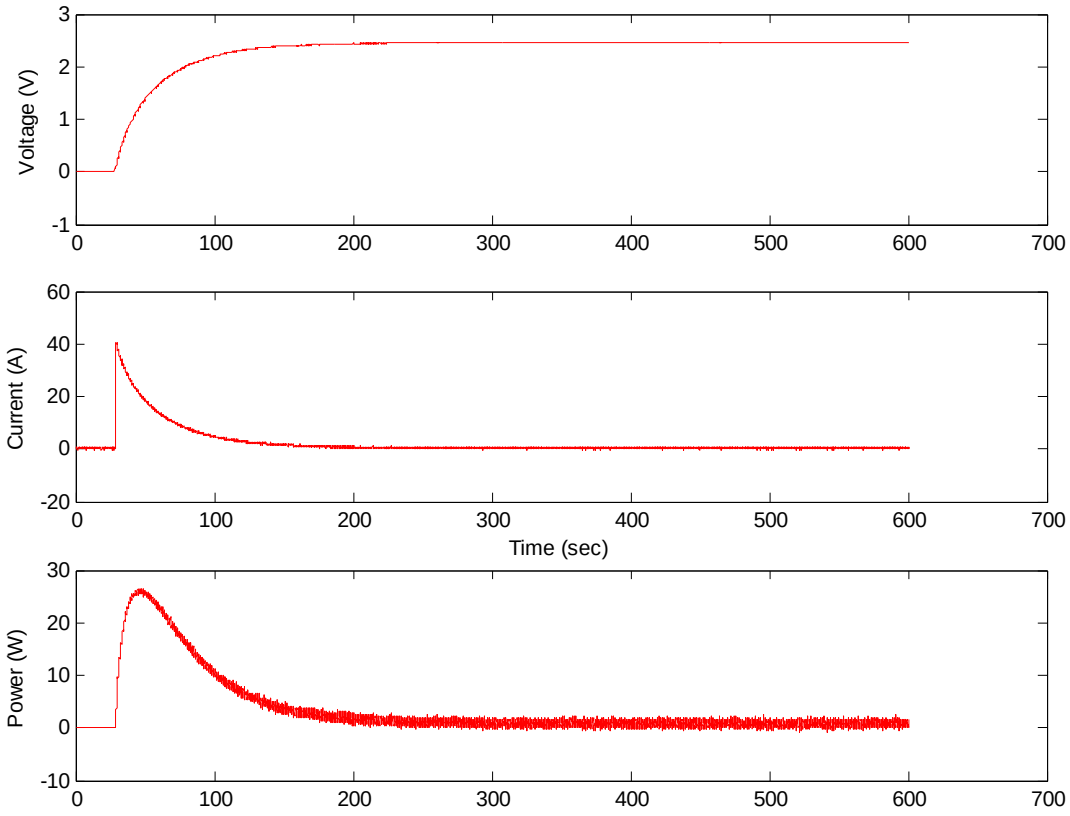

Figure A1.2-2: Plotted Matlab Data of 50 A Charge Cycle at T= -25°C

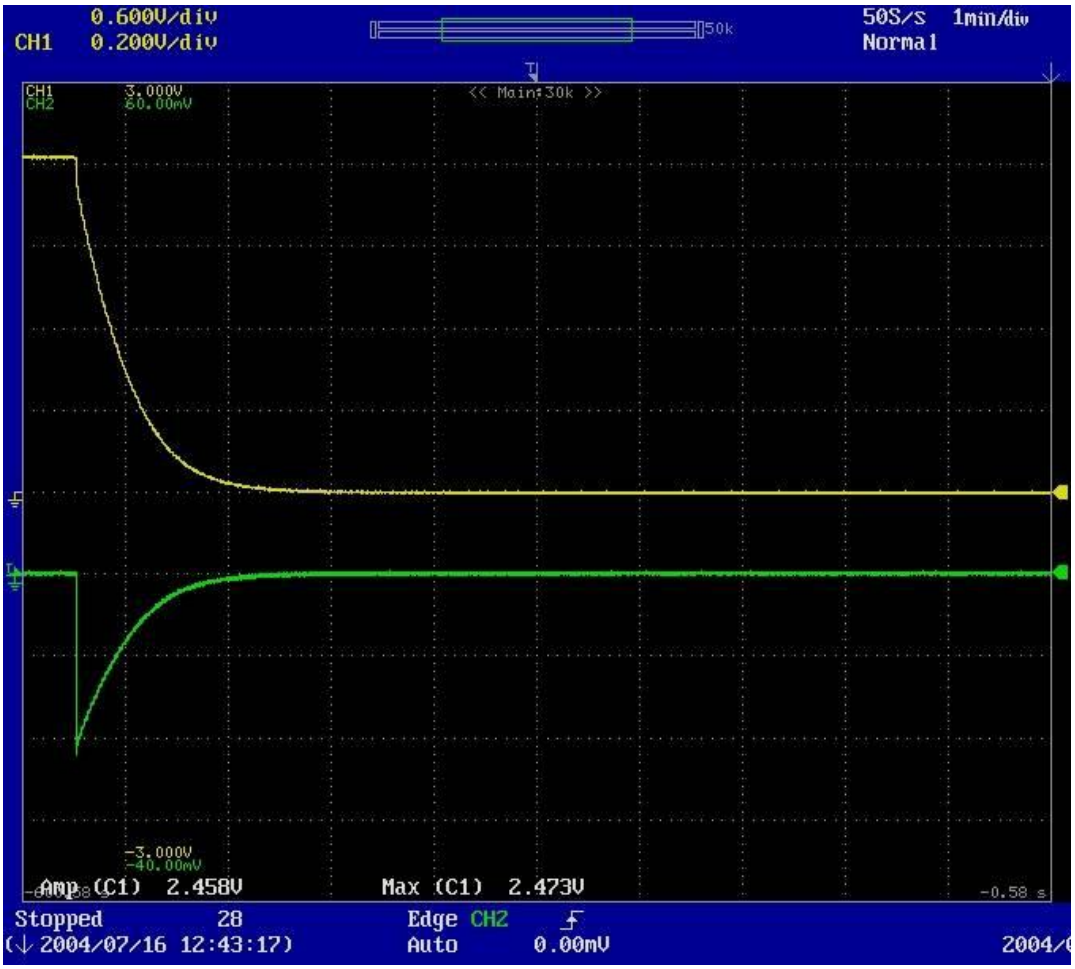

Figure A1.2-3: Oscilloscope Screen Capture of 50 A Discharge Cycle at T= -25°C (Timescale: 1 min/div)

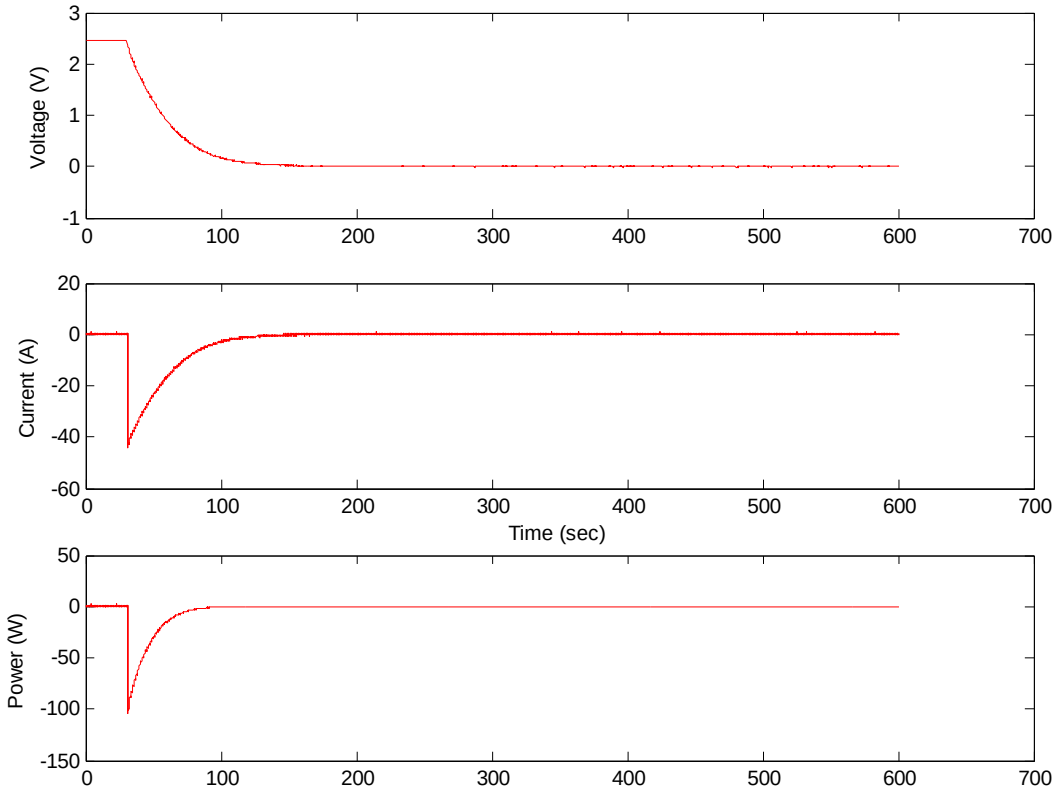

Figure A1.2-4: Plotted Matlab Data of 50 A Discharge Cycle at T= -25°C

Figure A1.2-5: Oscilloscope Screen Capture of 50 A Charge Cycle at T= 0^{o}C (Timescale: 1 min/div)

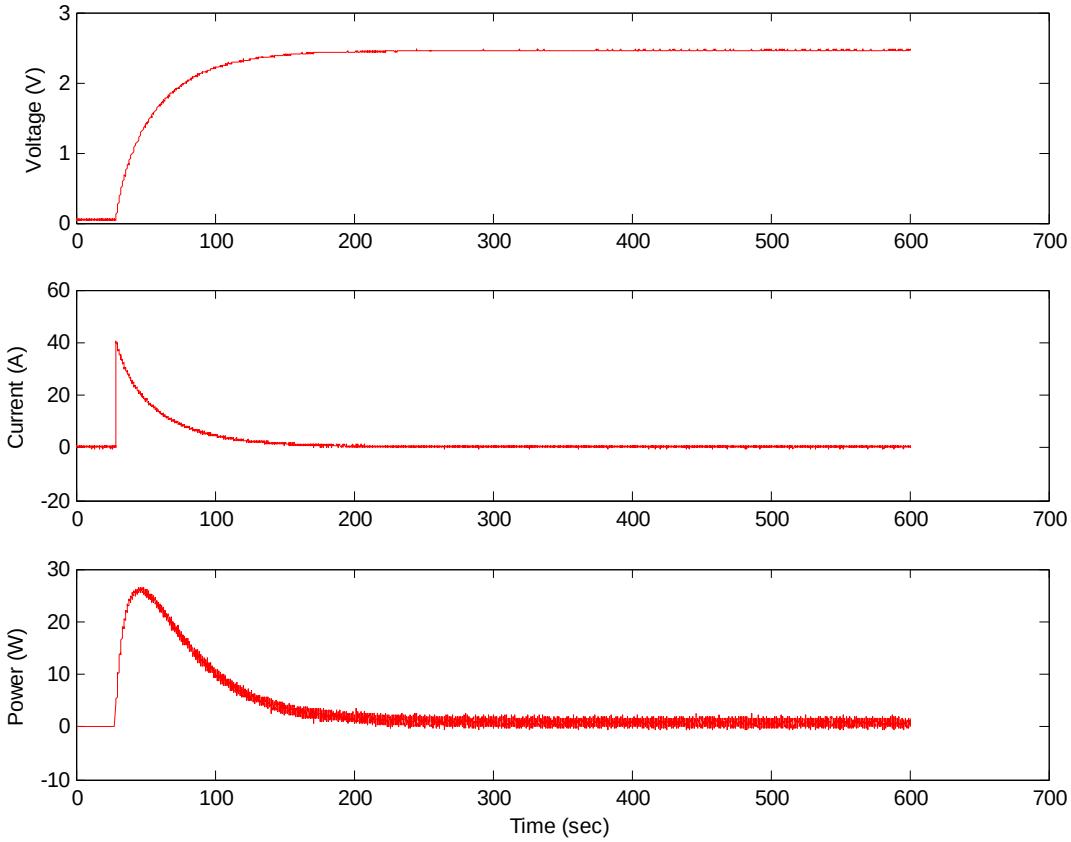

Figure A1.2-6: Plotted Matlab Data of 50 A Charge Cycle at T= 0^{o}C

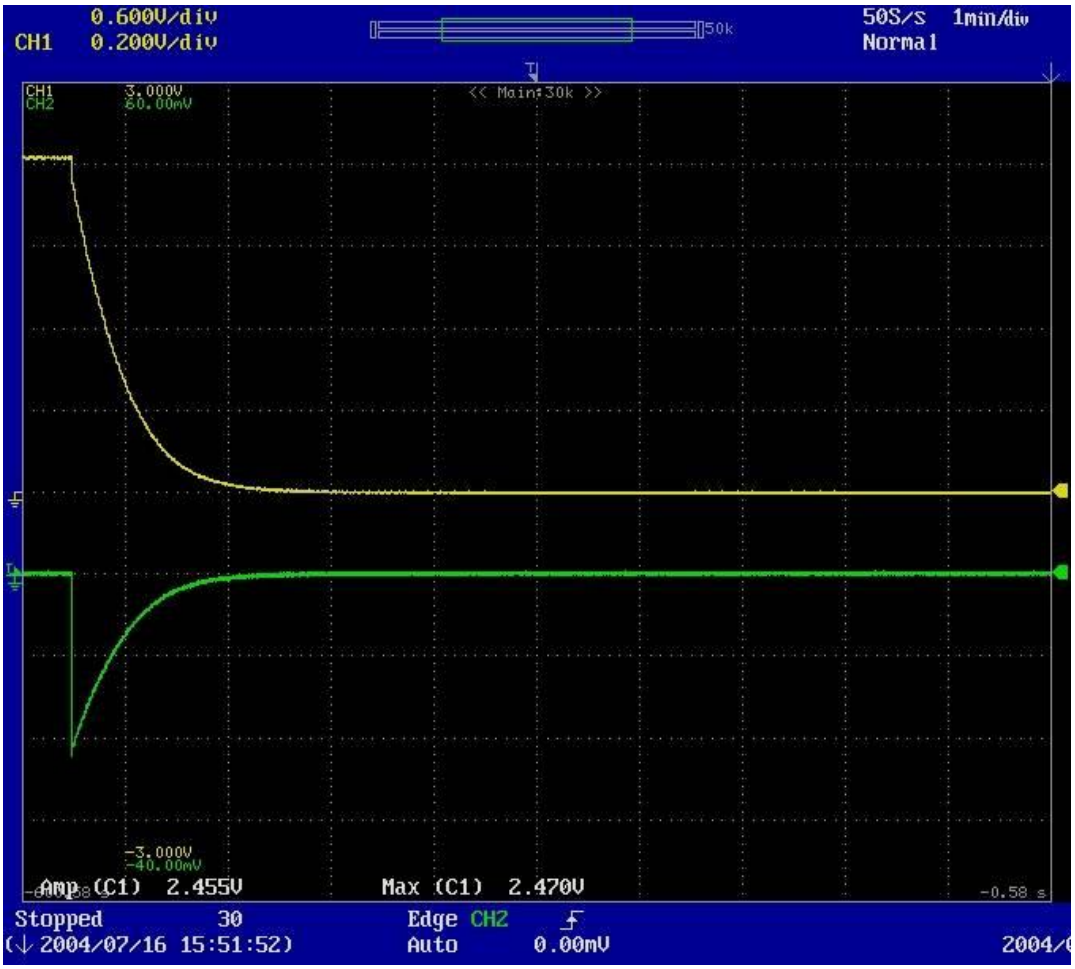

Figure A1.2-7: Oscilloscope Screen Capture of 50 A Discharge Cycle at T= 0^{o}C (Timescale: 1 min/div)

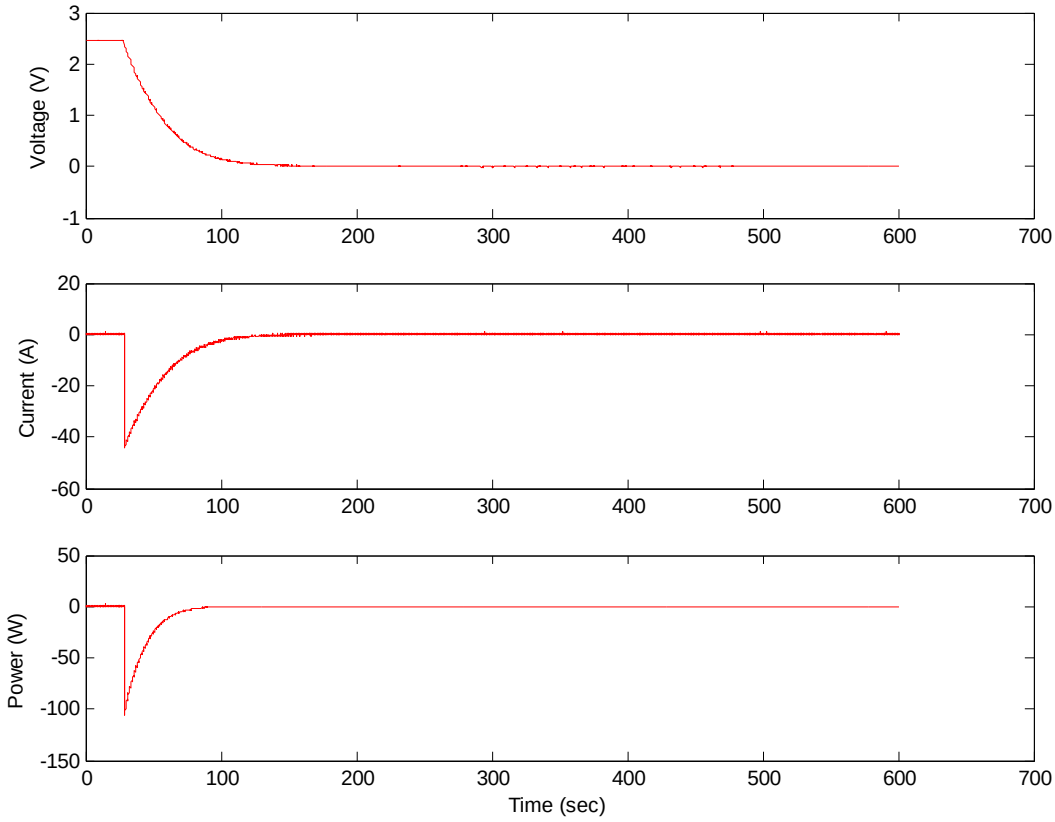

Figure A1.2-8: Plotted Matlab Data of 50 A Discharge Cycle at T= 0°C

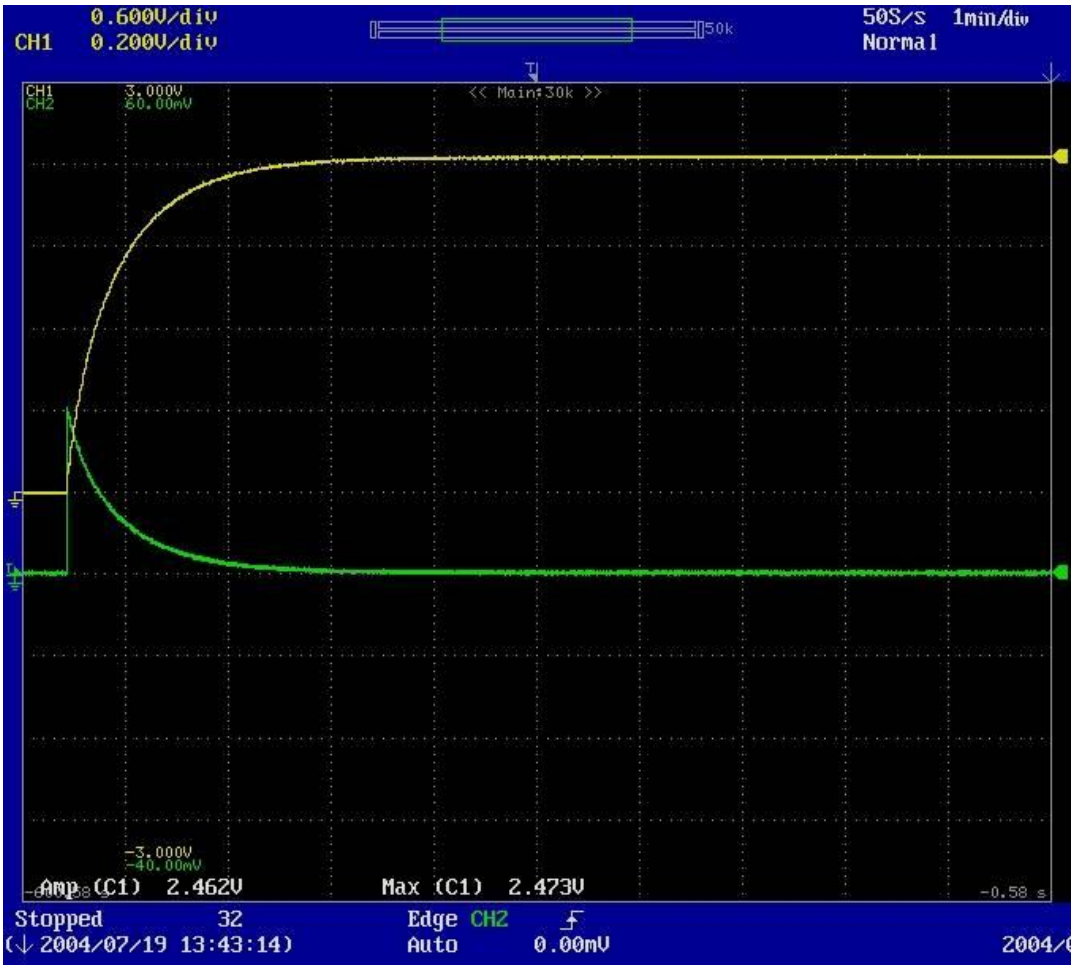

Figure A1.2-9: Oscilloscope Screen Capture of 50 A Charge Cycle at T= 25°C (Timescale: 1 min/div)

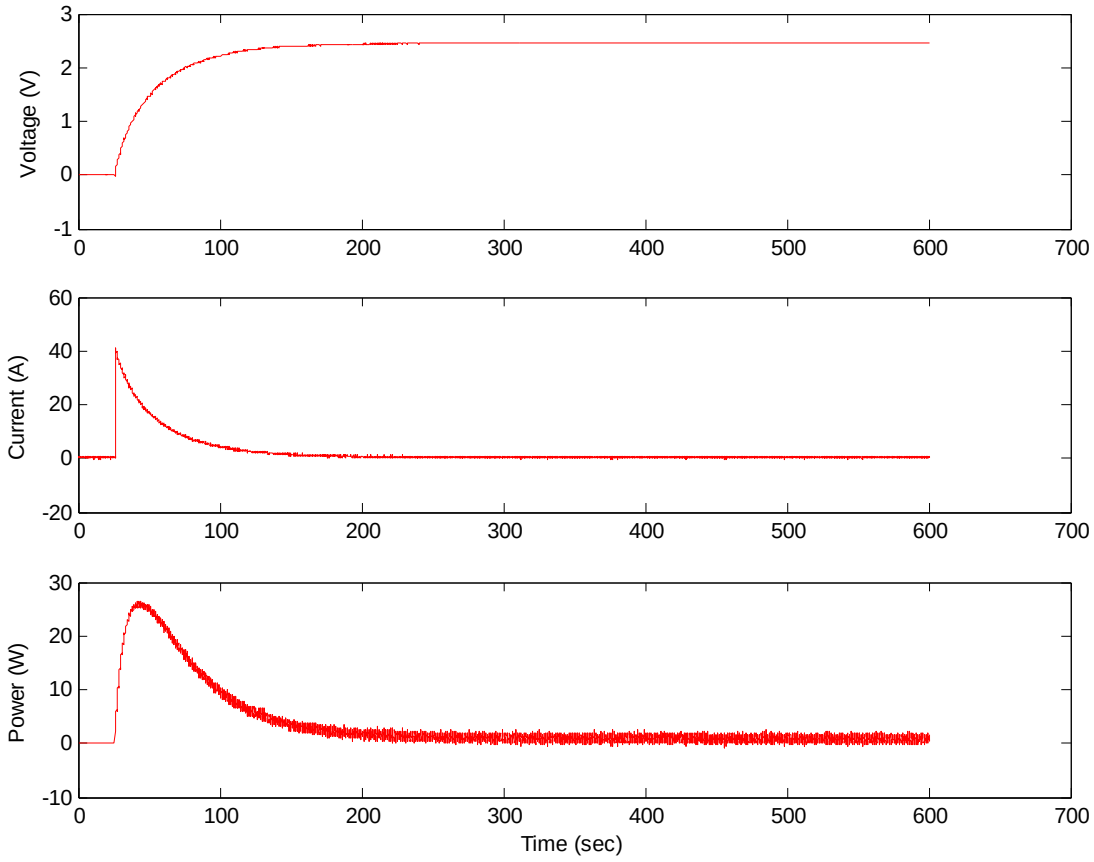

Figure A1.2-10: Plotted Matlab Data of 50 A Charge Cycle at T= 25^{o}C

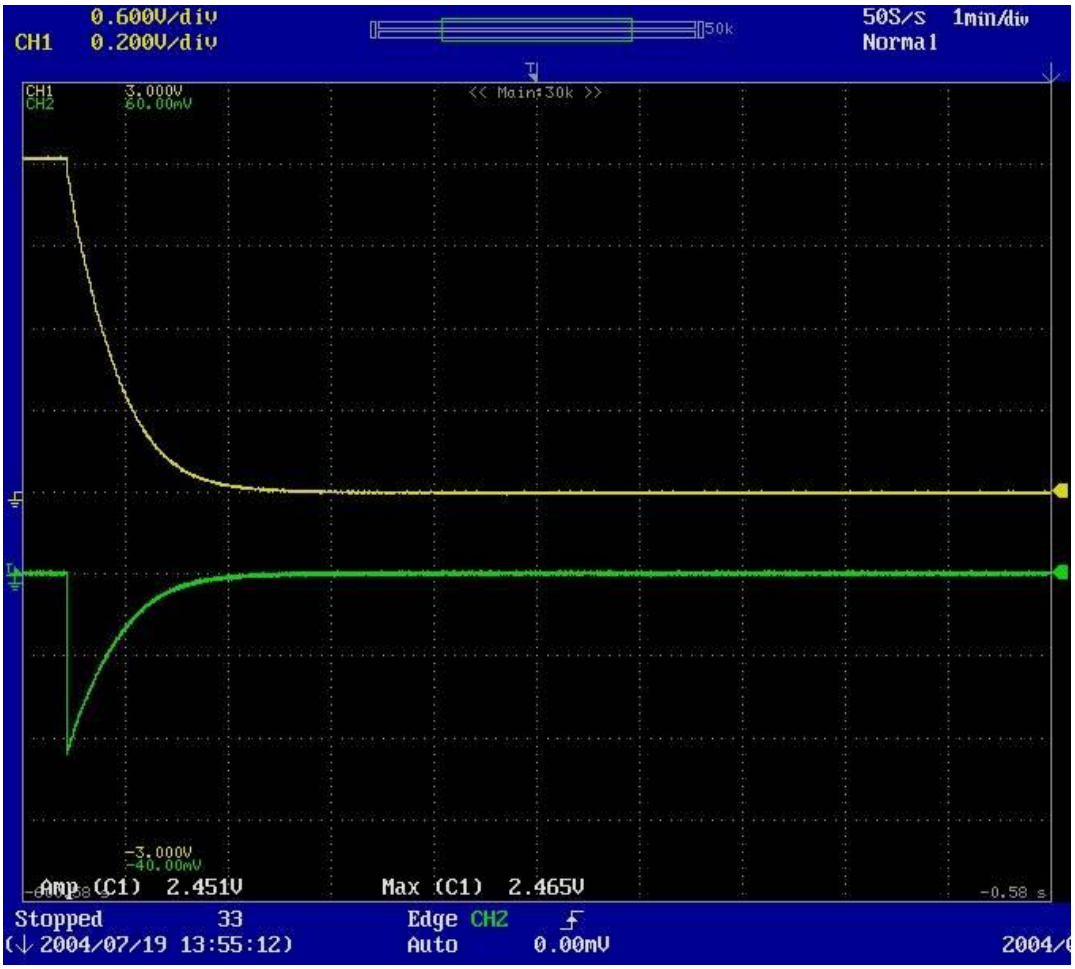

Figure A1.2-11: Oscilloscope Screen Capture of 50 A Discharge Cycle at T= 25°C (Timescale: 1 min/div)

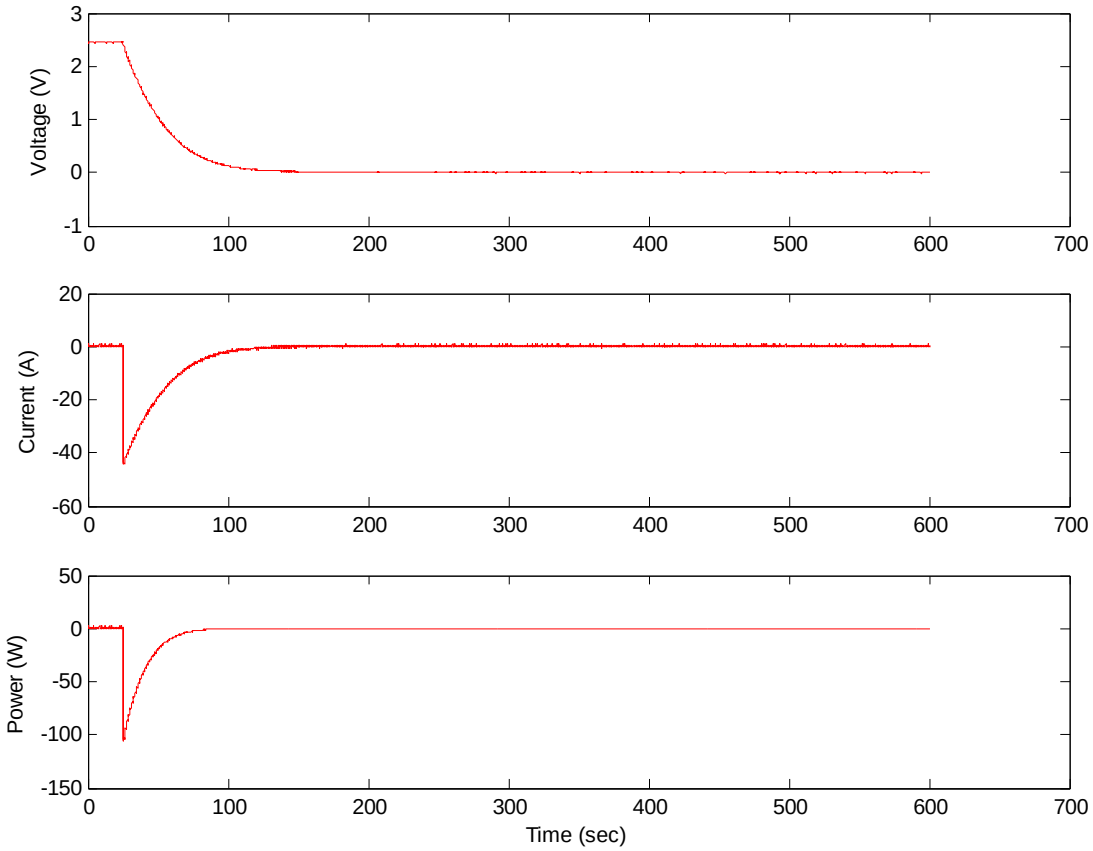

Figure A1.2-12: Plotted Matlab Data of 50 A Discharge Cycle at T= 25^{o}C

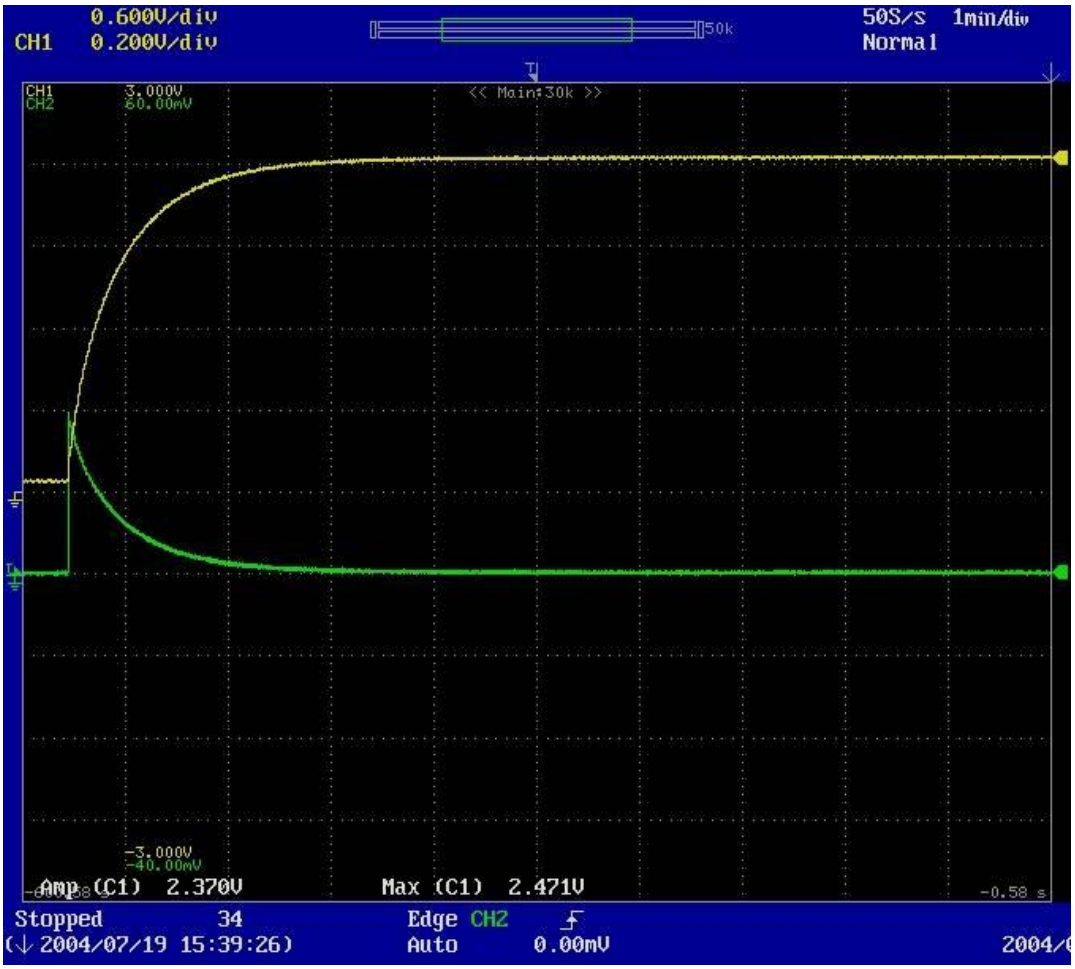

Figure A1.2-13: Oscilloscope Screen Capture of 50 A Charge Cycle at T= 50°C (Timescale: 1 min/div)

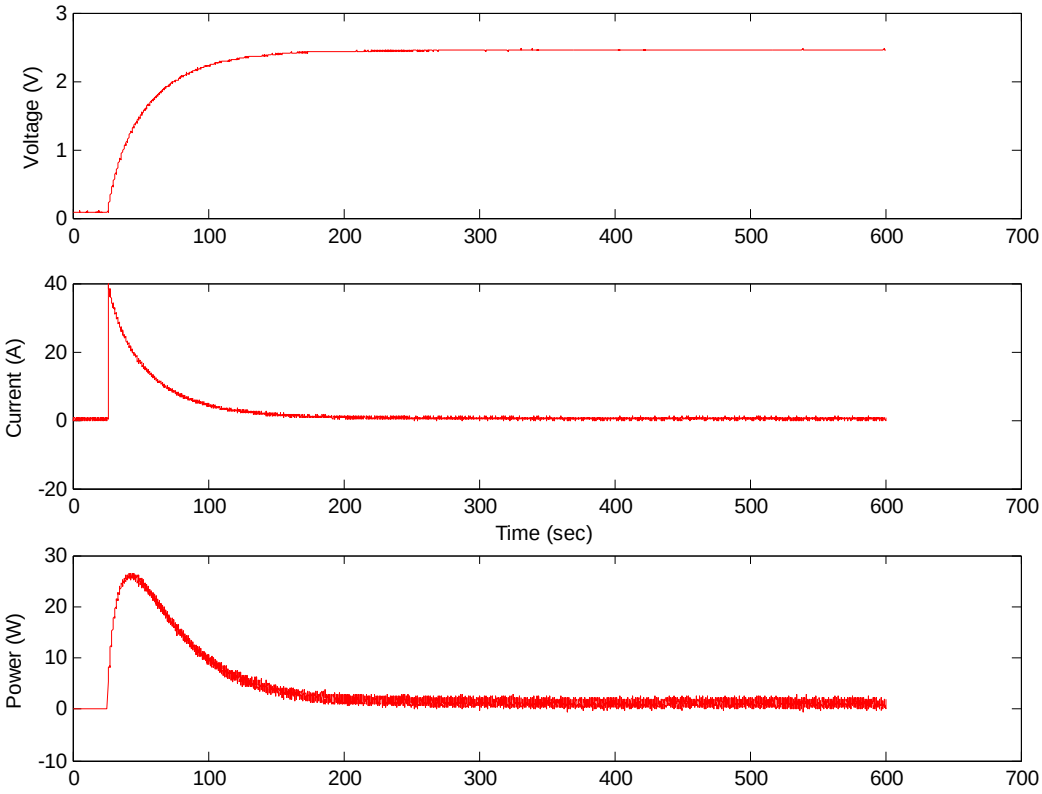

Figure A1.2-14: Plotted Matlab Data of 50 A Charge Cycle at T= 50^{o}C

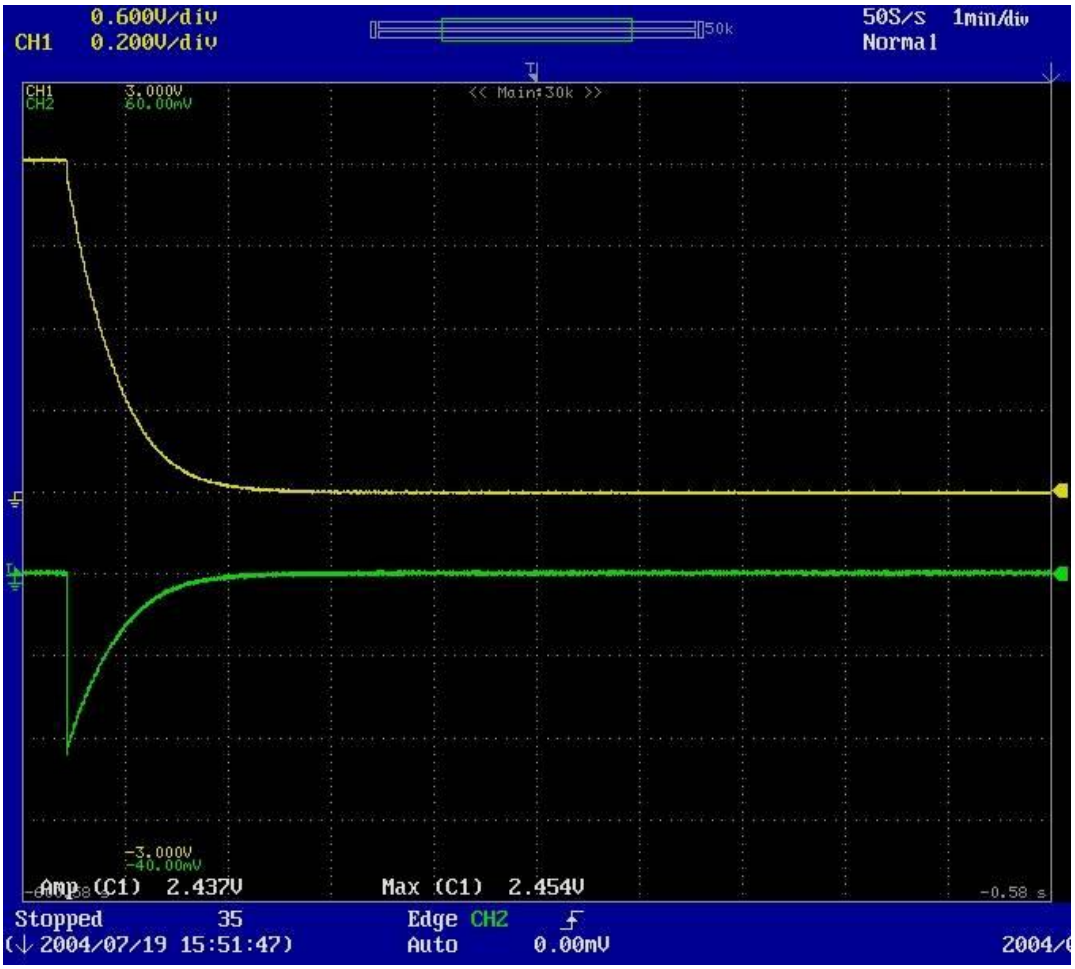

Figure A1.2-15: Oscilloscope Screen Capture of 50 A Discharge Cycle at T= 50°C (Timescale: 1 min/div)

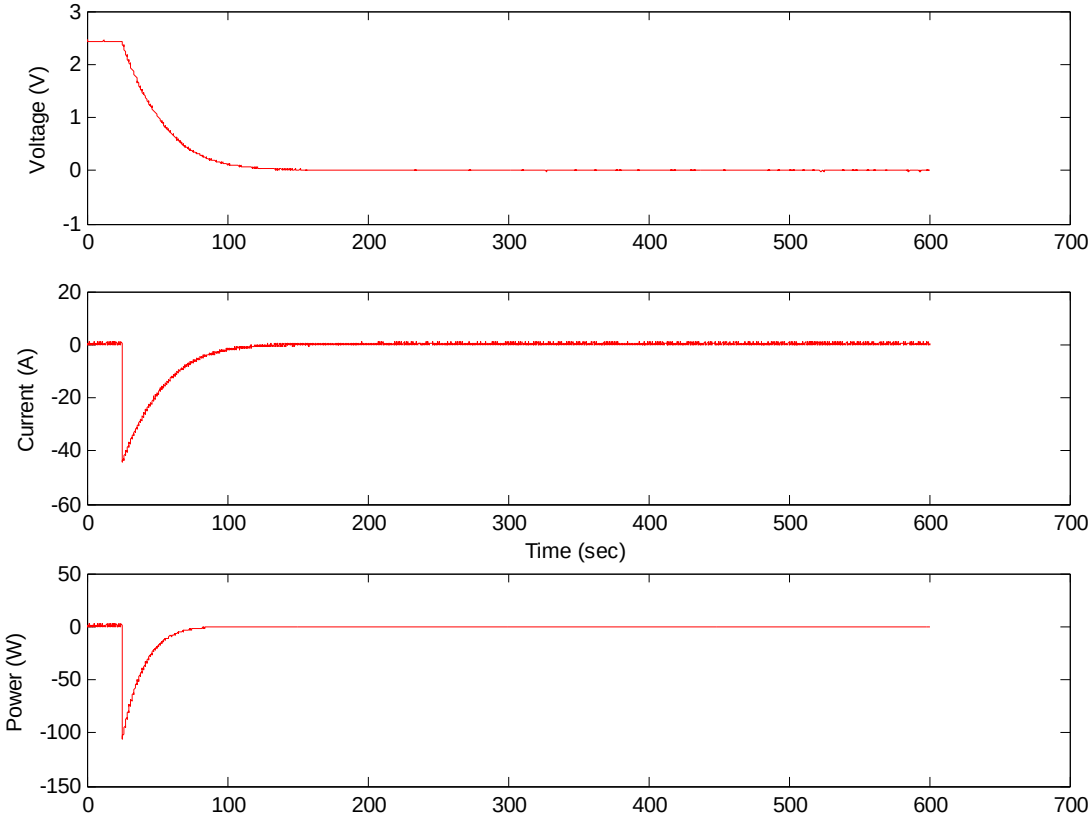

Figure A1.2-16: Plotted Matlab Data of 50 A Discharge Cycle at T= 50^{o}C

A1.3 450 F 60 A Results

Figure A1.3-1 Oscilloscope Screen Capture of 60 A Charge Cycle at T= -25°C (Timescale: 1 min/div)

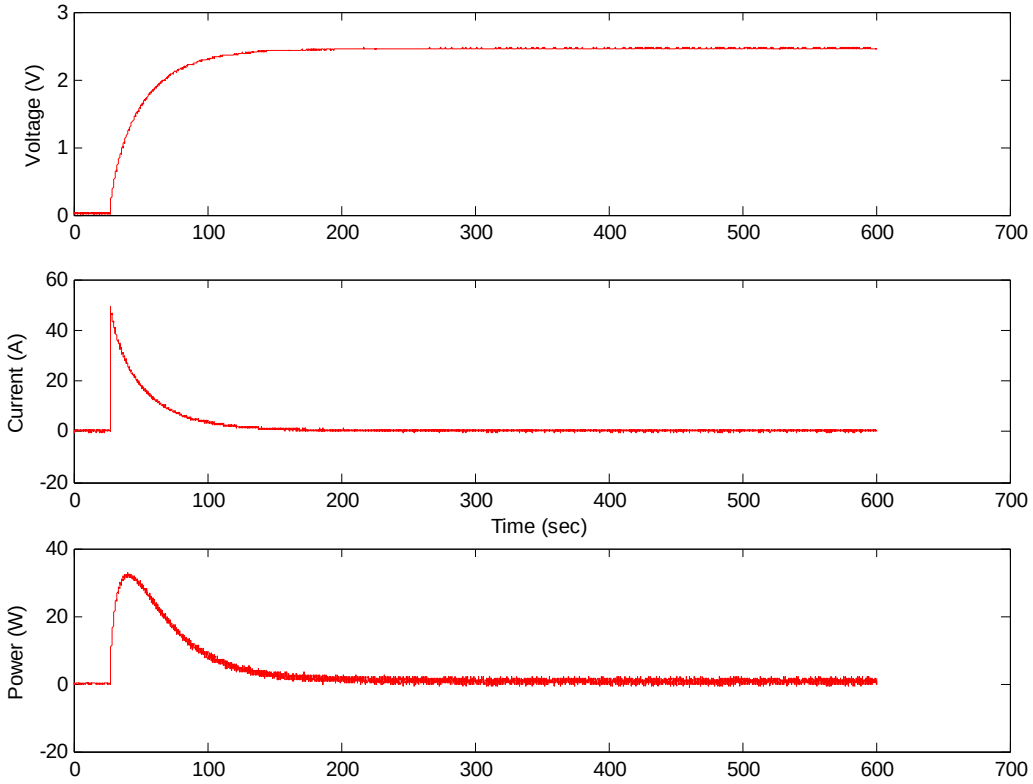

Figure A1.3-2: Plotted Matlab Data of 60 A Charge Cycle at T= -25^{o}C

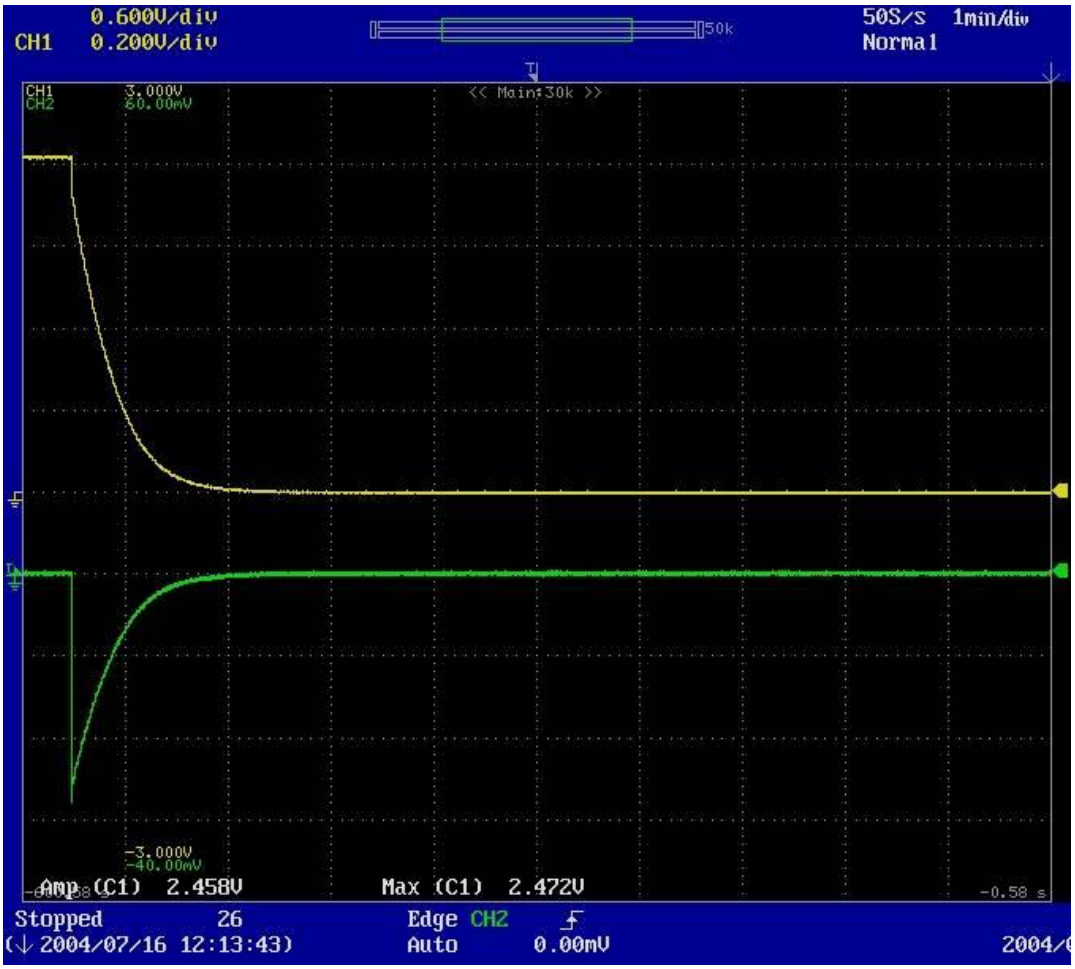

Figure A1.3-3: Plotted Matlab Data of 60 A Discharge Cycle at T= -25°C (Timescale: 1 min/div)

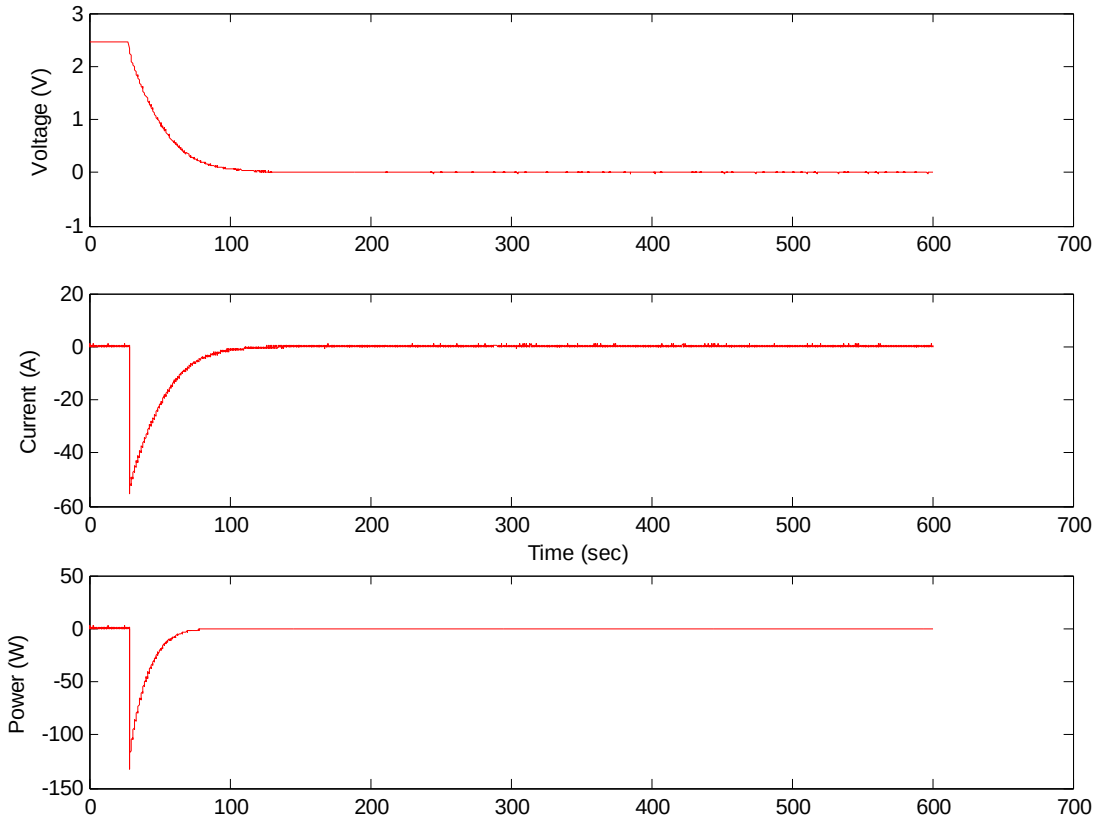

Figure A1.3-4: Plotted Matlab Data of 60 A Discharge Cycle at T= -25^{o}C

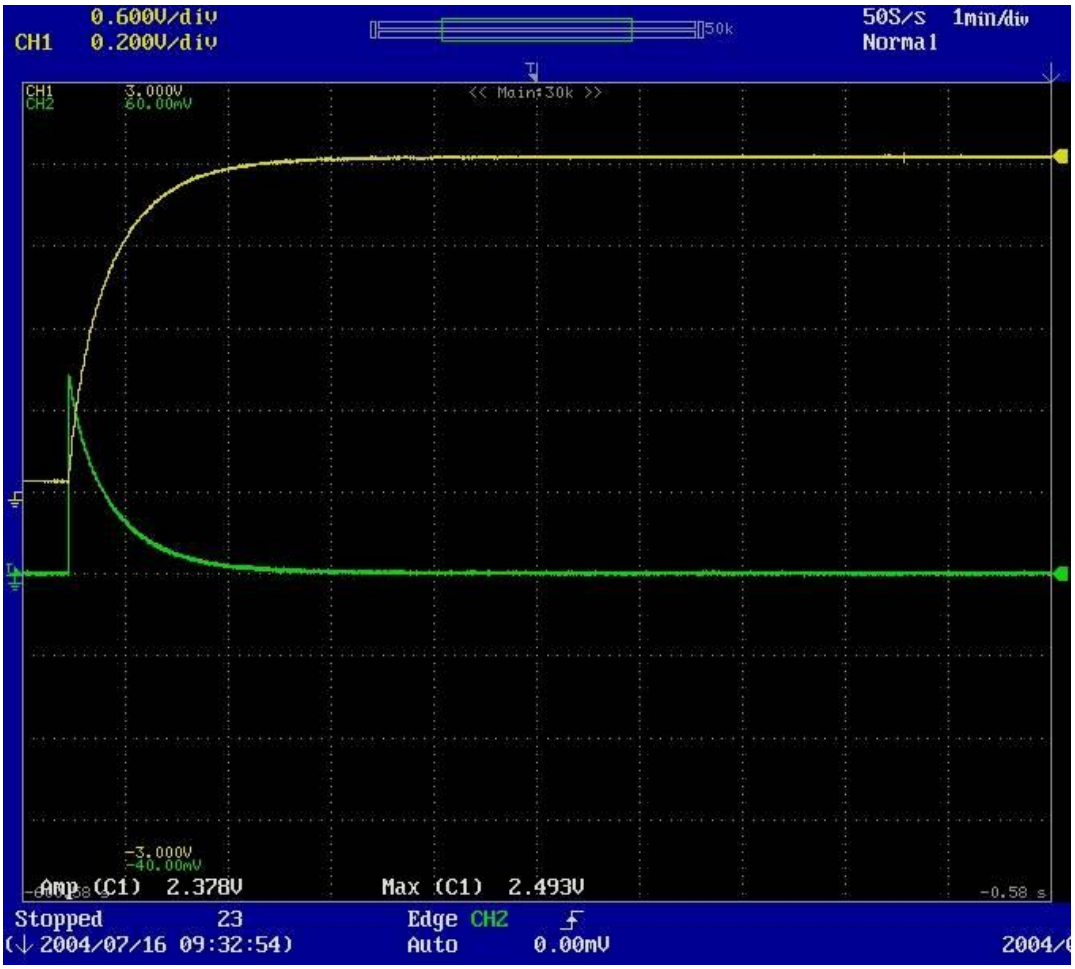

Figure A1.3-5: Oscilloscope Screen Capture of 60 A Charge Cycle at T= 0°C (Timescale: 1 min/div)

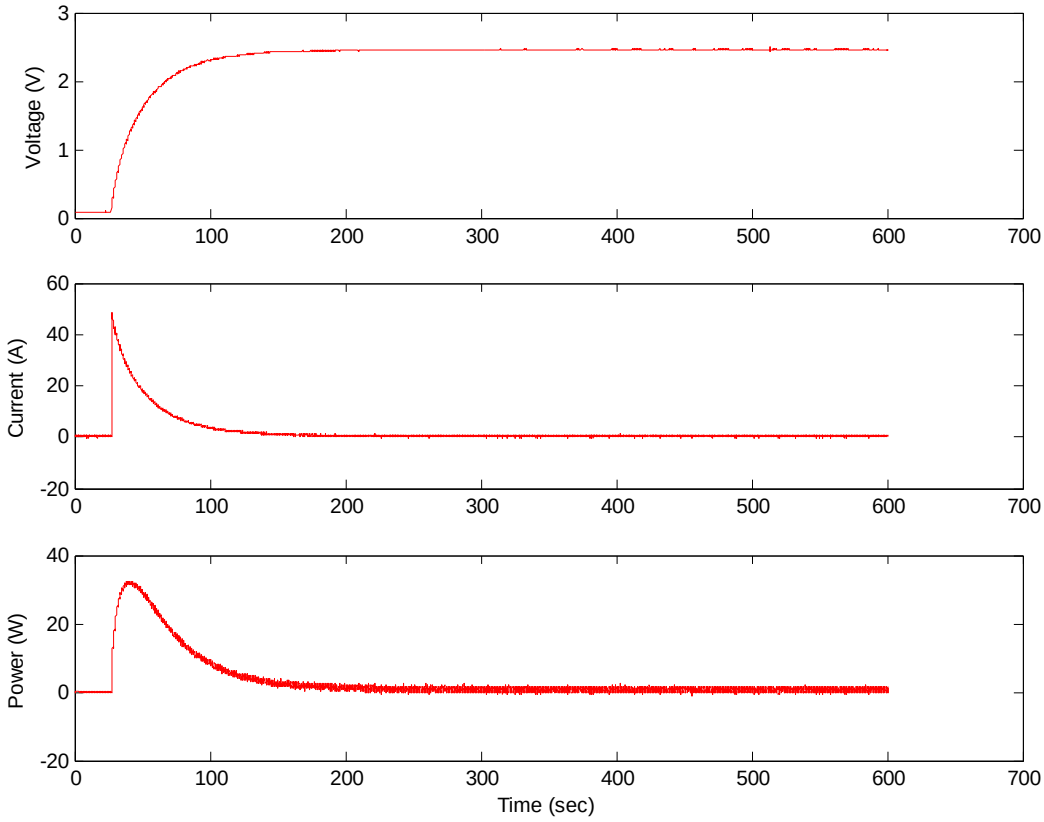

Figure A1.3-6: Plotted Matlab Data of 60 A Charge Cycle at T= 0^{o}C

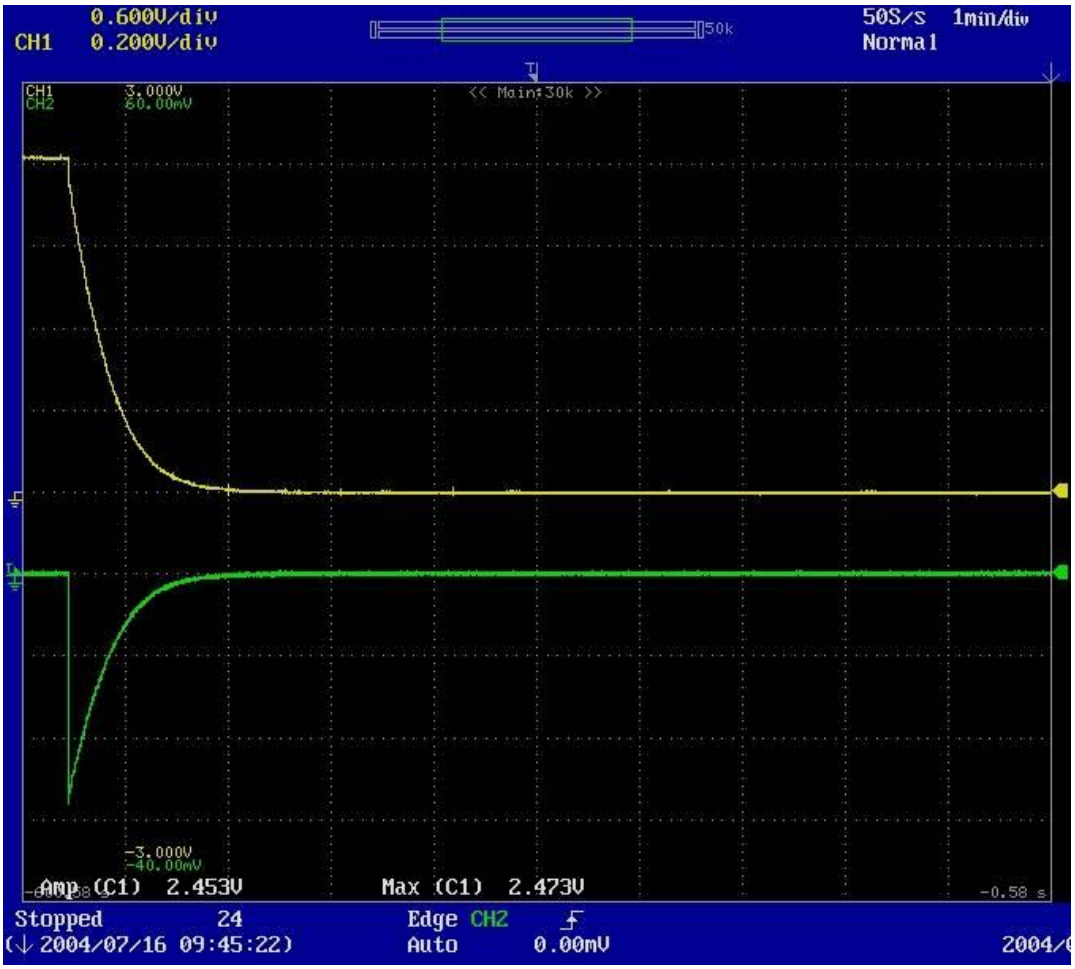

Figure A1.3-7: Oscilloscope Screen Capture of 60 A Discharge Cycle at T= 0^{o}C (Timescale: 1 min/div)

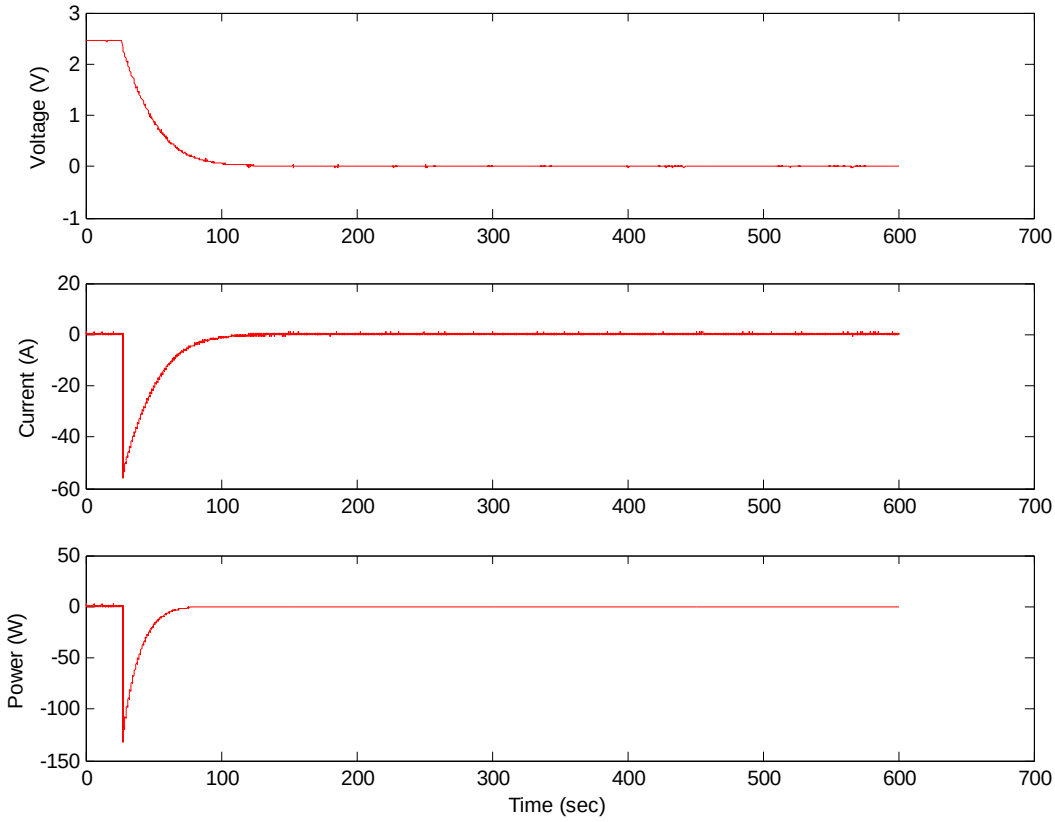

Figure A1.3-8: Plotted Matlab Data of 60 A Discharge Cycle at T= 0^{o}C

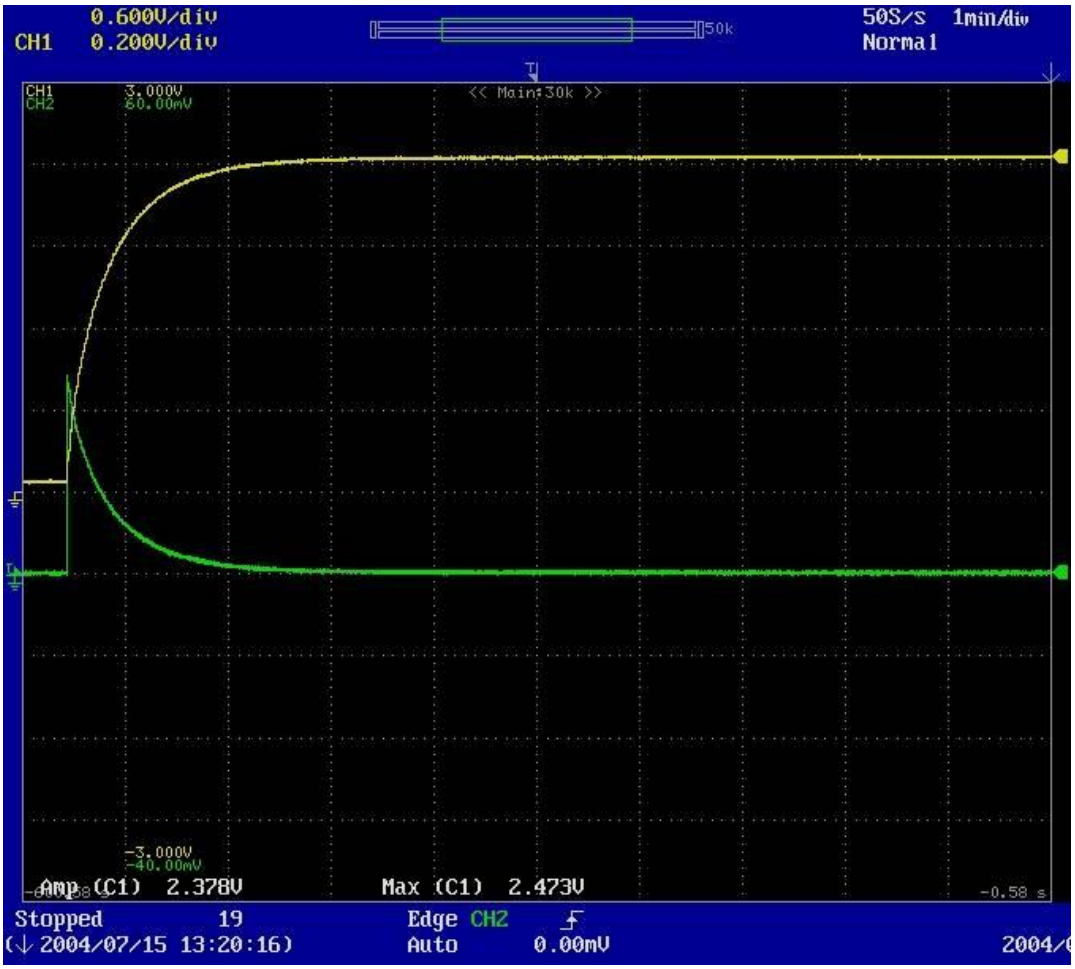

Figure A1.3-9: Oscilloscope Screen Capture of 60 A Charge Cycle at T= 25°C (Timescale: 1 min/div)

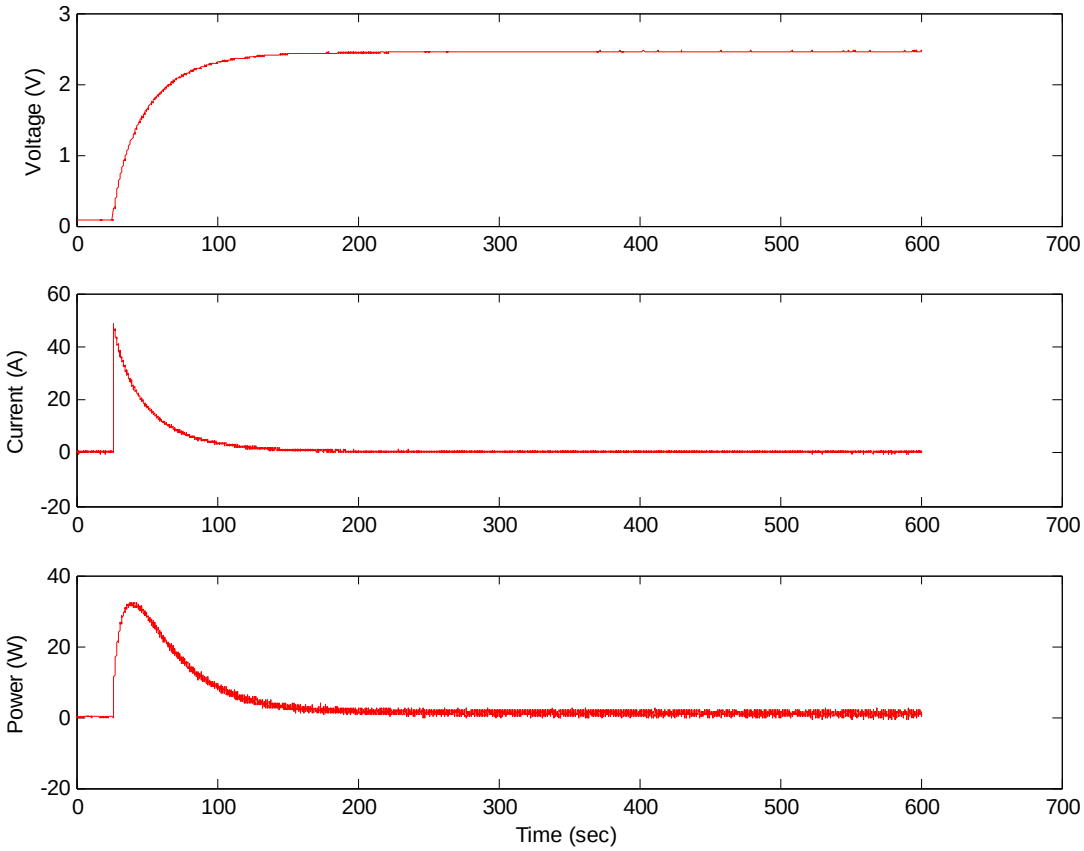

Figure A1.3-10: Plotted Matlab Data of 60 A Charge Cycle at T= 25^{o}C

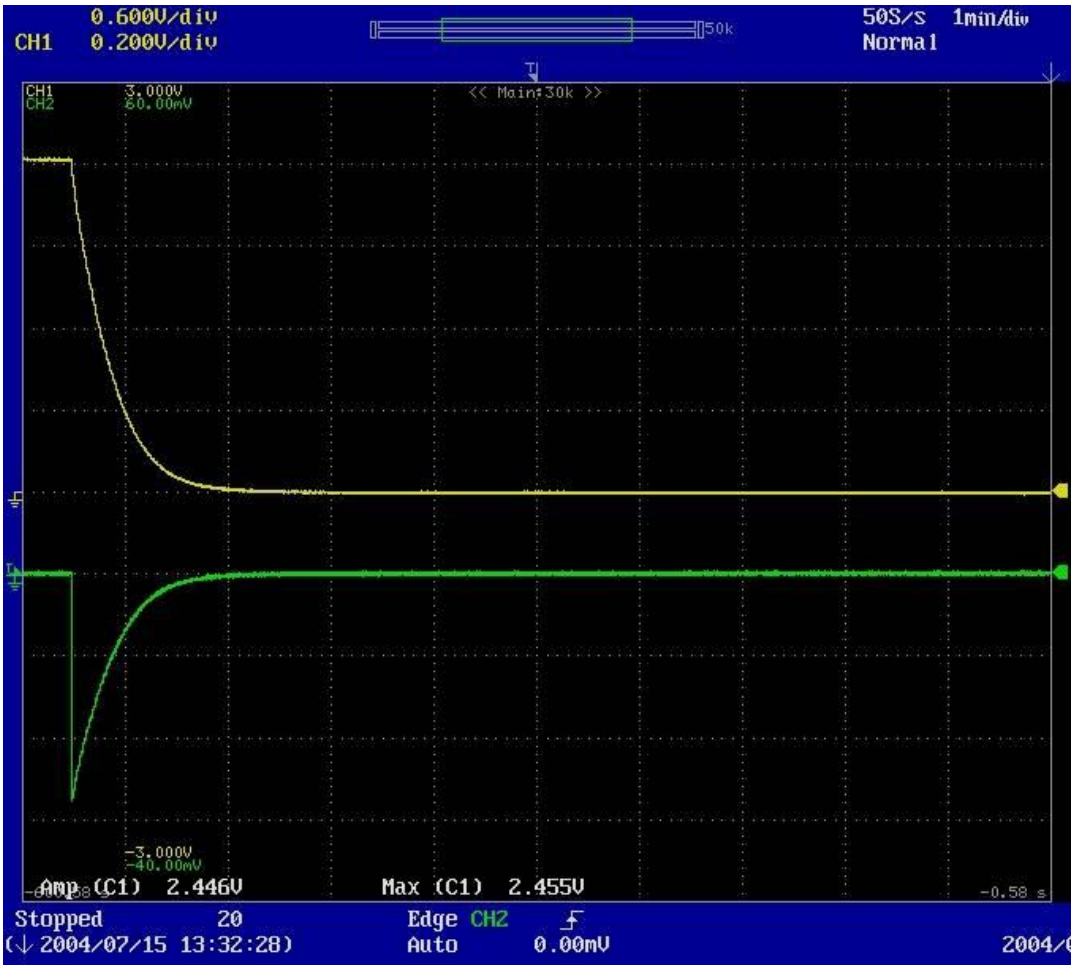

Figure A1.3-11: Oscilloscope Screen Capture of 60 A Discharge Cycle at T= 25°C (Timescale: 1 min/div)

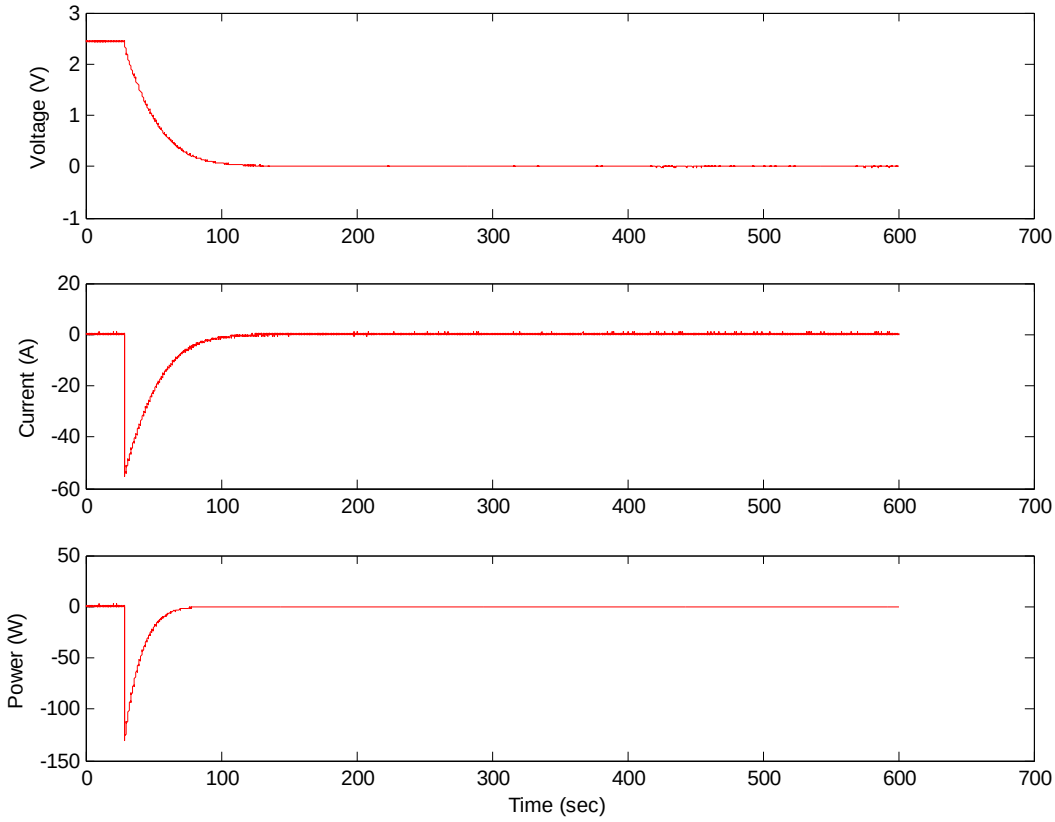

Figure A1.3-12: Plotted Matlab Data of 60 A Discharge Cycle at T= 25^{o}C

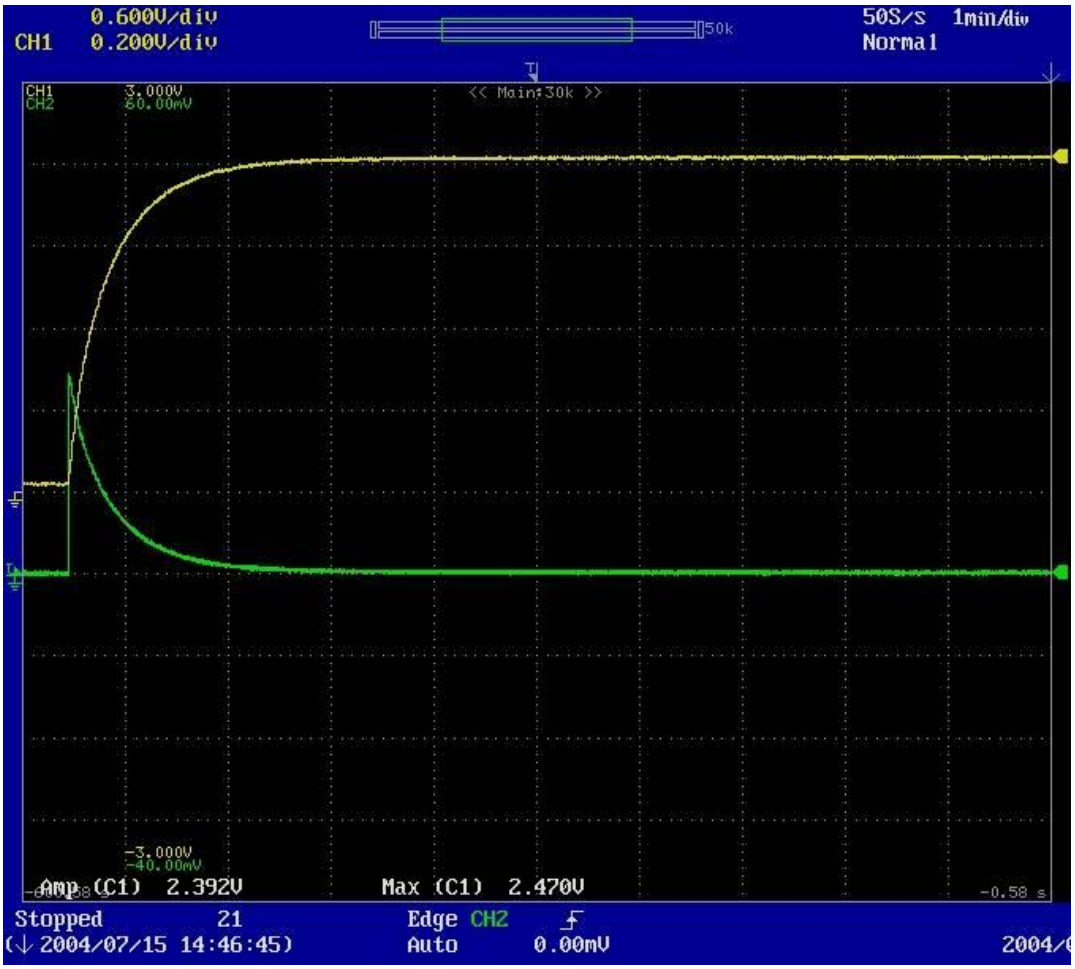

Figure A1.3-13: Oscilloscope Screen Capture of 60 A Charge Cycle at T= 50°C (Timescale: 1 min/div)

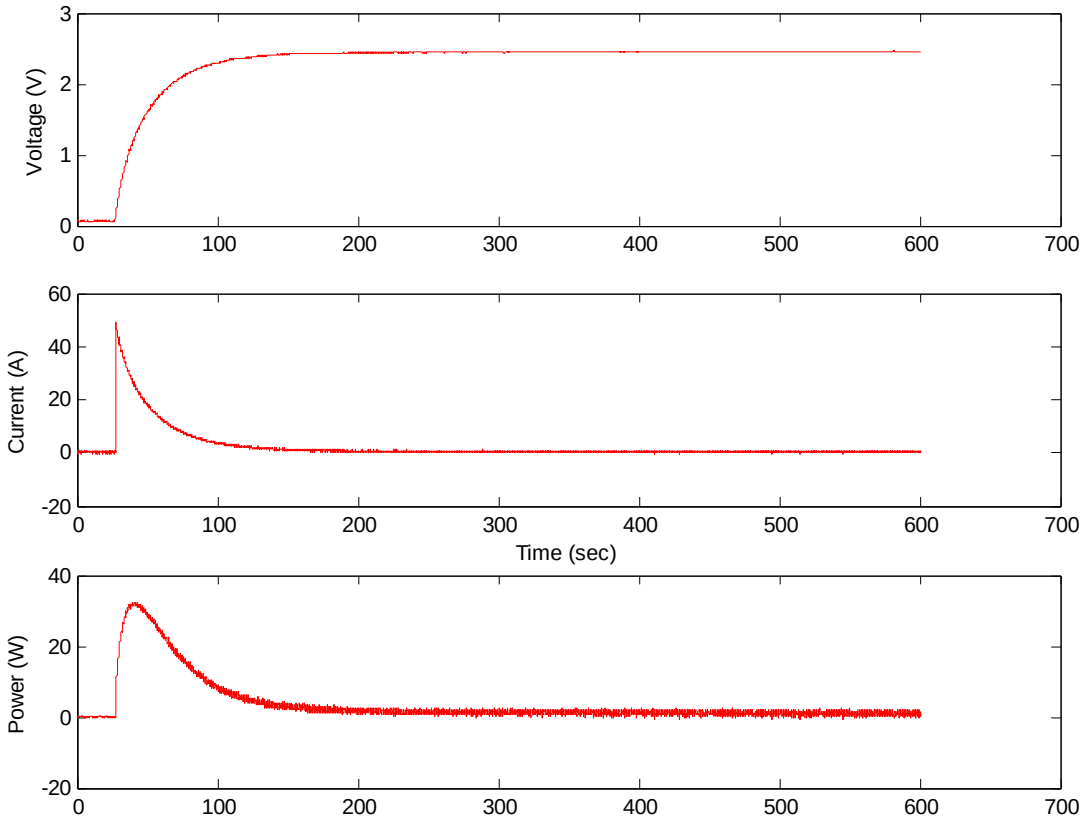

Figure A1.3-14: Figure Plotted Matlab Data of 60 A Charge Cycle at T= 50^{o}C

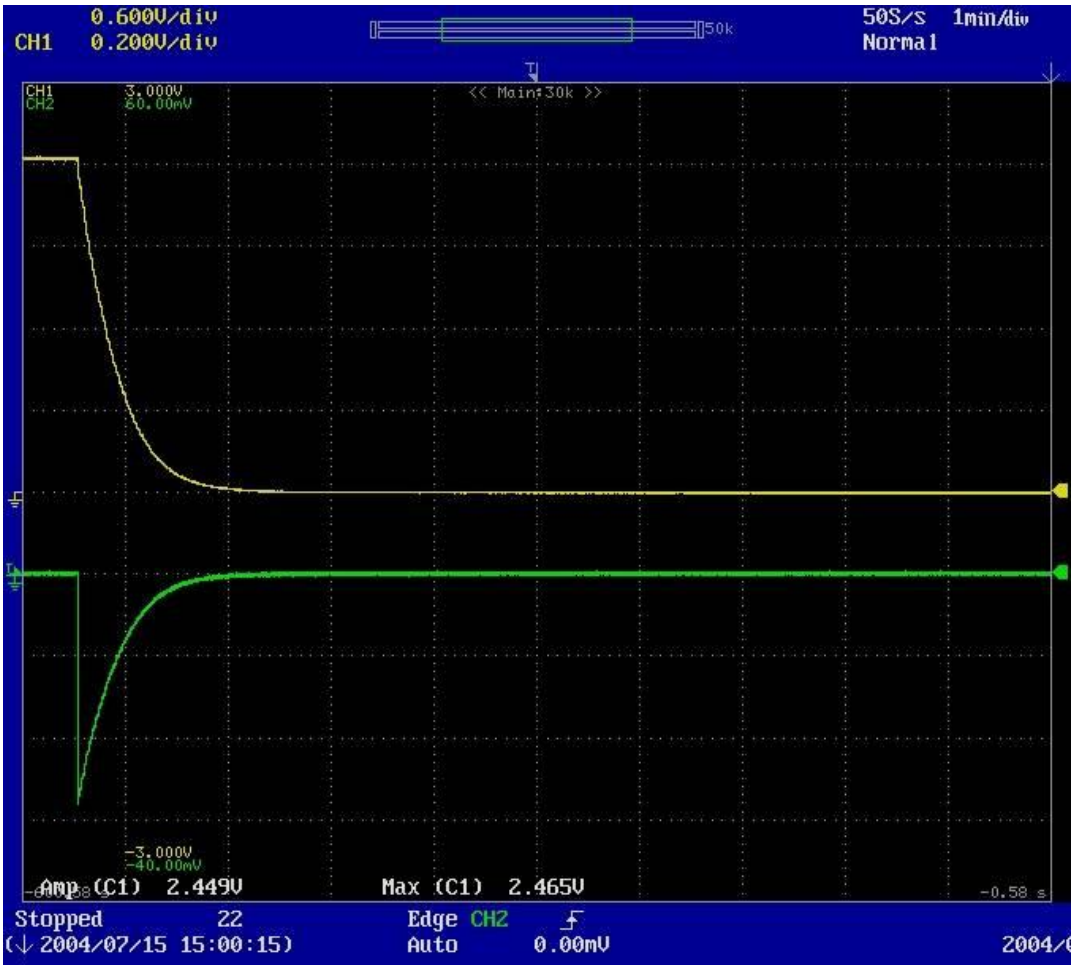

Figure A1.3-15: Oscilloscope Screen Capture of 60 A Discharge Cycle at T= 50°C (Timescale: 1 min/div)

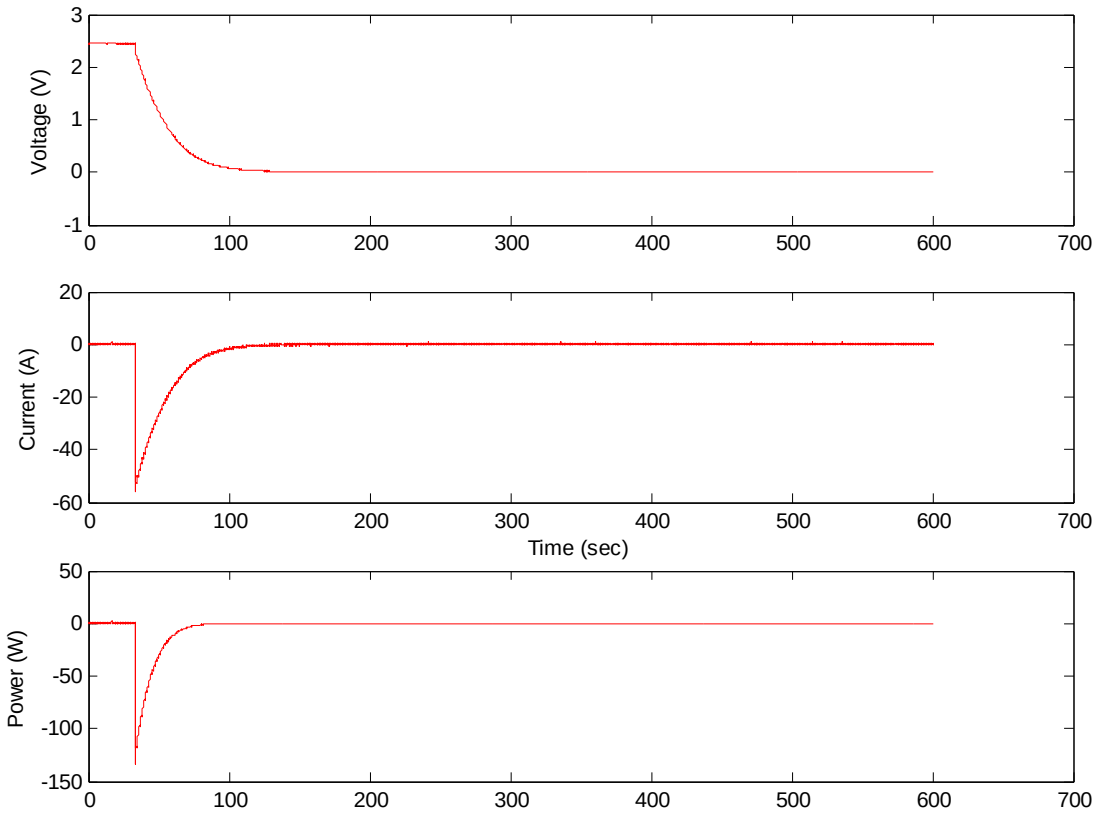

Figure A1.3-16: Plotted Matlab Data of 60 A Discharge Cycle at T= 50^{o}C

A2. 900 F Ultracapacitor Experiment Results

The results for the 900 F are shown in this section. The results are broken into three sub-categories that are based on the current charge and discharge levels. Within each current level, there are four temperatures: -25°C, 0°C, 25°C and 50°C. After each oscilloscope screen capture is the corresponding Matlab plots of the data.

A2.1 900 F 25 A Results

Figure A2.1-1: Oscilloscope Screen Capture of 25 A Charge Cycle at T= -25°C (Timescale: 1 min/div)

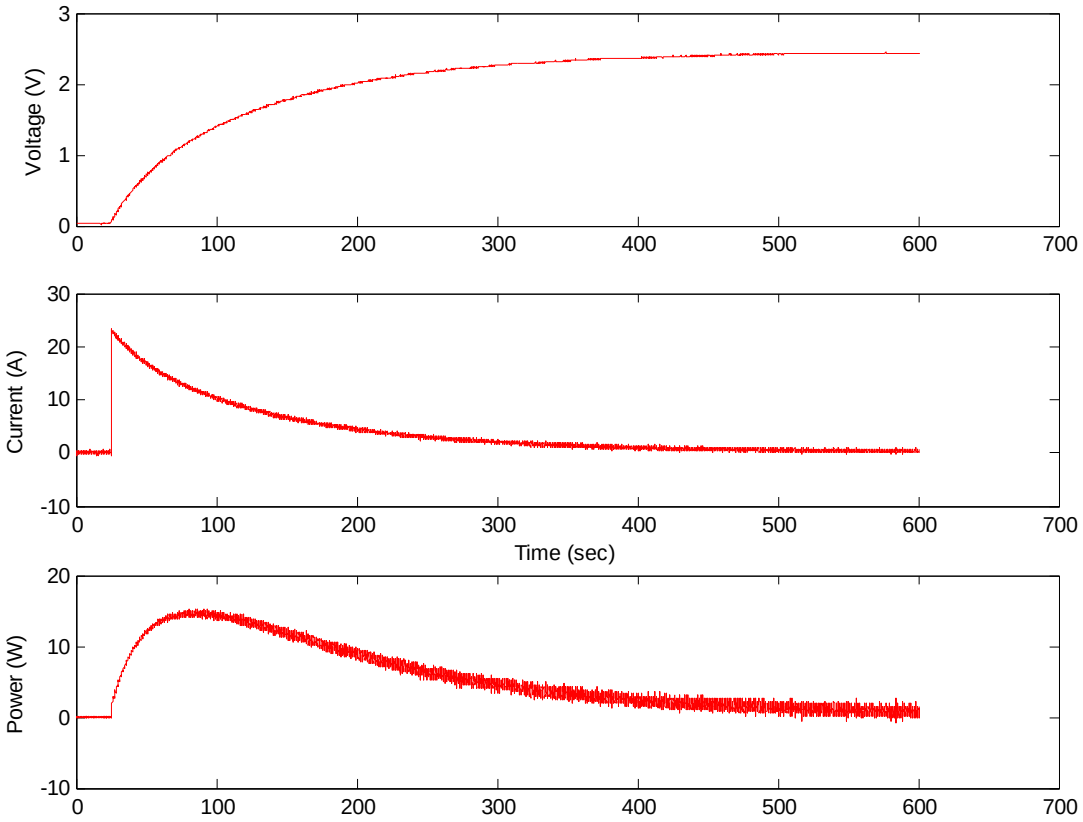

Figure A2.1-2: Plotted Matlab Data of 25 A Charge Cycle at T= -25°C

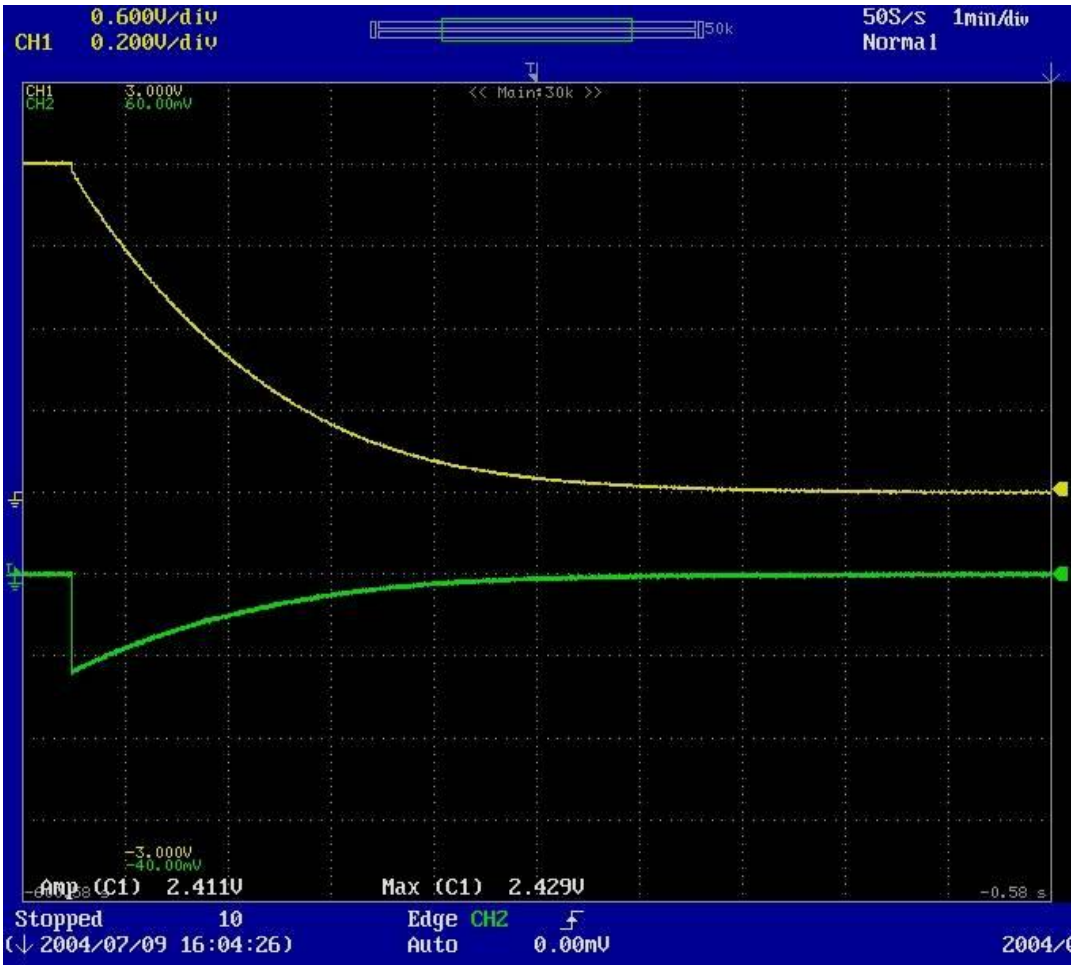

Figure A2.1-3: Oscilloscope Screen Capture of 25 A Discharge Cycle at T= -25°C (Timescale: 1 min/div)

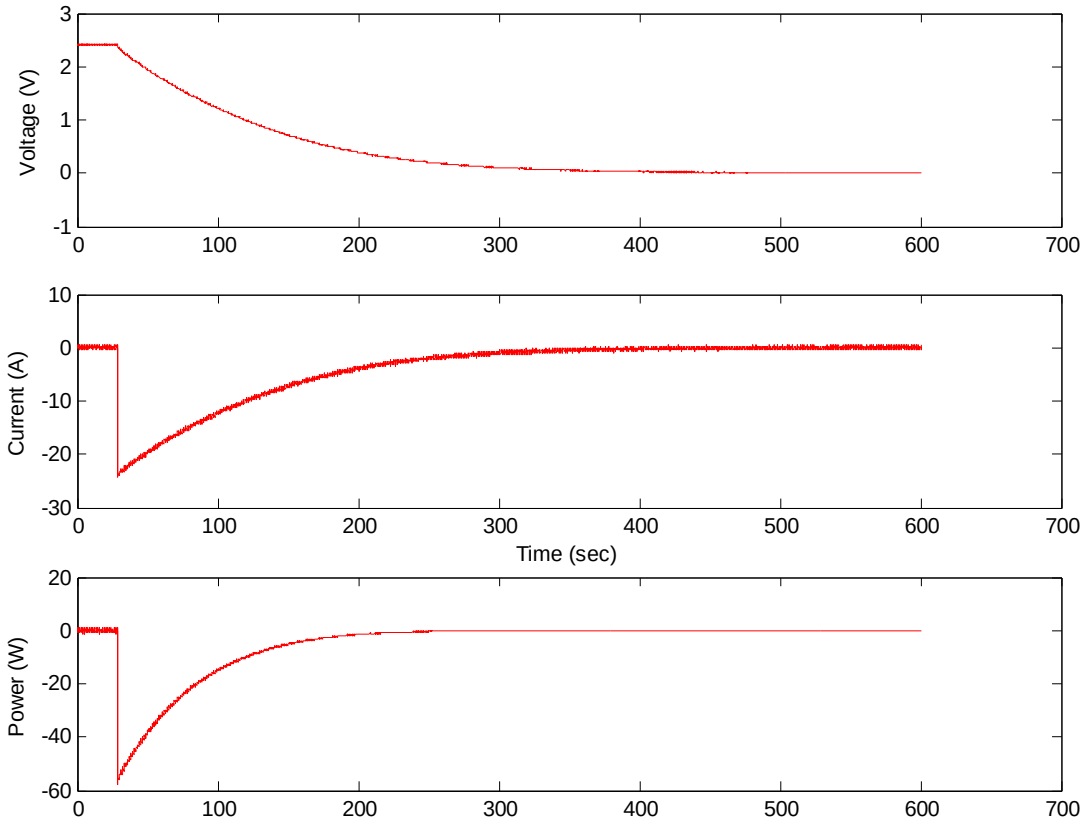

Figure A2.1-4: Plotted Matlab Data of 25 A Discharge Cycle at T= -25°C

Figure A2.1-5: Oscilloscope Screen Capture of 25 A Charge Cycle at T= 0^{o}C (Timescale: 1 min/div)

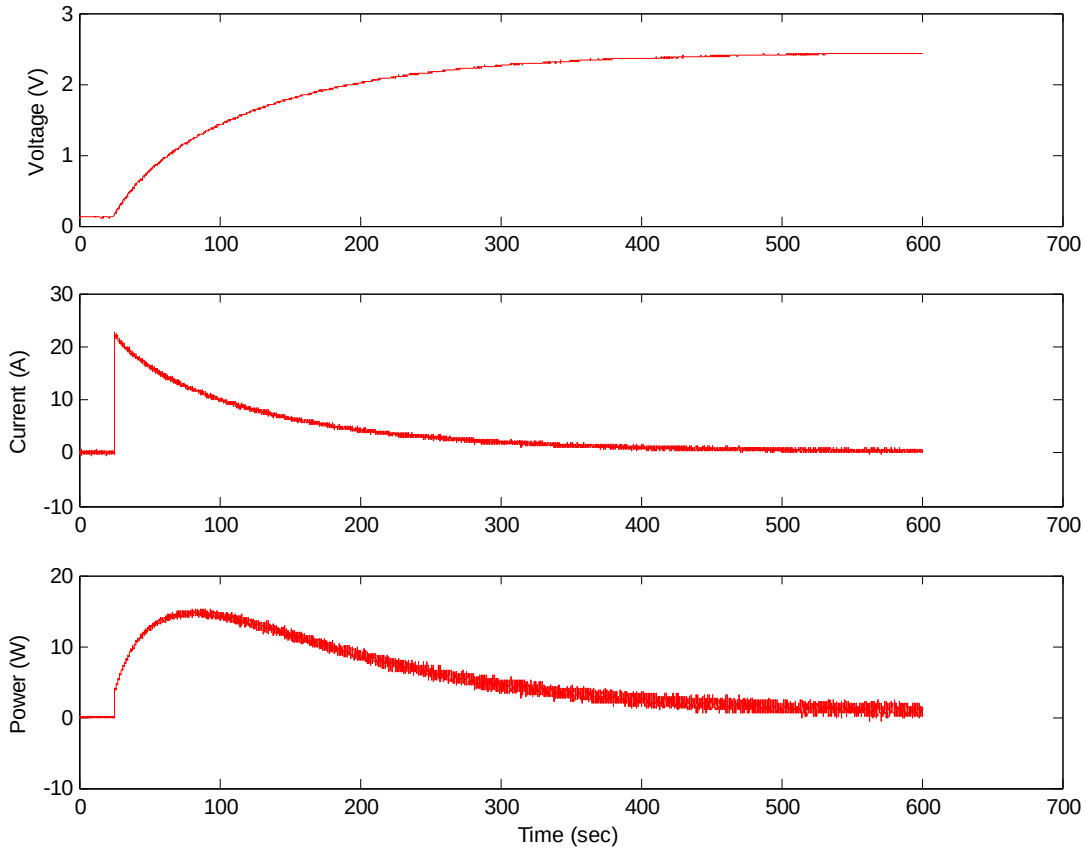

Figure A2.1-6: Plotted Matlab Data of 25 A Charge Cycle at T= 0°C

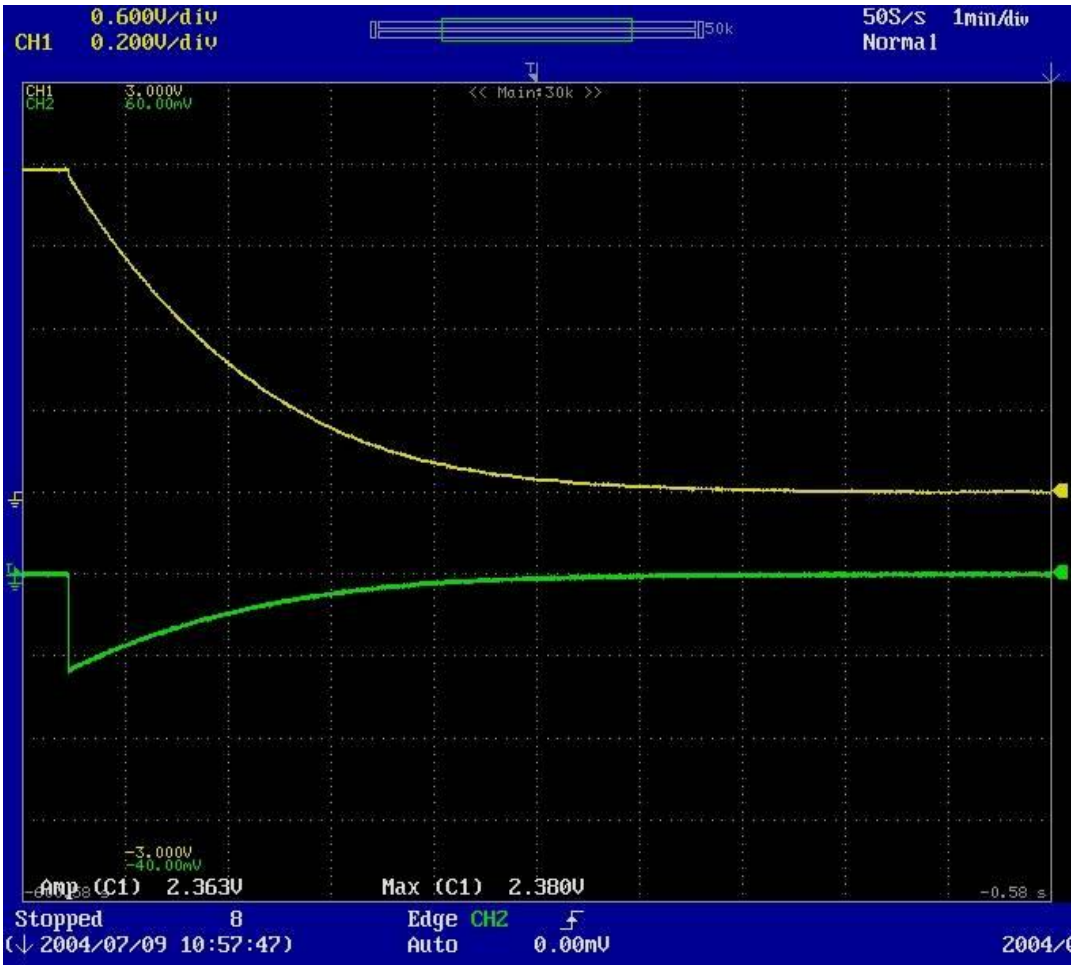

Figure A2.1-7: Oscilloscope Screen Capture of 25 A Discharge Cycle at T= 0^{o}C (Timescale: 1 min/div)

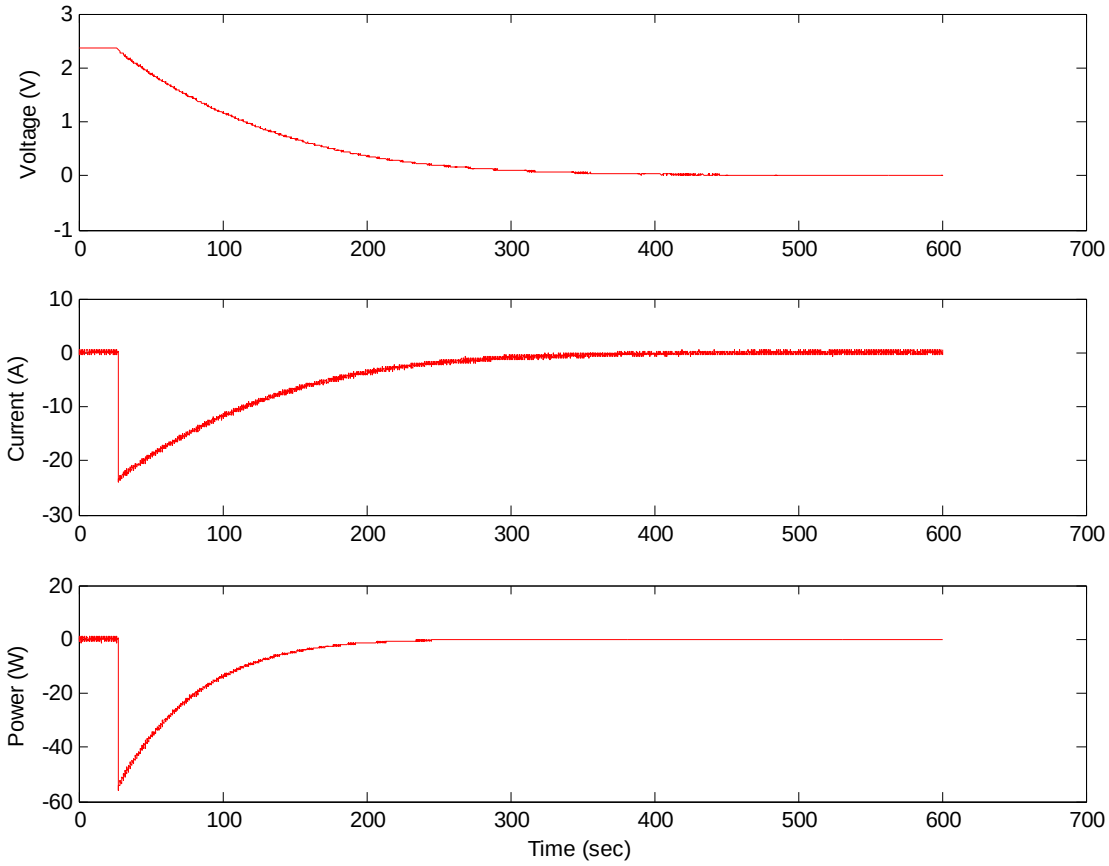

Figure A2.1-8: Plotted Matlab Data of 25 A Discharge Cycle at T= 0°C

Figure A2.1-9: Oscilloscope Screen Capture of 25 A Charge Cycle at T= 25°C (Timescale: 1 min/div)

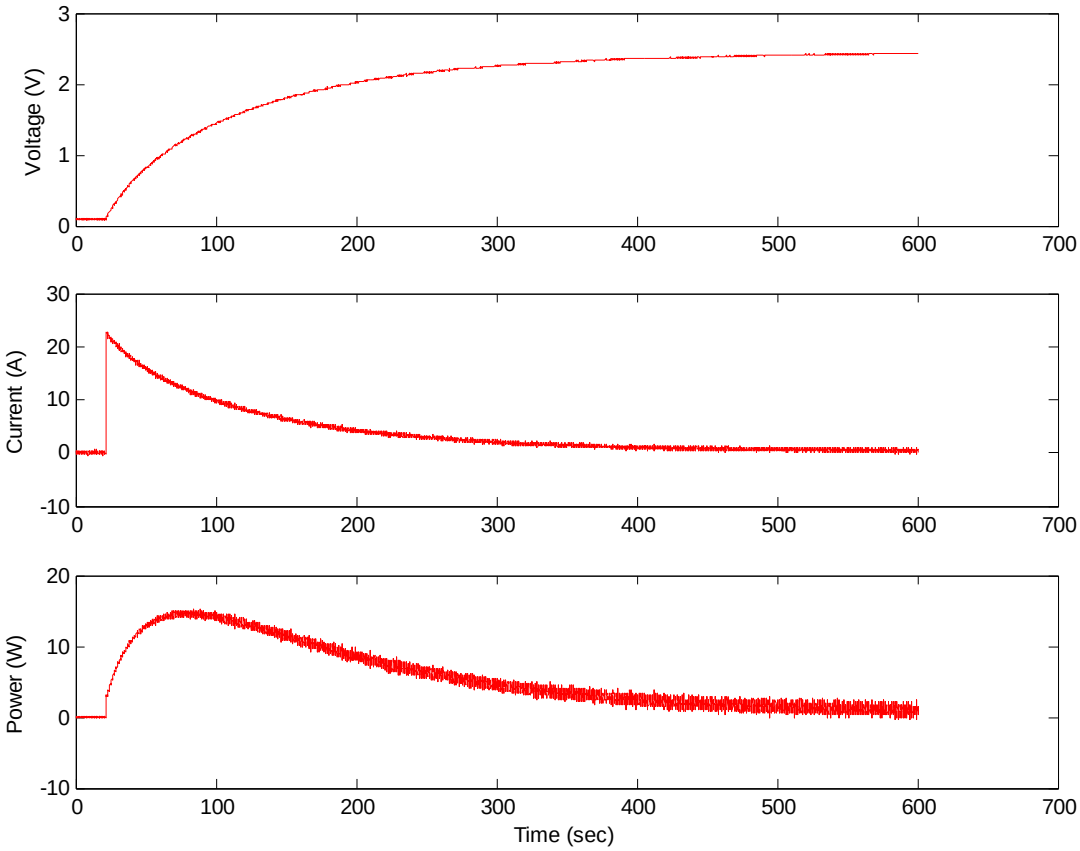

Figure A2.1-10: Plotted Matlab Data of 25 A Charge Cycle at T= 25°C

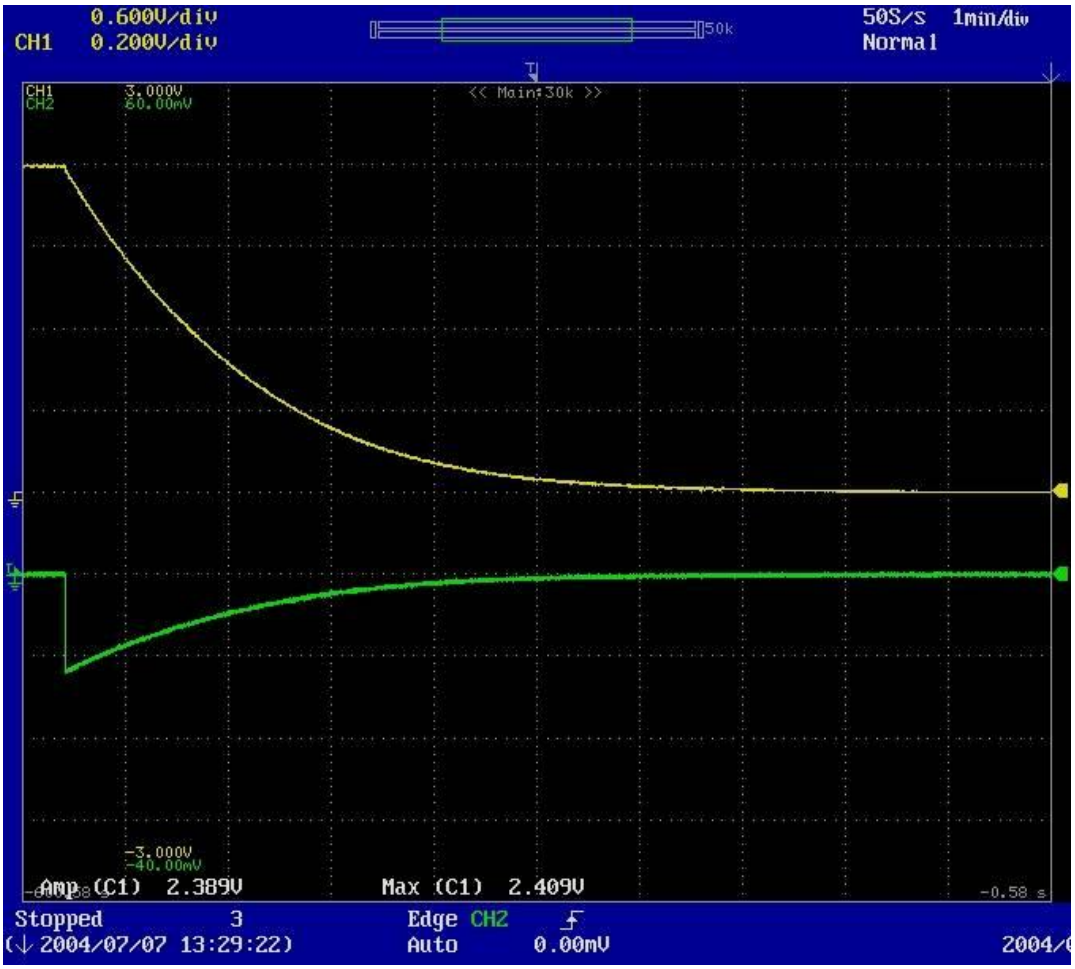

Figure A2.1-11: Oscilloscope Screen Capture of 25 A Discharge Cycle at T=25°C (Timescale: 1 min/div)

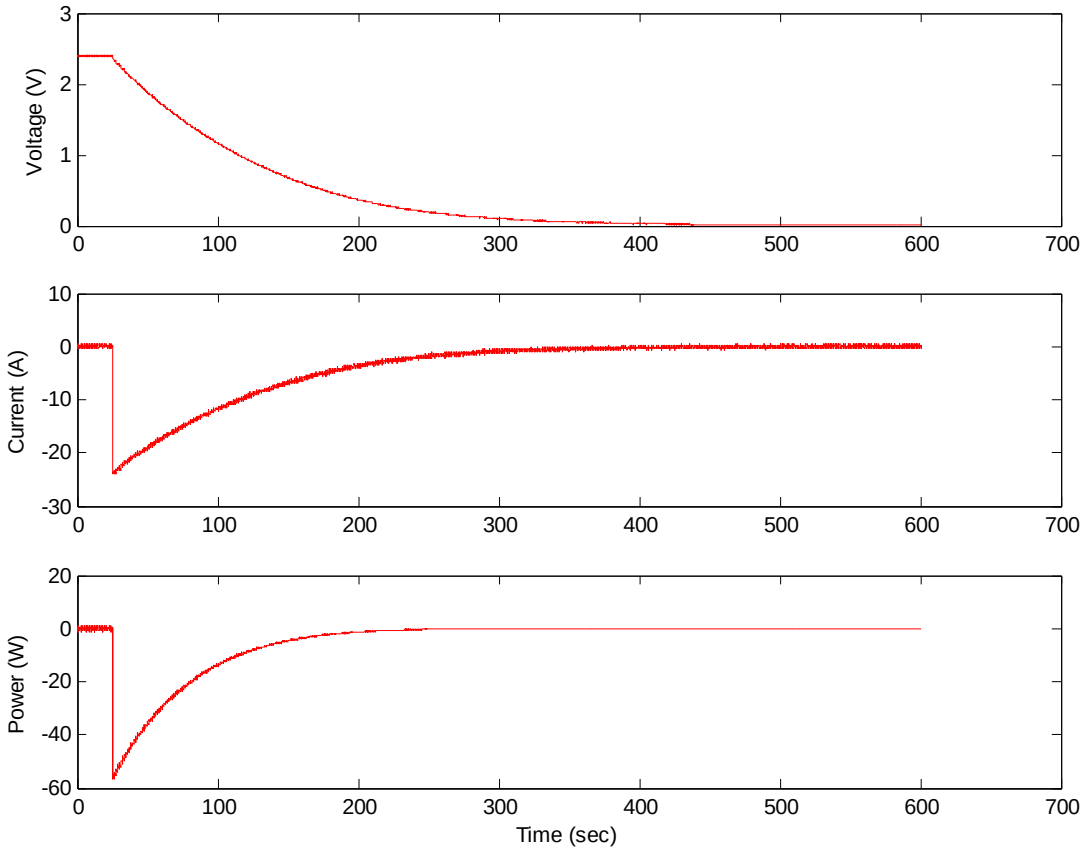

Figure A2.1-12: Plotted Matlab Data of 25 A Discharge Cycle at T=25°C

Figure A2.1-13: Oscilloscope Screen Capture of 25 A Charge Cycle at T= 50°C (Timescale: 1 min/div)

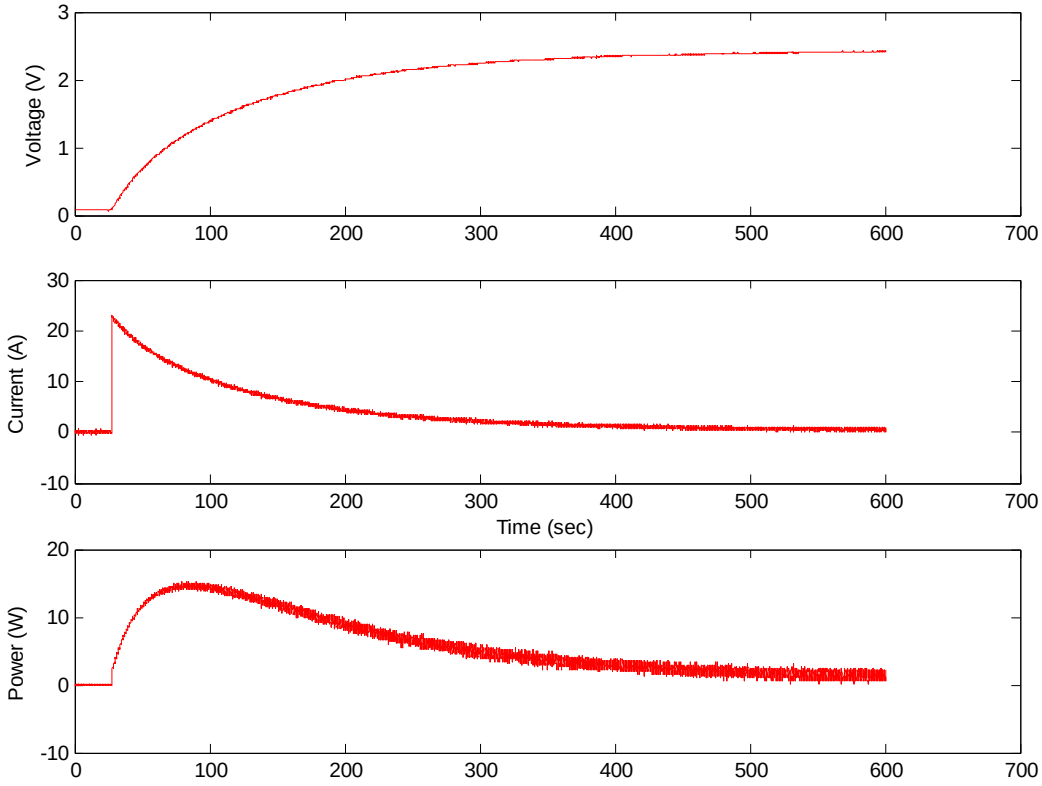

Figure A2.1-14: Plotted Matlab Data of 25 A Charge Cycle at T=50°C

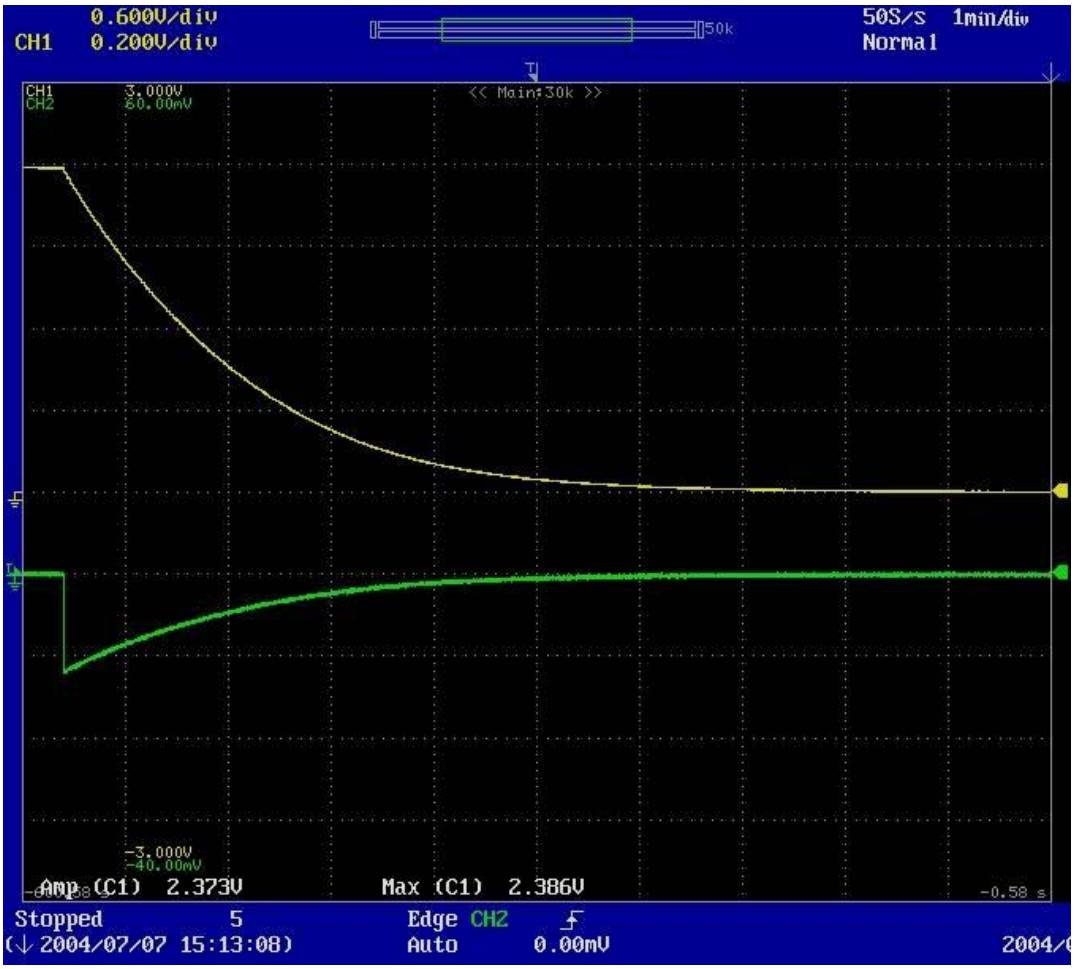

Figure A2.1-15: Oscilloscope Screen Capture of 25 A Discharge Cycle at T=50°C (Timescale: 1 min/div)

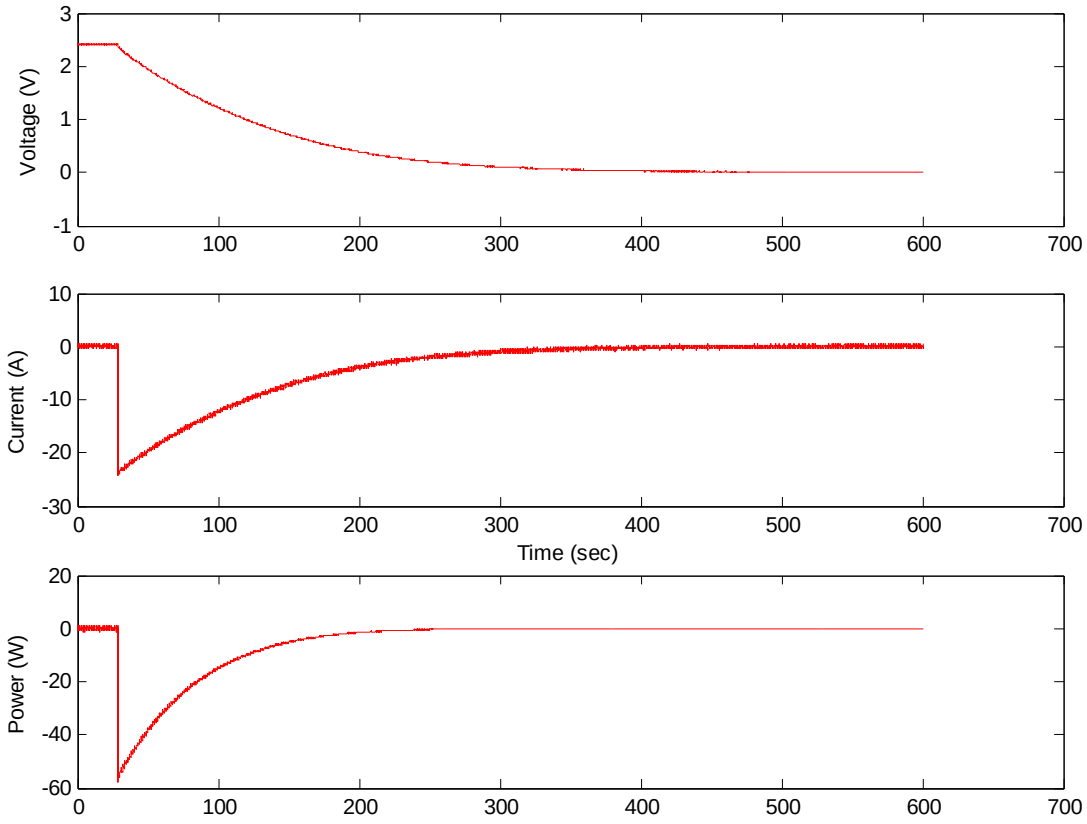

Figure A2.1-16: Plotted Matlab Data of 25 A Discharge Cycle at T=50°C

Figure A2.2-1: Oscilloscope Screen Capture of 50 A Charge Cycle at T= -25°C (Timescale: 1 min/div)

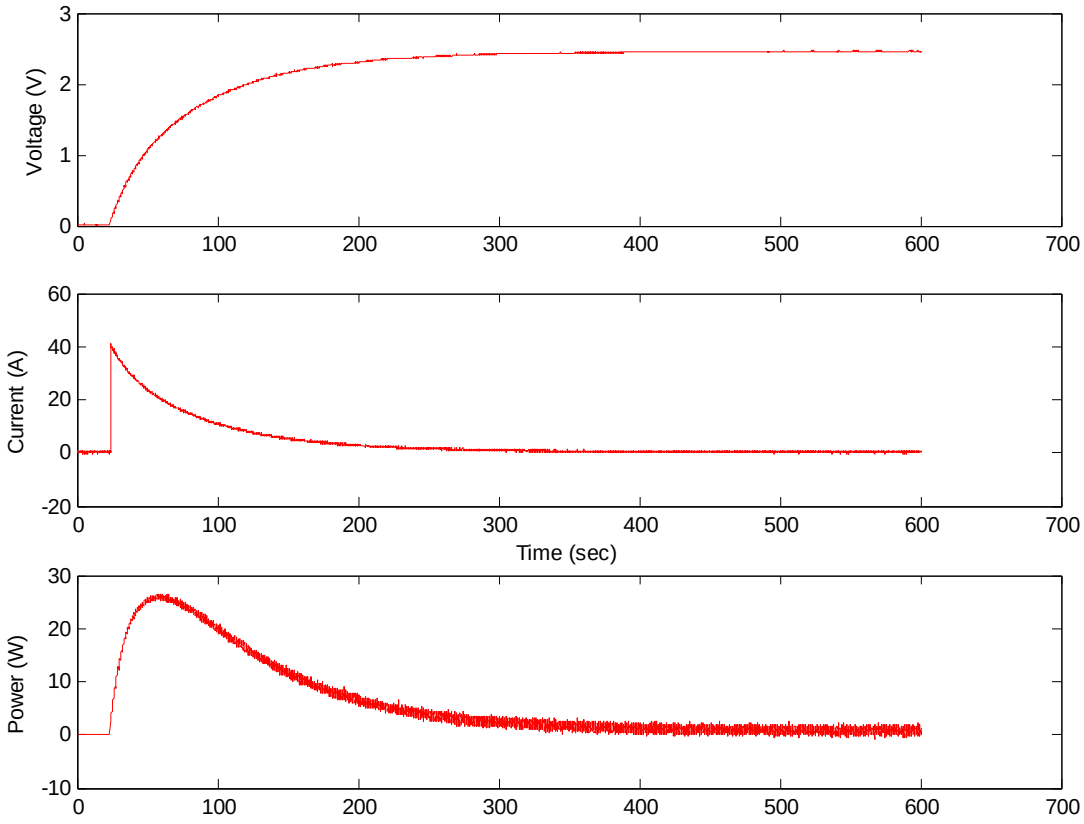

Figure A2.2-2: Plotted Matlab Data of 50 A Charge Cycle at T= -25°C

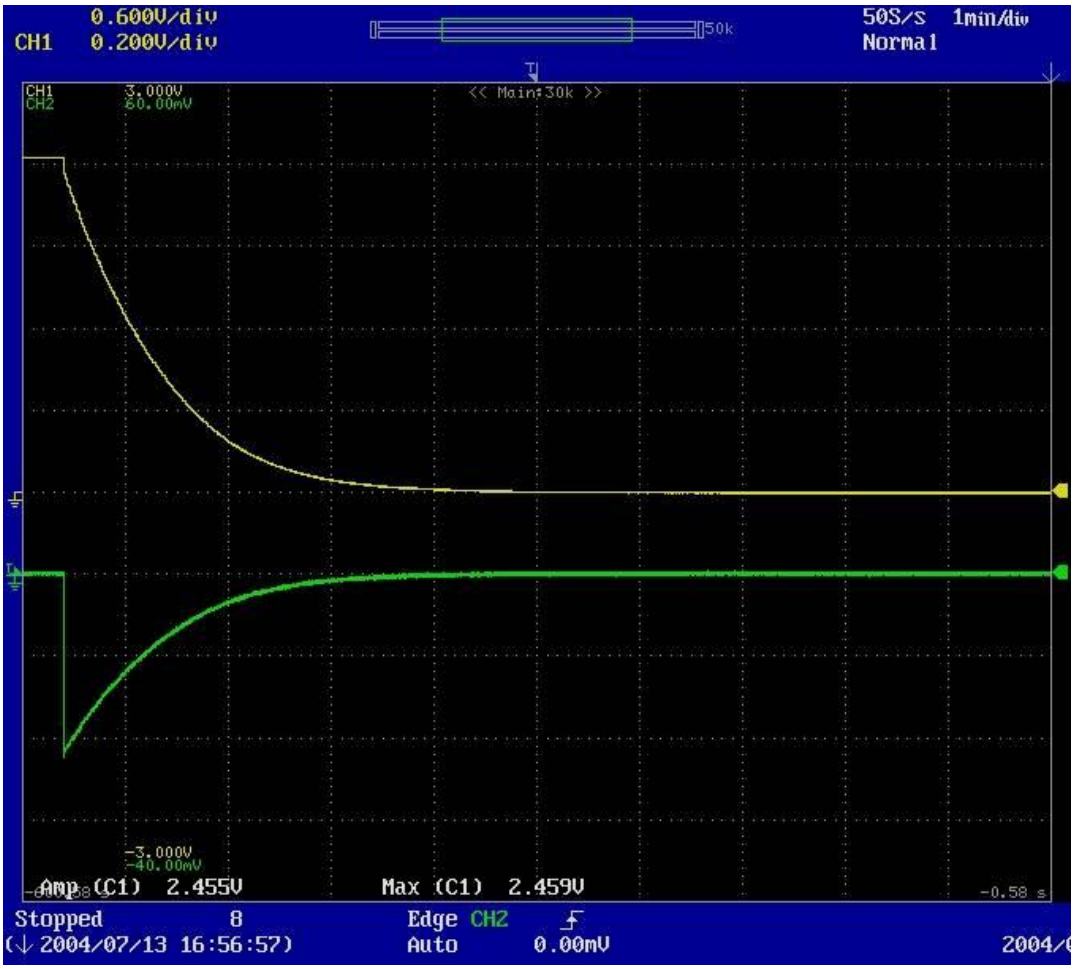

Figure A2.2-3: Oscilloscope Screen Capture of 50 A Discharge Cycle at T= -25°C (Timescale: 1 min/div)

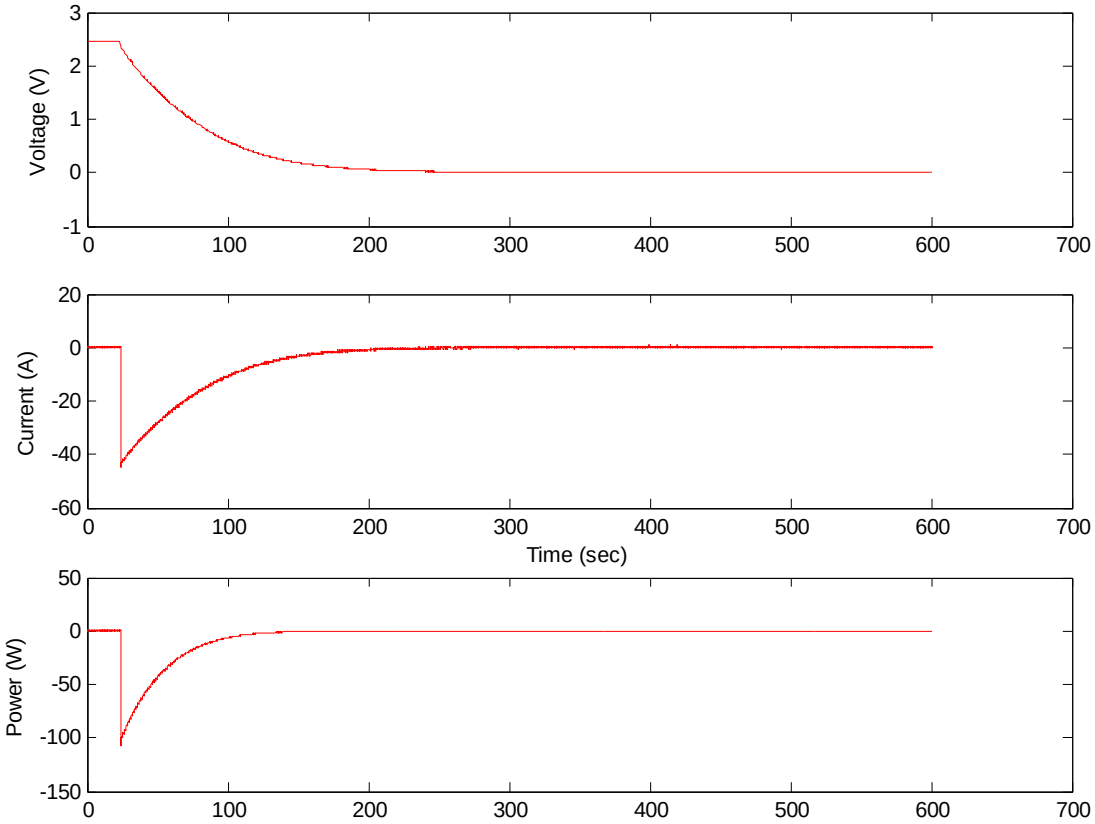

Figure A2.2-4: Plotted Matlab Data of 50 A Discharge Cycle at T= -25^{o}C

Figure A2-2-5: Oscilloscope Screen Capture of 50 A Charge Cycle at T= 0^{o}C (Timescale: 1 min/div)

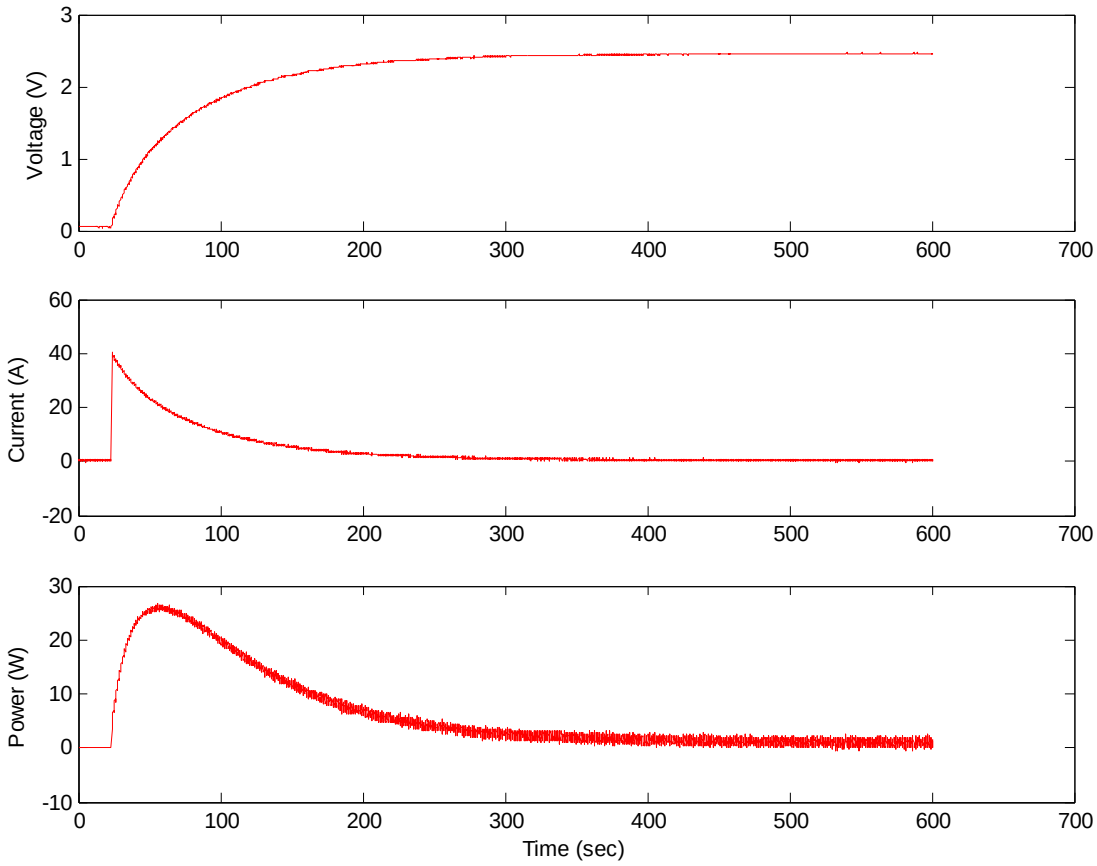

Figure A2.2-6: Plotted Matlab Data of 50 A Charge Cycle at T= 0°C

Figure A2.2-7: Oscilloscope Screen Capture of 50 A Discharge Cycle at T= 0^{o}C (Timescale: 1 min/div)

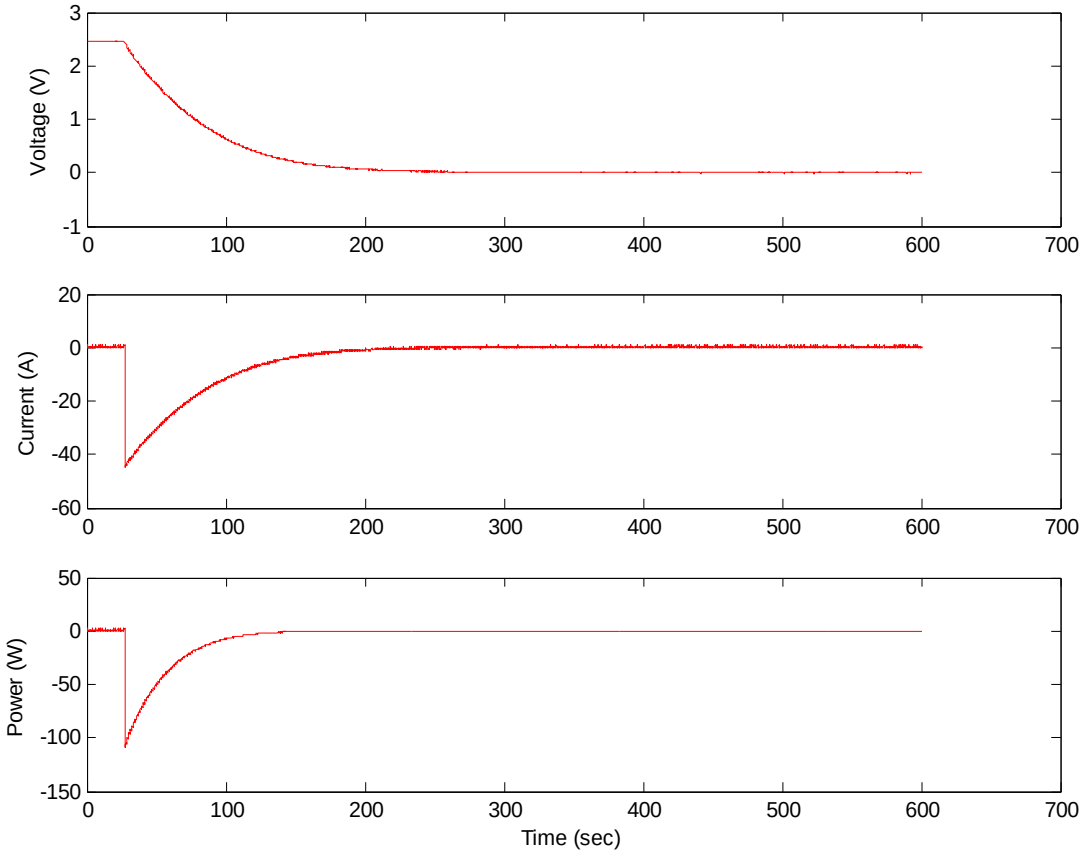

Figure A2.2-8: Plotted Matlab Data of 50 A Discharge Cycle at T= 0^{o}C

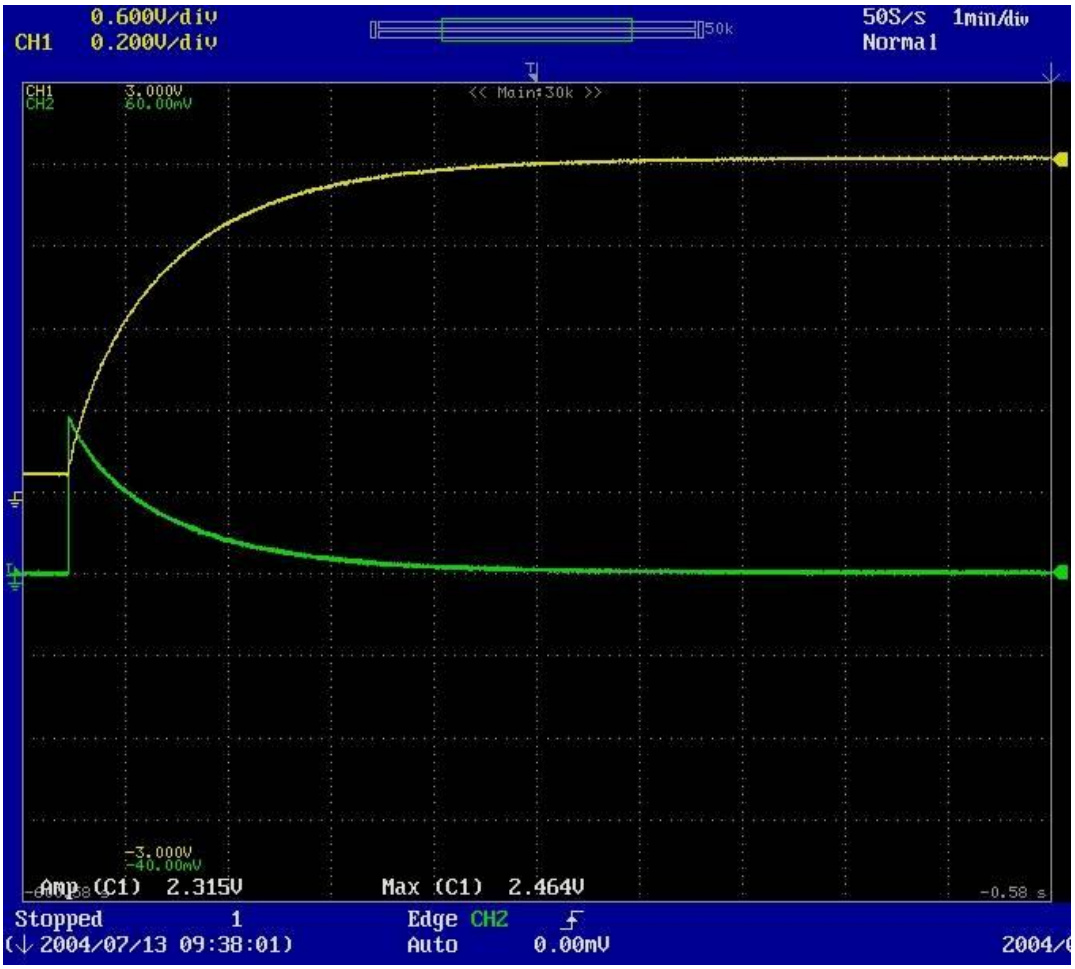

Figure A2.2-9: Oscilloscope Screen Capture of 50 A Charge Cycle at T= 25°C (Timescale: 1 min/div)

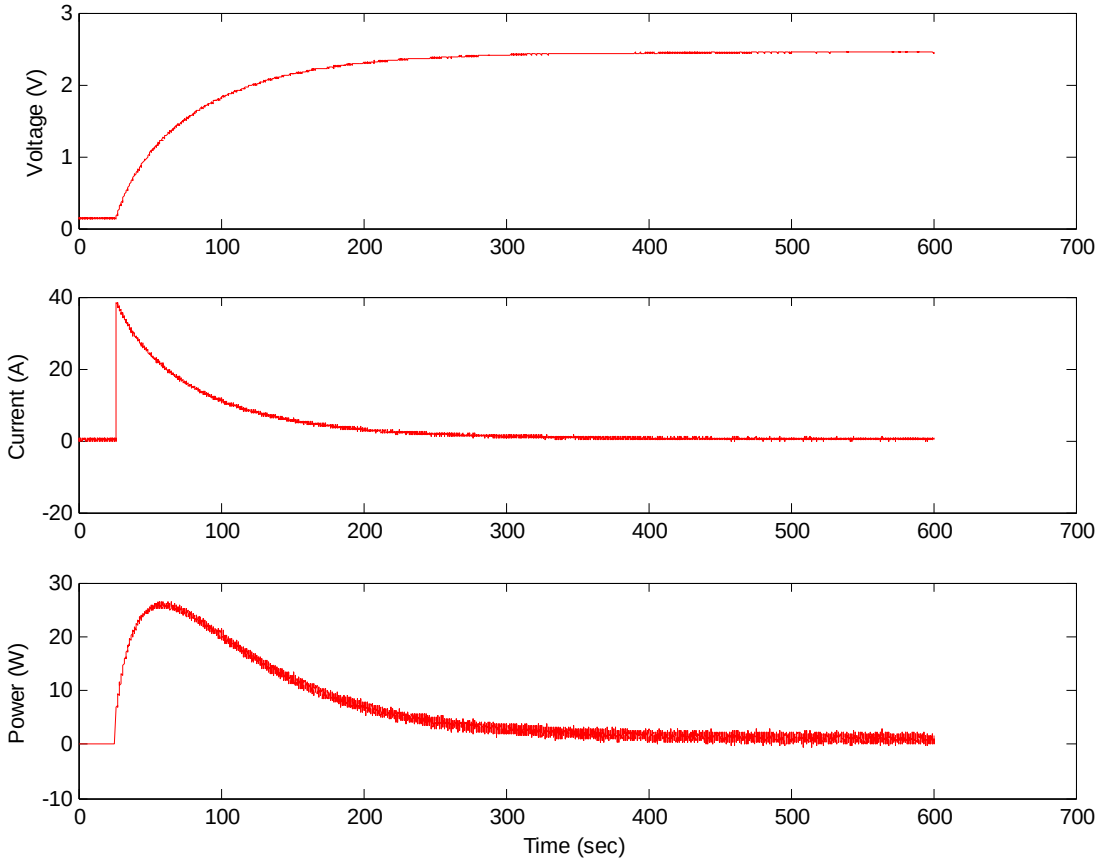

Figure A2.2-10: Plotted Matlab Data of 50 A Charge Cycle at T= 25°C

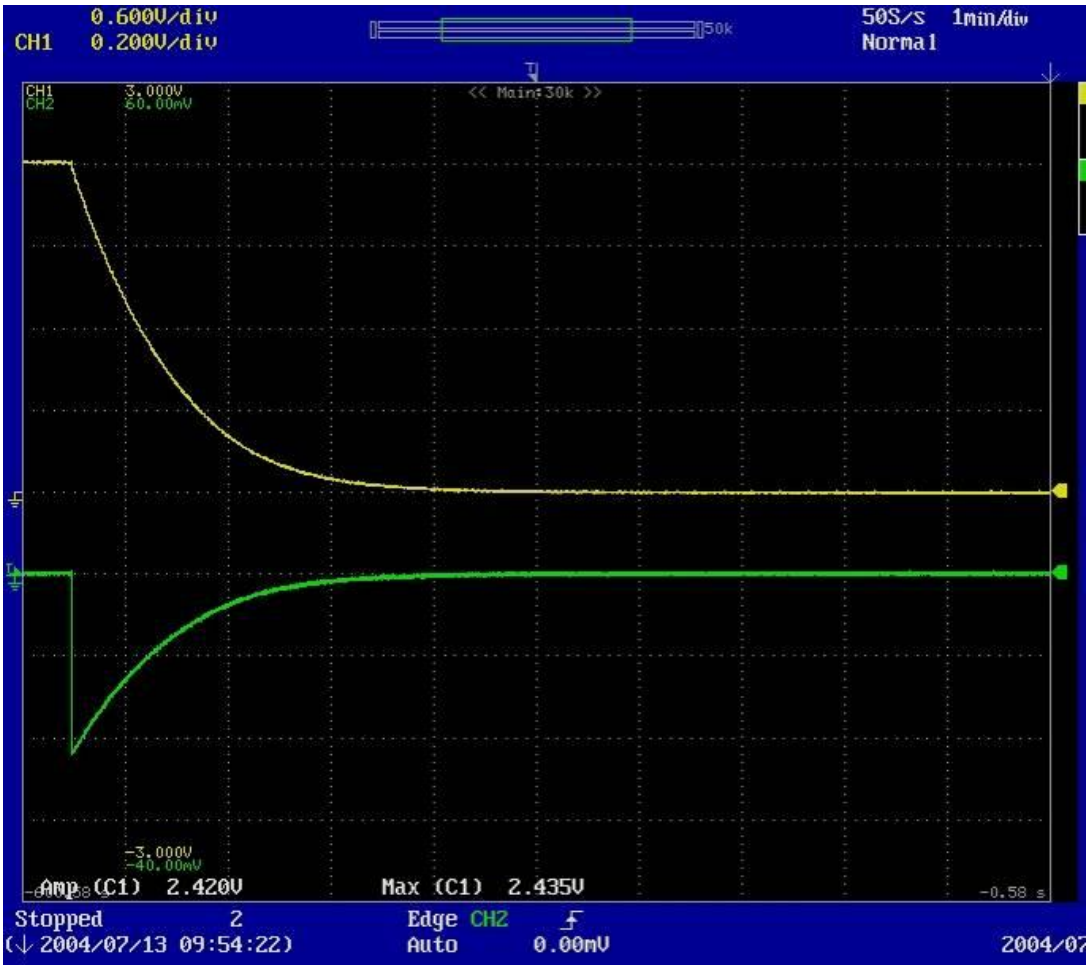

Figure A2.2-11: Oscilloscope Screen Capture of 50 A Discharge Cycle at T=25°C (Timescale: 1 min/div)

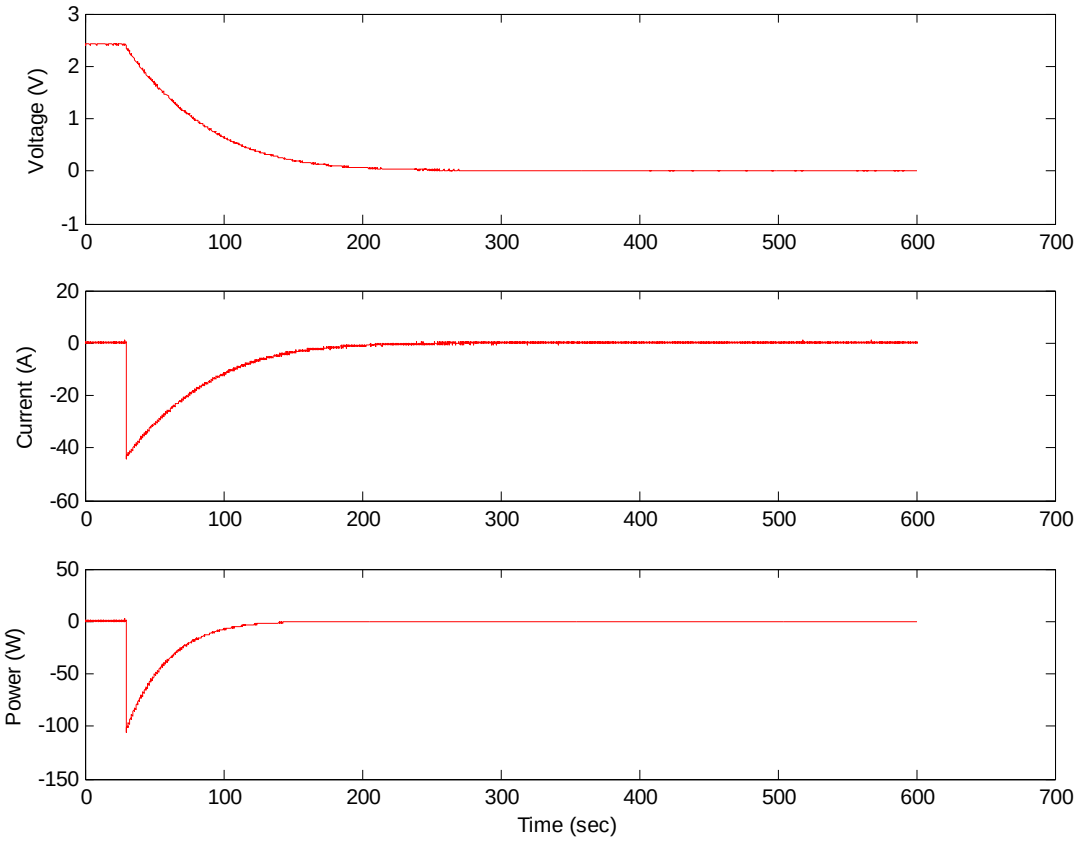

Figure A2.2-12: Plotted Matlab Data of 50 A Discharge Cycle at T= 25oC

Figure A2.2-13: Oscilloscope Screen Capture of 50 A Charge Cycle at T= 50°C (Timescale: 1 min/div)

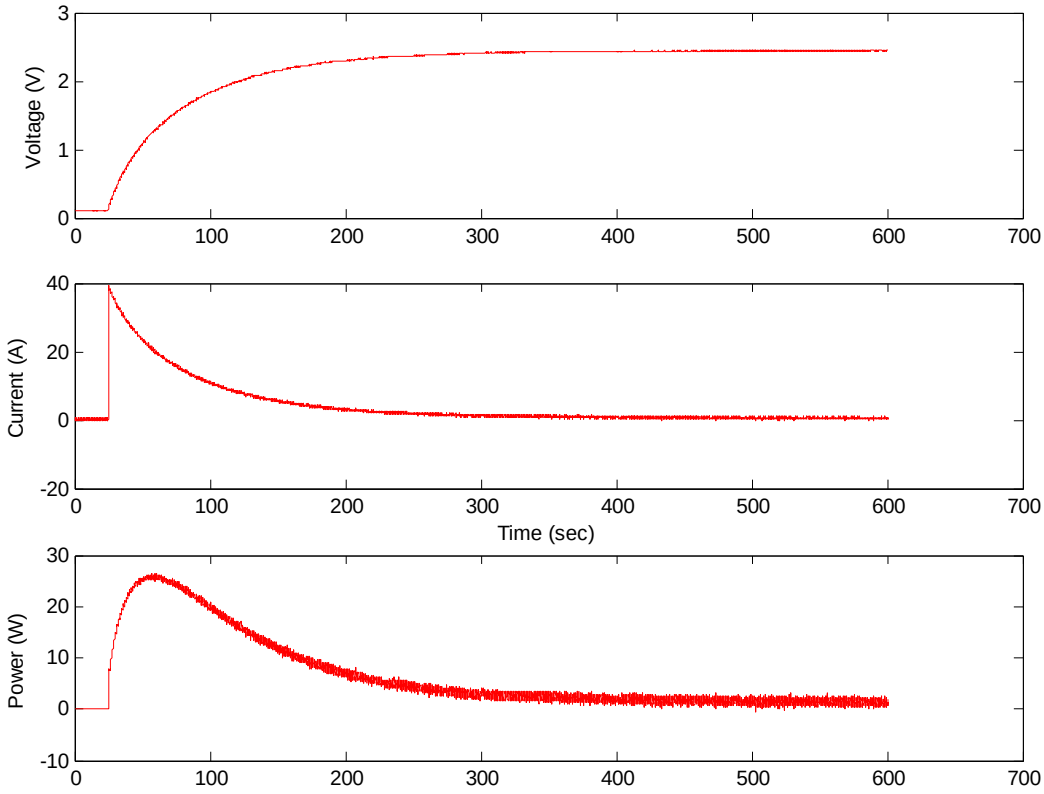

Figure A2.2-14: Plotted Matlab Data of 50 A Charge Cycle at T=50°C

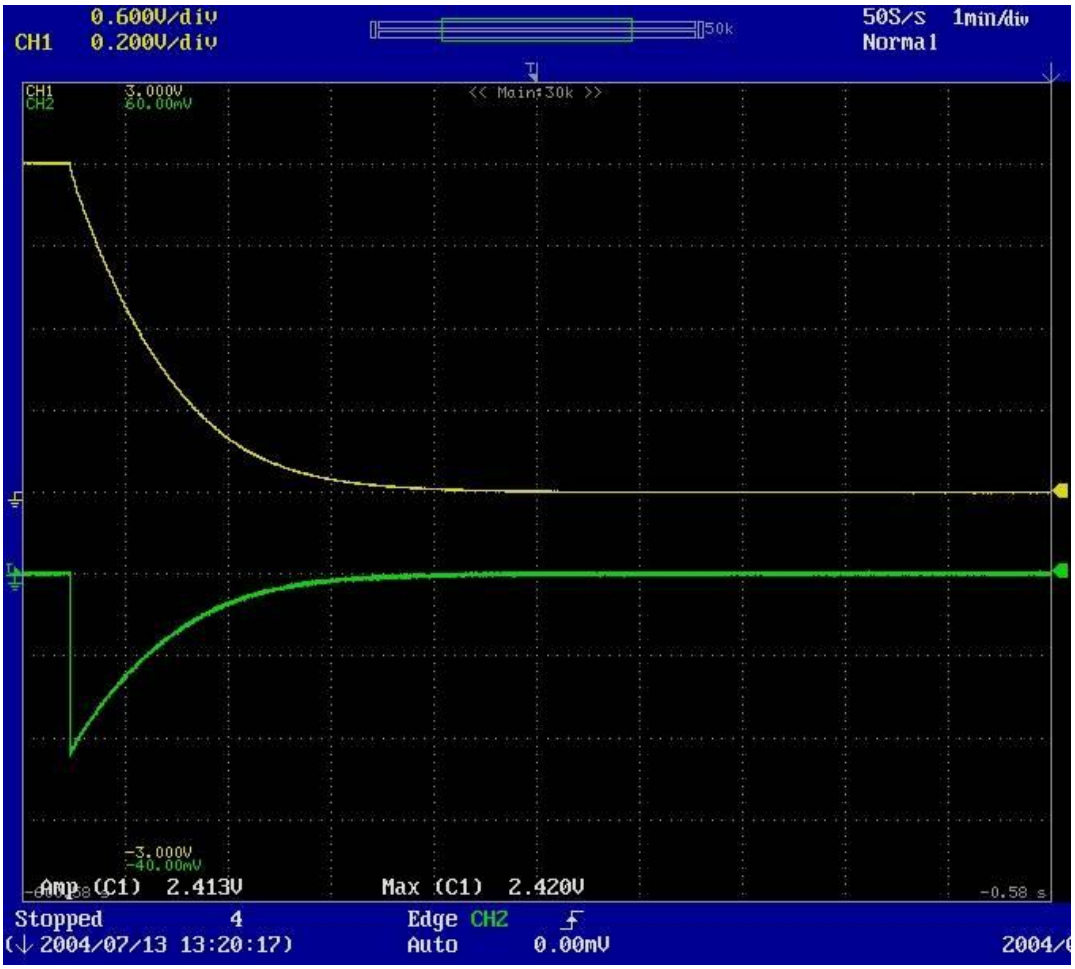

Figure A2.2-15: Oscilloscope Screen Capture of 50 A Discharge Cycle at T=50°C (Timescale: 1 min/div)

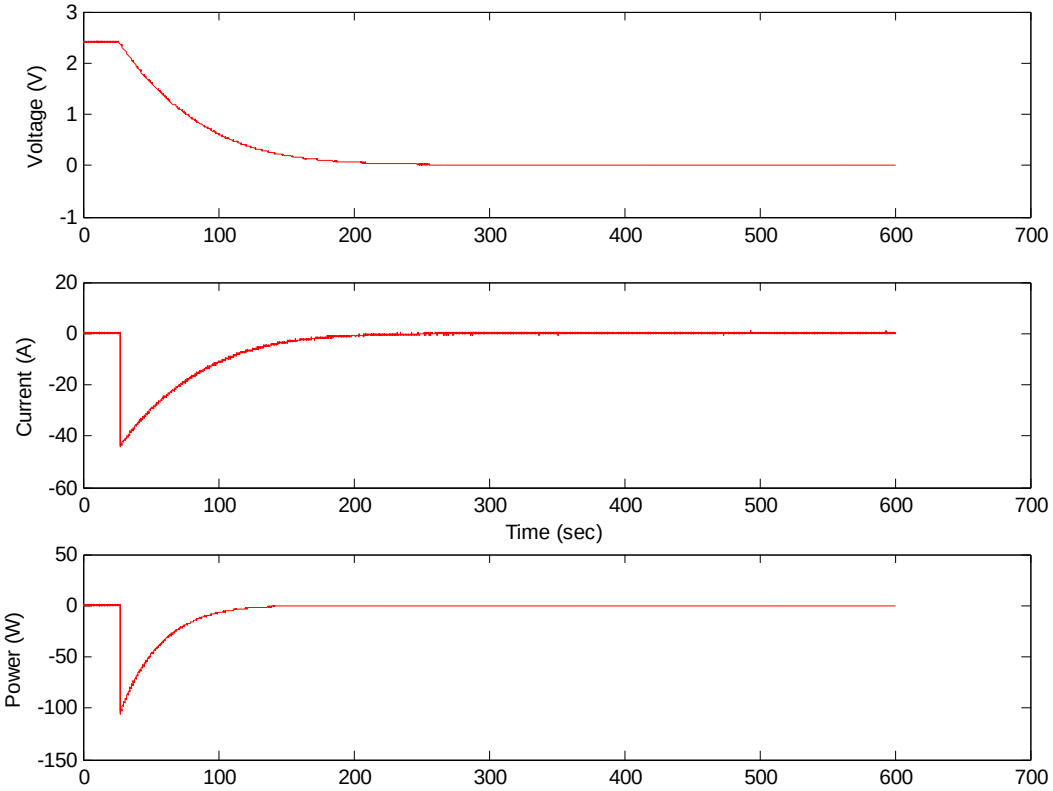

Figure A2.2-16: Plotted Matlab Data of 50 A Discharge Cycle at T=50°C

Figure A2.3-1: Oscilloscope Screen Capture of 60 A Charge Cycle at T= -25°C (Timescale: 1 min/div)

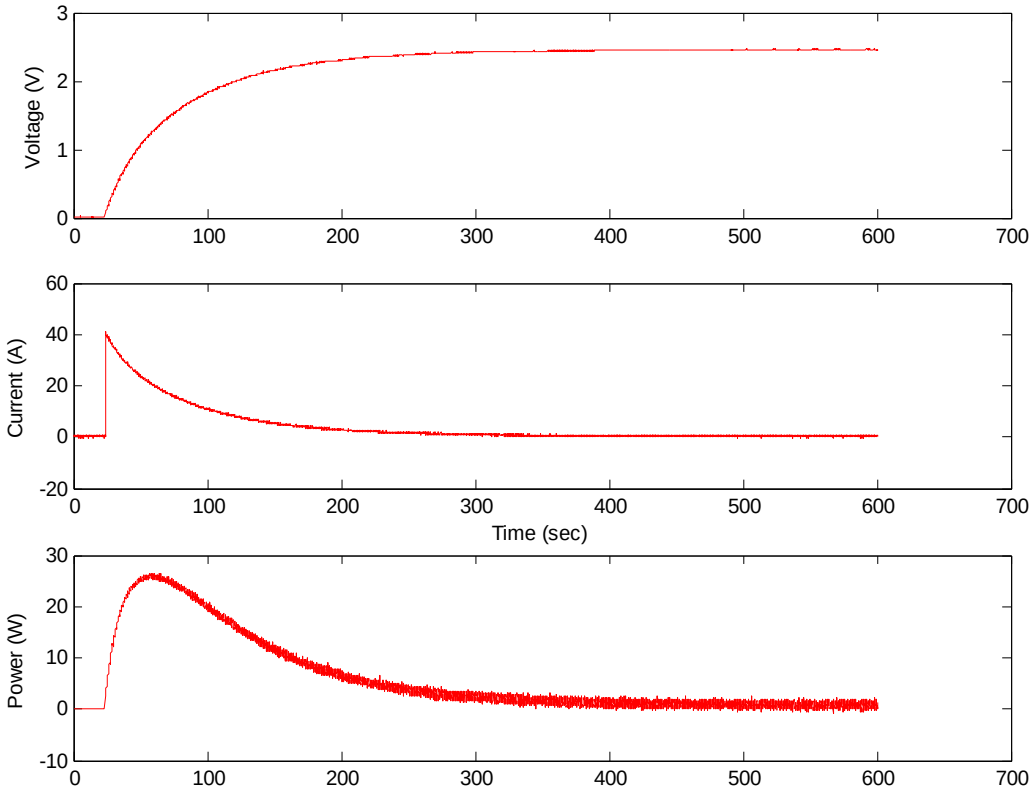

Figure A2.3-2: Plotted Matlab Data of 60 A Charge Cycle at T= -25°C

Figure A2.3-3: Oscilloscope Screen Capture of 60 A Discharge Cycle at T= -25°C (Timescale: 1 min/div)

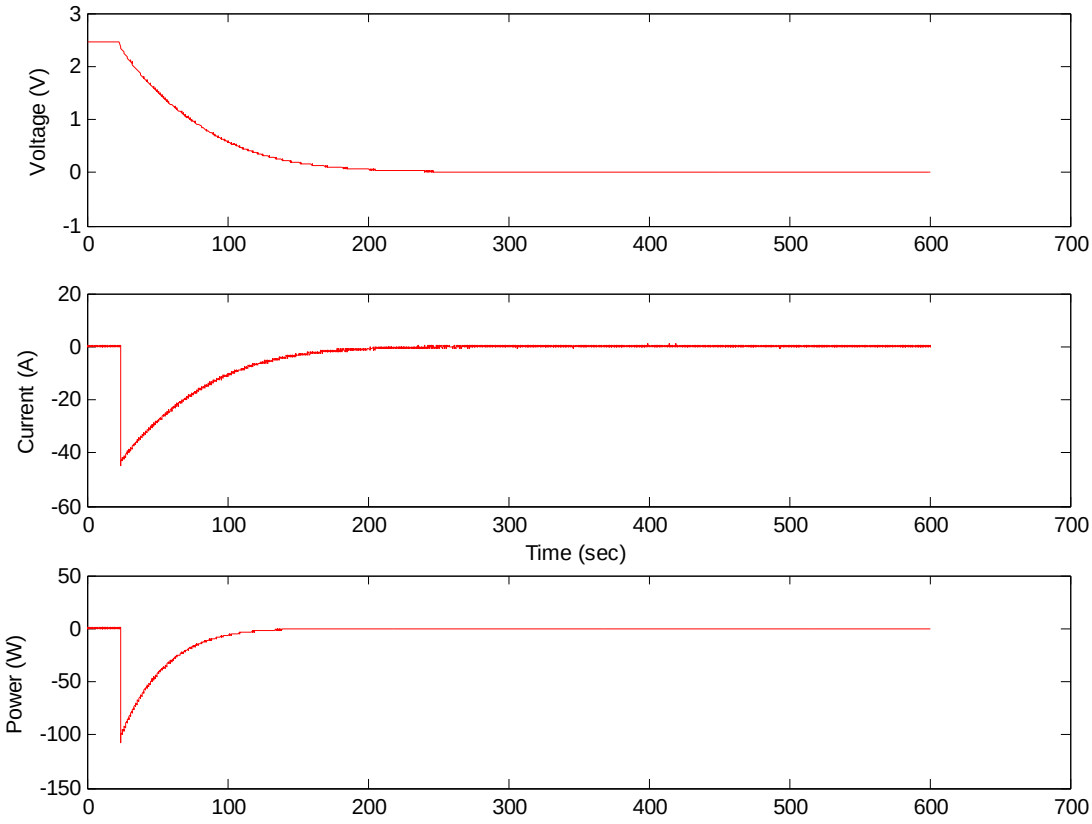

Figure A2.3-4: Plotted Matlab Data of 60 A Discharge Cycle at T= -25°C

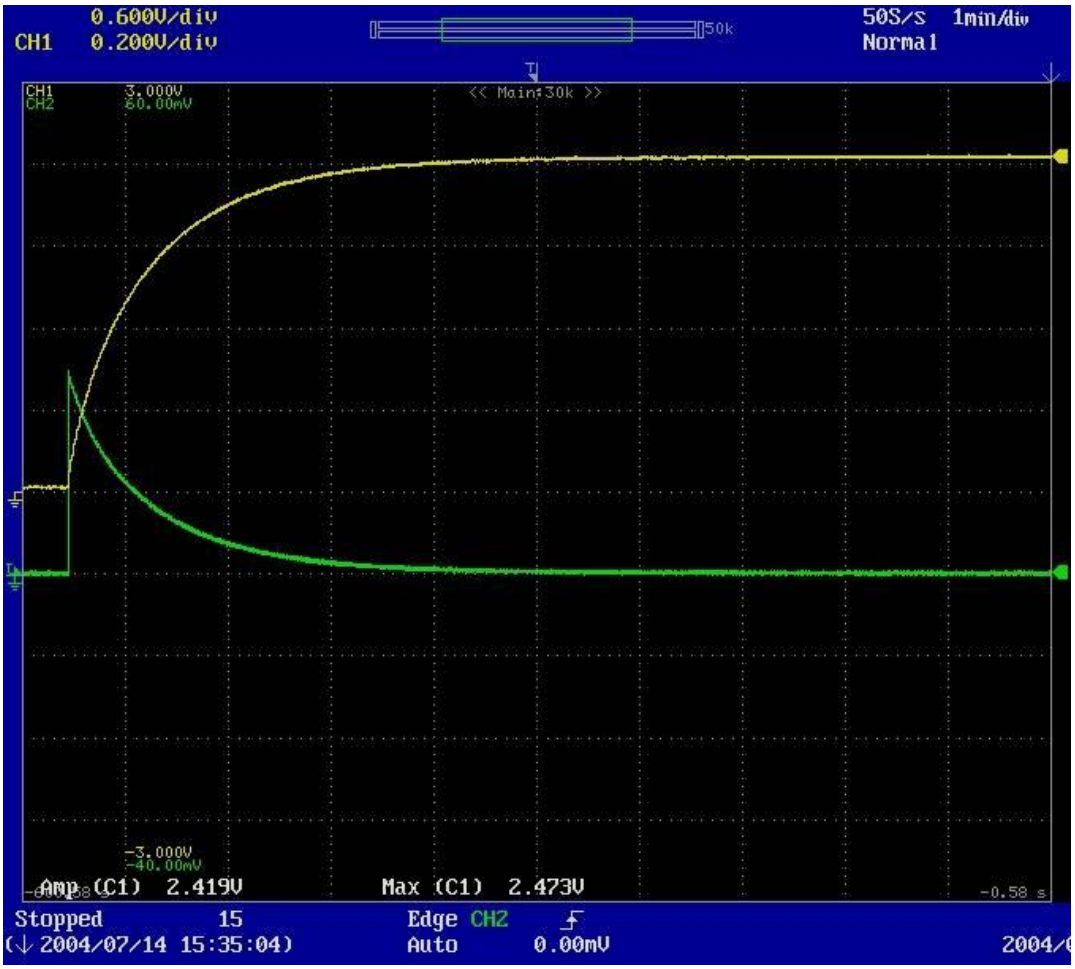

Figure A2.3-5: Oscilloscope Screen Capture of 60 A Charge Cycle at T= 0^{o}C (Timescale: 1 min/div)

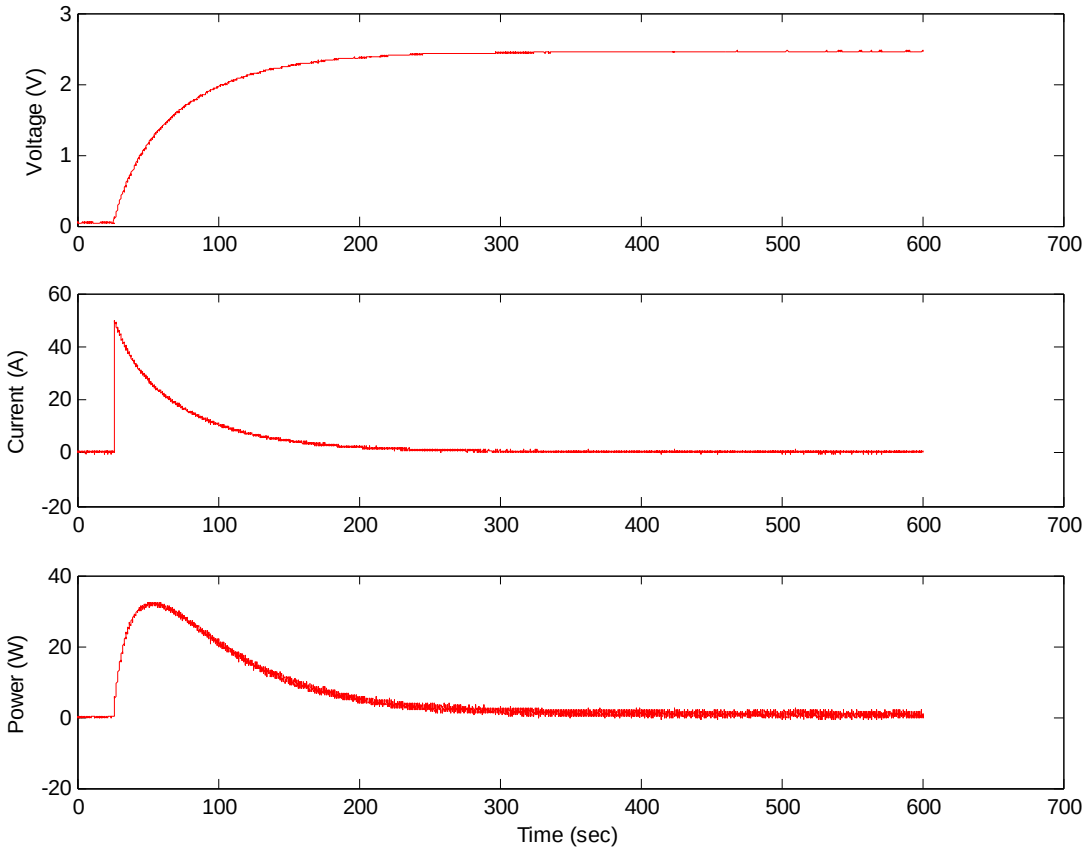

Figure A2.3-6: Plotted Matlab Data of 60 A Charge Cycle at T= 0^{o}C

Figure A2.3-7: Oscilloscope Screen Capture of 60 A Discharge Cycle at T= 0^{o}C (Timescale: 1 min/div)

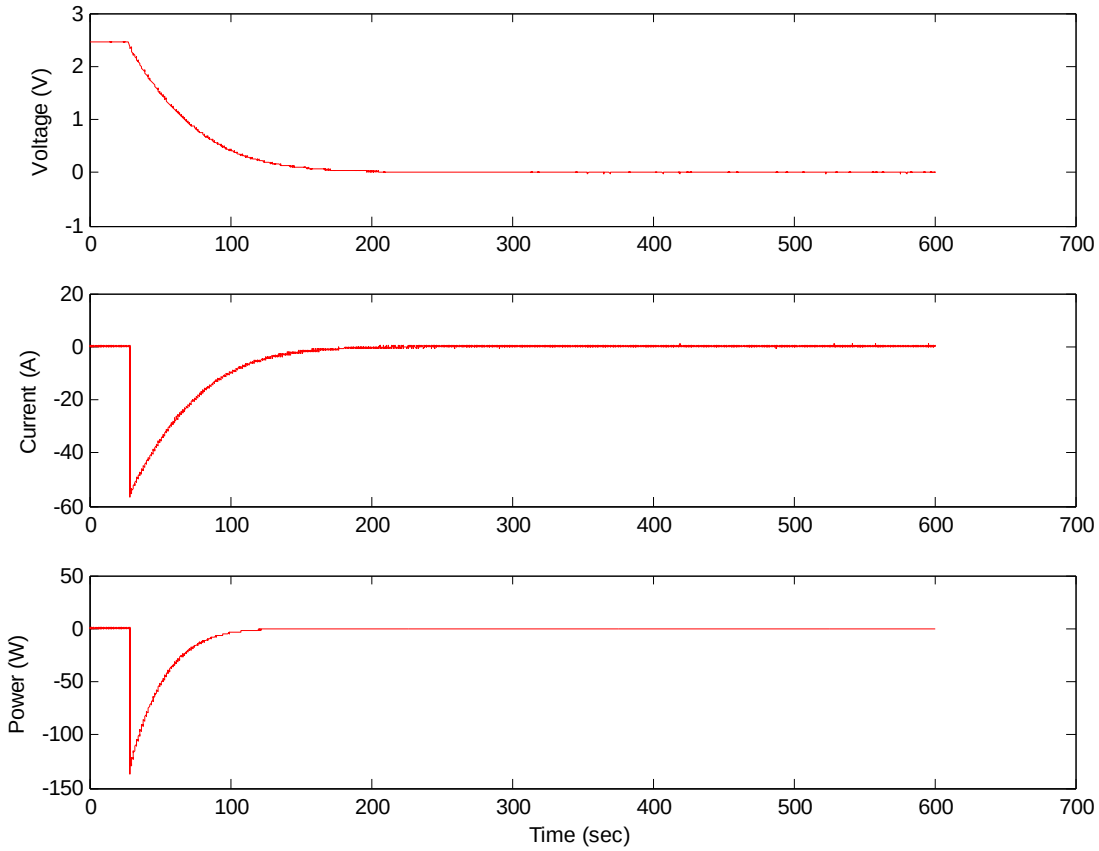

Figure A2.3-8: Plotted Matlab Data of 60 A Discharge Cycle at T= 0^{o}C

Figure A2.3-9: Oscilloscope Screen Capture of 60 A Charge Cycle at T= 25°C (Timescale: 1 min/div)

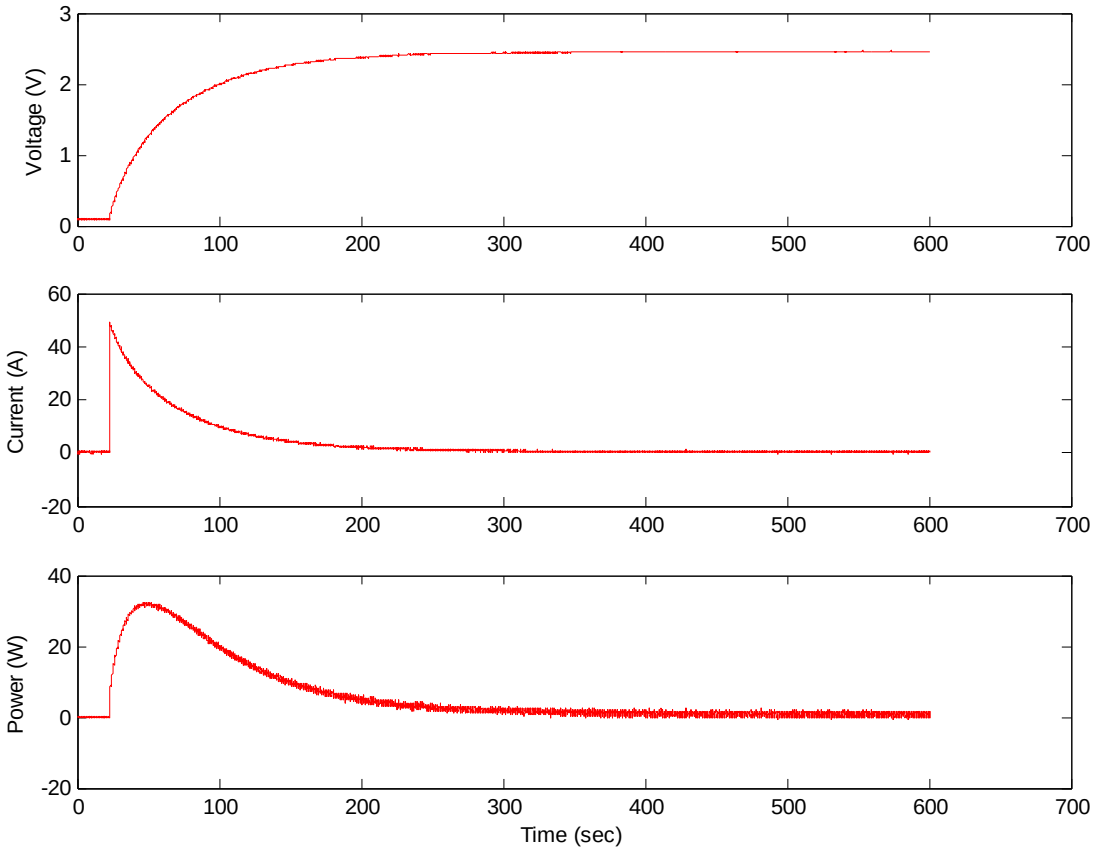

Figure A2.3-10: Plotted Matlab Data of 60 A Charge Cycle at T= 25°C

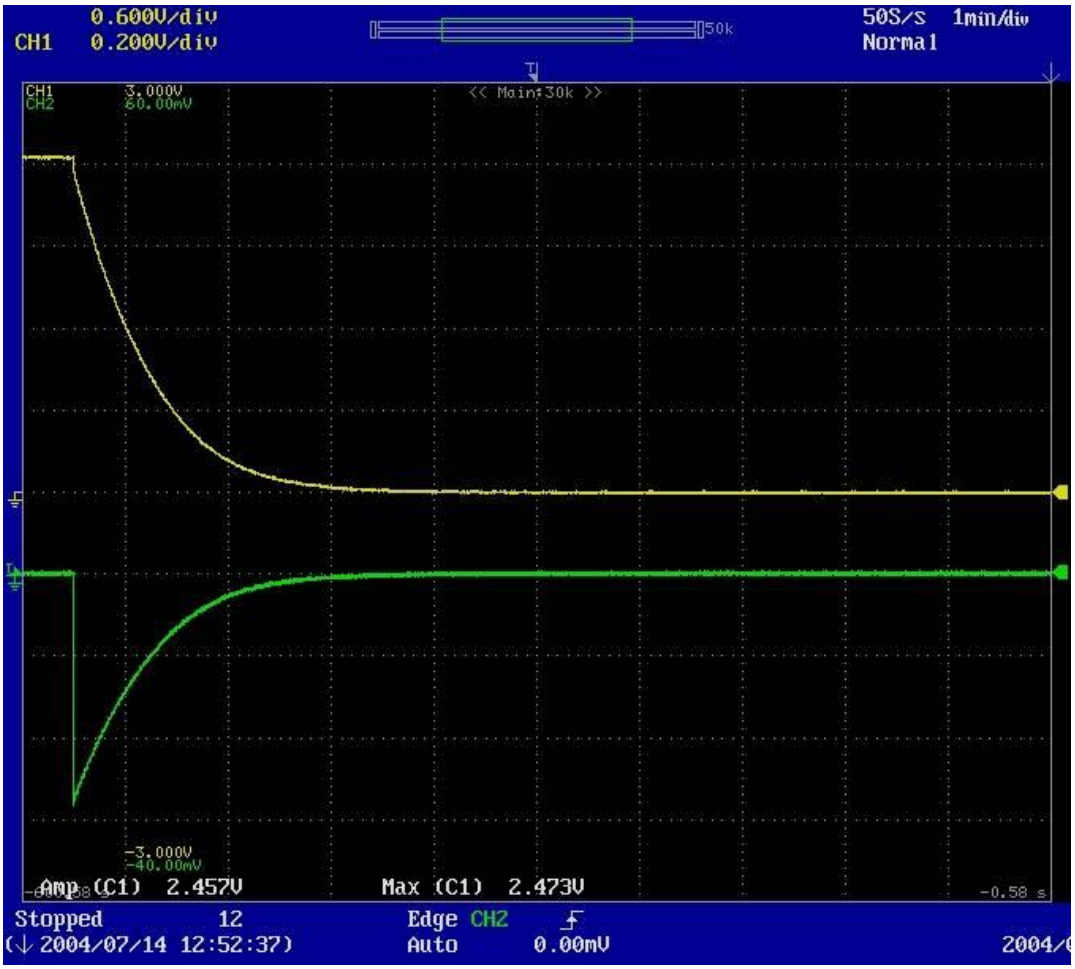

Figure A2.3-11: Oscilloscope Screen Capture of 60 A Discharge Cycle at T=25°C (Timescale: 1 min/div)

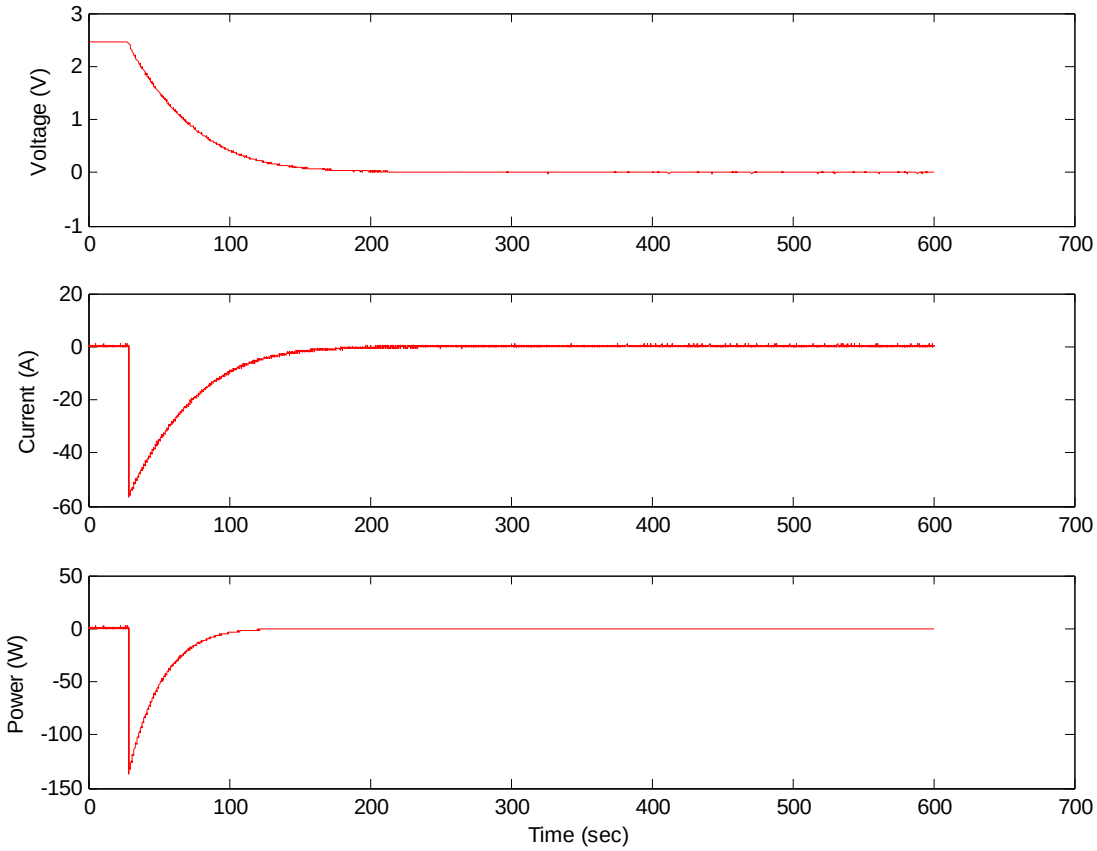

Figure A2.3-12: Plotted Matlab Data of 60 A Discharge Cycle at T=25°C

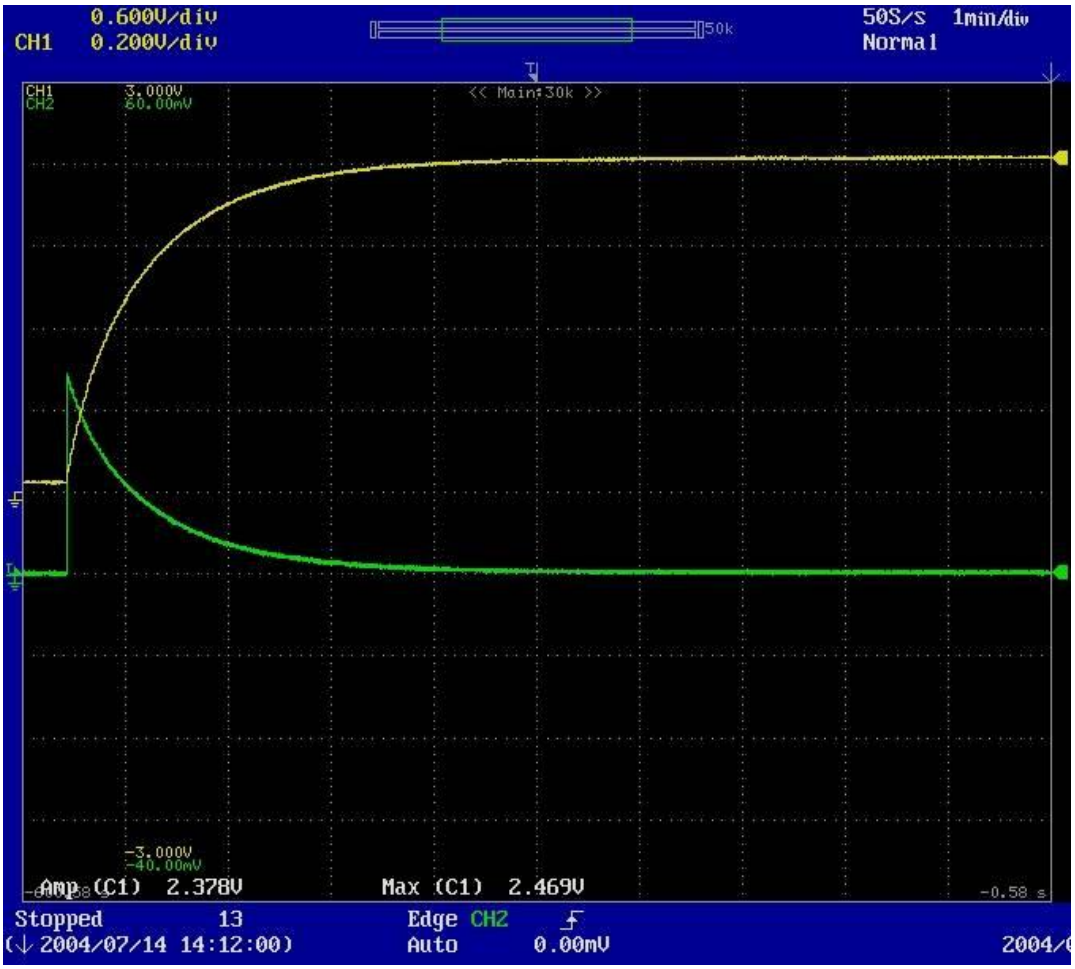

Figure A2.3-13: Oscilloscope Screen Capture of 60 A Charge Cycle at T= 50°C (Timescale: 1 min/div)

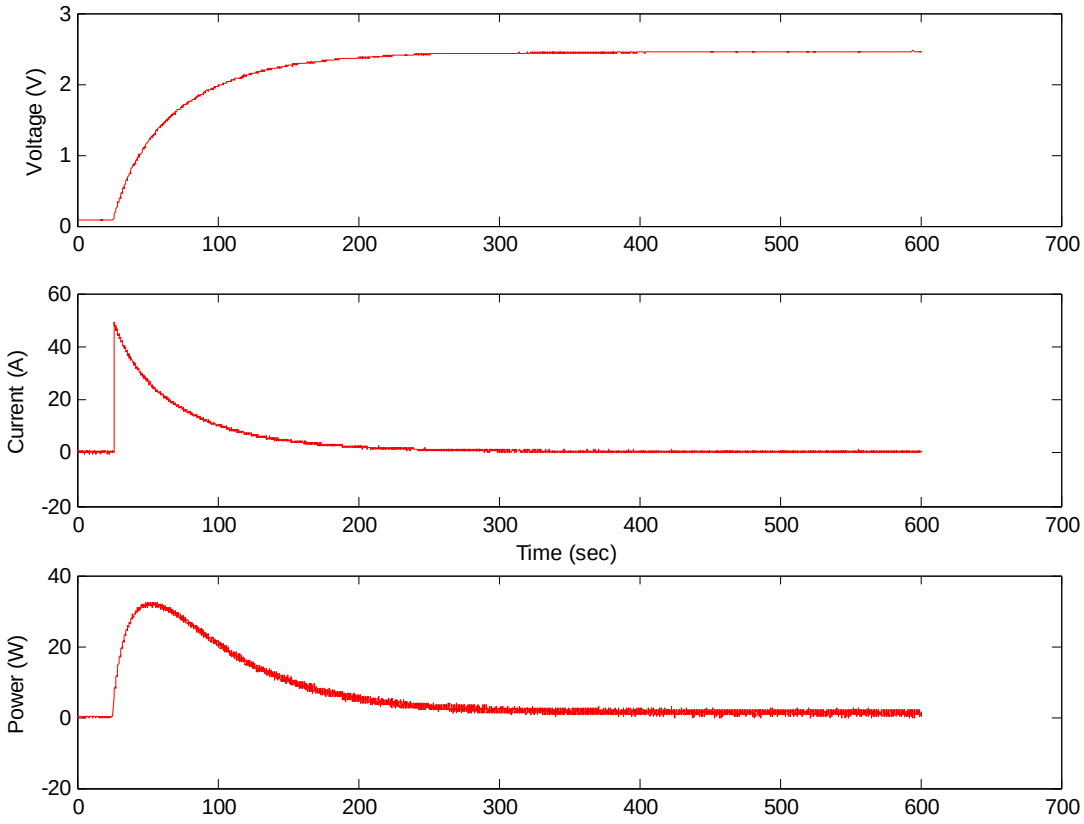

Figure A2.3-14: Plotted Matlab Data of 60 A Charge Cycle at T=50°C

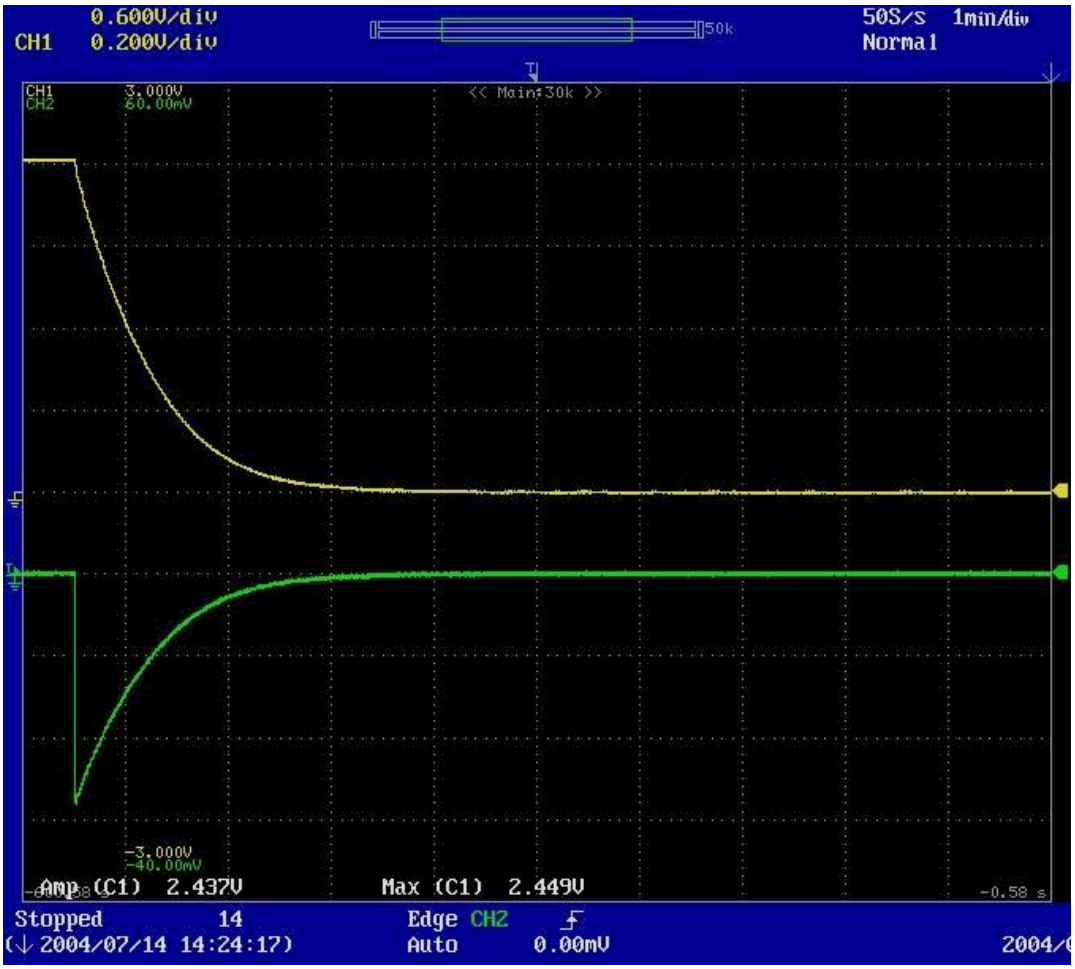

Figure A2.3-15: Oscilloscope Screen Capture of 60 A Discharge Cycle at T= 50°C (Timescale: 1 min/div)

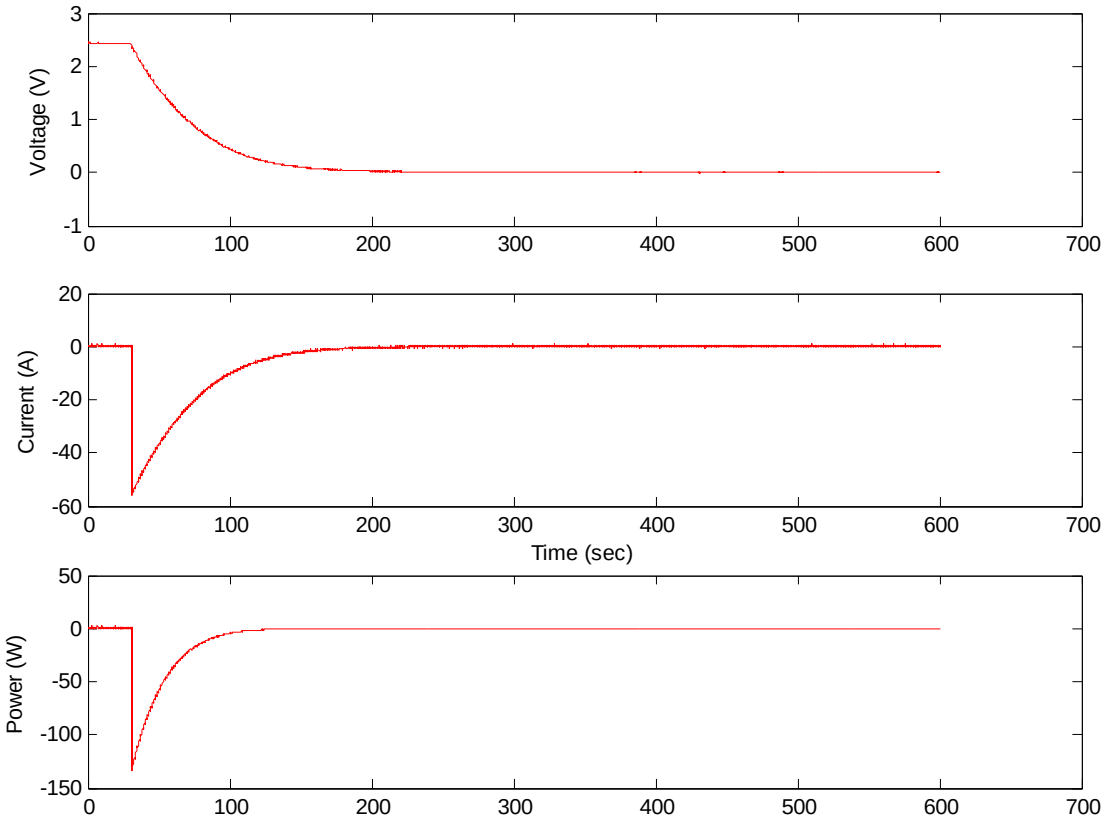

Figure A2.3-16: Plotted Matlab Data of 60 A Discharge Cycle at T=50°C

A3. 1800 F Ultracapacitor Experiment Results

The results for the 1800 F are shown in this section. The results are broken into three sub-categories that are based on the current charge and discharge levels. Within each current level, there are four temperatures: -25°C, 0°C, 25°C and 50°C. After each oscilloscope screen capture is the corresponding Matlab plots of the data.

A3.1 1800 F 25 A Results

Figure A3.1-1: Oscilloscope Screen Capture of 25 A Charge Cycle at T= -25°C (Timescale: 1 min/div)

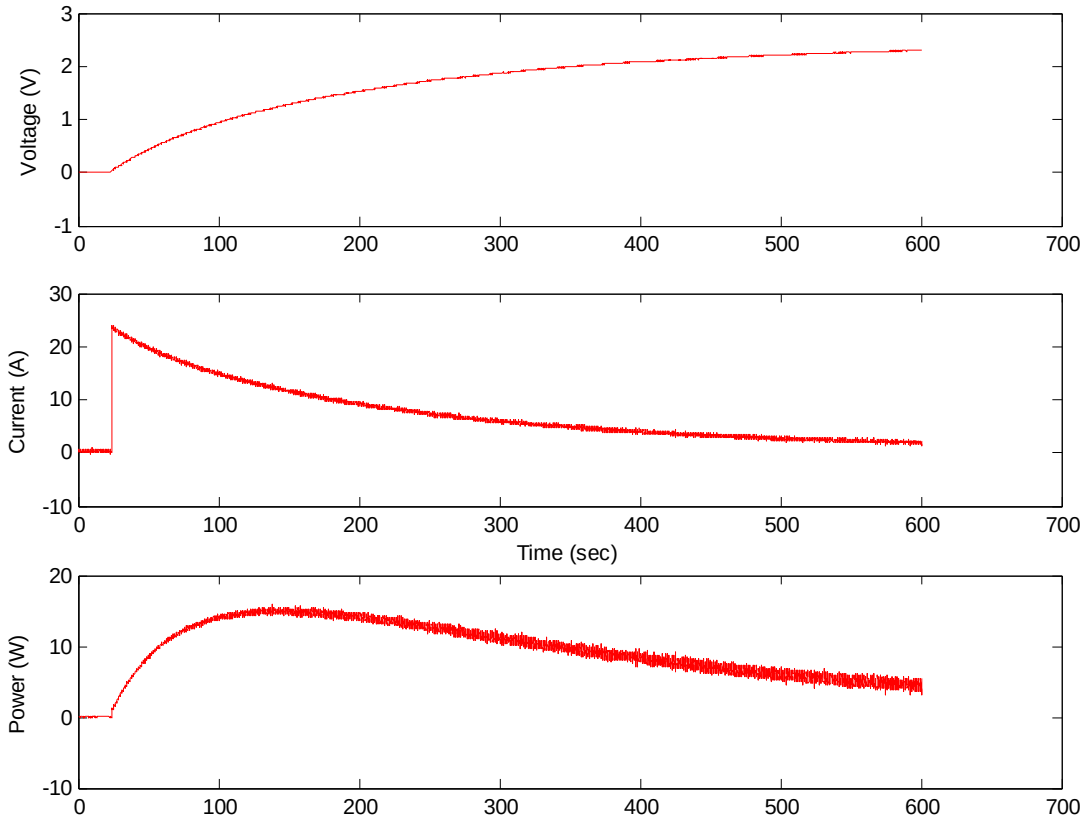

Figure A3.1-2: Plotted Matlab Data of 25 A Charge Cycle at T= -25°C

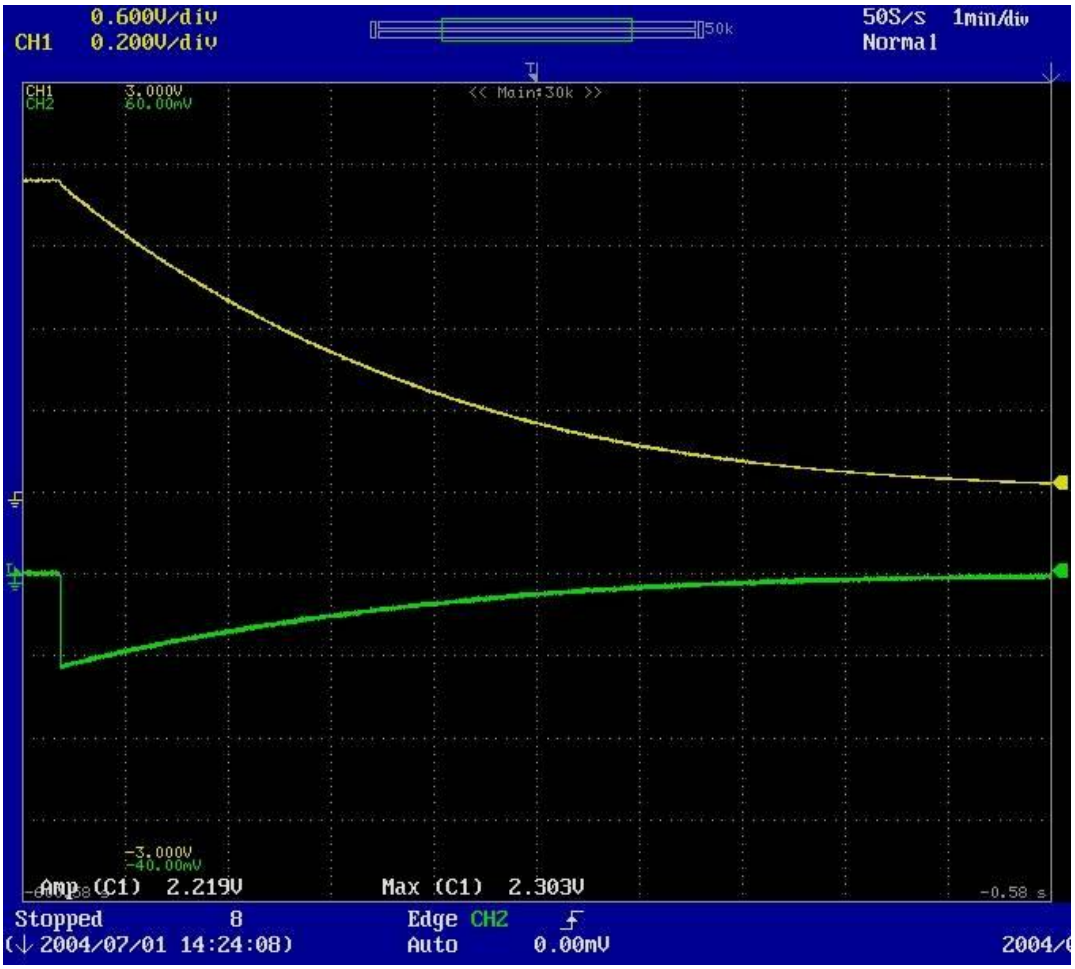

Figure A3.1-3: Oscilloscope Screen Capture of 25 A Discharge Cycle at T= -25°C (Timescale: 1 min/div)

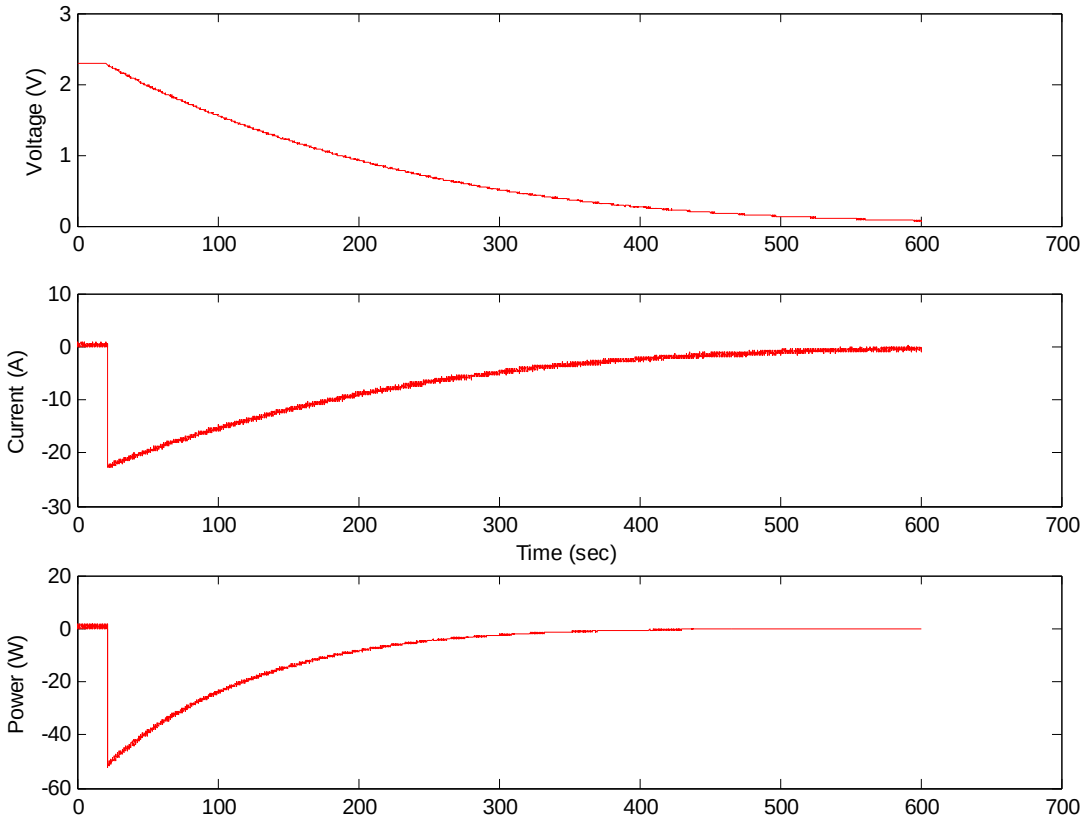

Figure A3.1-4: Plotted Matlab Data of 25 A Discharge Cycle at T= -25^{o}C

Figure A3.1-5: Oscilloscope Screen Capture of 25 A Charge Cycle at T= 0^{o}C (Timescale: 1 min/div)

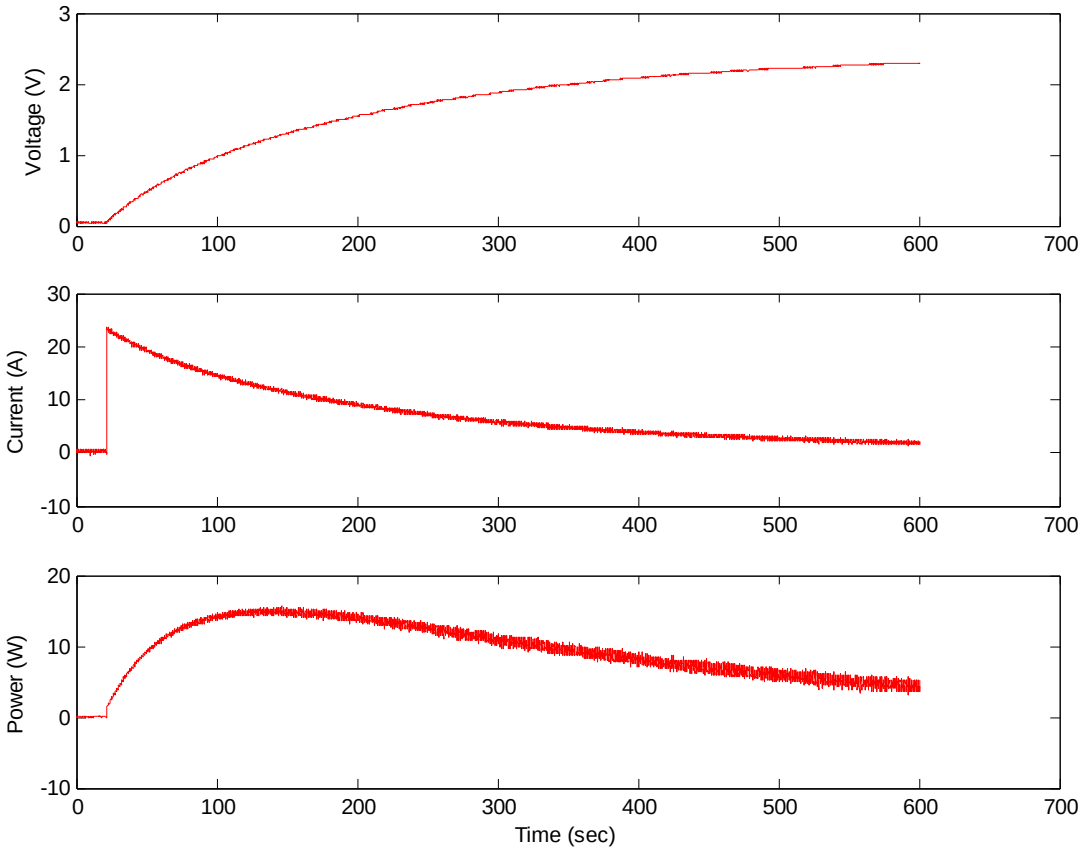

Figure A3.1-6: Plotted Matlab Data of 25 A Charge Cycle at T= 0^{o}C

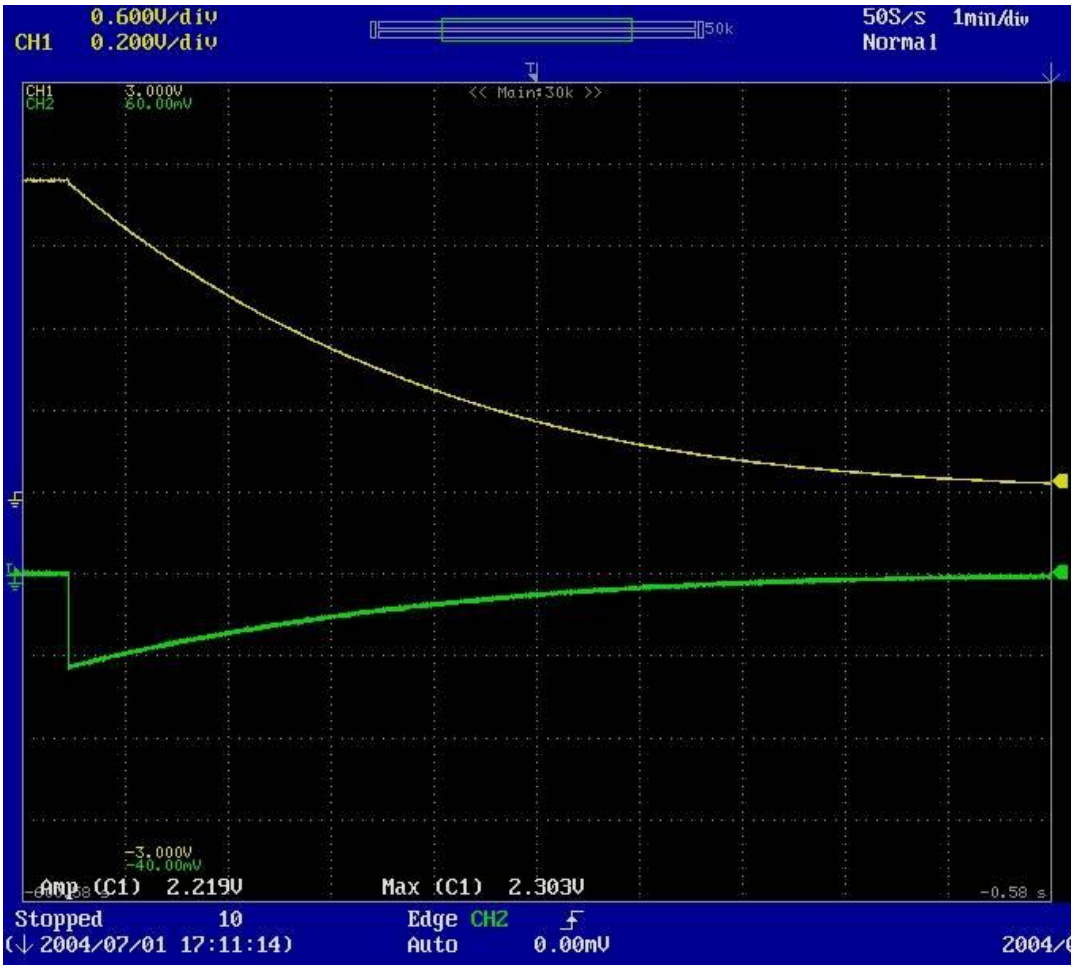

Figure A3.1-7: Oscilloscope Screen Capture of 25 A Discharge Cycle at T= 0^{o}C (Timescale: 1 min/div)

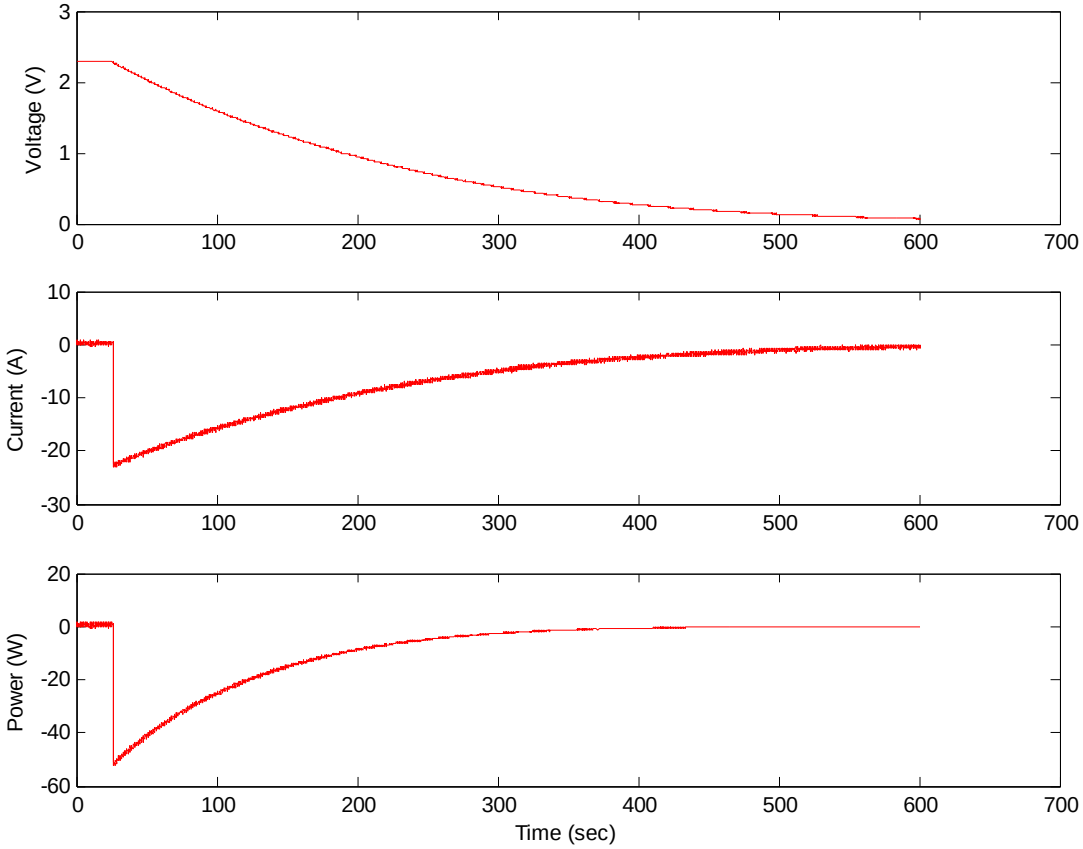

Figure A3.1-8: Plotted Matlab Data of 25 A Discharge Cycle at T= 0^{o}C

Figure A3.1-9: Oscilloscope Screen Capture of 25 A Charge Cycle at T= 25°C (Timescale: 1 min/div)

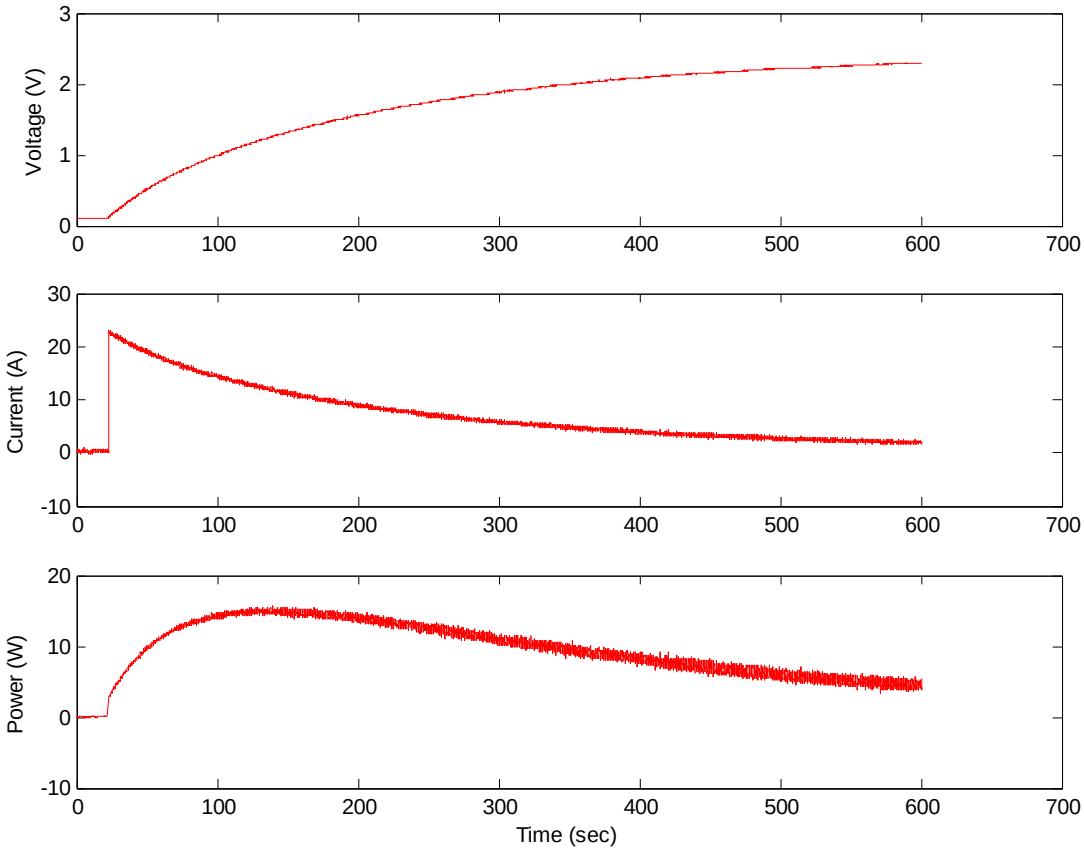

Figure A3.1-10: Plotted Matlab Data of 25 A Charge Cycle at T= 25°C

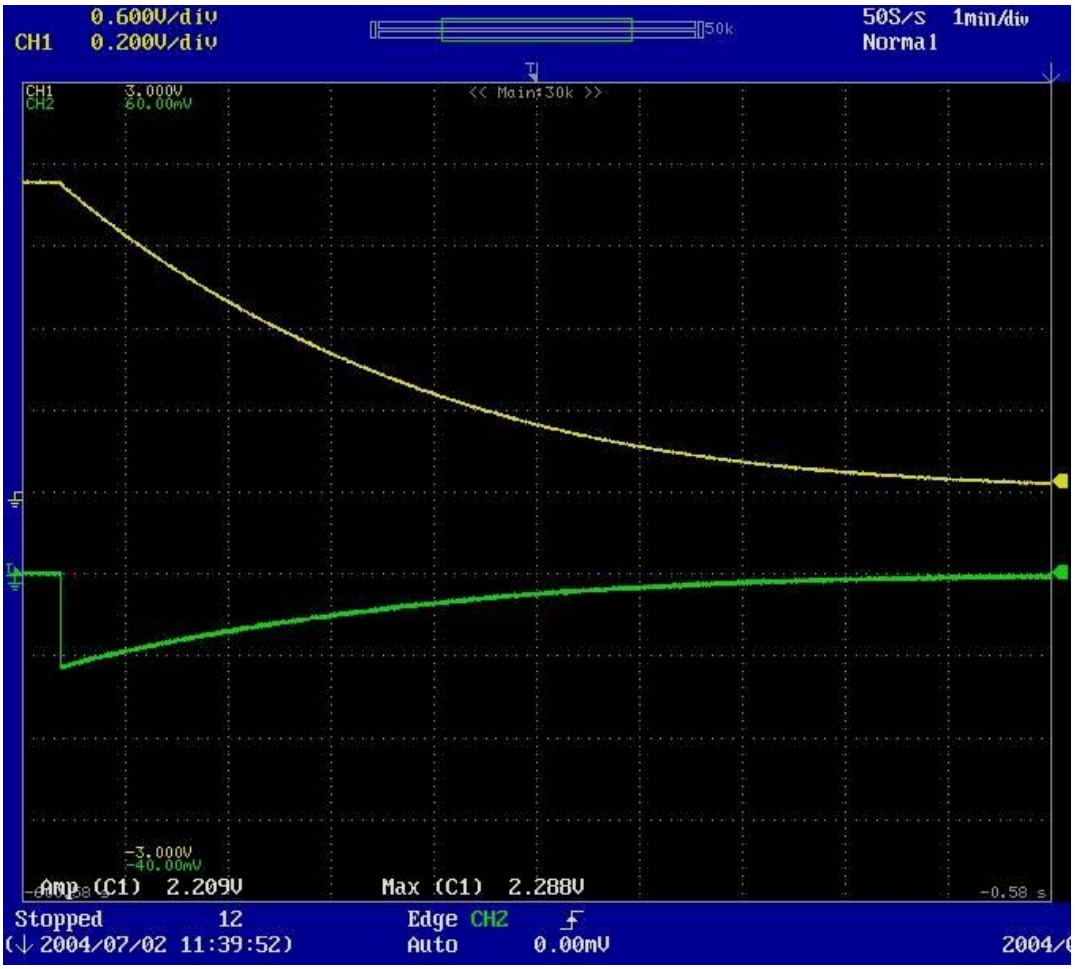

Figure A3.1-11: Oscilloscope Screen Capture of 25 A Discharge Cycle at T=25°C (Timescale: 1 min/div)

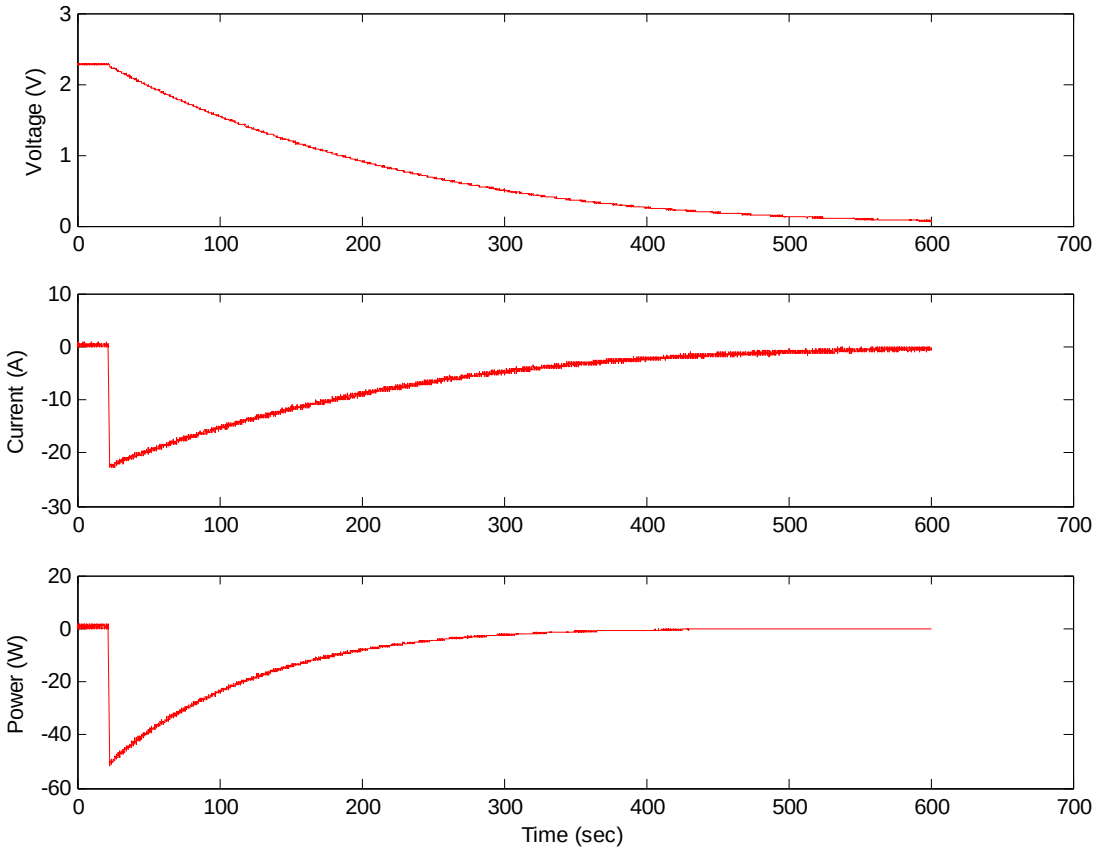

Figure A3.1-12: Plotted Matlab Data of 25 A Discharge Cycle at T=25°C

Figure A3.1-13: Oscilloscope Screen Capture of 25 A Charge Cycle at T= 50°C (Timescale: 1 min/div)

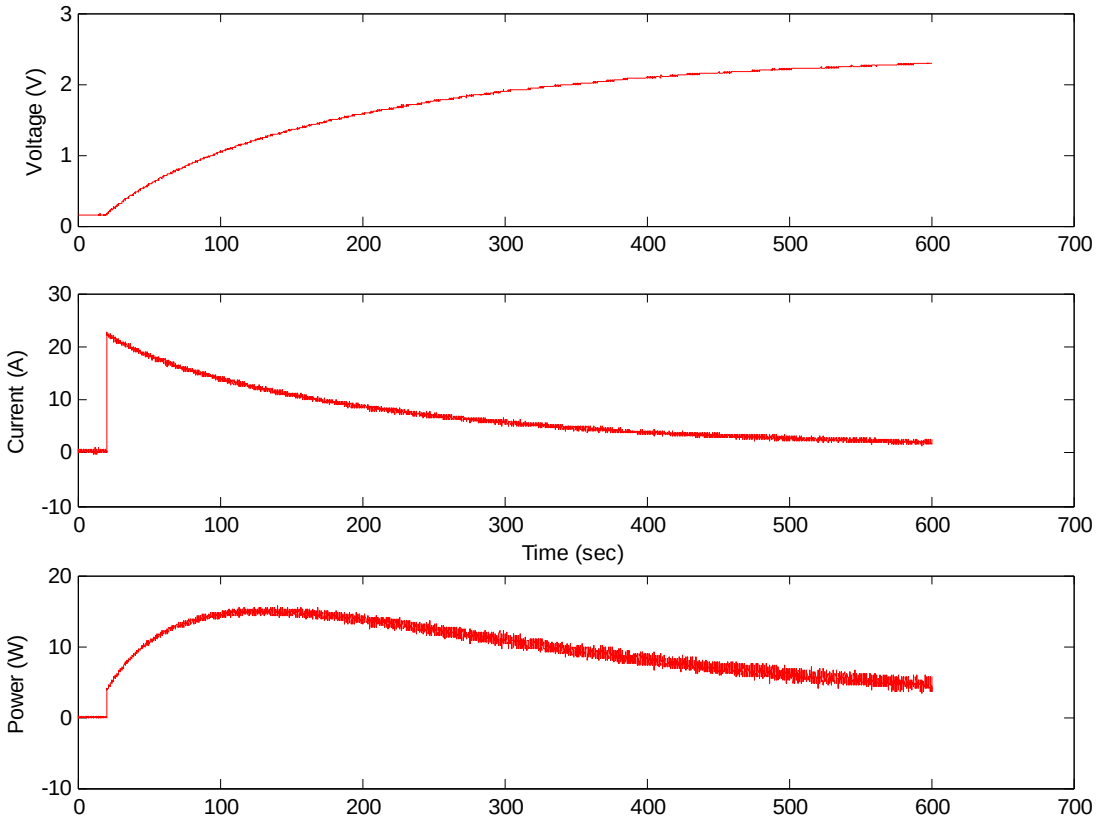

Figure A3.1-14: Plotted Matlab Data of 25 A Charge Cycle at T=50^{o}C

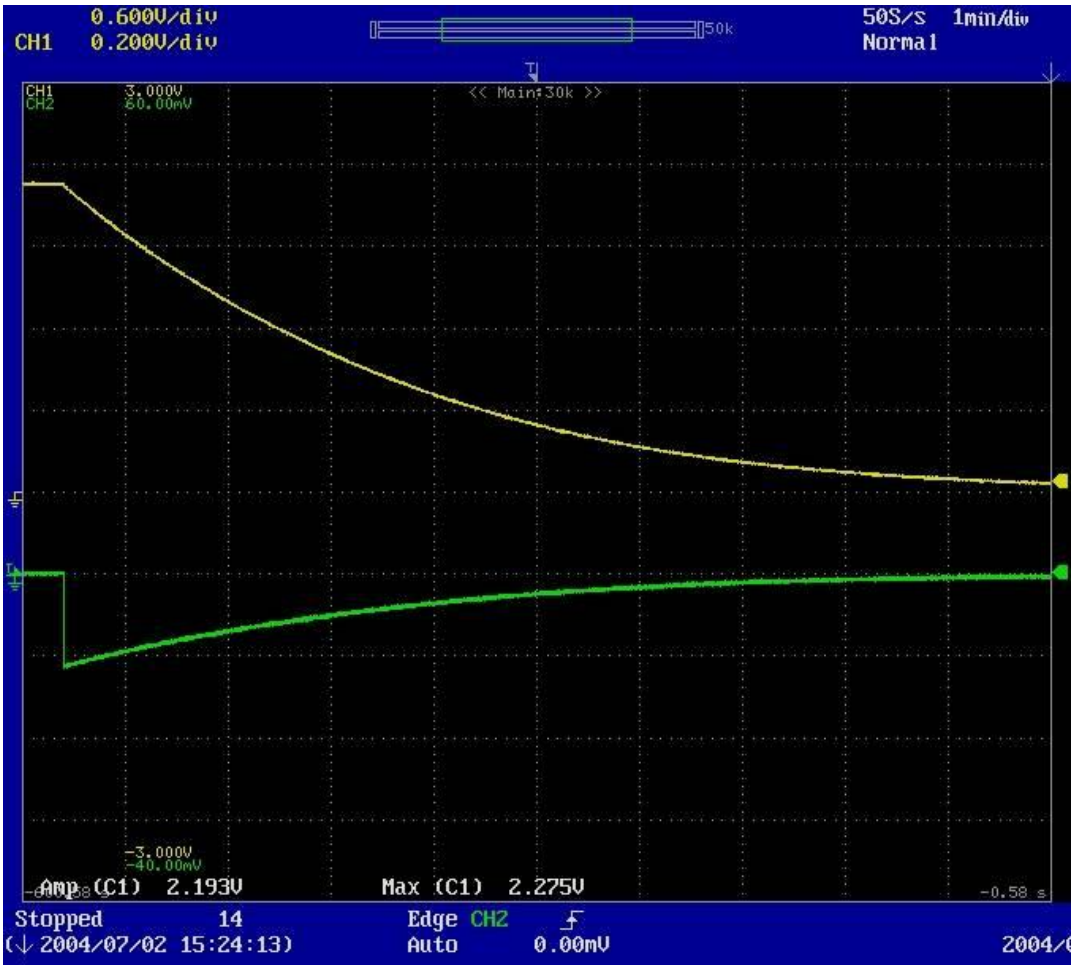

Figure A3.1-15: Oscilloscope Screen Capture of 25 A Discharge Cycle at T= 50°C (Timescale: 1 min/div)

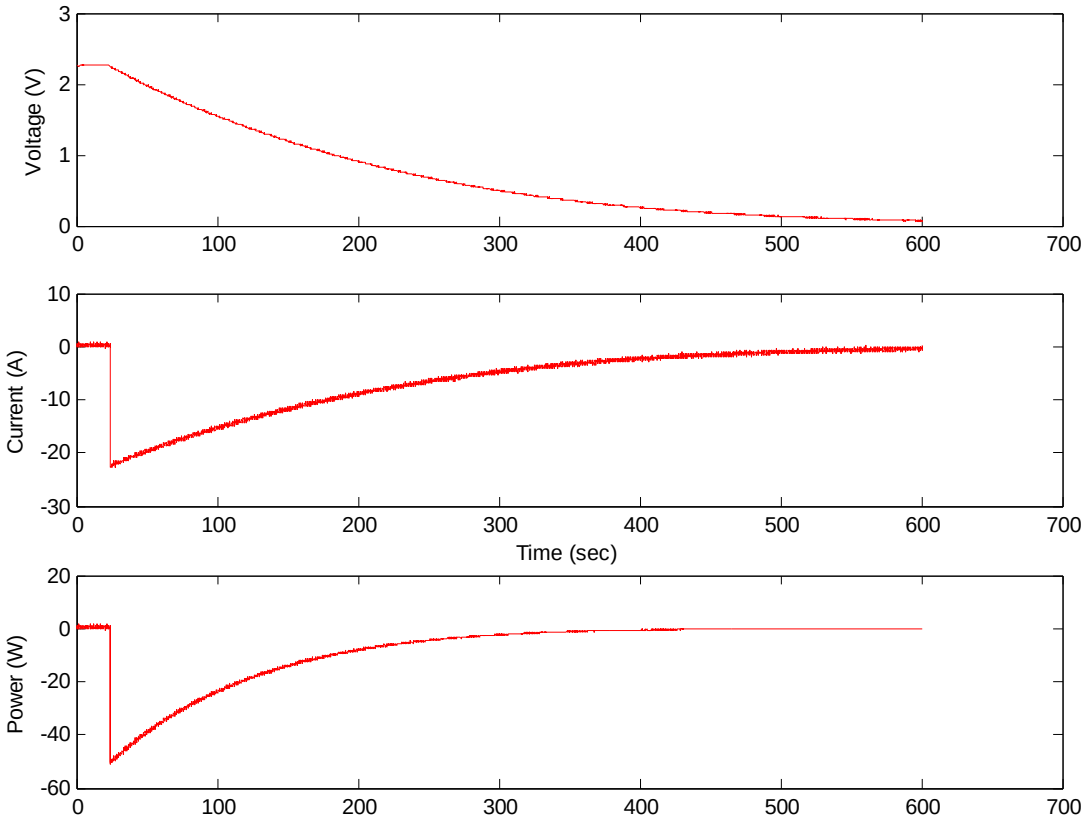

Figure A3.1-16: Plotted Matlab Data of 25 A Discharge Cycle at T=50°C

A3.2 1800 F 50 A Results

Figure A3.2-1: Oscilloscope Screen Capture of 50 A Charge Cycle at T= -25°C (Timescale: 1 min/div)

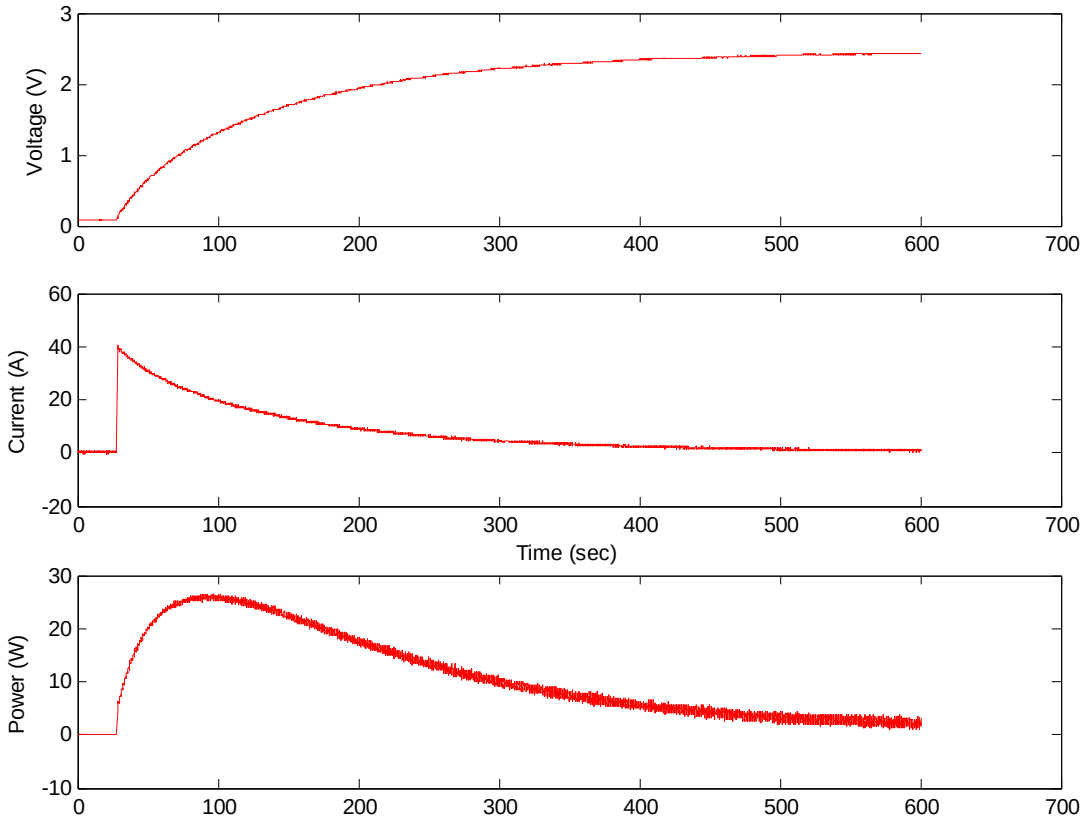

Figure A3.2-2: Plotted Matlab Data of 50 A Charge Cycle at T= -25°C

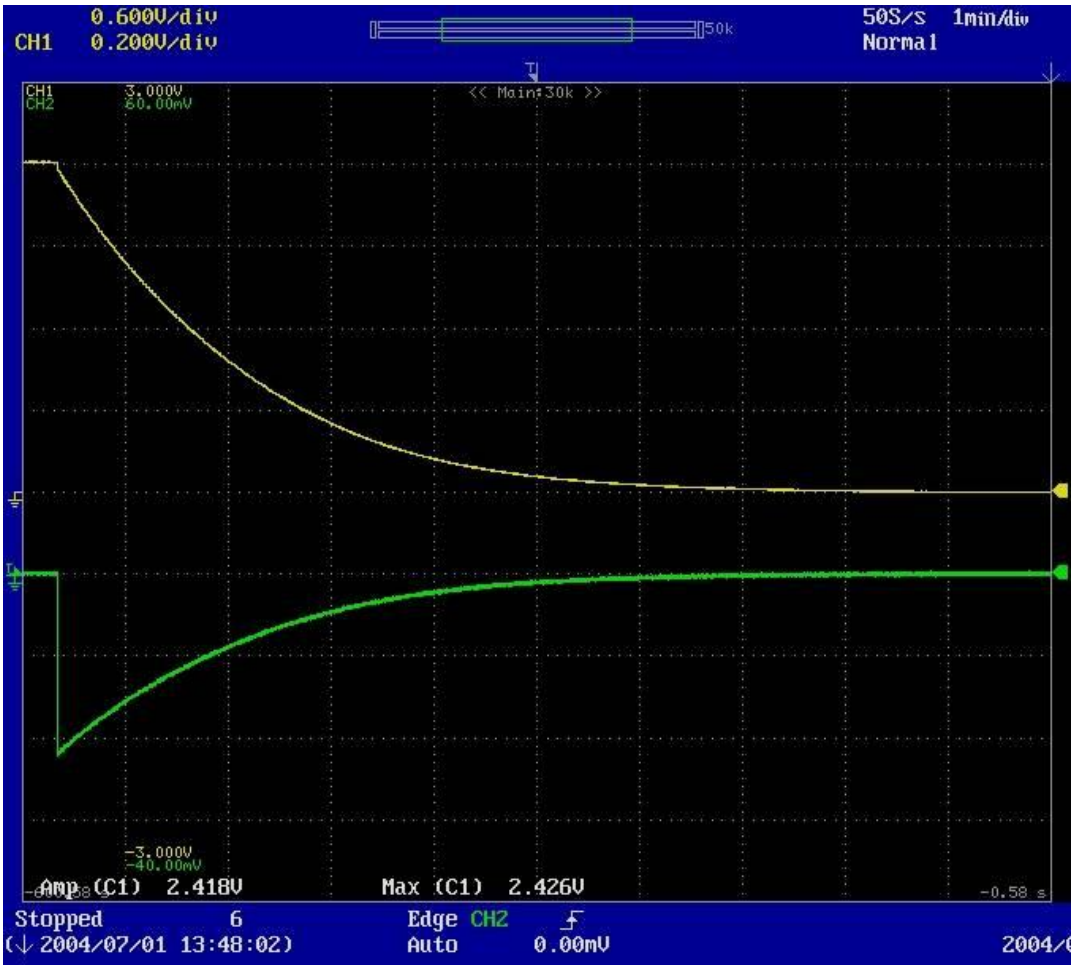

Figure A3.2-3: Oscilloscope Screen Capture of 50 A Discharge Cycle at T= -25°C (Timescale: 1 min/div)

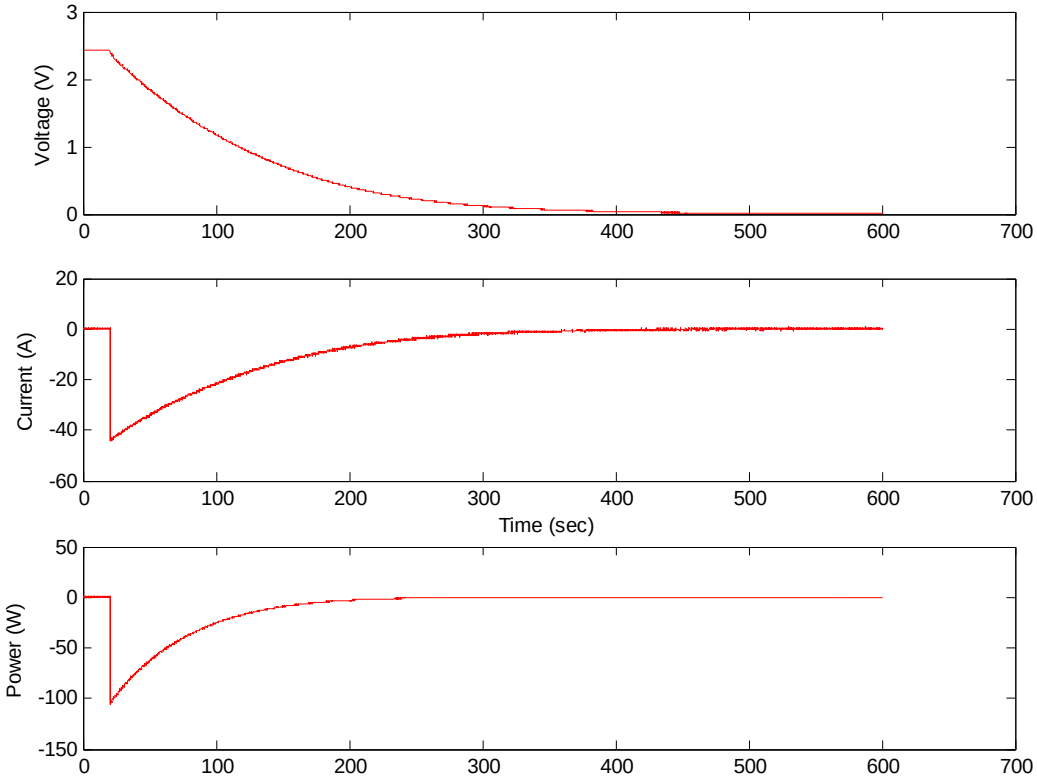

Figure A3.2-4: Plotted Matlab Data of 50 A Discharge Cycle at T= -25°C

Figure A3.2-5: Oscilloscope Screen Capture of 50 A Charge Cycle at T= 0^{o}C (Timescale: 1 min/div)

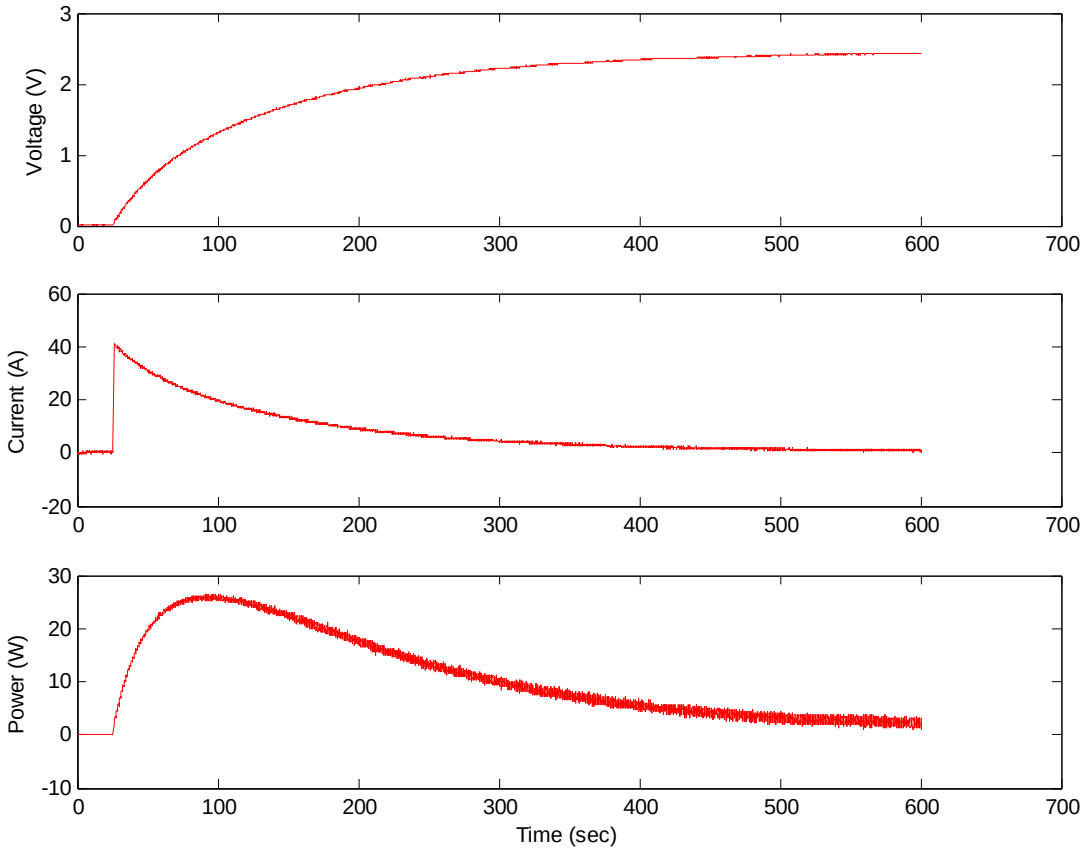

Figure A3.2-6: Plotted Matlab Data of 50 A Charge Cycle at T= 0^{o}C

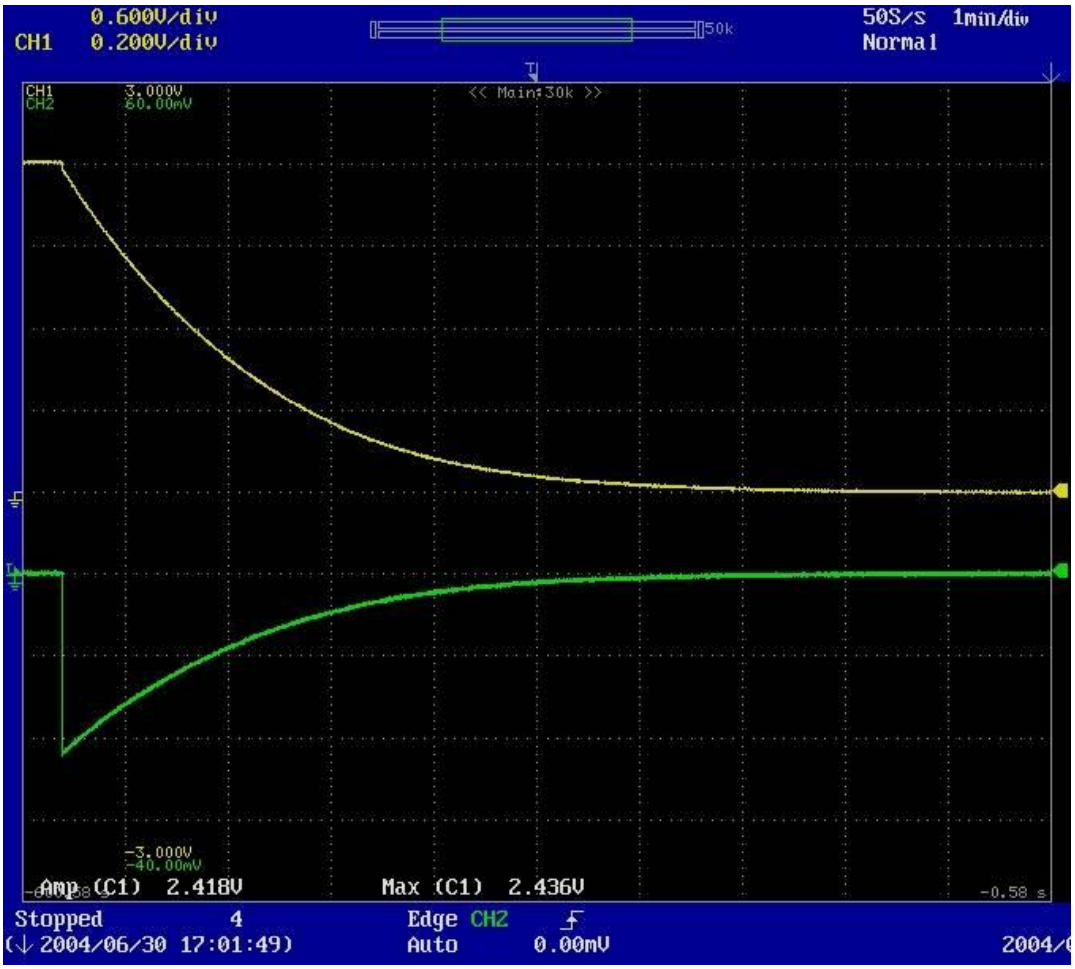

Figure A3.2-7: Oscilloscope Screen Capture of 50 A Discharge Cycle at T= 0^{0}C (Timescale: 1 min/div)

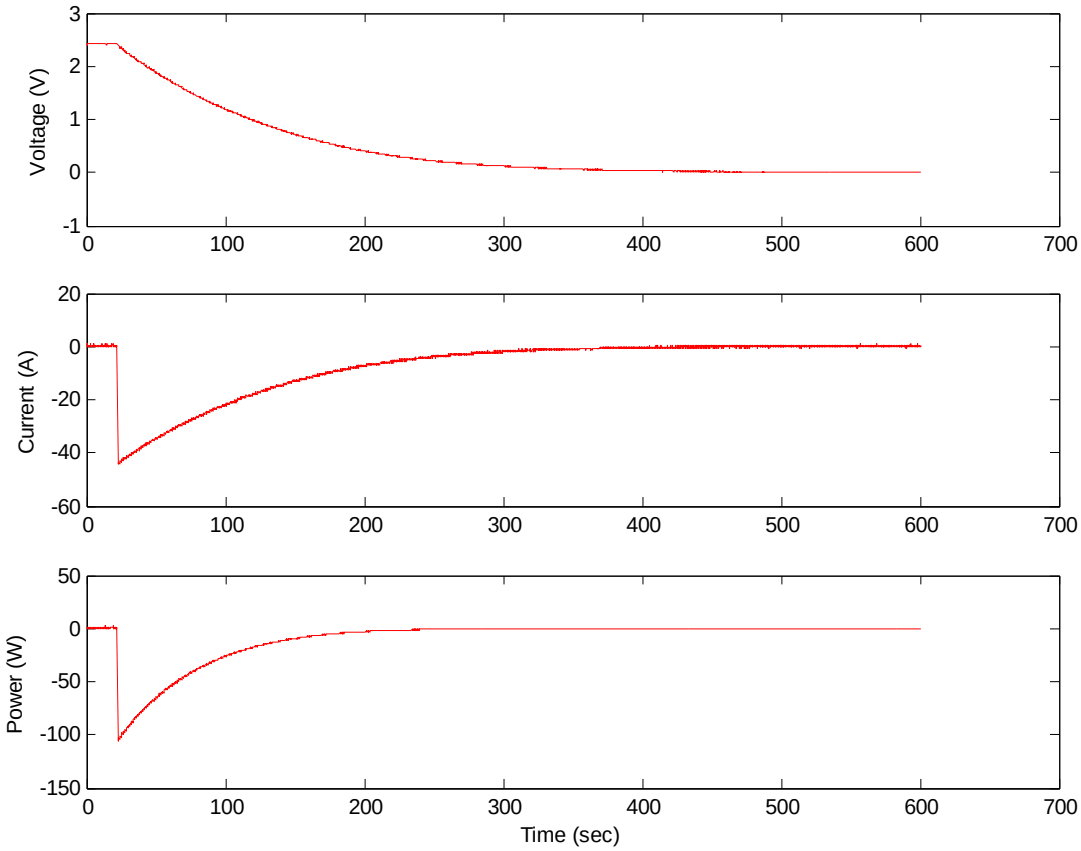

Figure A3.2-8: Plotted Matlab Data of 50 A Discharge Cycle at T= 0^{o}C

Figure A3.2-9: Oscilloscope Screen Capture of 50 A Charge Cycle at T= 25°C (Timescale: 1 min/div)

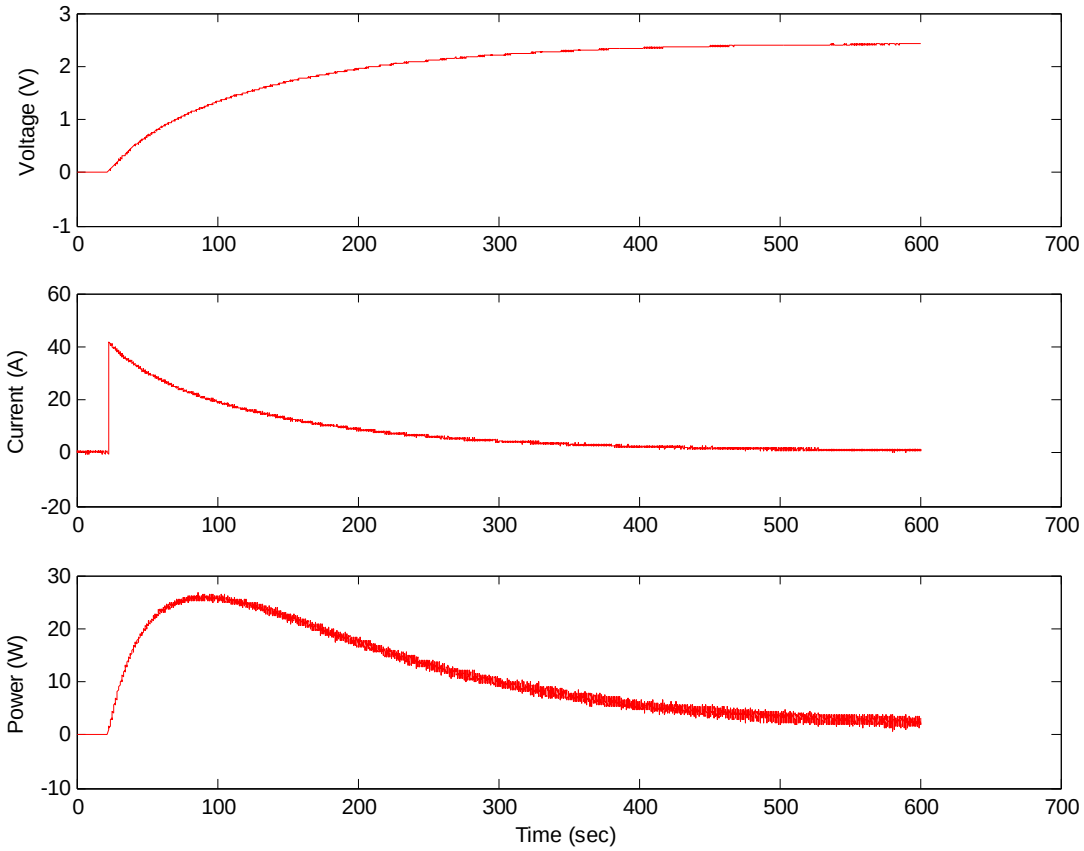

Figure A3.2-10: Plotted Matlab Data of 50 A Charge Cycle at T= 25°C

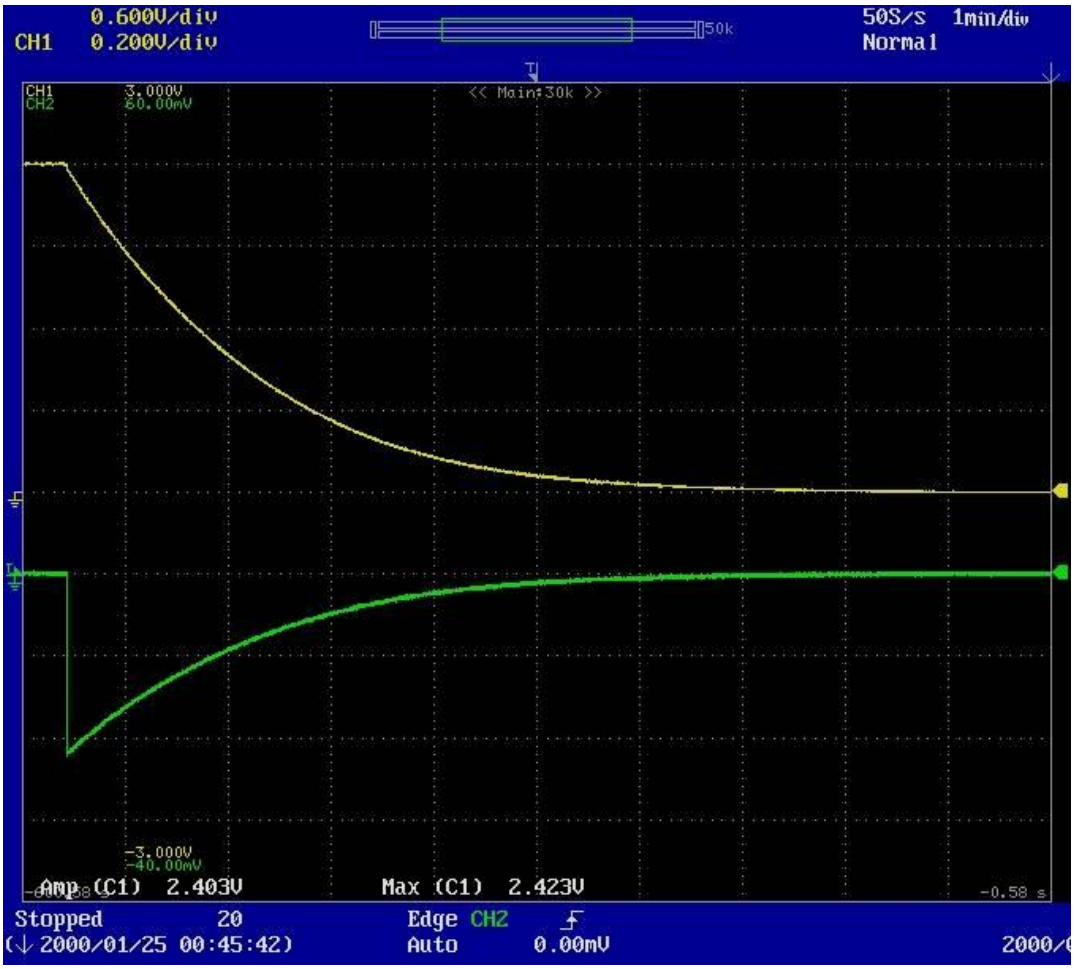

Figure A3.2-11: Oscilloscope Screen Capture of 50 A Discharge Cycle at T=25°C (Timescale: 1 min/div)

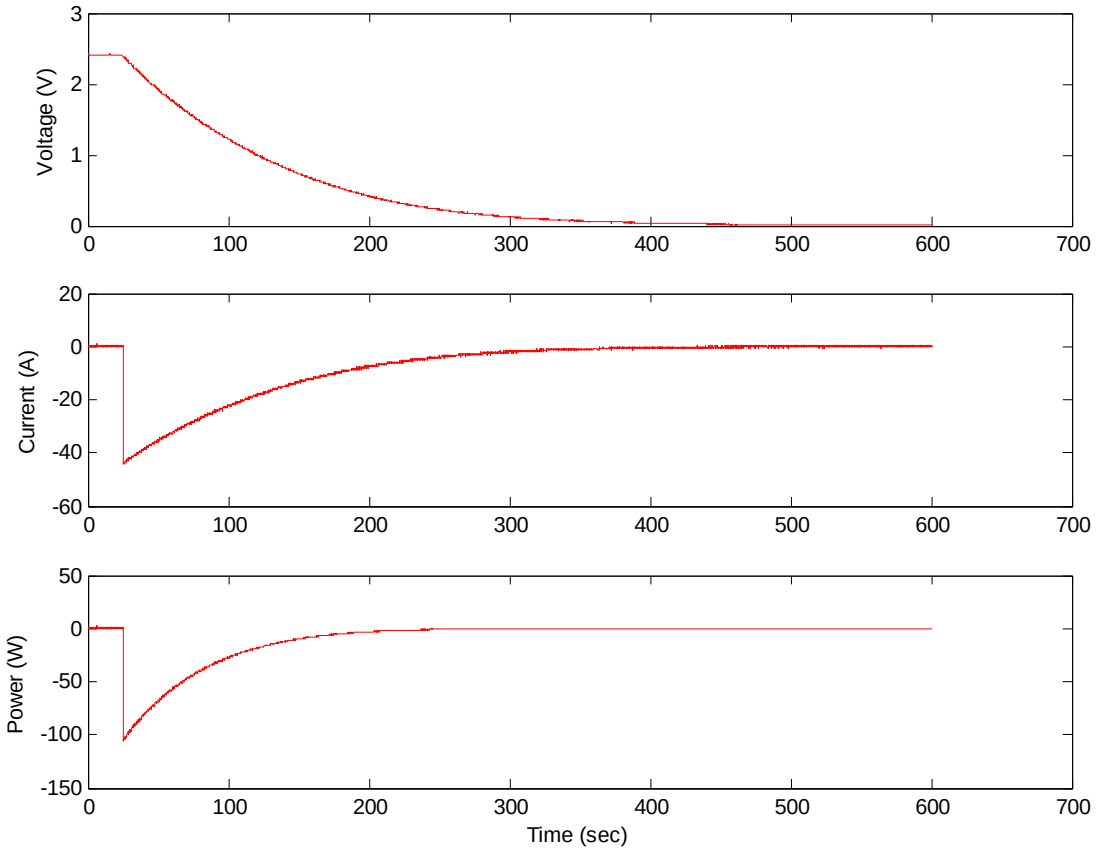

Figure A3.2-12: Plotted Matlab Data of 50 A Discharge Cycle at T=25°C

Figure A3.2-13: Oscilloscope Screen Capture of 50 A Charge Cycle at T= 50°C (Timescale: 1 min/div)

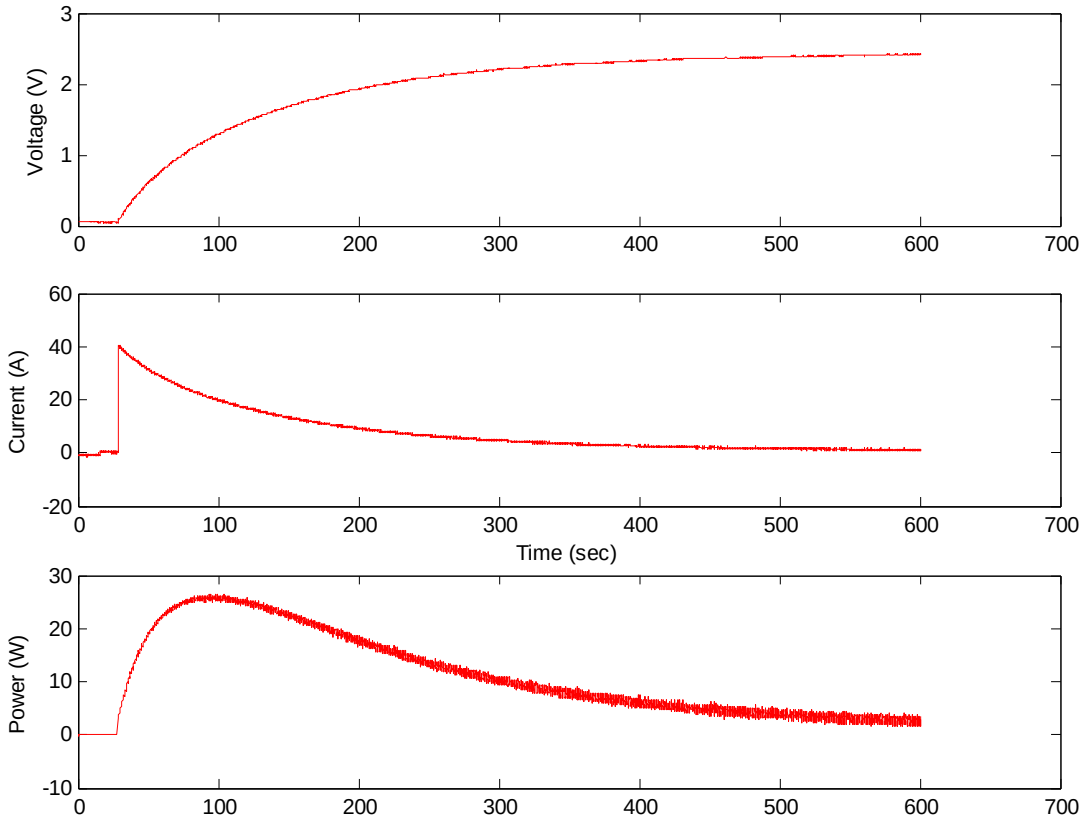

Figure A3.2-14: Plotted Matlab Data of 50 A Charge Cycle at T=50°C

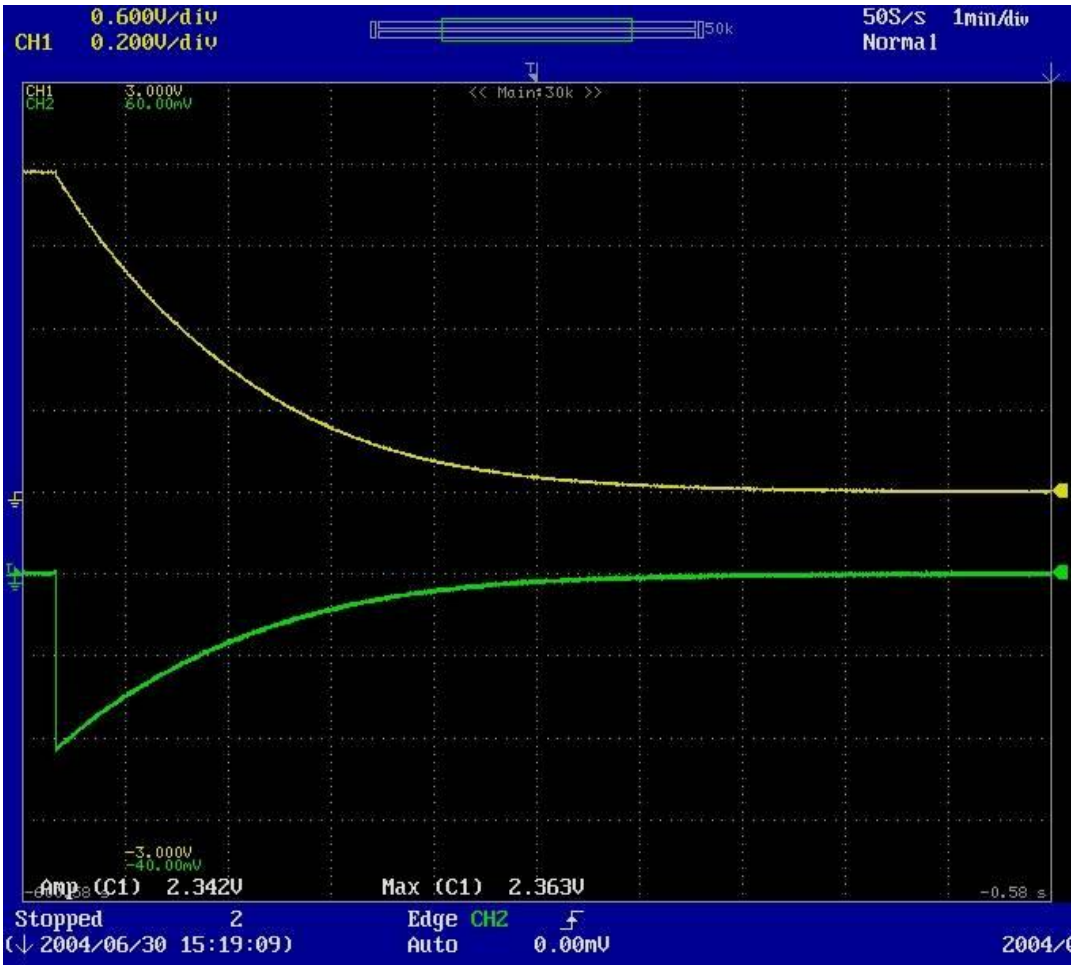

Figure A3.2-15: Oscilloscope Screen Capture of 50 A Discharge Cycle at T= 50°C (Timescale: 1 min/div)

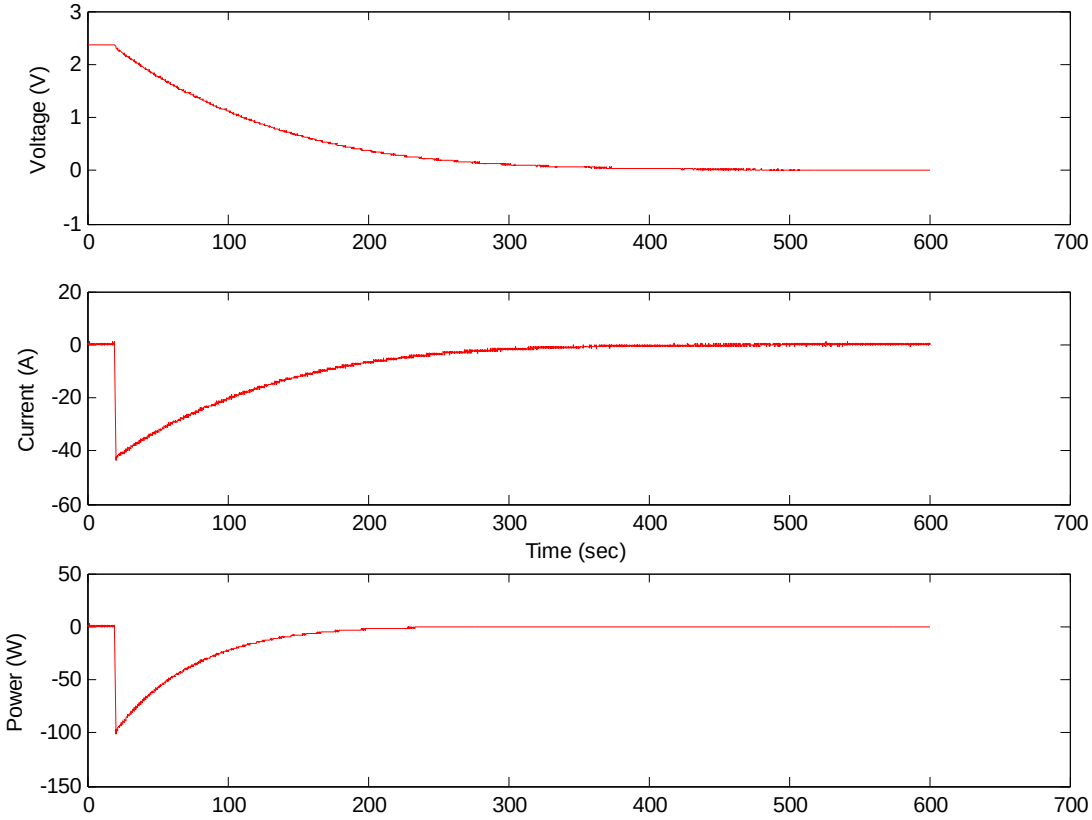

Figure A3.2-16: Plotted Matlab Data of 50 A Discharge Cycle at T=50°C

A3.3 1800 F 60 A Results

Figure A3.3-1: Oscilloscope Screen Capture of 60 A Charge Cycle at T= -25^{o}C (Timescale: 1 min/div)

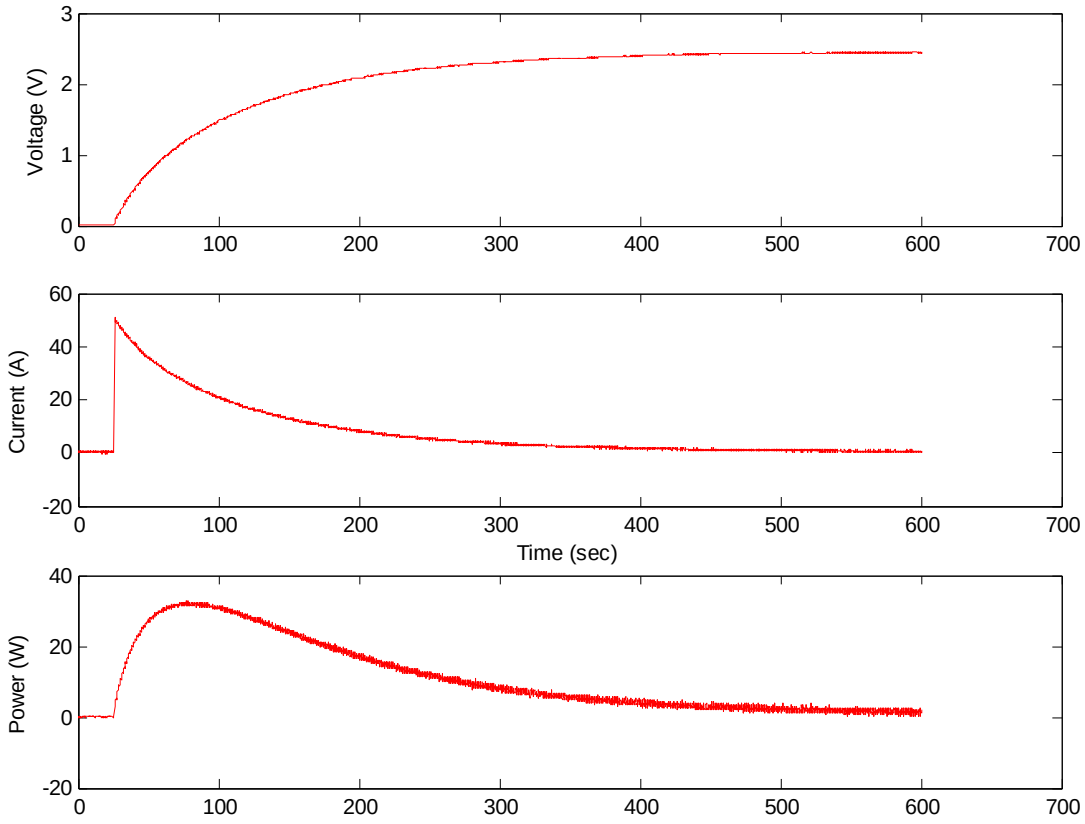

Figure A3.3-2: Plotted Matlab Data of 60 A Charge Cycle at T= -25°C

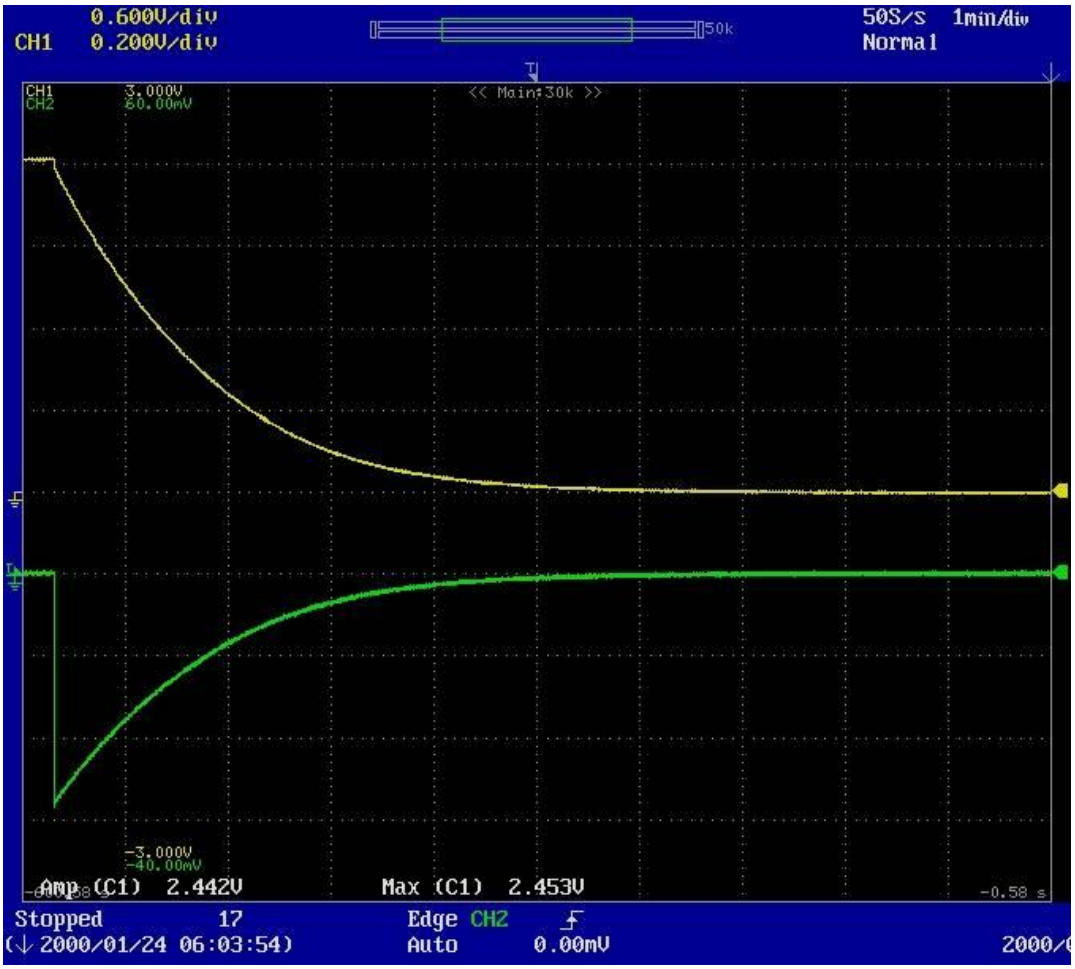

Figure A3.3-3: Oscilloscope Screen Capture of 60 A Discharge Cycle at T= -25°C (Timescale: 1 min/div)

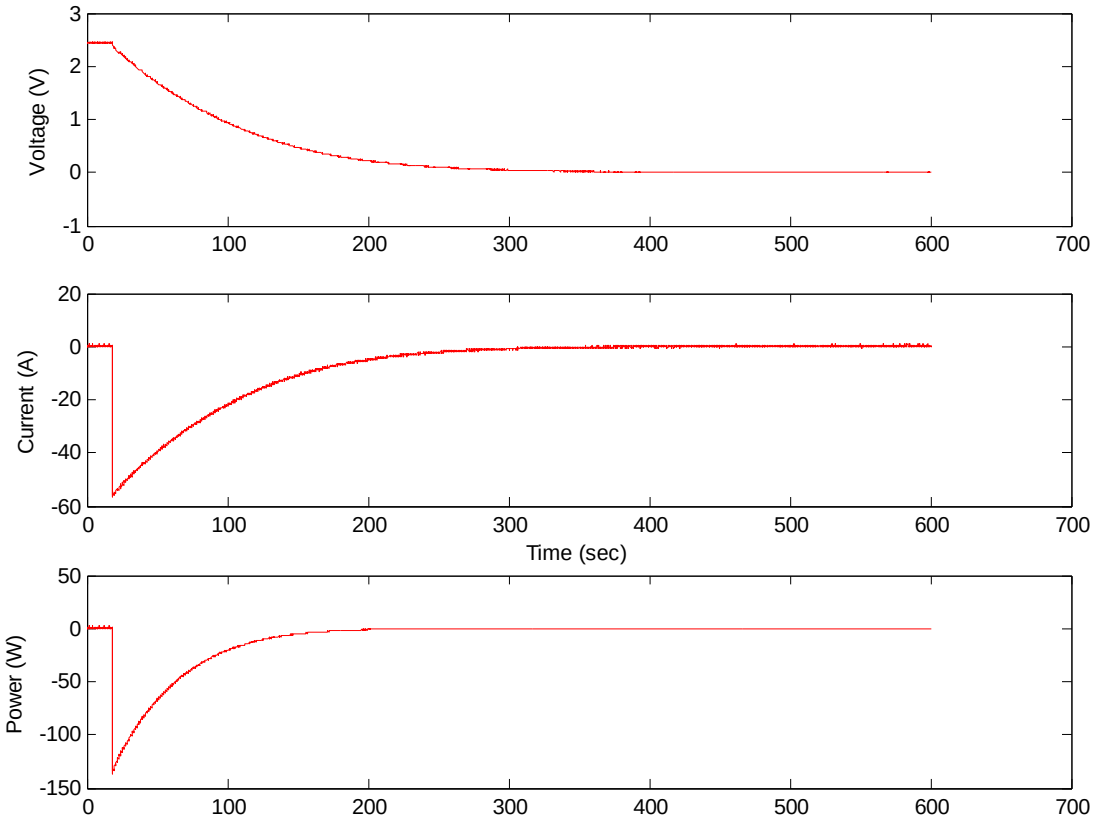

Figure A3.3-4: Plotted Matlab Data of 60 A Discharge Cycle at T= -25°C

Figure A3.3-5: Oscilloscope Screen Capture of 60 A Charge Cycle at T= 0^{o}C (Timescale: 1 min/div)

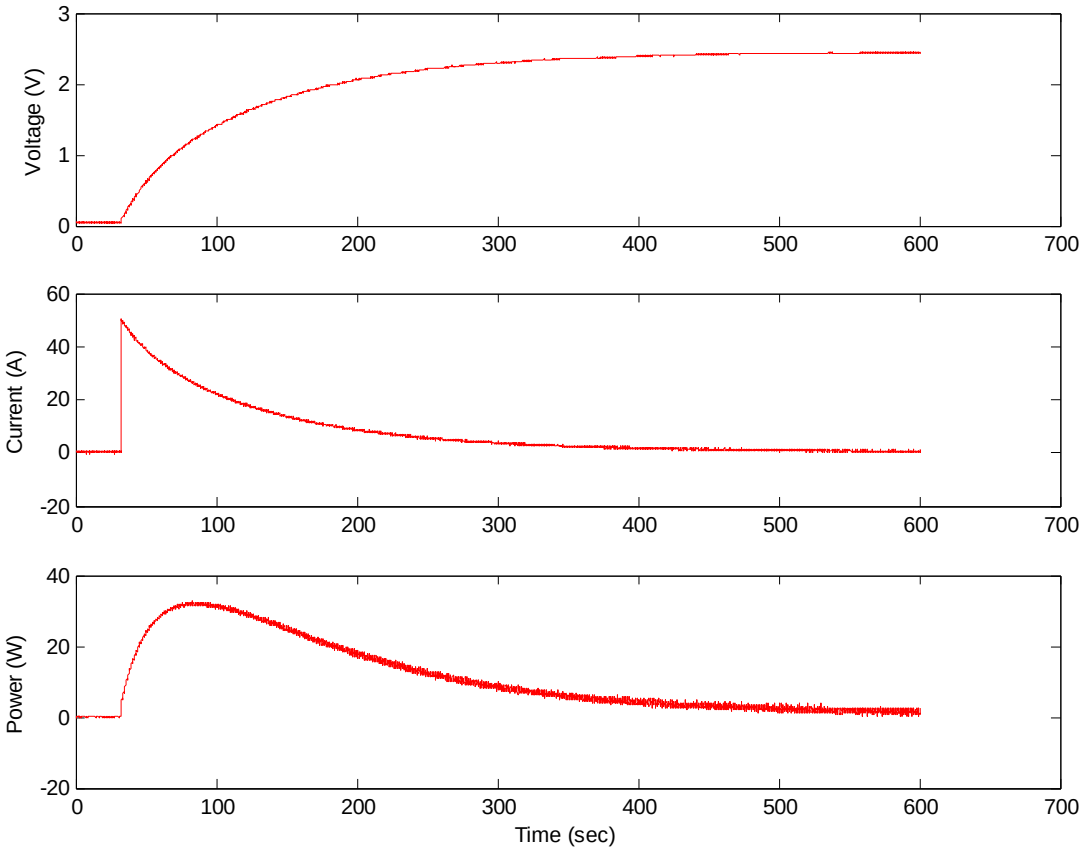

Figure A3.3-6: Plotted Matlab Data of 60 A Charge Cycle at T= 0^{o}C

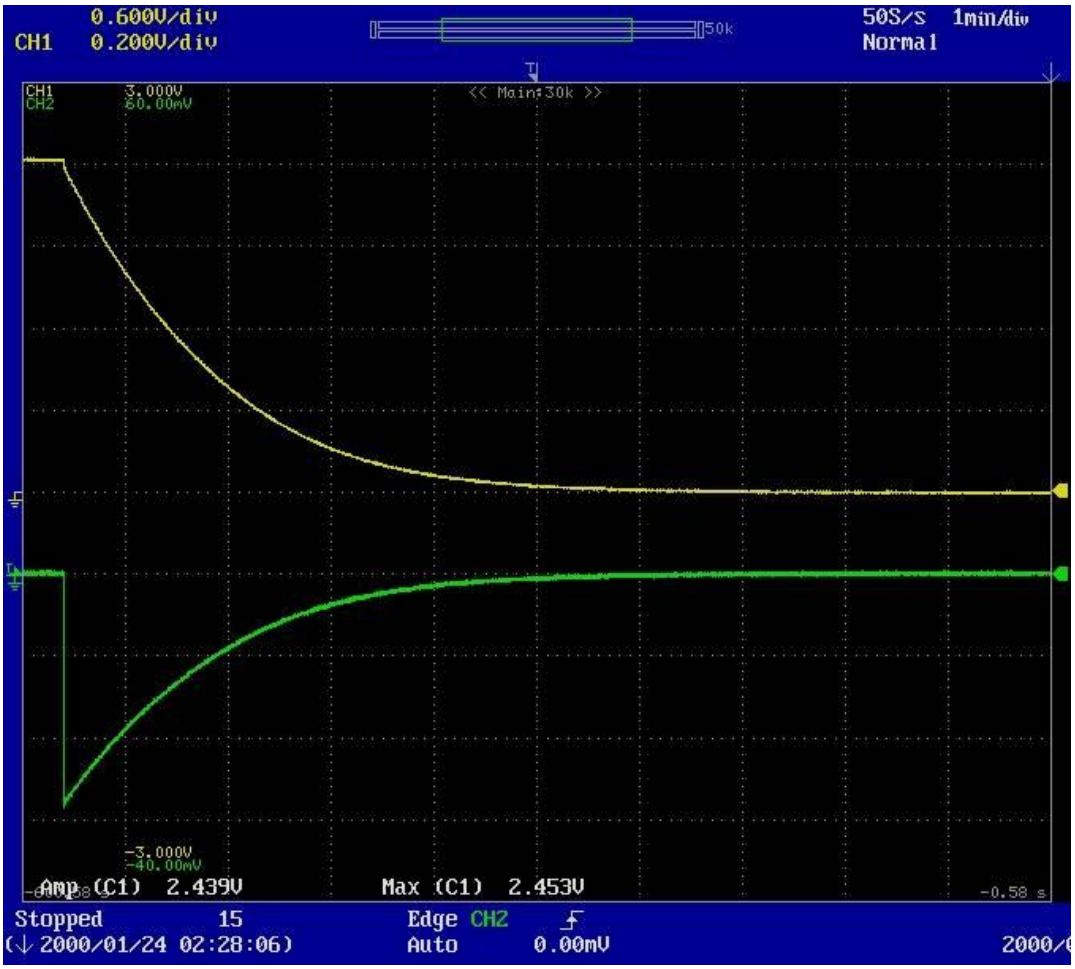

Figure A3.3-7: Oscilloscope Screen Capture of 60 A Discharge Cycle at T= 0^{o}C (Timescale: 1 min/div)

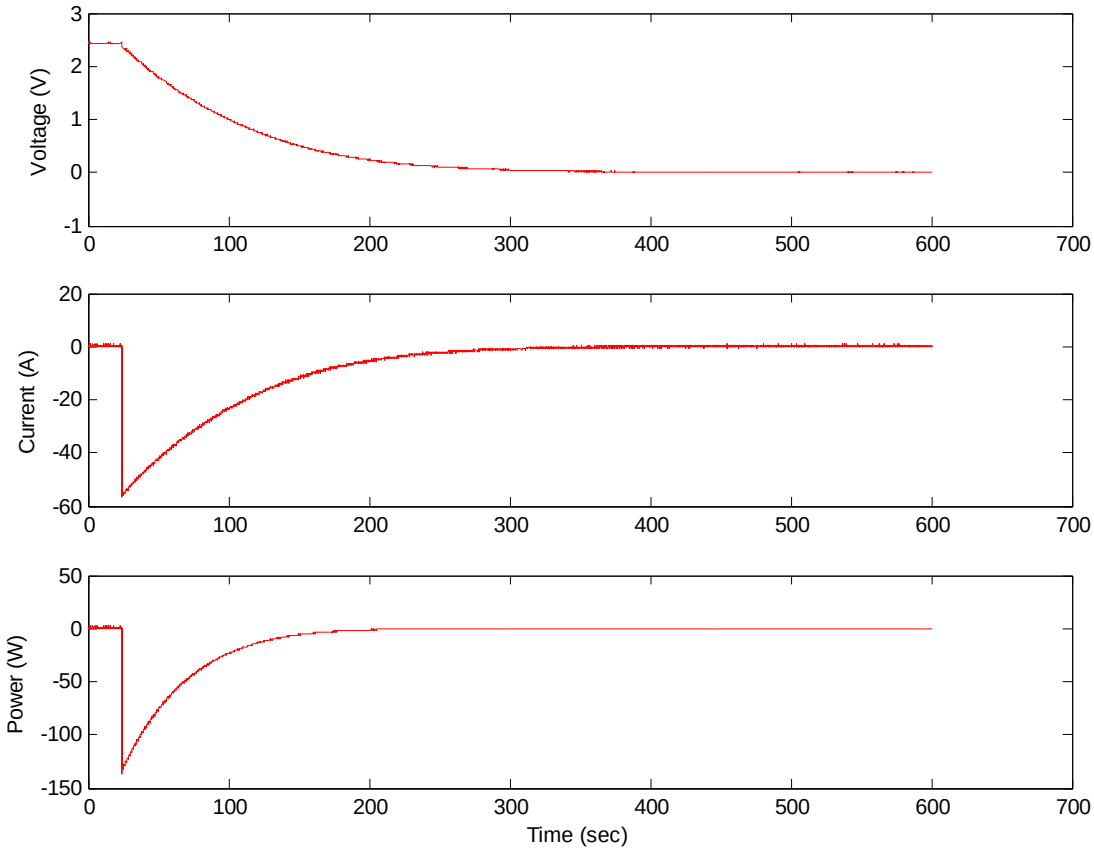

Figure A3.3-8: Plotted Matlab Data of 60 A Discharge Cycle at T= 0^{o}C

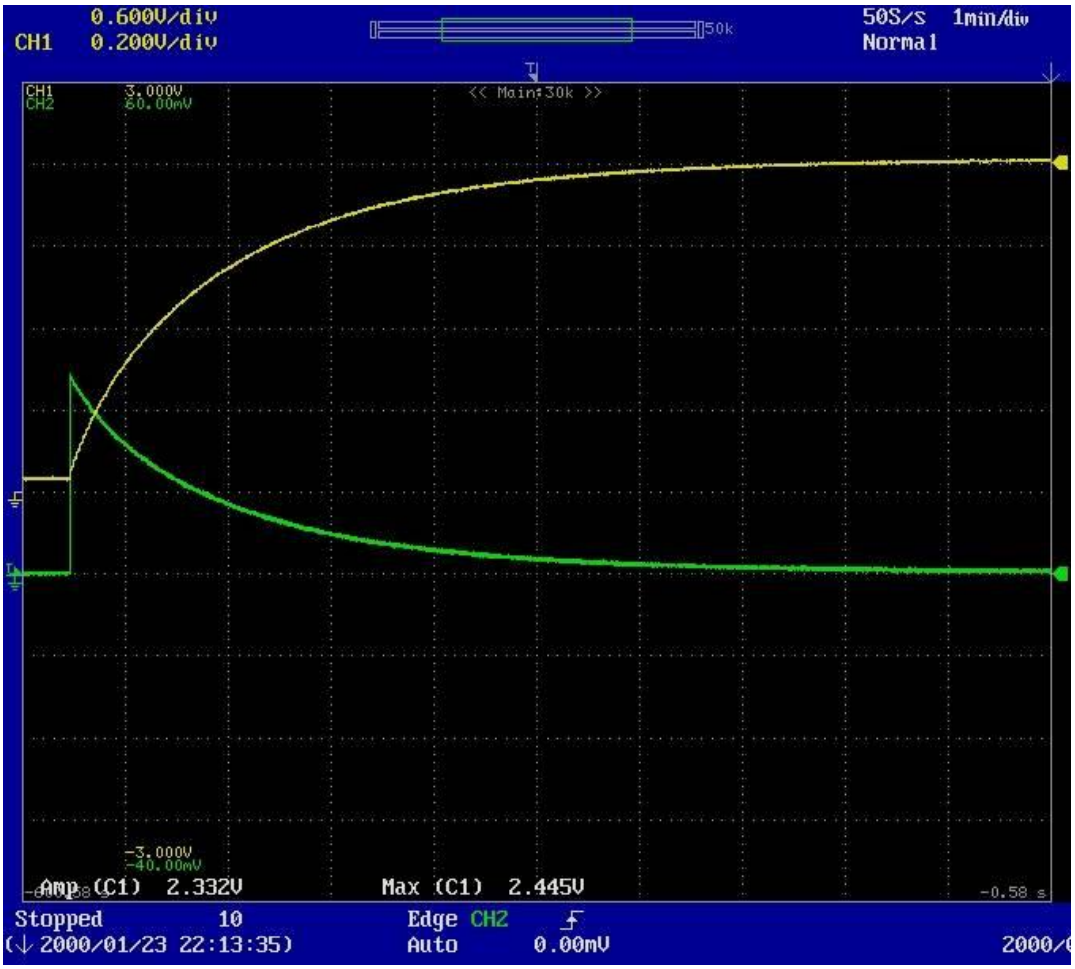

Figure A3.3-9: Oscilloscope Screen Capture of 60 A Charge Cycle at T= 25°C (Timescale: 1 min/div)

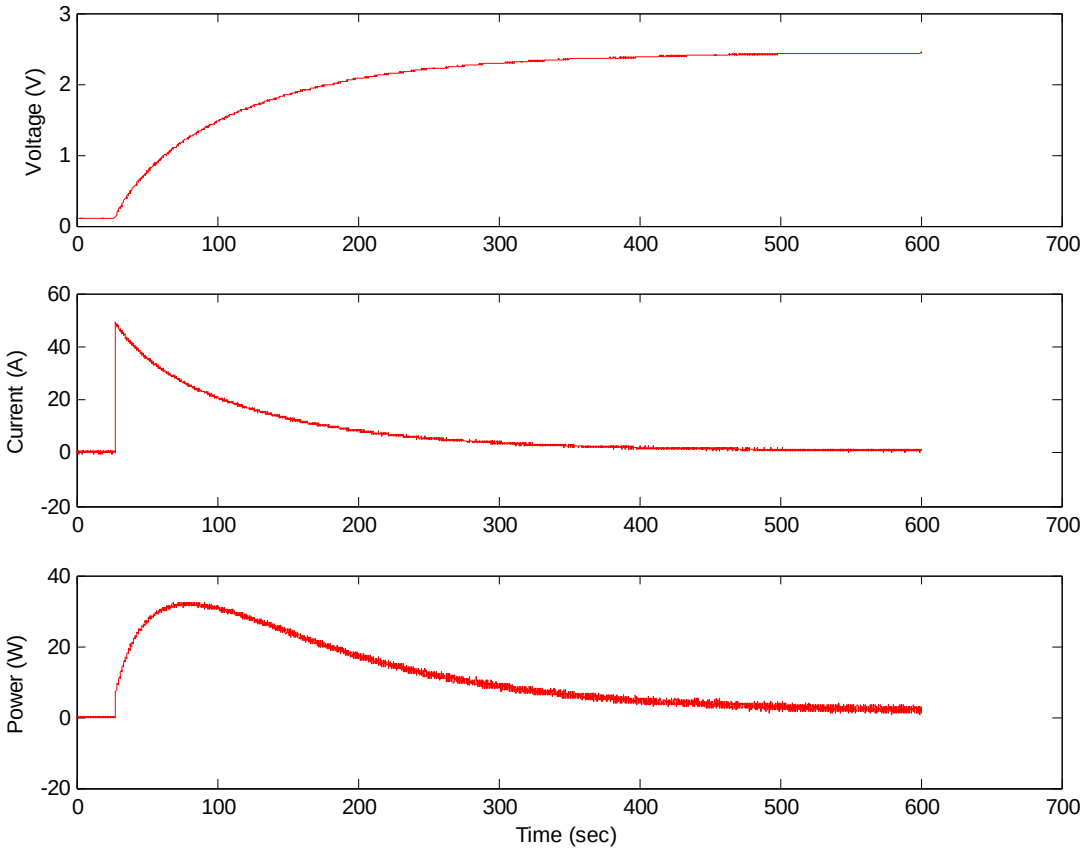

Figure A3.3-10: Plotted Matlab Data of 60 A Charge Cycle at T= 25°C

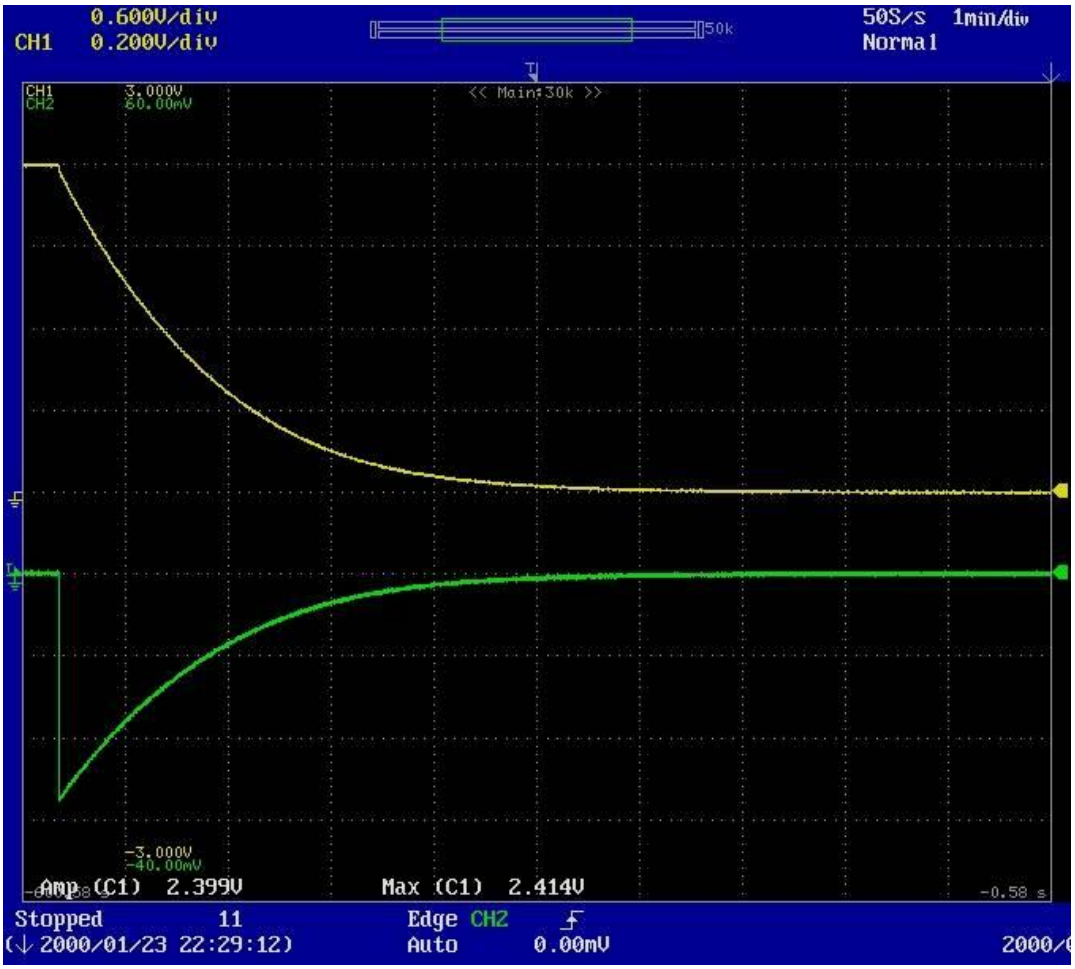

Figure A3.3-11: Oscilloscope Screen Capture of 60 A Discharge Cycle at T= 25°C (Timescale: 1 min/div)

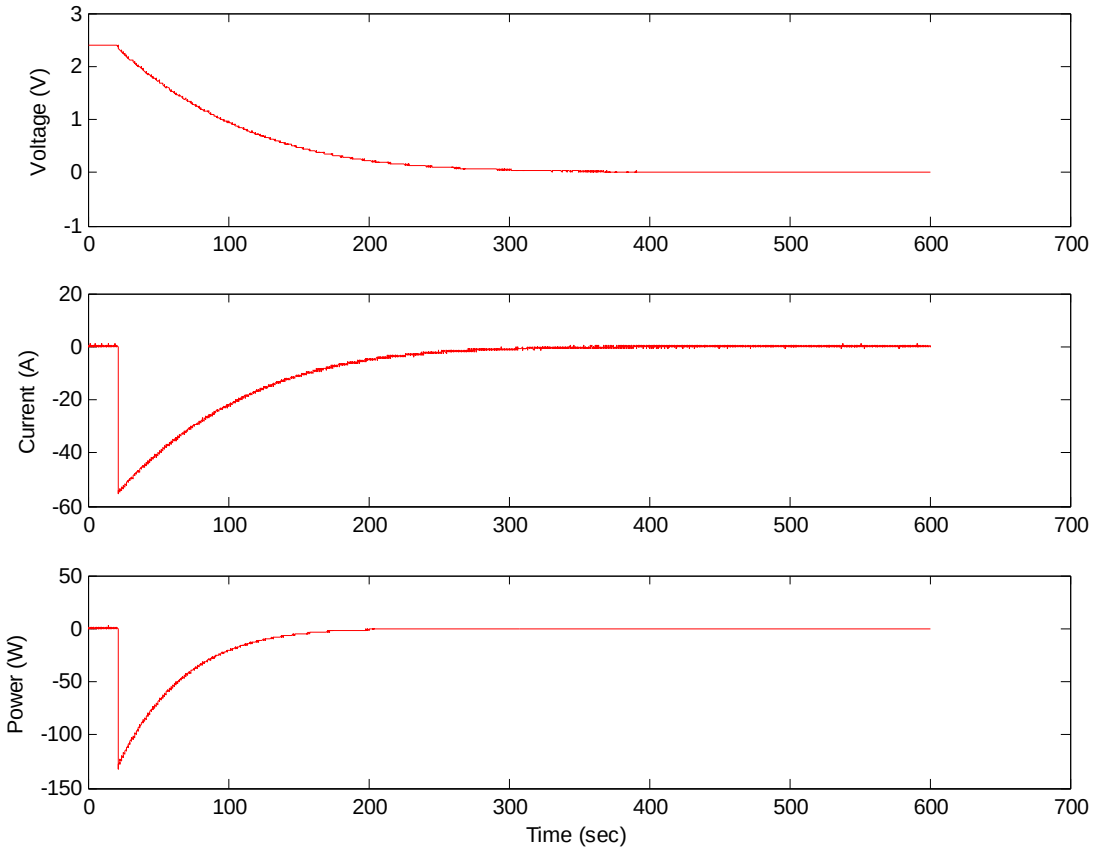

Figure A3.3-12: Plotted Matlab Data of 60 A Discharge Cycle at T=25°C

Figure A3.3-13: Oscilloscope Screen Capture of 60 A Charge Cycle at T= 50°C (Timescale: 1 min/div)

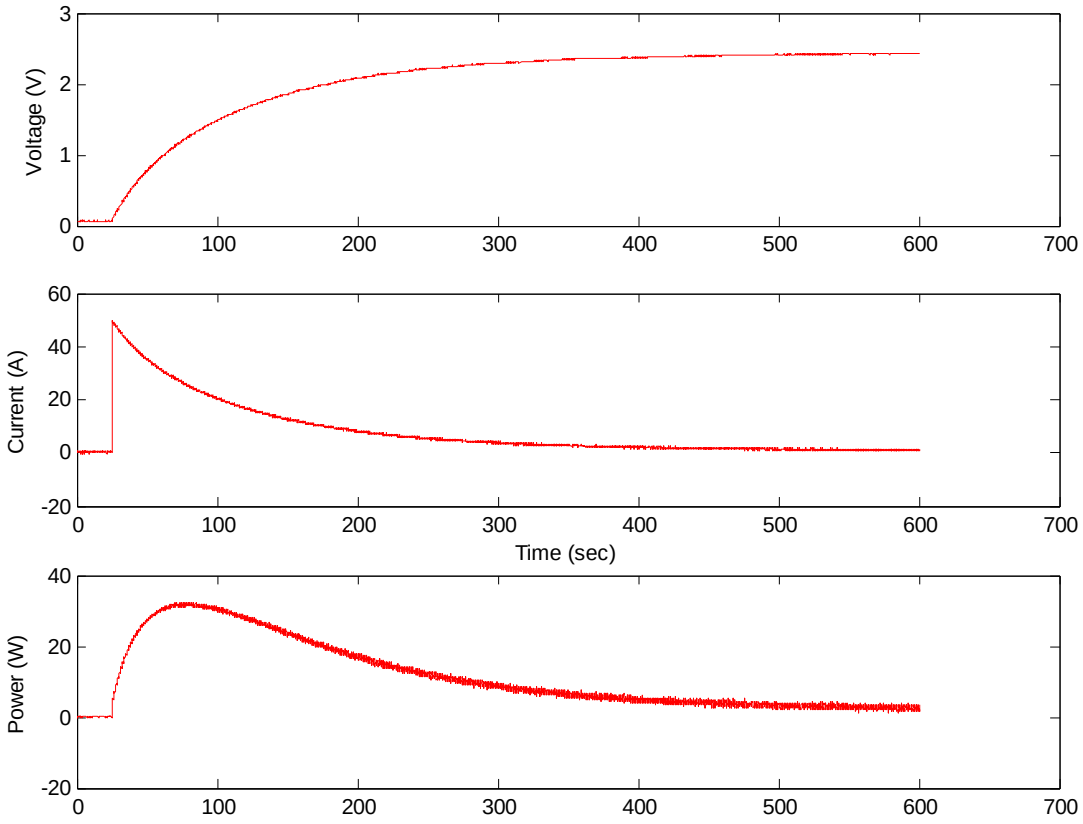

Figure A3.3-14: Plotted Matlab Data of 60 A Charge Cycle at T=50°C

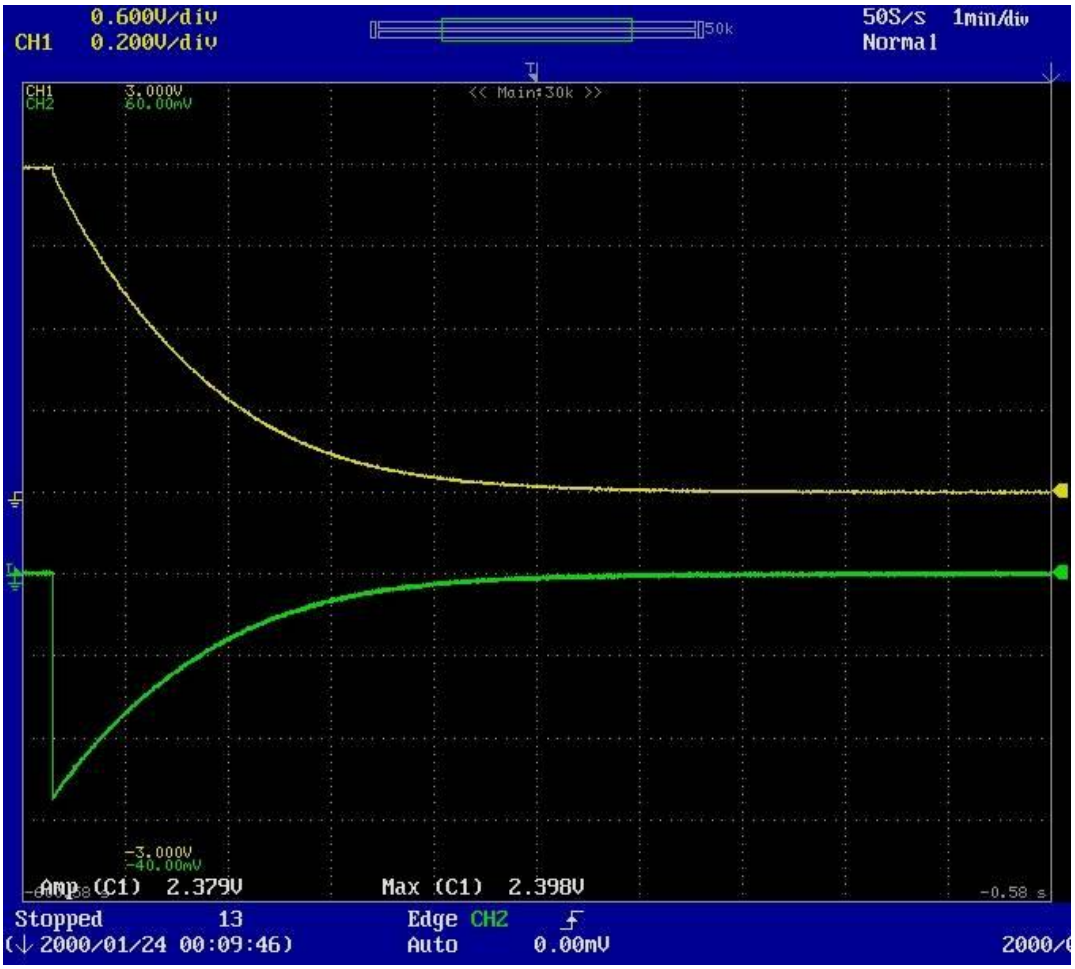

Figure A3.3-15: Oscilloscope Screen Capture of 60 A Discharge Cycle at T= 50°C (Timescale: 1 min/div)

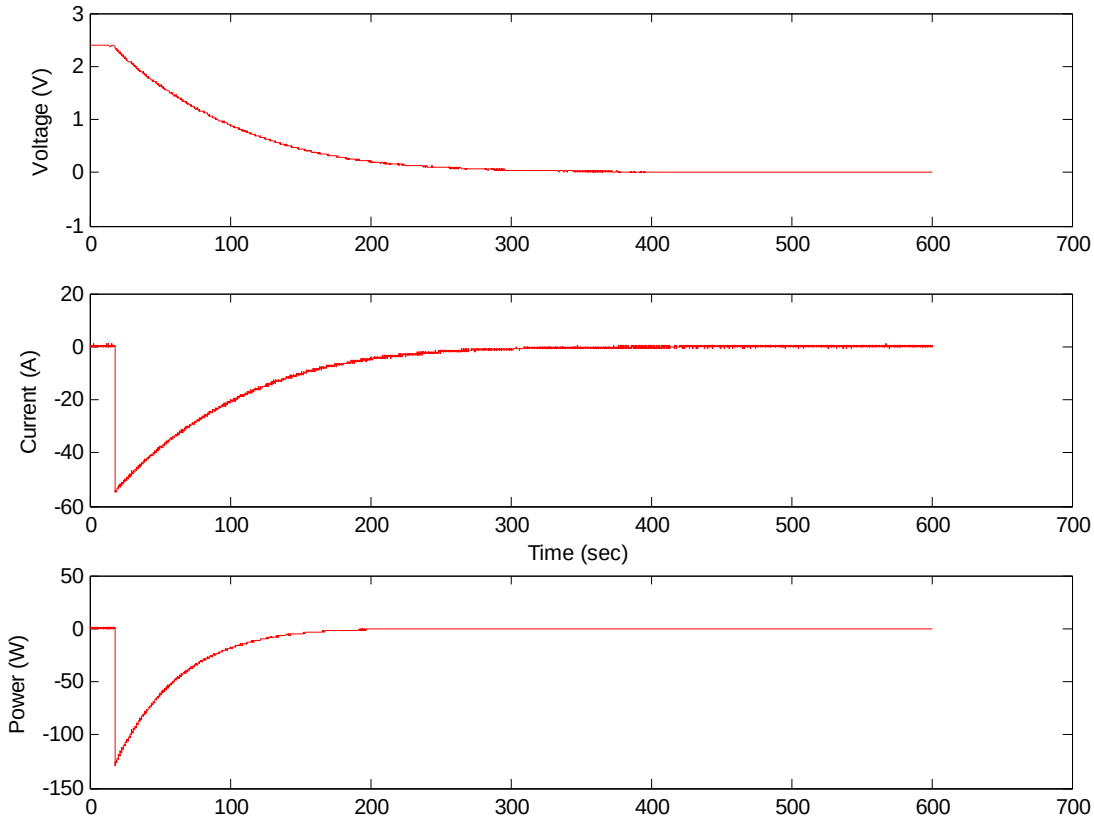

Figure A3.3-16: Plotted Matlab Data of 60 A Discharge Cycle at T=50°C

Appendix B

This Appendix B contains the best fit coefficients of the best fit curves obtained from Matlab. In addition, Matlab plots of the best fit curves for the 450, 900, and 1800 F ultracapacitors are contained.

B1. Best Fit Curve Coefficients

The best fit curve coefficients for the 450, 900, and 1800 F ultracapacitor are contained within this section of the Appendix B**.**

Table B1.1: 450 F Ultracapacitor 25 A Voltage Coefficients

Temperature	A	B	C	D	R^2
-25°C Charge	2.394	$5.506e^{-5}$	-3.73	-.01955	.9988
-25 °C Discharge	.5394	-.0201	3.891	-.0201	.9984
0 °C Charge	2.392	$5.605e^{-5}$	-3.862	-.01964	.9988
0 °C Discharge	6.394	-.02369	-3.462	-.0451	.9999
25 °C Charge	2.385	$5.898e^{-5}$	-3.535	-.01942	.9988
25 °C Discharge	4	.02038	.7022	.02038	.9986
50 °C Charge	2.384	$6.008e^{-5}$	-3.839	-.02007	.9987
50 °C Discharge	1.468	-.02056	2.769	-.02056	.9987
50 °C Discharge	1.468	-.02056	2.769	-.02056	.9987

Table B1.2: 450 F Ultracapacitor 25 A Current Coefficients

Temperature	A	B	C	D	R^2
-25°C Charge	-162.5	-.01684	195.8	-.01684	.9893
-25 °C Discharge	3.339	-.006036	-45.5	-.01784	.9979
0 °C Charge	37.08	.02135	2.426	.004368	.9973
0 °C Discharge	2.205	.004701	-43.28	.01843	.9979
25 °C Charge	31.29	.01631	$1.104e^{-6}$	.02244	.9886
25 °C Discharge	2.128	.004684	-47.09	.01861	.9978
50 °C Charge	36.8	-.02117	2.004	-.003152	.9972
50 °C Discharge	1.328	-.002908	-42.11	-.01923	.9978

Table B1.3: 450 F Ultracapacitor 50 A Voltage Coefficients

Temperature	A	B	C	D	R^2
-25°C Charge	2.434	$2.38e^{-5}$	-5.568	-.03237	.9982
-25 °C Discharge	7.581	-.03575	-.1822	-.03575	.9983
0 °C Charge	2.433	$2.401e^{-5}$	-5.567	-.03259	.9984
0 °C Discharge	7.296	-.03258	-.7285	-.01883	.9991
25 °C Charge	2.43	$2.663e^{-5}$	-5.256	-.03311	.9982
25 °C Discharge	10.19	-.02993	-4.331	-.02468	.9993
50 °C Charge	2.422	$3.269e^{-5}$	-5.099	-.03311	.9984
50 °C Discharge	6.375	-.0371	$3.571e^{-5}$	.007203	.9987

Table B1.4: 450 F Ultracapacitor 50 A Current Coefficients

Temperature	A	B	C	D	R^2
-25°C Charge	-520.4	-.02992	608	-.02992	.9929
-25 °C Discharge	1.202	-.003882	-132.9	-.03432	.9979
0 °C Charge	170.7	-.03012	-83.32	-.03012	.9931
0 °C Discharge	1.236	-.004368	-127	-.03508	.9980
25 °C Charge	39.84	-.02197	103.5	-.06703	.9963
25 °C Discharge	1.074	-.003541	-115.1	-.03564	.9982
50 °C Charge	87.03	-.03387	1.424	-.002749	.9977
50 °C Discharge	.7864	-.002008	-116	-.03625	.9983

Table B1.5: 450 F Ultracapacitor 60 A Voltage Coefficients

Temperature	A	B	C	D	R^2
-25°C Charge	2.44	$1.845e^{-5}$	-6.243	-.03921	.9981
-25 °C Discharge	8.601	-.03993	-.07536	-.02279	.999
0 °C Charge	2.439	$1.955e^{-5}$	-6.149	-.03922	.9982
0 °C Discharge	8.613	-.04084	-.7971	-.02371	.9991
25 °C Charge	2.43	$2.631e^{-5}$	-5.975	-.03952	.9981
25 °C Discharge	9.412	-.04106	-.9145	-.02448	.9991
50 °C Charge	2.426	$2.917e^{-5}$	-6.479	-.04051	.9982
50 °C Discharge	11.15	-.04226	-.7626	-.02405	.9992

Table B1.6: 450 F Ultracapacitor 60 A Current Coefficients

Temperature	A	B	C	D	R^2
-25°C Charge	450.2	-.03674	-328.5	-.03674	.994
-25 °C Discharge	6.702	-.0139	-191.1	-.04063	.998
0 °C Charge	58.47	-.02731	187.1	-.08238	.9972
0 °C Discharge	1.021	-.004018	-195	-.0445	.9982
25 °C Charge	1.053e4	-.03632	-1.041e4	-.03632	.9915
25 °C Discharge	11.14	-.01739	-207.8	-.04117	.9982
50 °C Charge	137.9	-.04167	1.689	-.003401	.9978
50 °C Discharge	19.99	-.02094	-255.2	-.04084	.9984

Table B1.7: 900 F Ultracapacitor 25 A Voltage Coefficients

Temperature	A	B	C	D	R^2
-25°C Charge	2.261	.00014	-2.783	-.01117	.9992
-25 °C Discharge	7.032	-.01332	-4.269	-.01902	.9999
0 °C Charge	2.263	$1.331e^{-4}$	-2.663	-.01102	.9993
0 °C Discharge	8.727	-.01389	-5.987	-.01787	.9999
25 °C Charge	2.241	$1.439e^{-4}$	-2.597	-.01128	.9993
25 °C Discharge	1.818	-.01056	1.4	-.01056	.9979
50 °C Charge	2.241	$1.349e^{-4}$	-2.835	-.01148	.9993
50 °C Discharge	4.321	-.008903	-1.244	-.00632	.9981

Table B1.8: 900 F Ultracapacitor 25 A Current Coefficients

Temperature	A	B	C	D	R^2
-25°C Charge	35.01	-.009038	-8.407	-.009038	.9948
-25 °C Discharge	-33.77	-.01058	-	-	.9962
0 °C Charge	21.63	-.01235	6.136	-.00472	.9983
0 °C Discharge	-32.93	-.01073	-	-	-
25 °C Charge	15.8	-.006793	13.28	-.02048	.9986
25 °C Discharge	32.59	-.01071	-	-	.9965
50 °C Charge	-36.03	-.00884	62.43	-.00884	.9912
50 °C Discharge	-51.92	-.01296	24.68	-.02169	.999

Table B1.9: 900 F Ultracapacitor 50 A Voltage Coefficients

Temperature	A	B	C	D	R^2
-25°C Charge	2.386	$6.118e^{-5}$	-3.349	-.01776	.9988
-25 °C Discharge	1.071	-.01892	2.793	.01892	.998
0 °C Charge	2.382	$6.348e^{-5}$	-3.266	-.01773	.9989
0 °C Discharge	7.296	-.02319	-4.39	-.03921	.9998
25 °C Charge	2.376	$6.275e^{-5}$	-3.339	-.01761	.9989
25 °C Discharge	5.145	-.01661	-.9736	-.01087	.9992
50 °C Charge	2.366	$6.649e^{-5}$	-3.284	-.01794	.9989
50 °C Discharge	6.622	-.02278	-3.64	-.04071	.9984

Table B1.10: 900 F Ultracapacitor 50 A Current Coefficients

Temperature	A	B	C	D	R^2
-25°C Charge	30.99	-.01178	37.1	-.03363	.9988
-25 °C Discharge	13.47	-.008617	-81.45	-.01601	.9988
0 °C Charge	51.43	-.02063	7.884	-.006542	.9988
0 °C Discharge	10.32	-.007616	-84.56	-.01643	.9989
25 °C Charge	12.9	-.007873	50.04	-.02291	.9987
25 °C Discharge	12.25	-.00871	-88.69	-.01659	.9989
50 °C Charge	5.4	-.004834	53.53	-.01987	.9987
50 °C Discharge	11.75	-.008602	-85.67	-.01665	.999

Table B1.11: 900 F Ultracapacitor 60 A Voltage Coefficients

Temperature	A	B	C	D	R^2
-25°C Charge	2.411	$4.203e^{-5}$	-3.959	-.02147	.9986
-25 °C Discharge	5.611	-.02078	-.8598	-.01274	.9991
0 °C Charge	2.409	$4.359e^{-5}$	-3.848	-.02148	.9986
0 °C Discharge	5.555	-.02108	-.8524	-.01294	.9991
25 °C Charge	2.404	$4.665e^{-5}$	-3.495	-.02155	.9987
25 °C Discharge	93.45	-.03497	-90.23	-.03625	.9999
50 °C Charge	2.399	$4.736e^{-5}$	-3.816	-.02186	.9987
50 °C Discharge	3.169	-.0245	2.128	-.0245	.9996

Table B1.12: 900 F Ultracapacitor 60 A Current Coefficients

Temperature	A	B	C	D	R^2
-25°C Charge	$-9.935e^{4}$	-.01965	$9.943e^{4}$	-.01965	.9959
-25 °C Discharge	15.58	-.0107	-126.6	-.02067	.9989
0 °C Charge	65.26	$-6.611e^{-4}$	29.91	$-2.595e^{-4}$	.9989
0 °C Discharge	14.49	-.01075	-124.5	-.02108	.9989
25 °C Charge	7.056	-.007137	70.84	-.02439	.9988
25 °C Discharge	12.65	-.01023	-124.6	-.0214	.999
50 °C Charge	-1199	-.01946	1274	-.01946	.9937
50 °C Discharge	14.15	-.01095	-130.8	-.02148	.9991

Table B1.13: 1800 F Ultracapacitor 25 A Voltage Coefficients

Temperature	A	B	C	D	R^2
-25°C Charge	1.988	$2.715e^{-4}$	-2.249	-.006953	.9996
-25 °C Discharge	10.02	-.007495	-7.603	-.008754	.9999
0 °C Charge	2.006	$2.562e^{-4}$	-2.203	-.006881	.9996
0 °C Discharge	49.65	-.007985	-47.18	-.00822	.9999
25 °C Charge	2.029	$2.339e^{-4}$	-2.17	-.006763	.9996
25 °C Discharge	5.499	-.007061	-3.071	-.009768	.9999
50 °C Charge	2.045	$2.161e^{-4}$	-2.093	-.006698	.9996
50 °C Discharge	4.15	-.006724	-1.744	-.01138	.9999

Table B1.14: 1800 F Ultracapacitor 25 A Current Coefficients

Temperature	A	B	C	D	R^2
-25°C Charge	18.19	-.003808	9.194	-.01301	.9989
-25 °C Discharge	-26.75	-.005694	-	-	.9947
0 °C Charge	16.97	-.003704	9.636	-.01201	.9989
0 °C Discharge	-27.59	-.005734	-	-	.9948
25 °C Charge	16.72	-.003652	9.386	-.01203	.9989
25 °C Discharge	-26.73	-.005748	-	-	.9951
50 °C Charge	3.605	-.001339	20.44	-.006182	.9983
50 °C Discharge	-26.83	-.0057	-	-	.9954

Table B1.15: 1800 F Ultracapacitor 50 A Voltage Coefficients

Temperature	A	B	C	D	R^2
-25°C Charge	2.238	$1.503e^{-4}$	-2.709	-.0102	.9994
-25 °C Discharge	5.368	-.01222	-2.713	-.01989	.9999
0 °C Charge	2.228	$1.587e^{-4}$	-2.743	-.01038	.9993
0 °C Discharge	5.559	-.01234	-2.857	-.01908	.9999
25 °C Charge	2.223	$1.579e^{-4}$	-2.686	-.01047	.9993
25 °C Discharge	6.258	-.01252	-3.503	-.0182	.9999
50 °C Charge	2.218	$1.535e^{-4}$	-2.791	-.0105	.9994
50 °C Discharge	4.048	-.01164	-1.471	-.02297	.9998

Table B1.16: 1800 F Ultracapacitor 50 A Current Coefficients

Temperature	A	B	C	D	R^2
-25°C Charge	35.55	-.01216	15.04	-.004789	.9992
-25 °C Discharge	-56.58	-.01012	-	-	.9965
0 °C Charge	36.39	-.01215	14.69	-.004759	.9992
0 °C Discharge	-58.07	-.01024	-	-	.9964
25 °C Charge	39.42	-.01134	10.23	-.003968	.999
25 °C Discharge	-59.52	-.01023	-	-	.9967
50 °C Charge	26.95	-.005839	28.35	-.01776	.9993
50 °C Discharge	-54.63	-.01031	-	-	.997

Table B1.17: 1800 F Ultracapacitor 60 A Voltage Coefficients

Temperature	A	B	C	D	R^2
-25°C Charge	2.298	$1.186e^{-4}$	-2.927	-.01221	.9992
-25 °C Discharge	1.804	-.0125	1.331	-.0125	.9979
0 °C Charge	2.293	$1.198e^{-4}$	-3.135	-.01217	.9992
0 °C Discharge	2.088	-.01262	1.299	-.01262	.998
25 °C Charge	2.286	$1.169e^{-4}$	-2.876	-.01215	.9993
25 °C Discharge	4.474	-.01462	-1.796	-.02938	.9998
50 °C Charge	2.284	$1.108e^{-4}$	-2.872	-.01237	.9993
50 °C Discharge	3.82	-.01094	-.8354	-.007285	.9991

Table B1.18: 1800 F Ultracapacitor 60 A Current Coefficients

Temperature	A	B	C	D	R^2
-25°C Charge	25.47	-.006717	42.59	-.01686	.9994
-25 °C Discharge	-74.11	-.01274	-	-	.9968
0 °C Charge	40.7	-.007872	37.92	-.02347	.9995
0 °C Discharge	-79.94	-.01282	-	-	.9969
25 °C Charge	32.32	-.007051	37.88	-.02076	.9993
25 °C Discharge	-75.73	-.01283	-	-	.9972
50 °C Charge	56.5	-.013	7.42	-.003407	.9991
50 °C Discharge	-71.77	-.01287	-	-	.9975

B2. 450 F Ultracapacitor Best Fit Curve Results

The results for the 450 F are shown in this section. The results are broken into three sub-categories that are based on the current charge and discharge levels. Each figure contains the best fit curves for the four temperatures: -25°C, 0°C, 25°C and 50°C.

B2.1 450 F Ultracapacitor 25 A Results

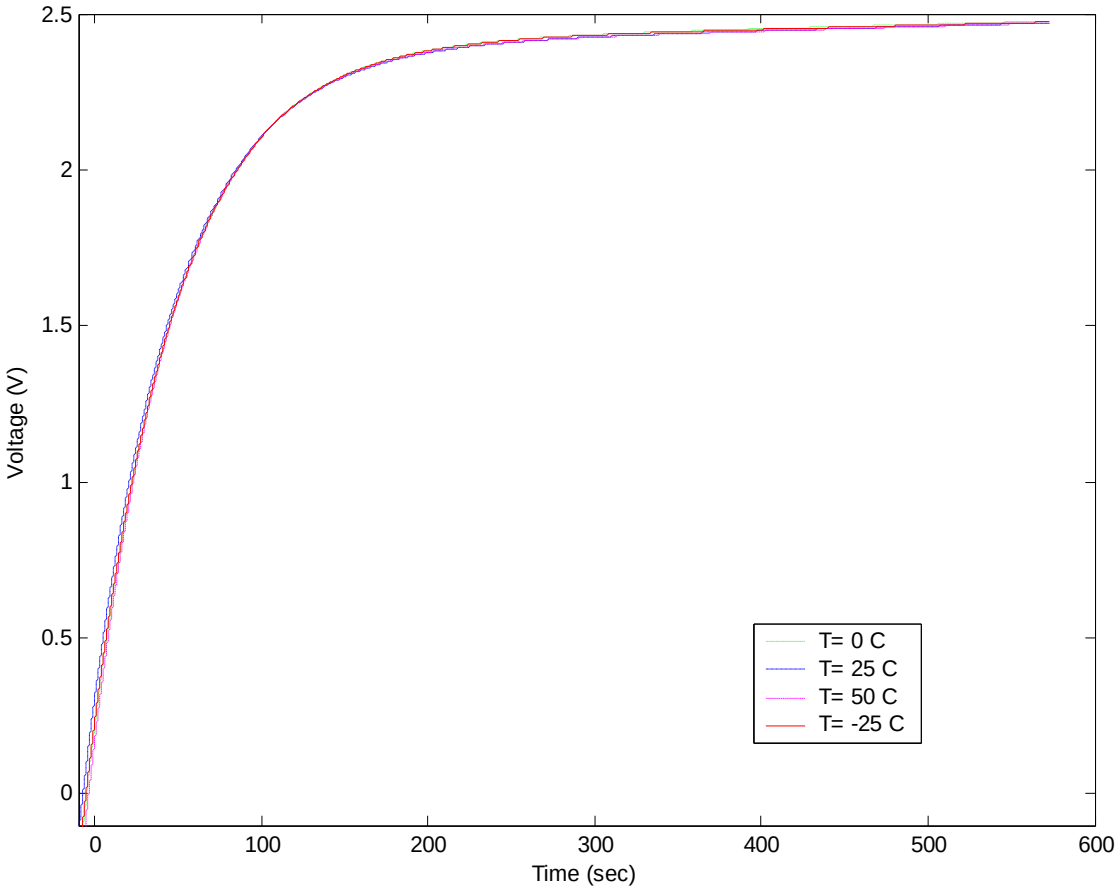

Figure B2.1-1: 25 A Charge Voltage Best Fit Curves

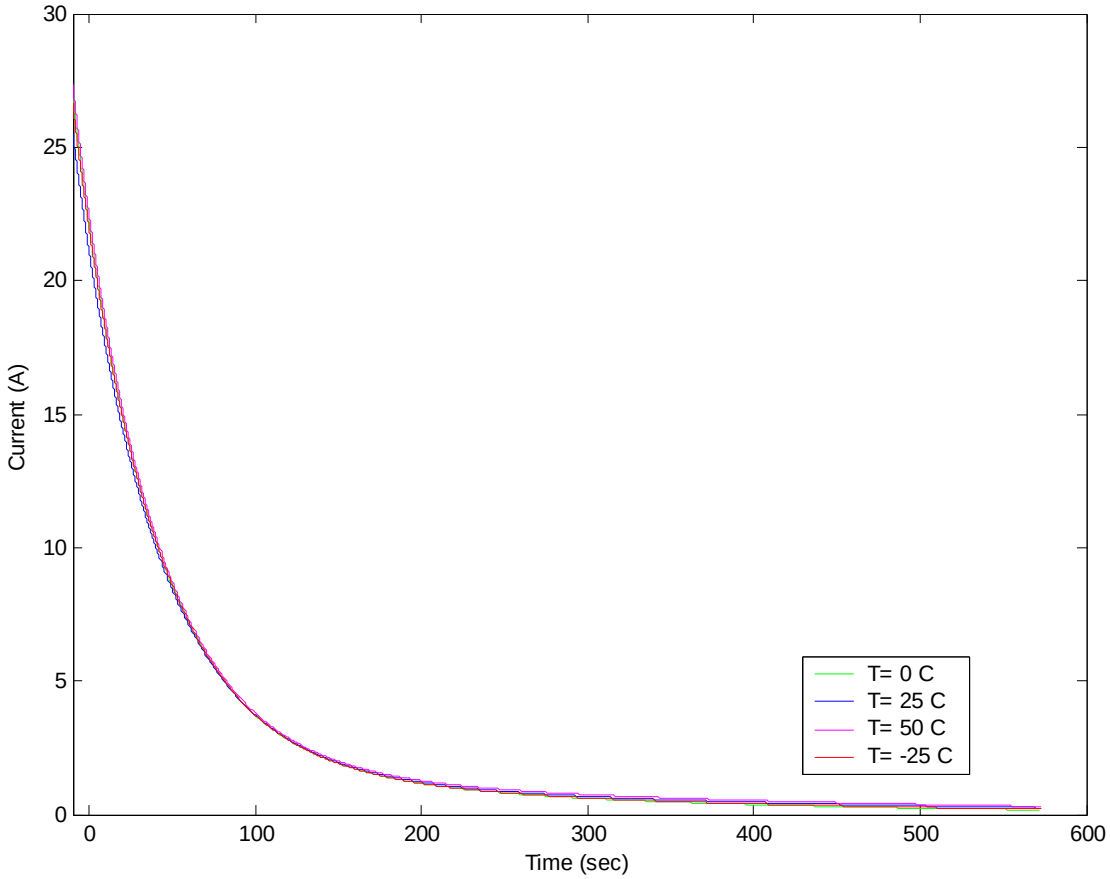

Figure B2.1-2: 25 A Charge Current Best Fit Curves

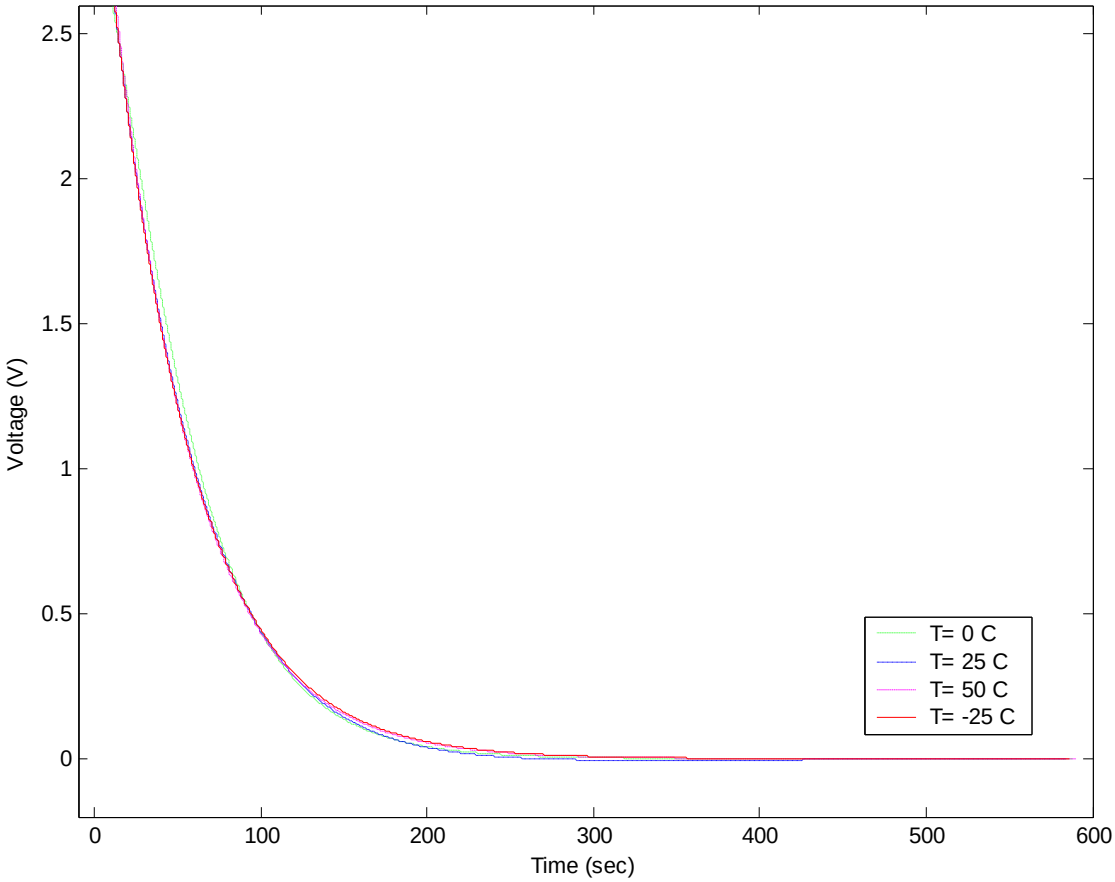

Figure B2.1-3: 25 A Discharge Voltage Best Fit Curves

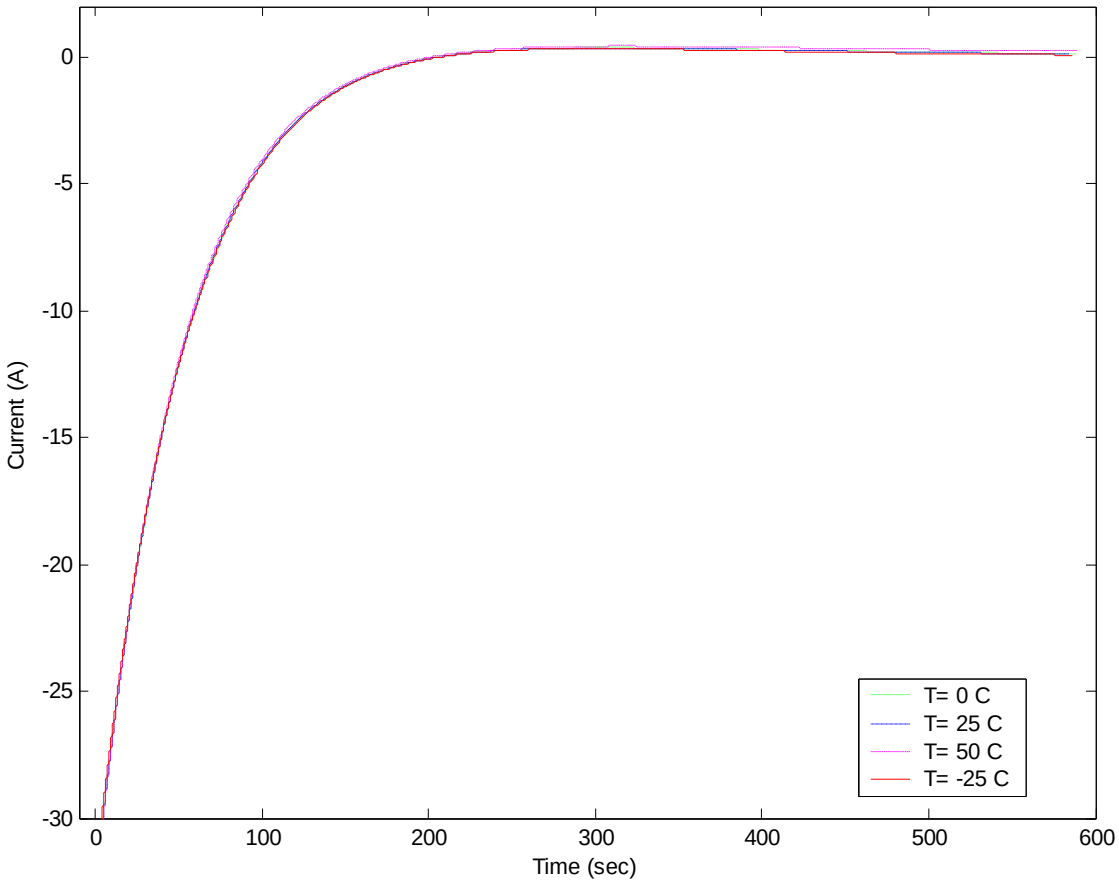

Figure B2.1-4: 25 A Discharge Current Best Fit Curves

B2.2 450 F Ultracapacitor 50 A Results

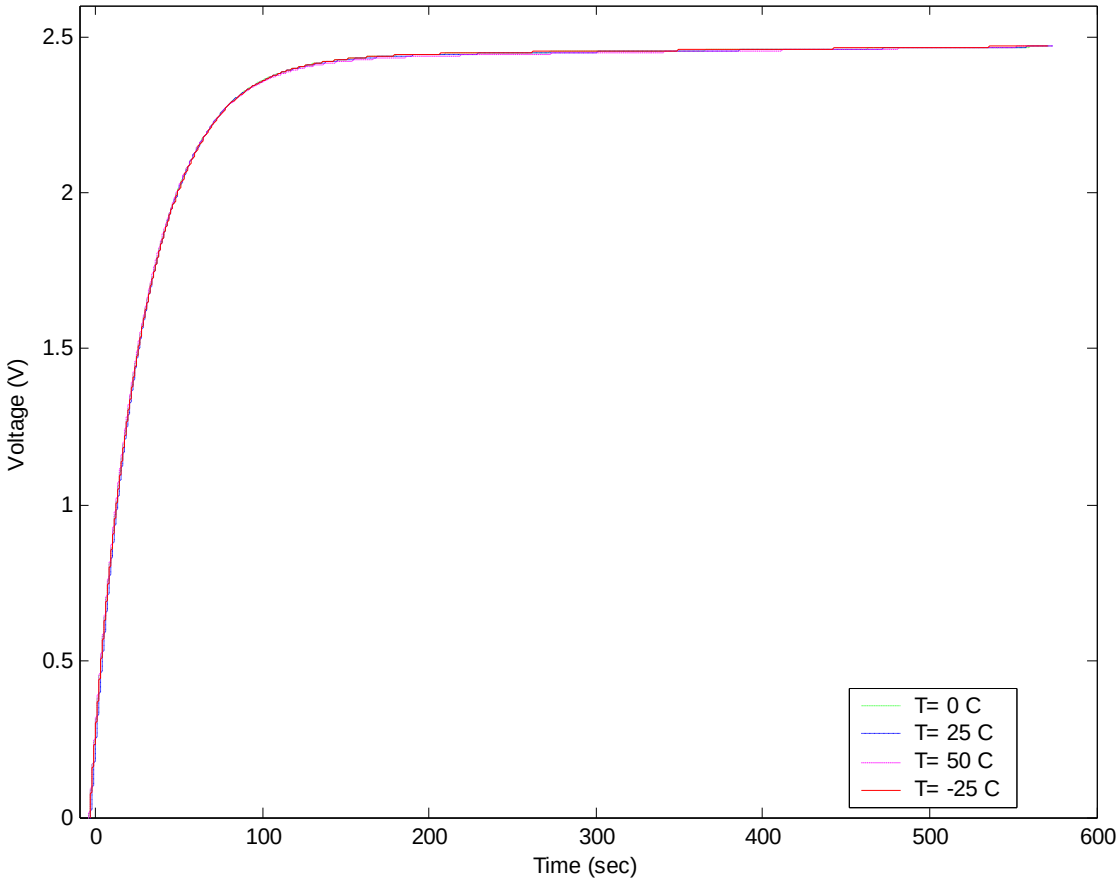

Figure B2.2-1: 50 A Charge Voltage Best Fit Curves

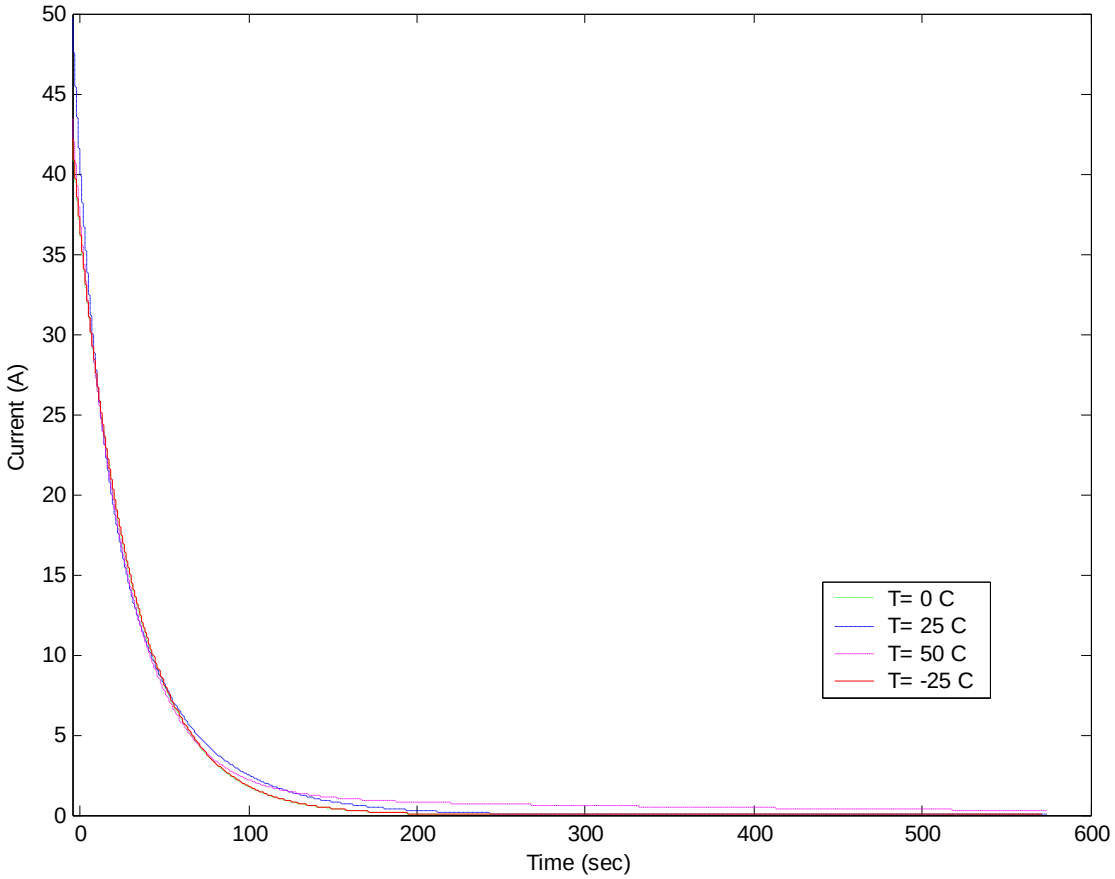

Figure B2.2-2: 50 A Charge Current Best Fit Curves

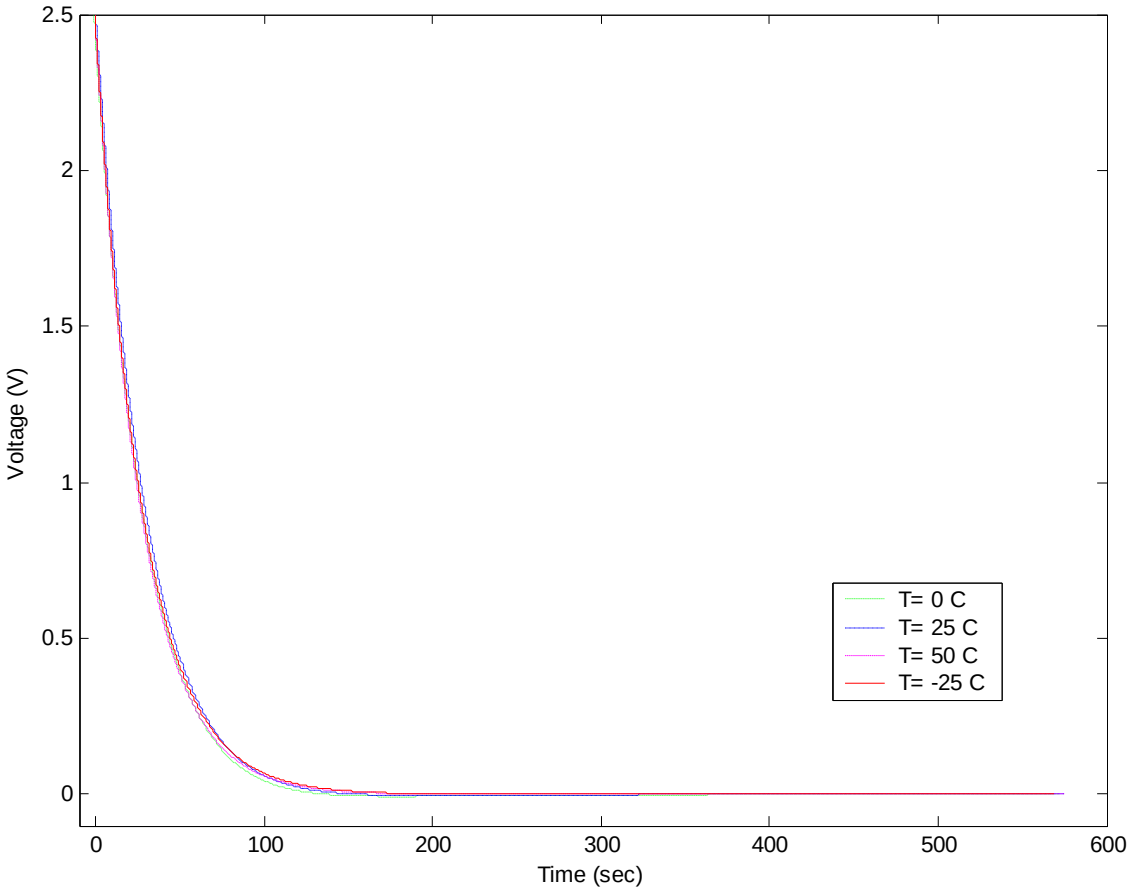

Figure B2.2-3: 50 A Discharge Voltage Best Fit Curves

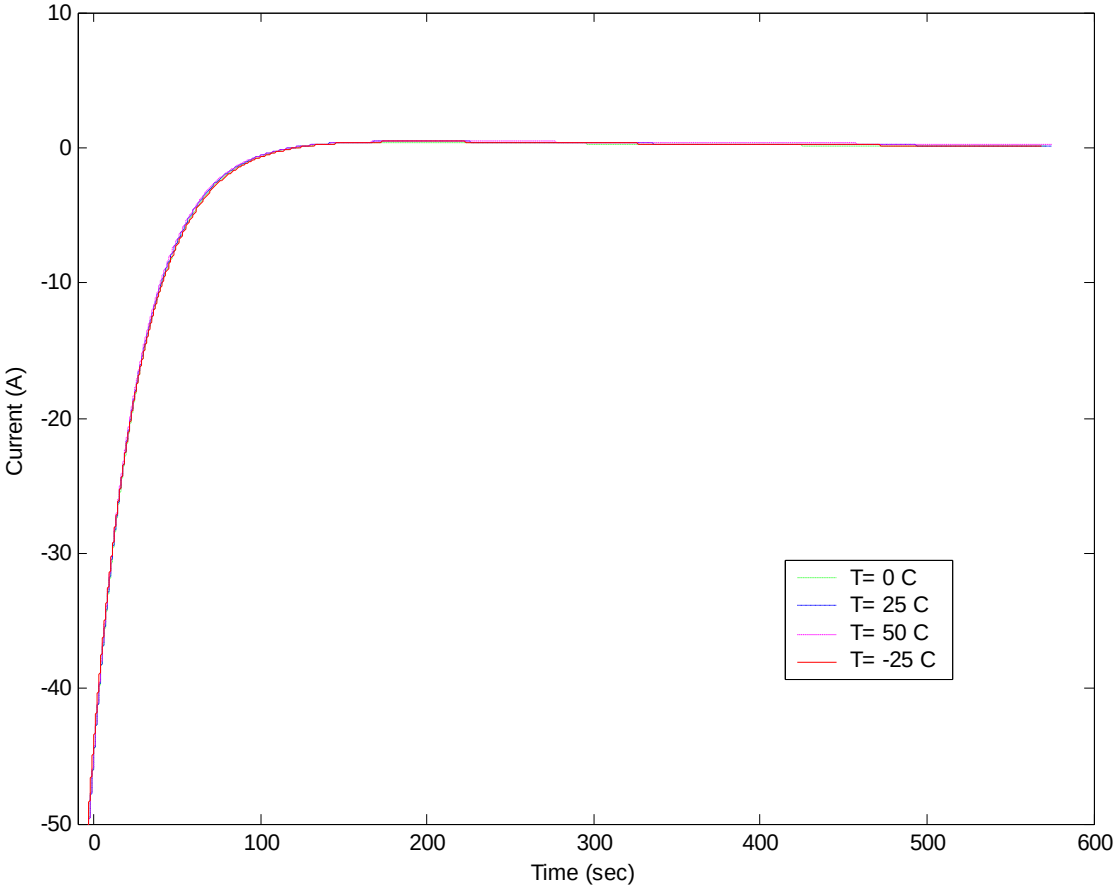

Figure B2.2-4: 50 A Discharge Current Best Fit Curves

B2.3 450 F Ultracapacitor 60 A Results

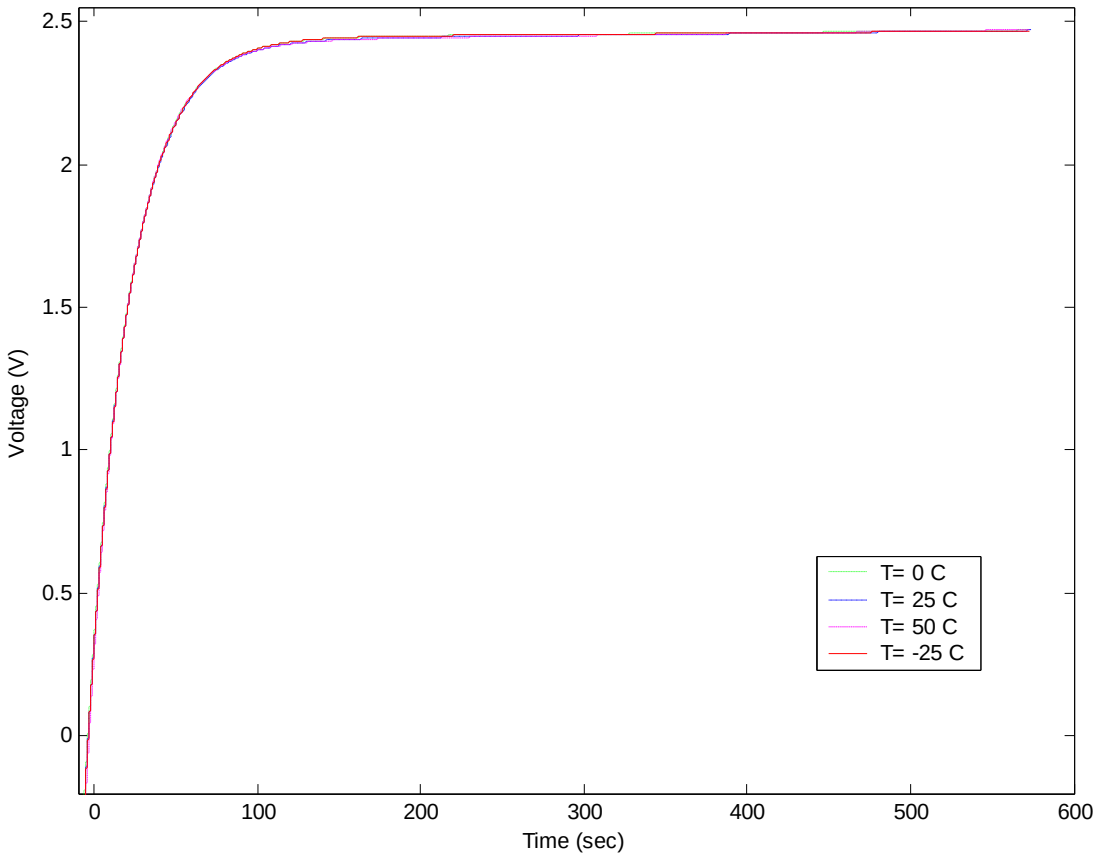

Figure B2.3-1: 60 A Charge Voltage Best Fit Curves

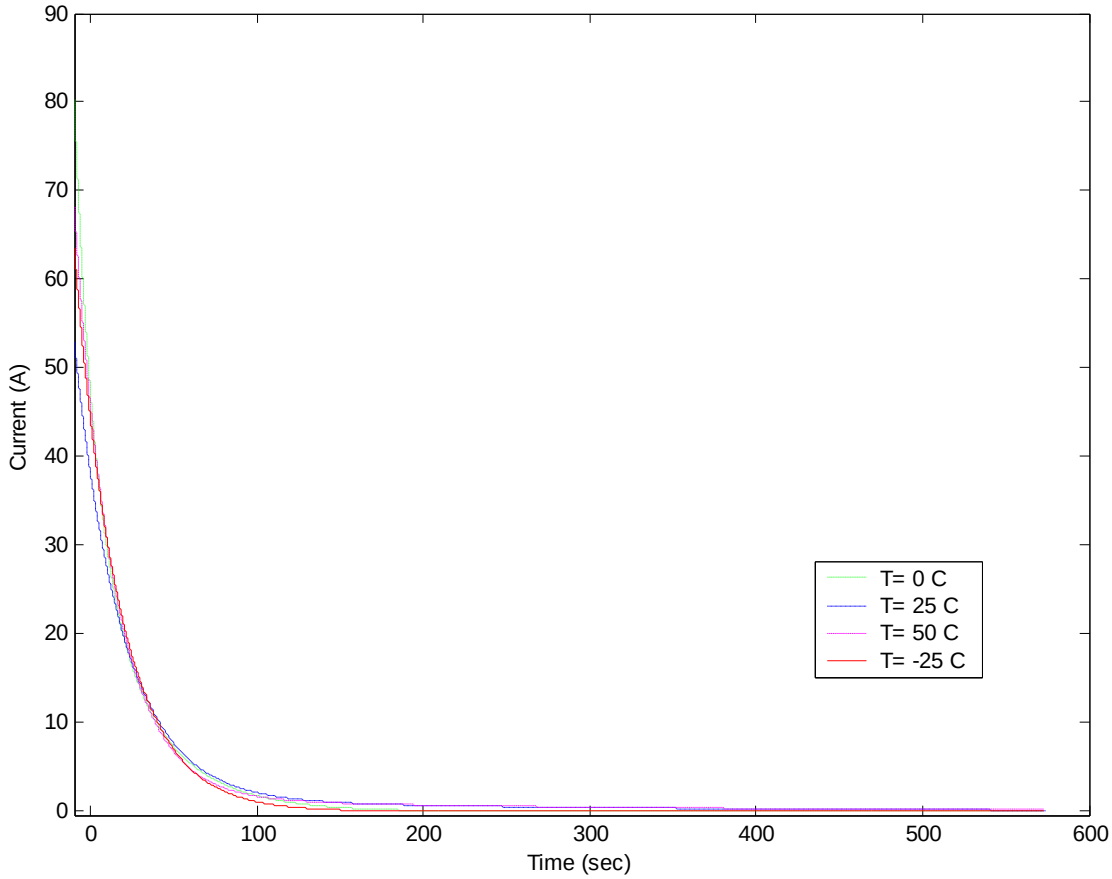

Figure B2.3-2: 60 A Charge Current Best Fit Curves

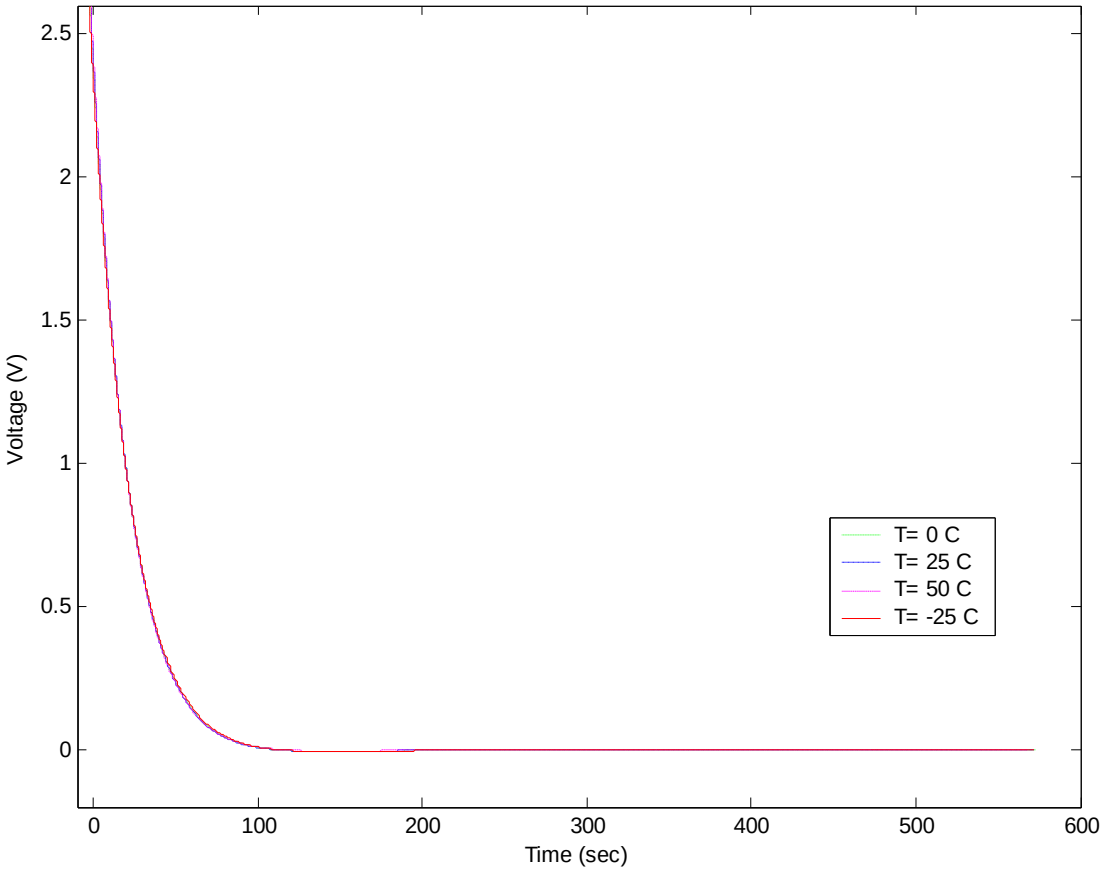

Figure B2.3-3: 60 A Discharge Voltage Best Fit Curves

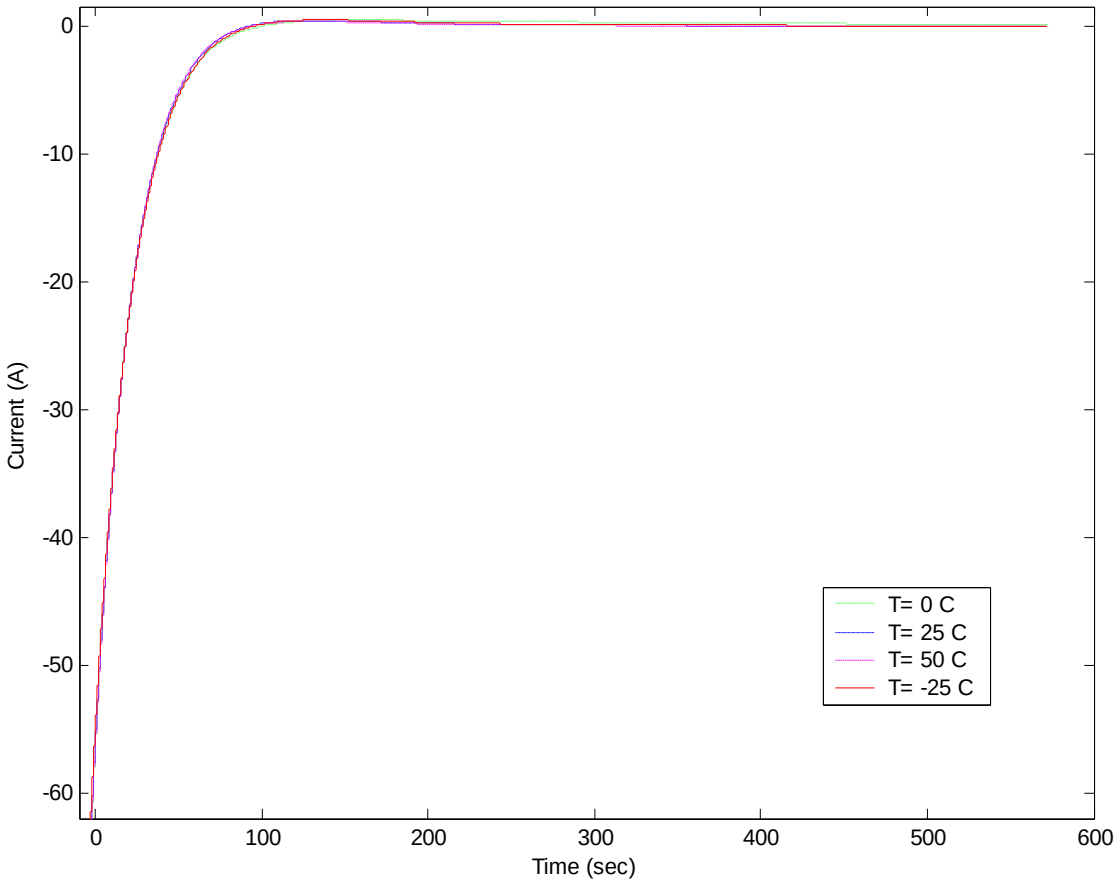

Figure B2.3-4: 60 A Discharge Current Best Fit Curves

B3. 900 F Ultracapacitor Best Fit Curve Results

The results for the 900 F are shown in this section. The results are broken into three sub-categories that are based on the current charge and discharge levels. Each figure contains the best fit curves for the four temperatures: -25^{o}C, 0^{o}C, 25^{o}C and 50^{o}C.

B3.1 900 F Ultracapacitor 25 A Results

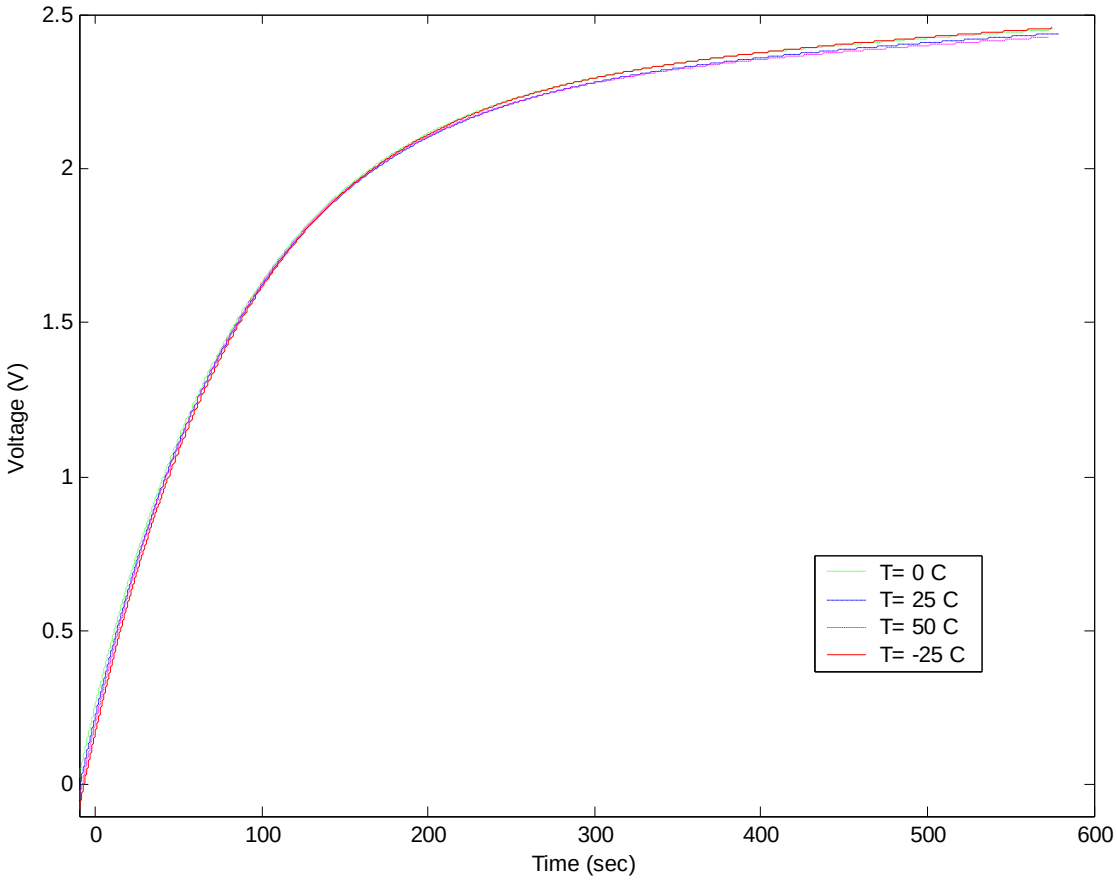

Figure B3.1-1: 25 A Charge Voltage Best Fit Curves

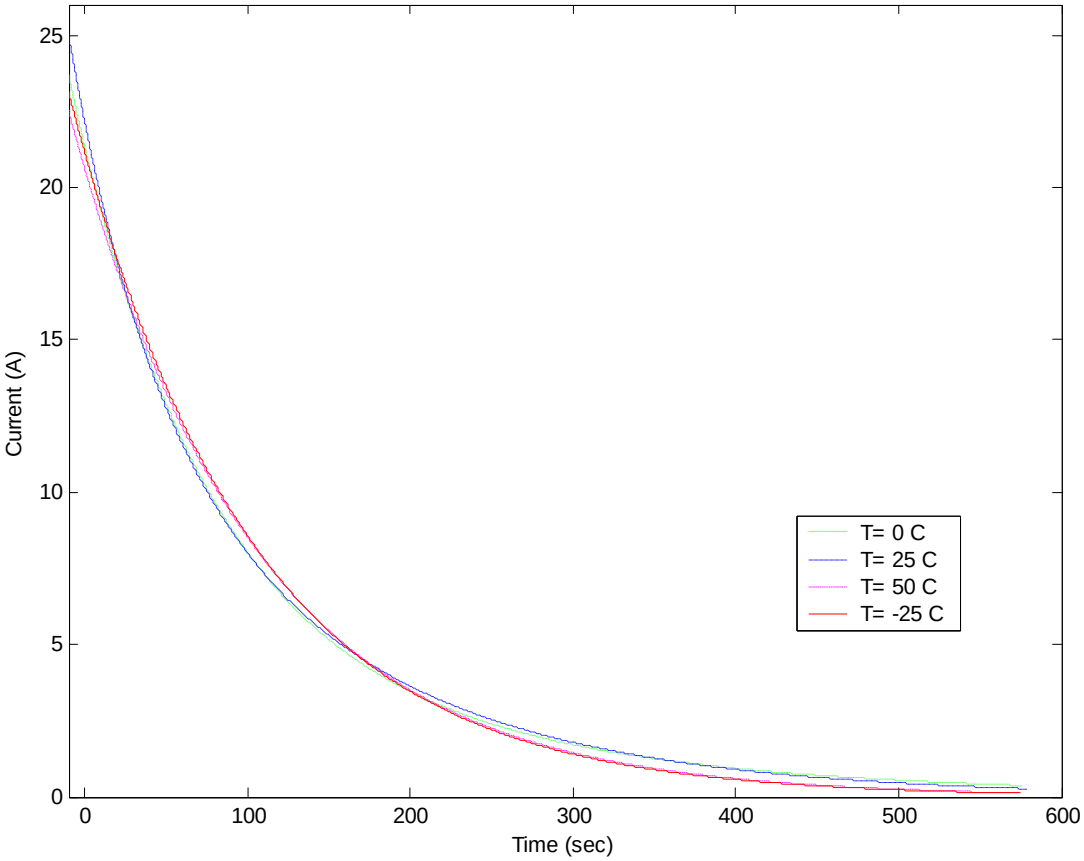

Figure B3.1-2: 25 A Charge Current Best Fit Curves

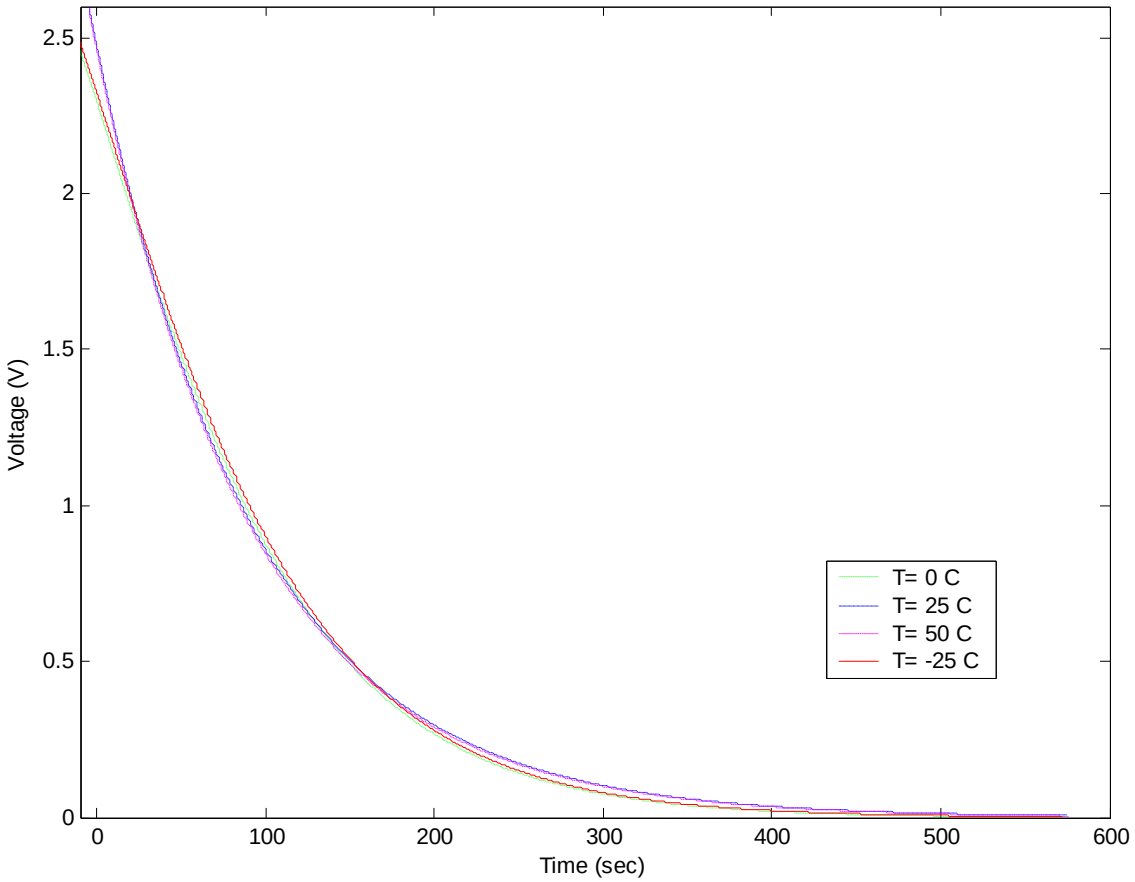

Figure B3.1-3: 25 A Discharge Voltage Best Fit Curves

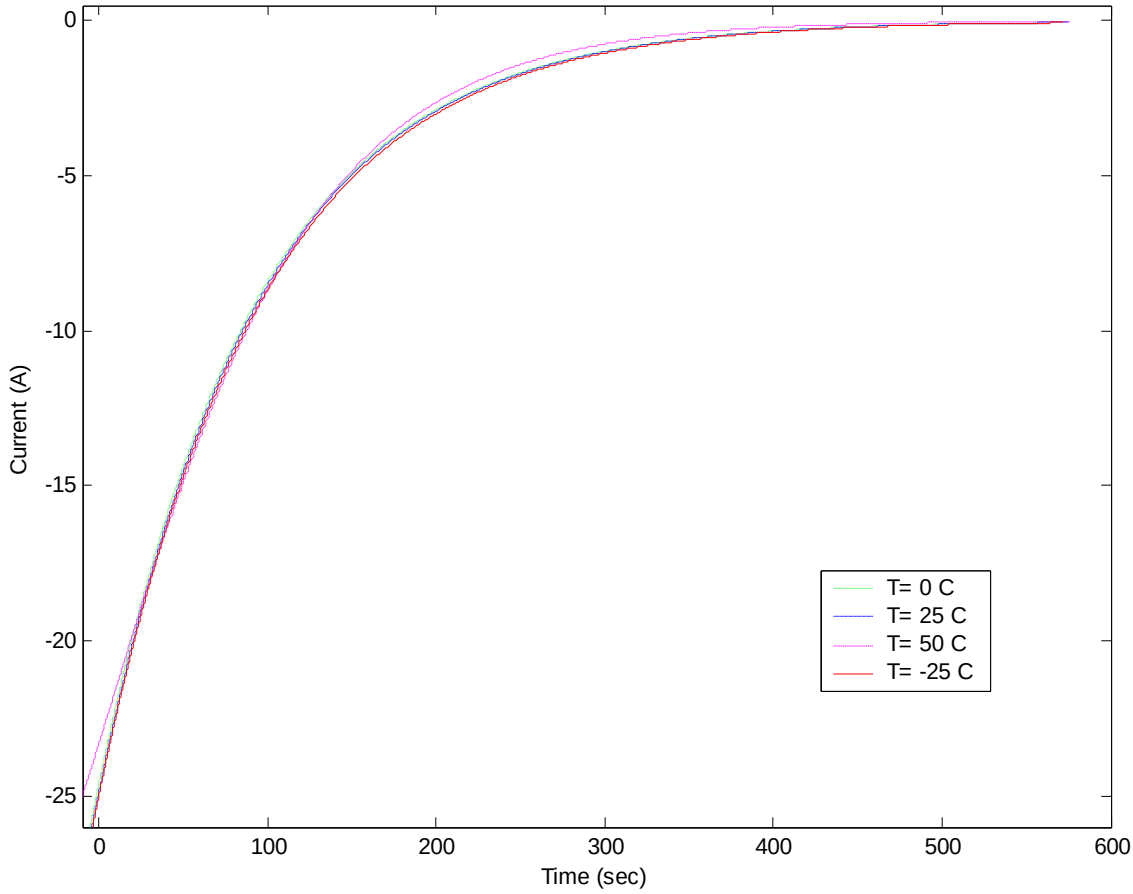

Figure B3.1-4: 25 A Discharge Current Best Fit Curves

B3.2 900 F Ultracapacitor 50 A Results

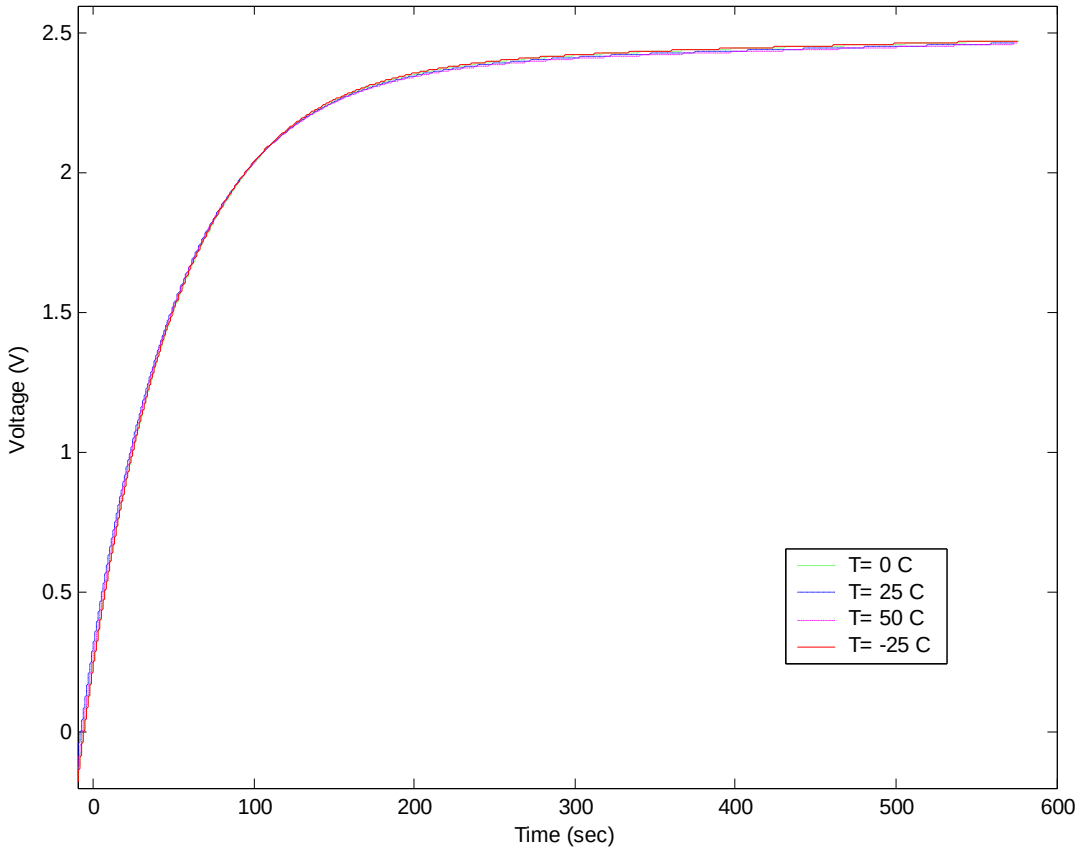

Figure B3.2-1: 50 A Charge Voltage Best Fit Curves

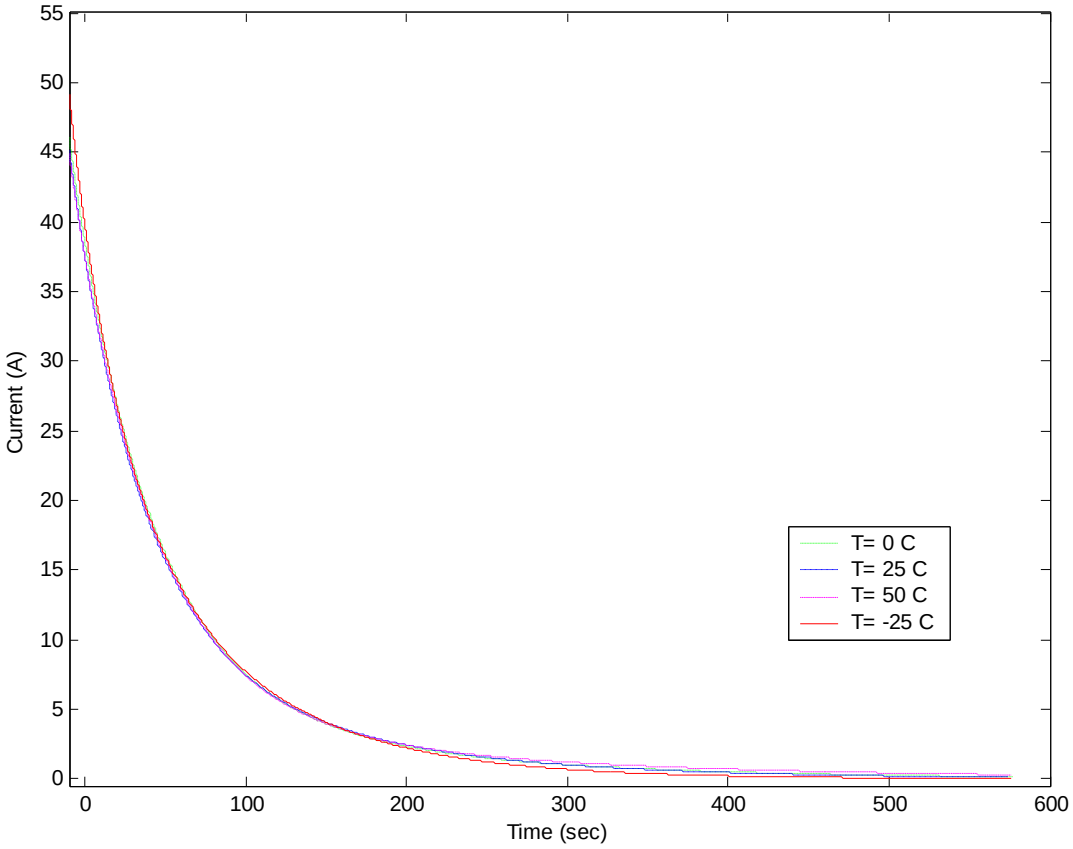

Figure B3.2-2: 50 A Charge Current Best Fit Curves

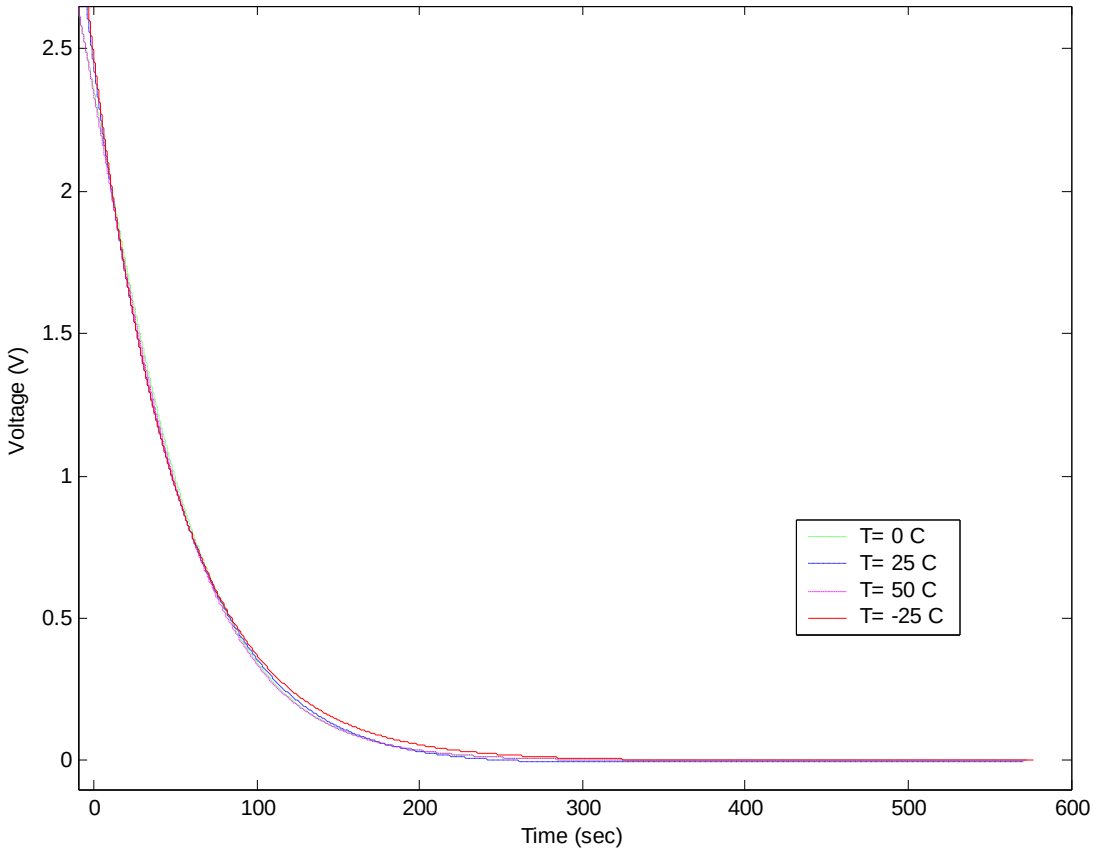

Figure B3.2-3: 50 A Discharge Voltage Best Fit Curves

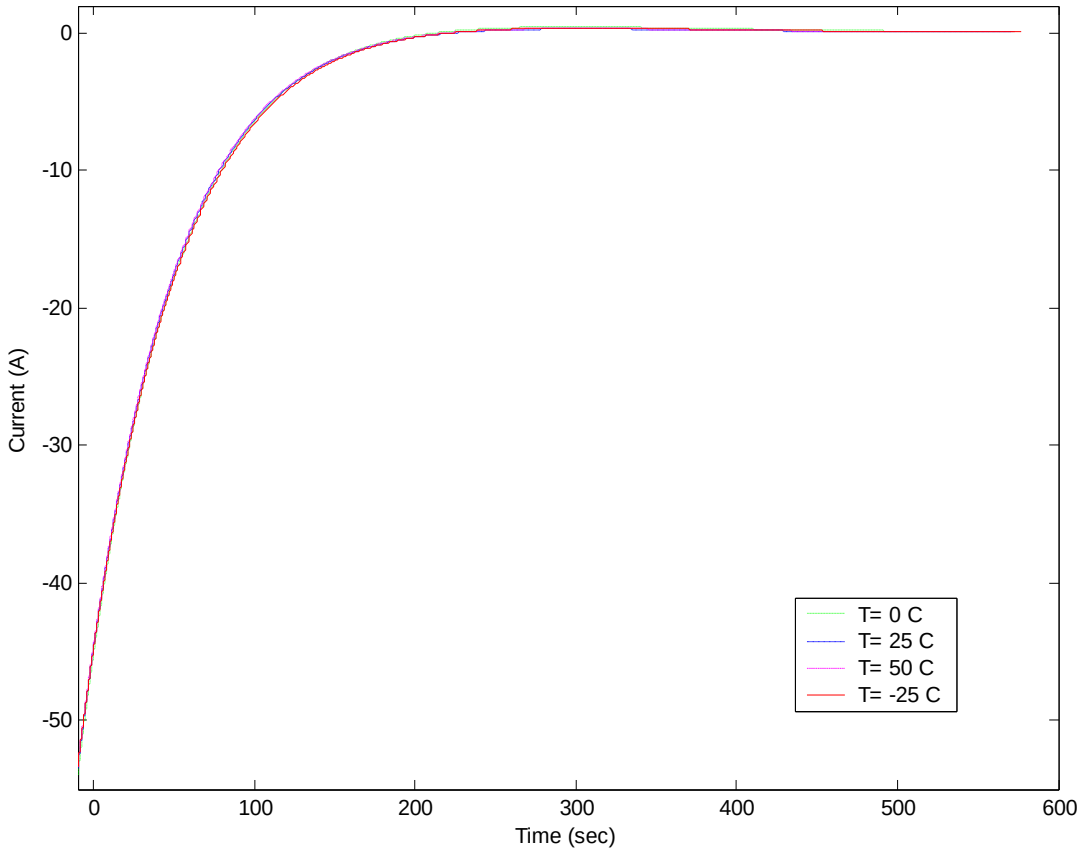

Figure B3.2-4: 50 A Discharge Current Best Fit Curves

B3.3 900 F Ultracapacitor 60 A Results

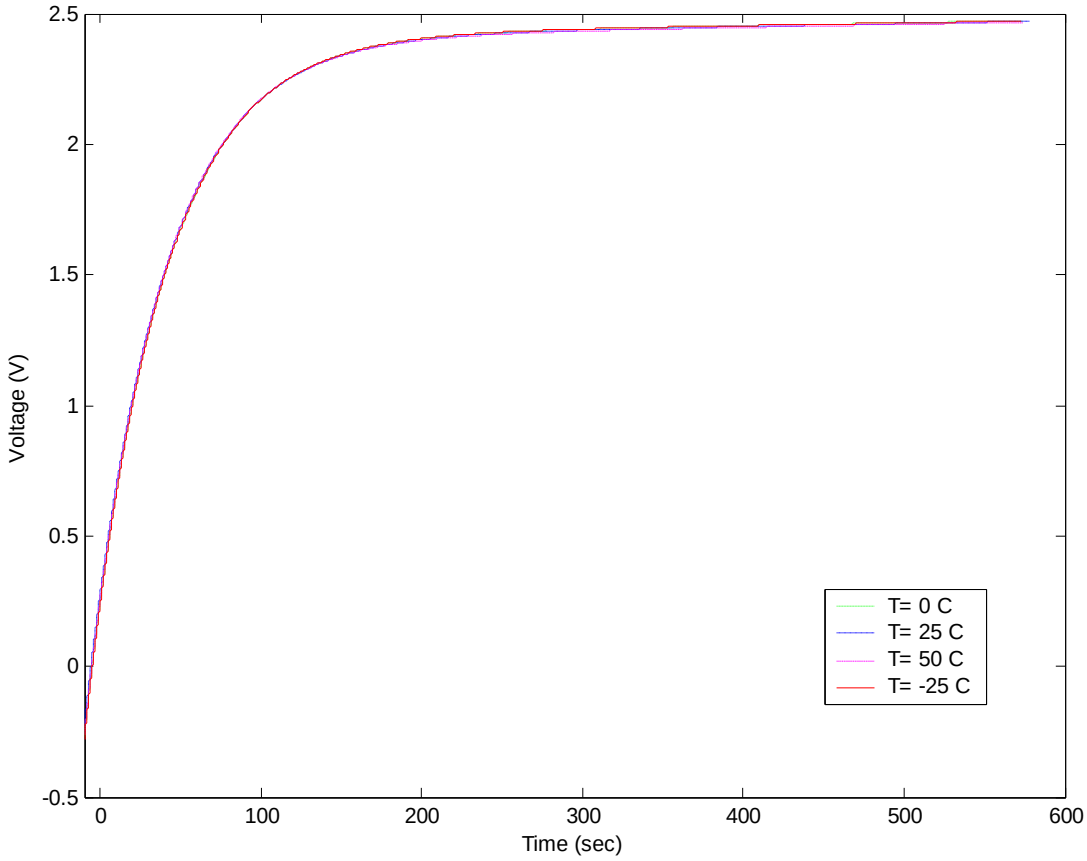

Figure B3.3-1: 60 A Charge Voltage Best Fit Curves

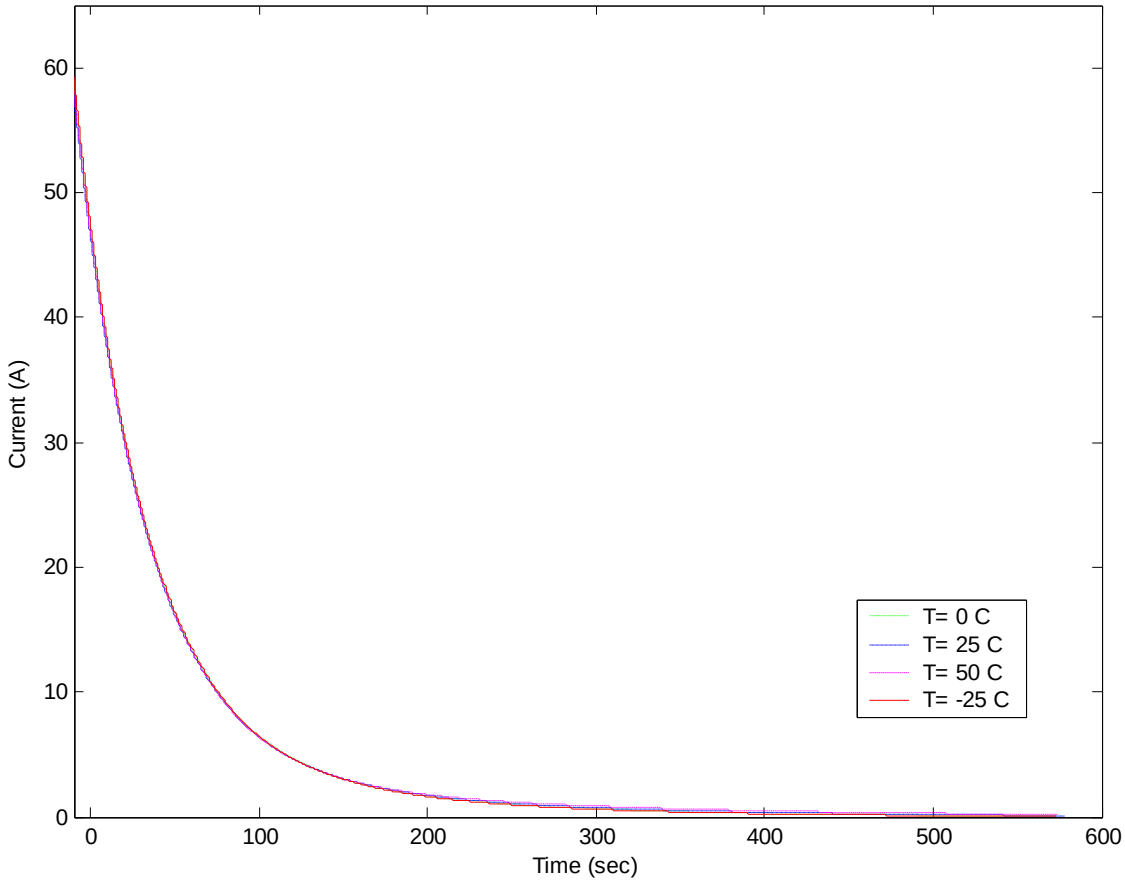

Figure B3.3-2: 60 A Charge Current Best Fit Curves

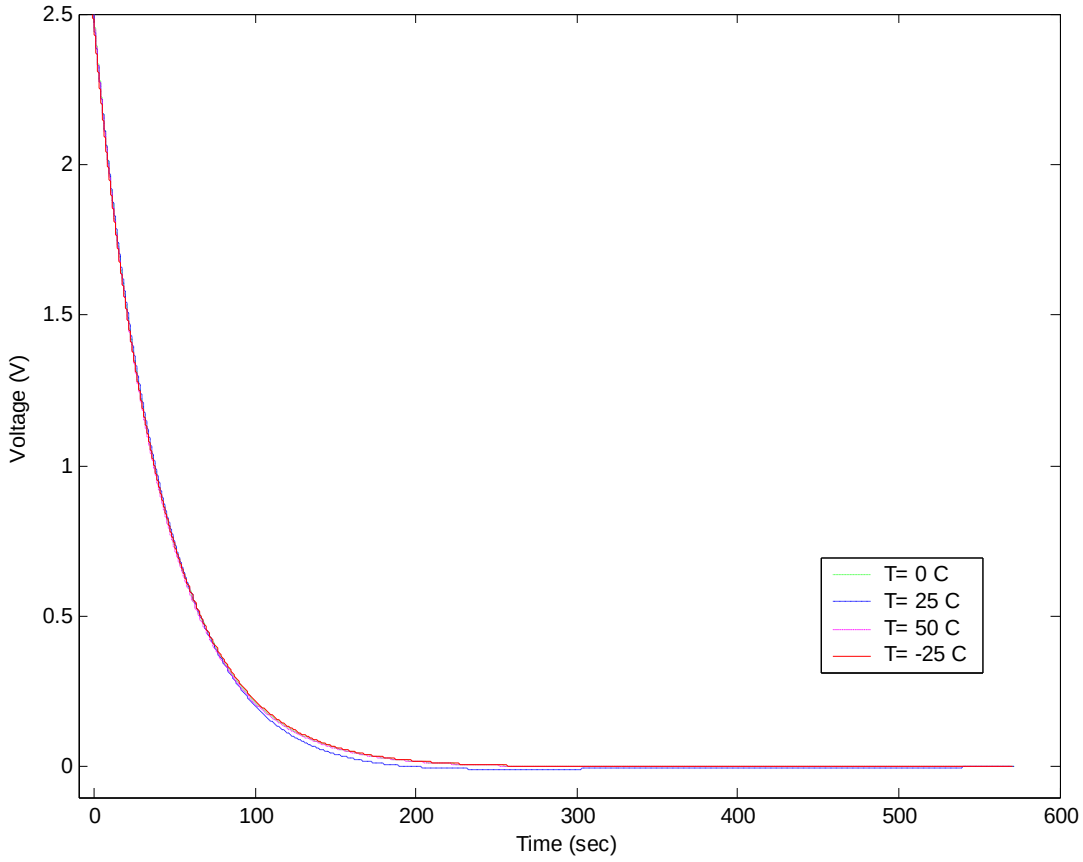

Figure B3.3-3: 60 A Discharge Voltage Best Fit Curves

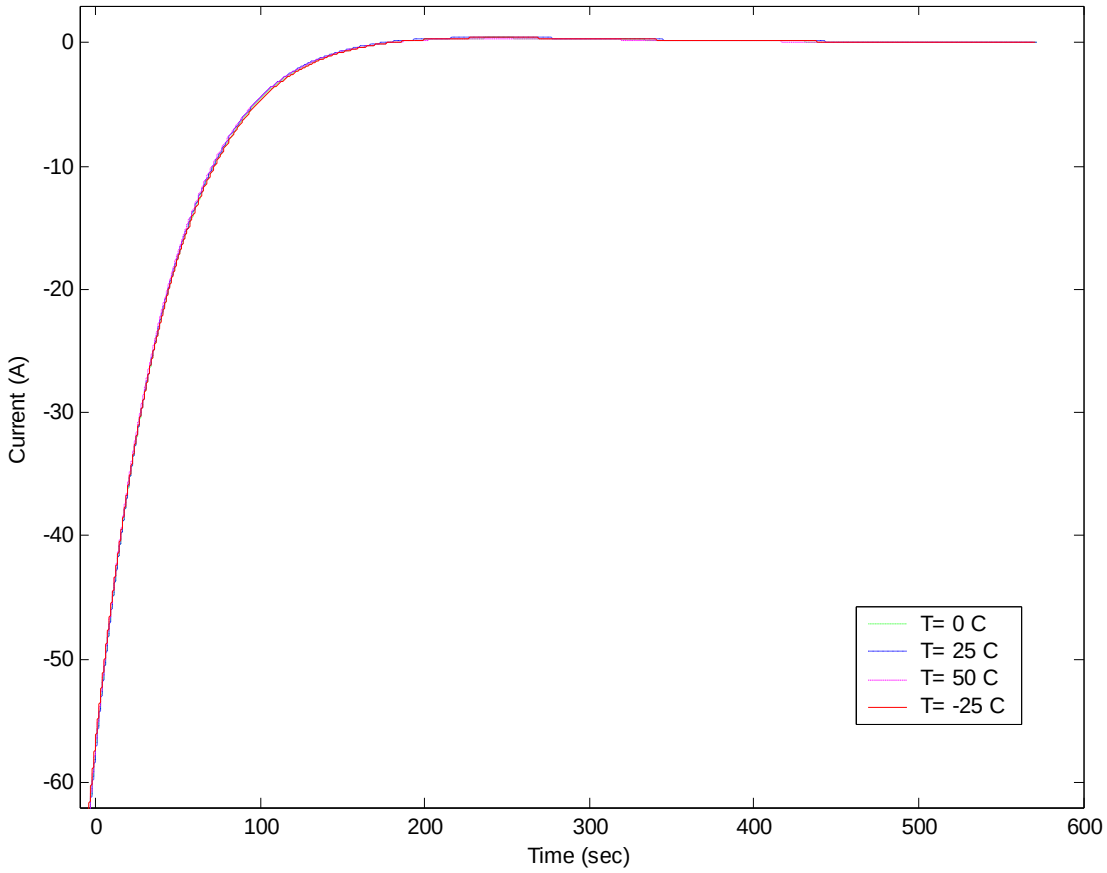

Figure B3.3-4: 60 A Discharge Current Best Fit Curves

B4. 1800 F Ultracapacitor Best Fit Curve Results

The results for the 1800 F are shown in this section. The results are broken into three sub-categories that are based on the current charge and discharge levels. Each figure contains the best fit curves for the four temperatures: -25°C, 0°C, 25°C and 50°C.

B4.1 1800 F Ultracapacitor 25 A Results

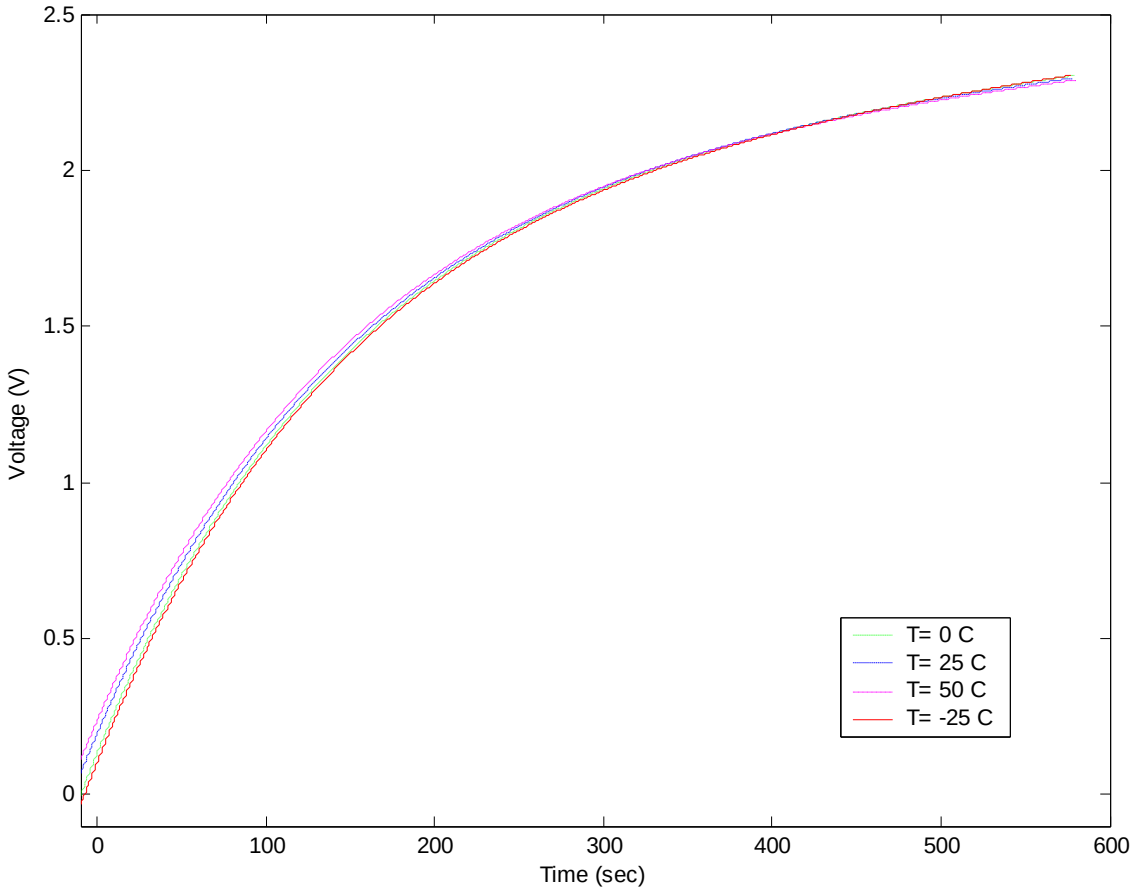

Figure B4.1-1: 25 A Charge Voltage Best Fit Curves

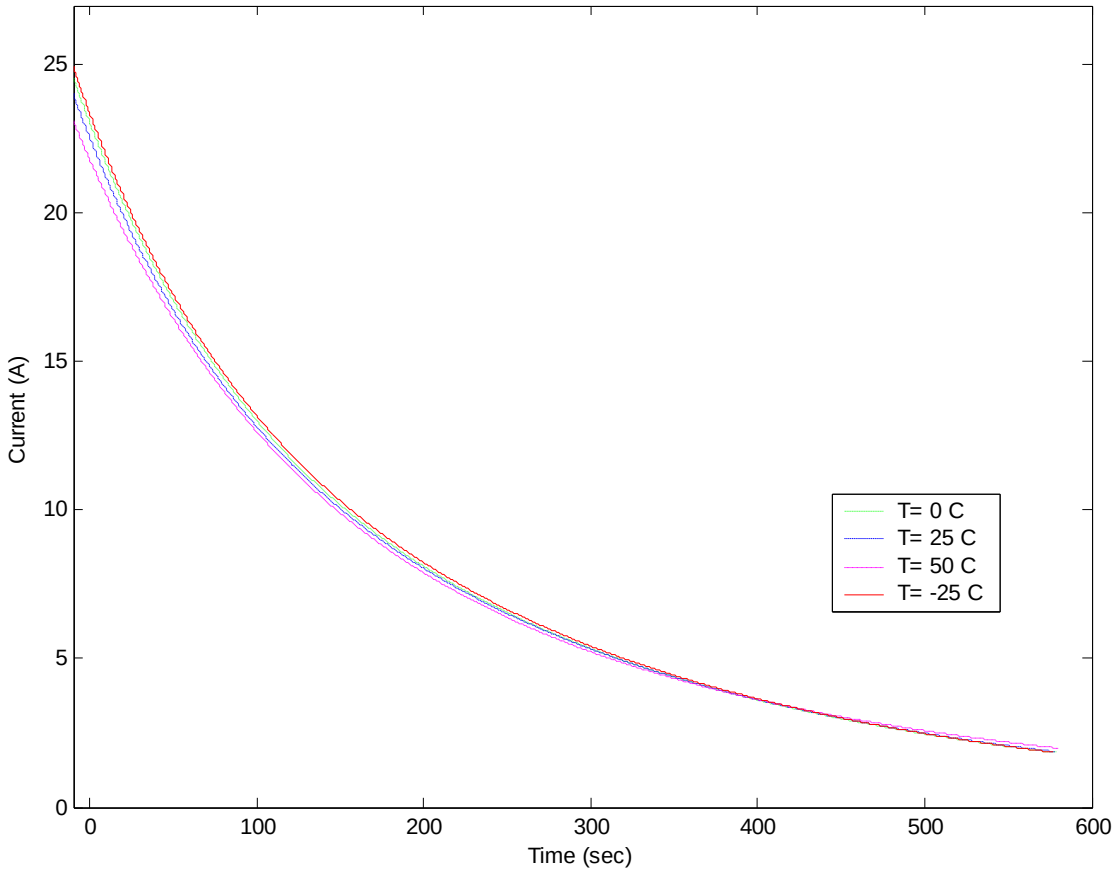

Figure B4.1-2: 25 A Charge Current Best Fit Curves

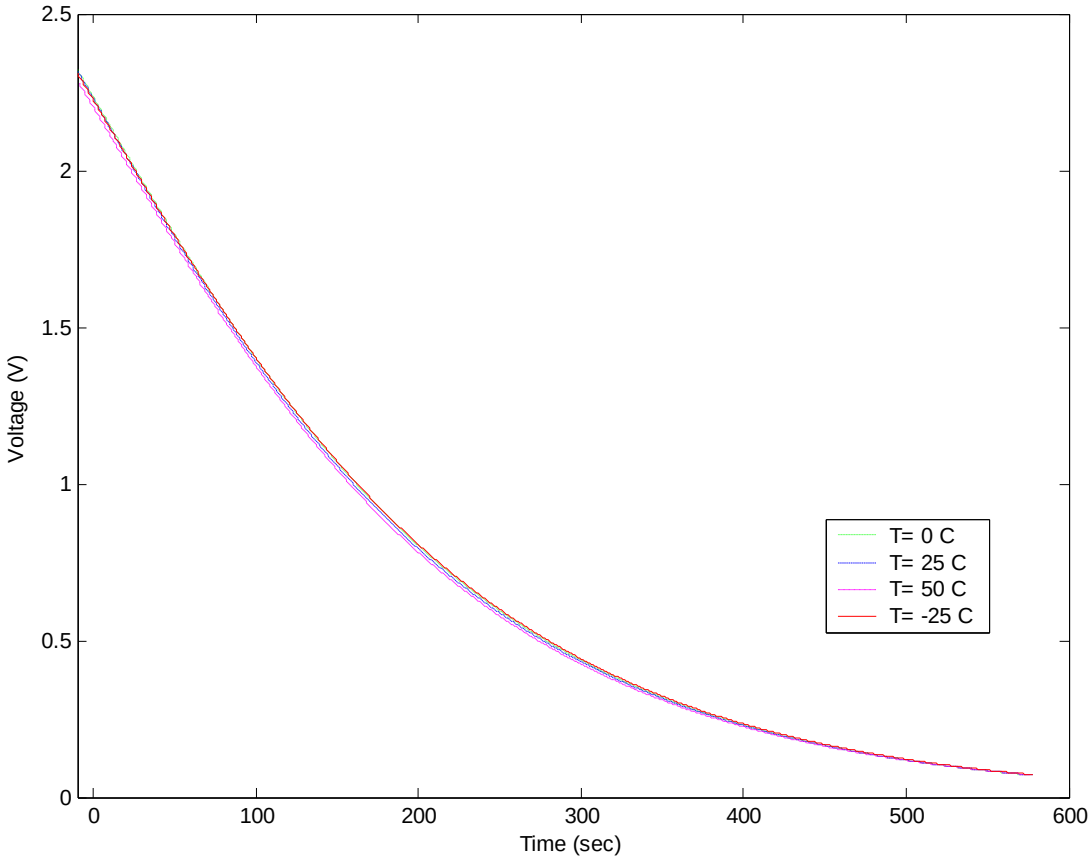

Figure B4.1-3: 25 A Discharge Voltage Best Fit Curves

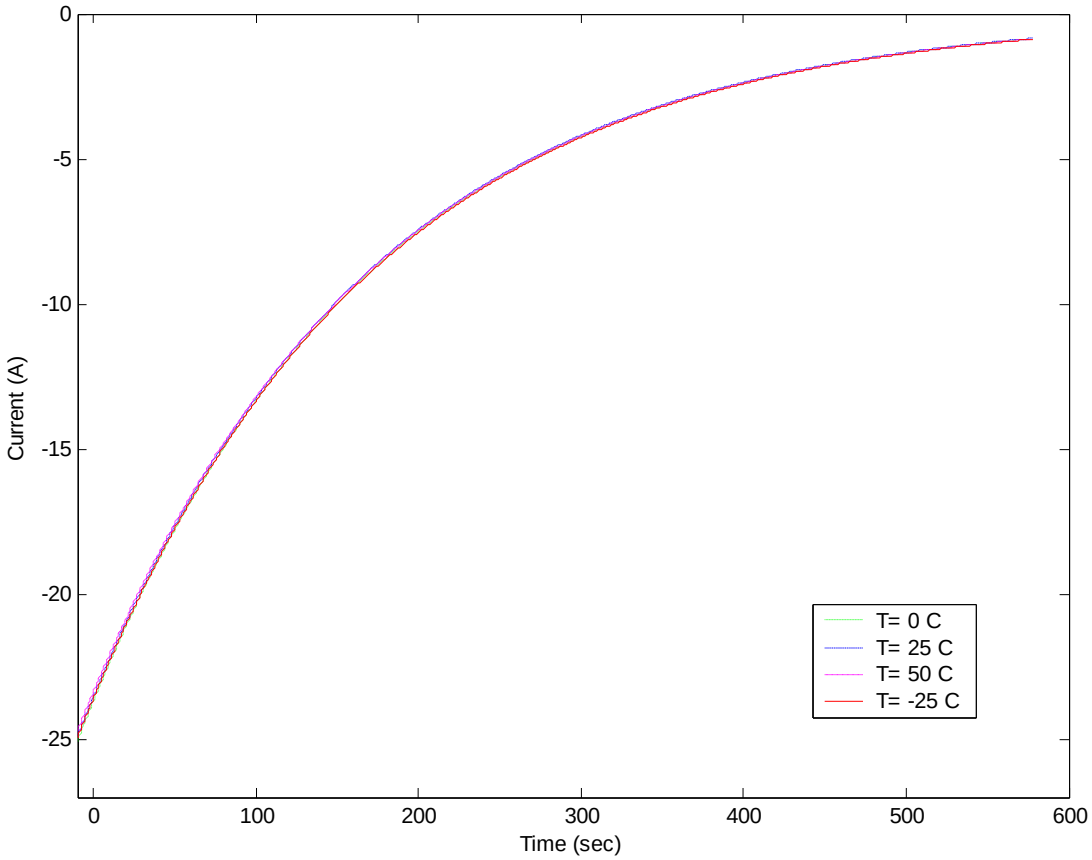

Figure B4.1-4: 25 A Discharge Current Best Fit Curves

B4.2 1800 F Ultracapacitor 50 A Results

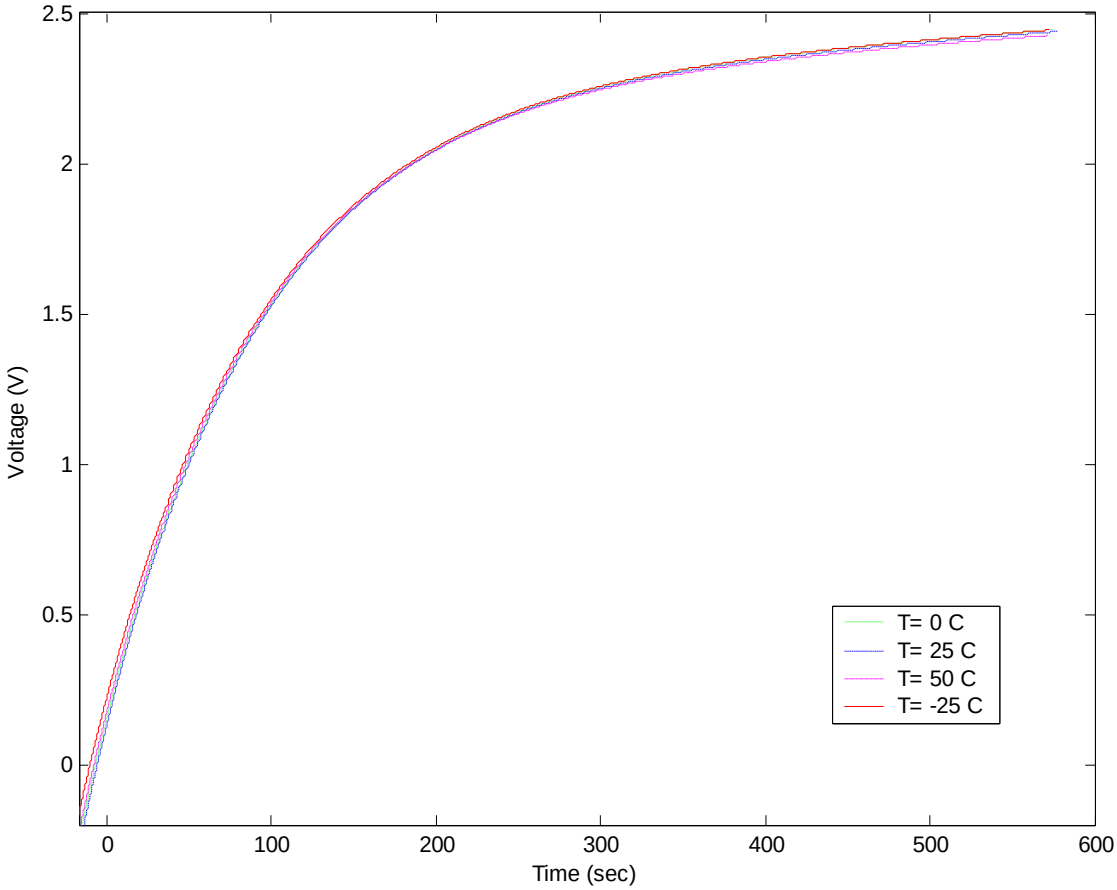

Figure B4.2-1: 50 A Charge Voltage Best Fit Curves

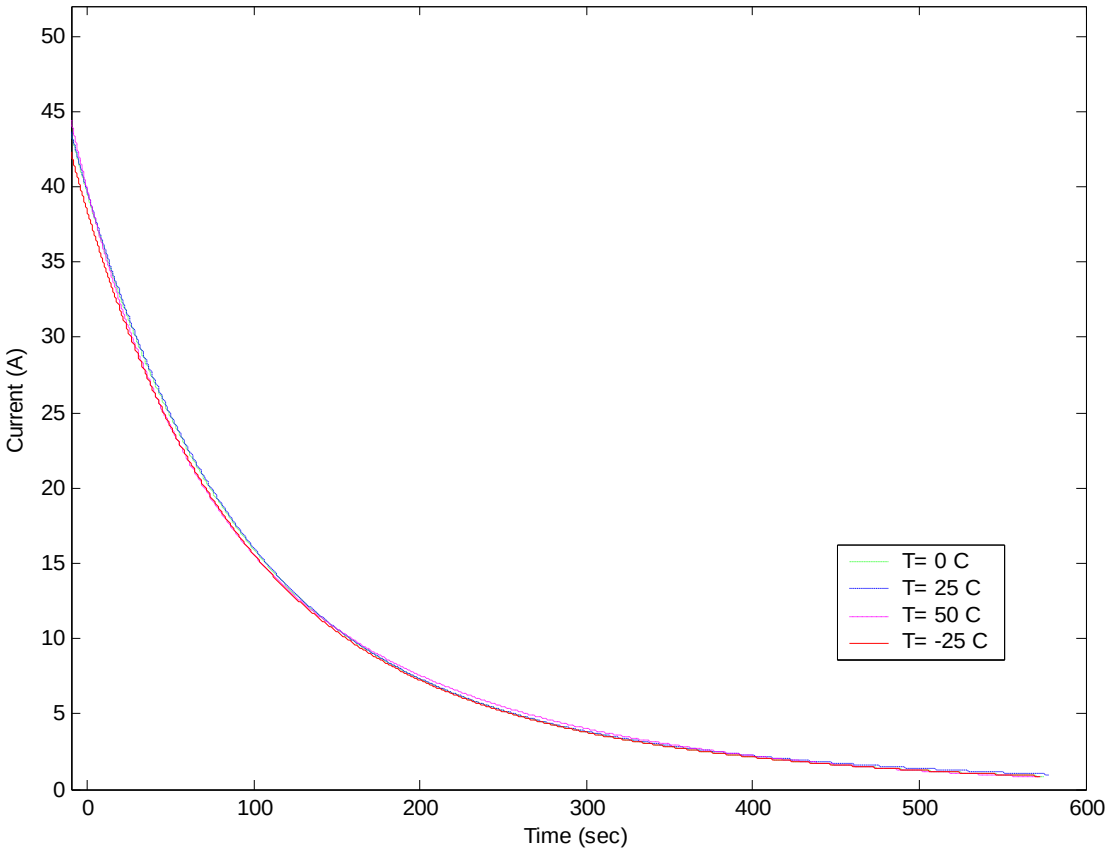

Figure B4.2-2: 50 A Charge Current Best Fit Curves

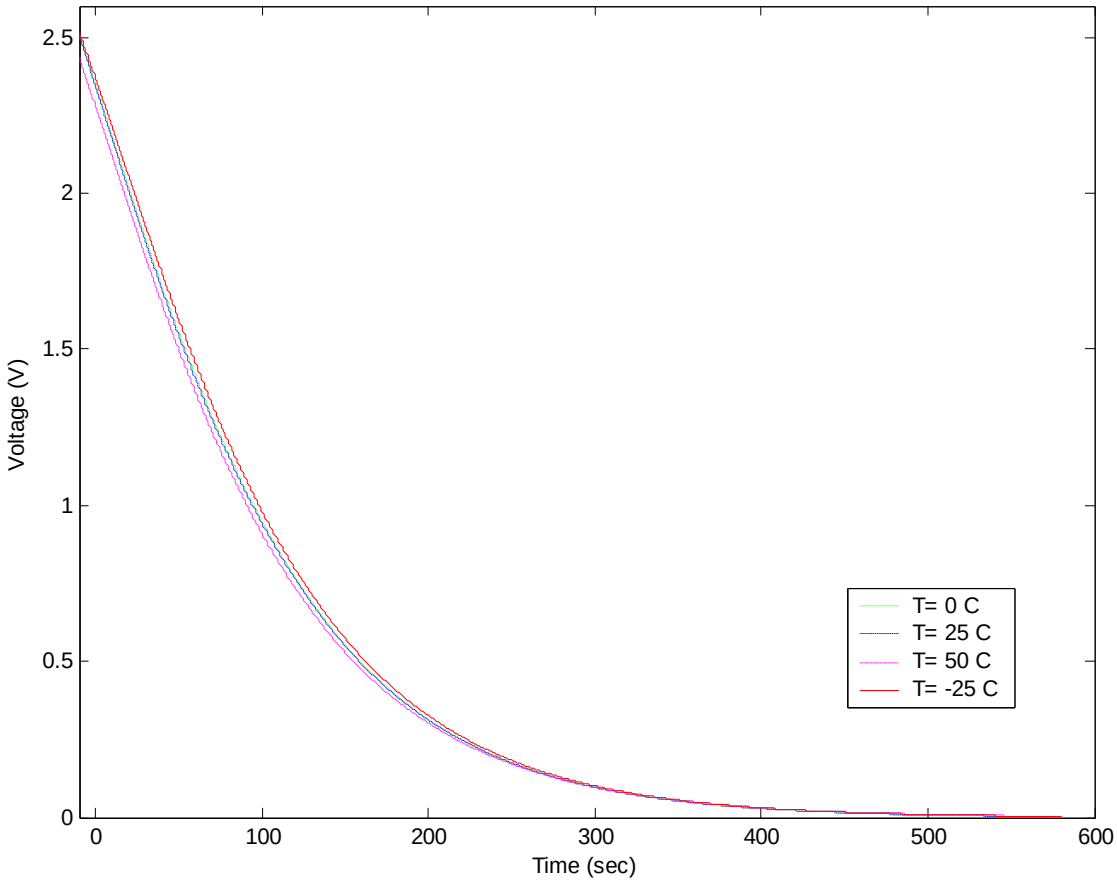

Figure B4.2-3: 50 A Discharge Voltage Best Fit Curves

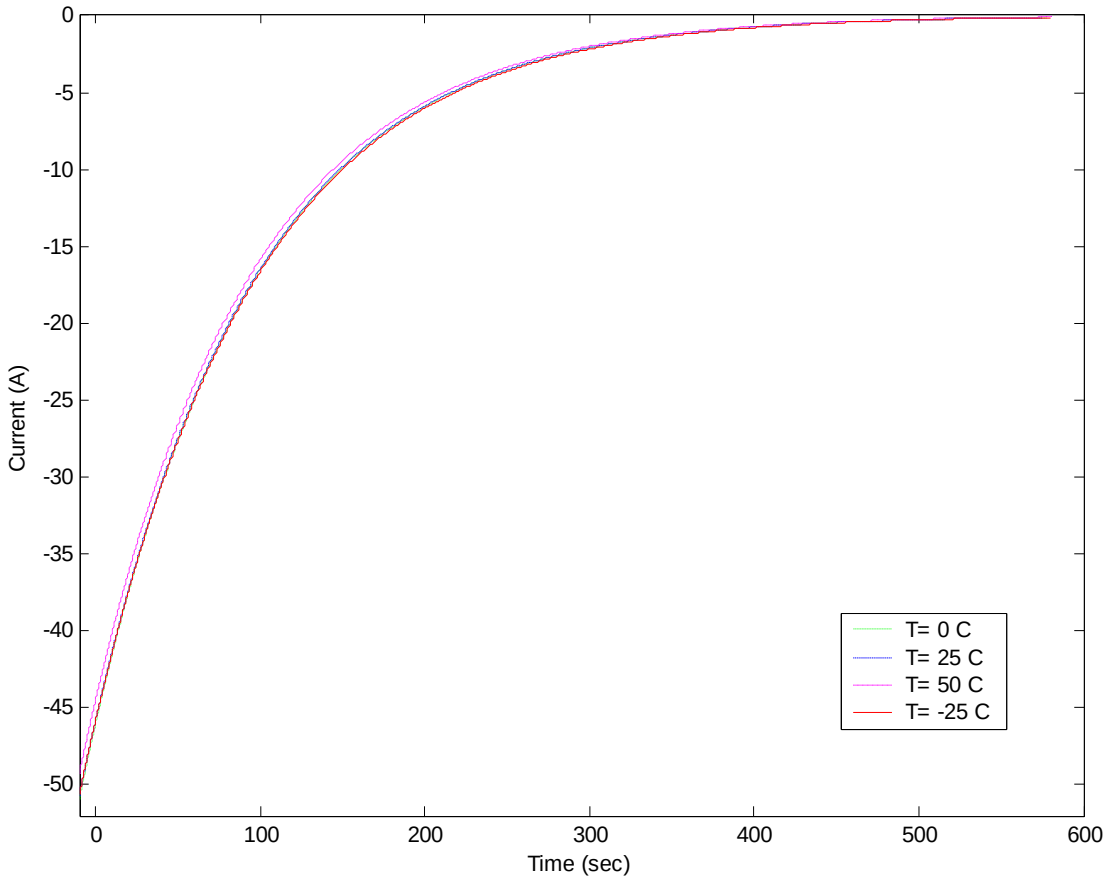

Figure B4.2-4: 50 A Discharge Current Best Fit Curves

B4.3 1800 F Ultracapacitor 60 A Results

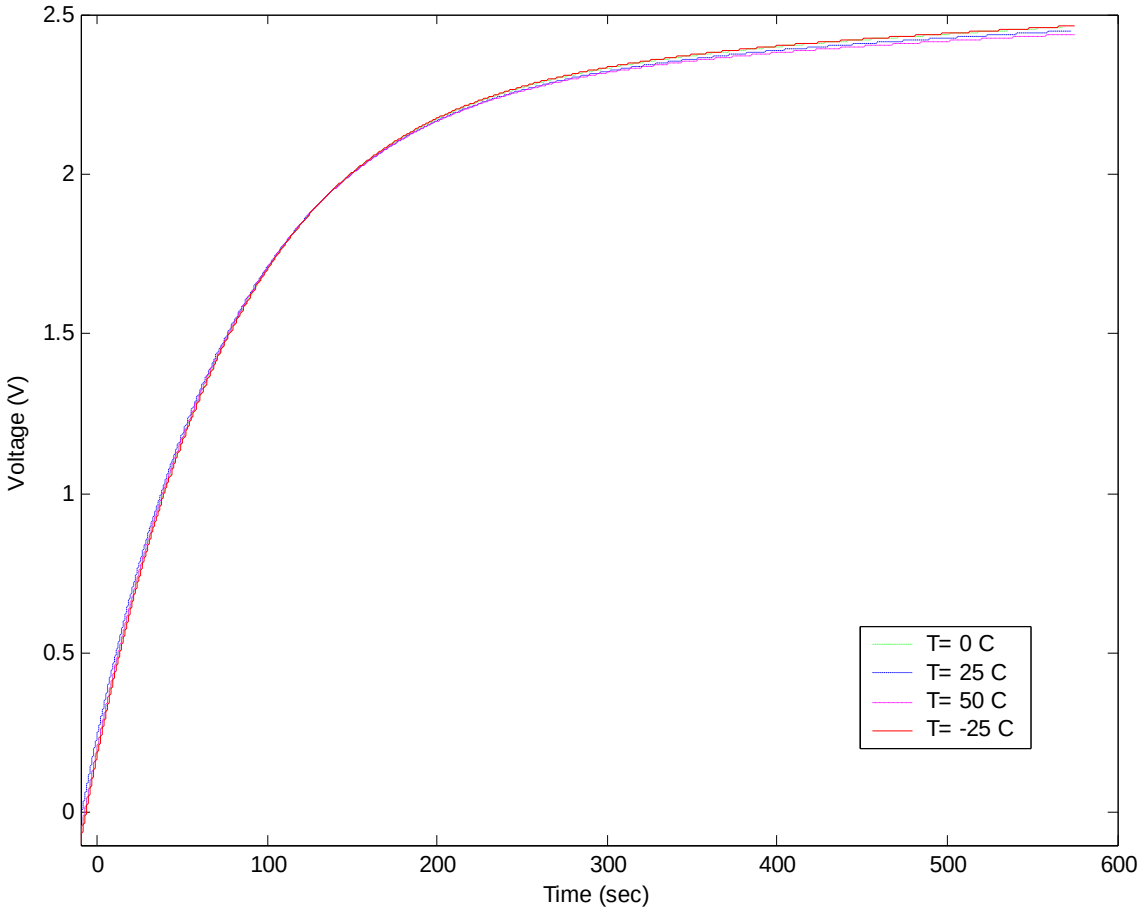

Figure B4.3-1: 60 A Charge Voltage Best Fit Curves

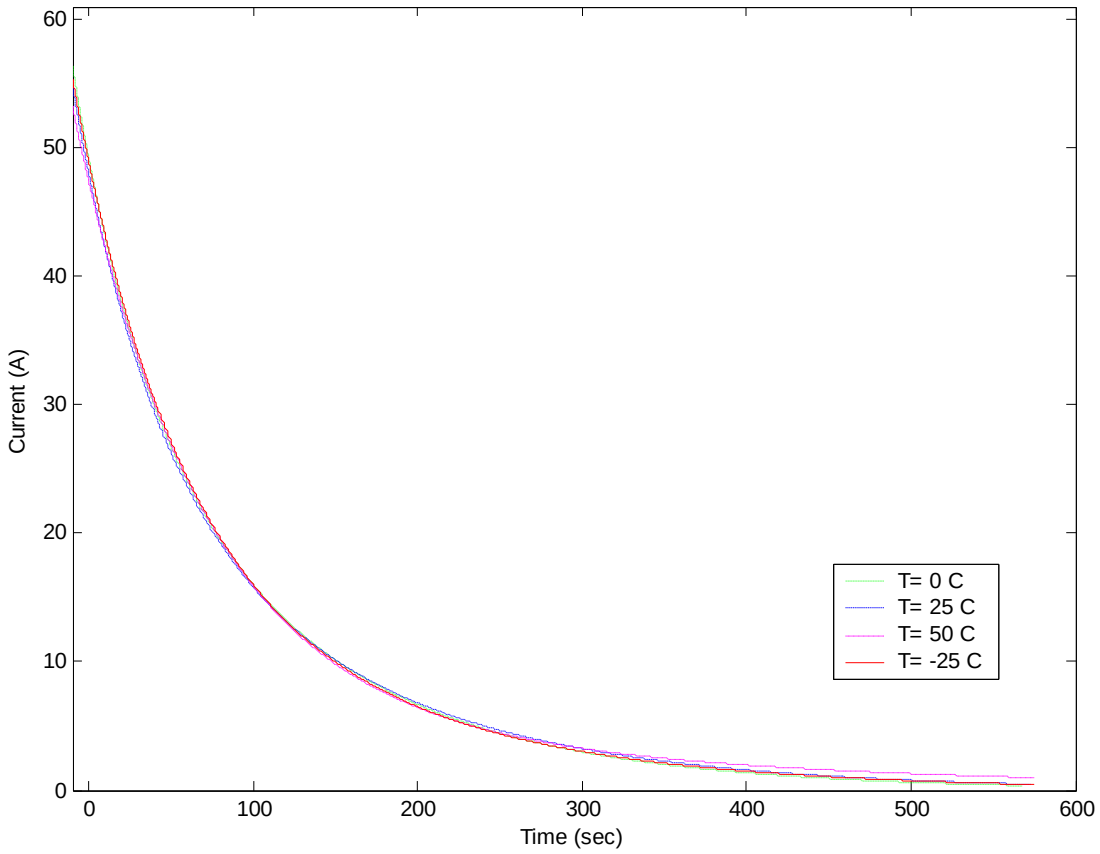

Figure B4.3-2: 60 A Charge Current Best Fit Curves

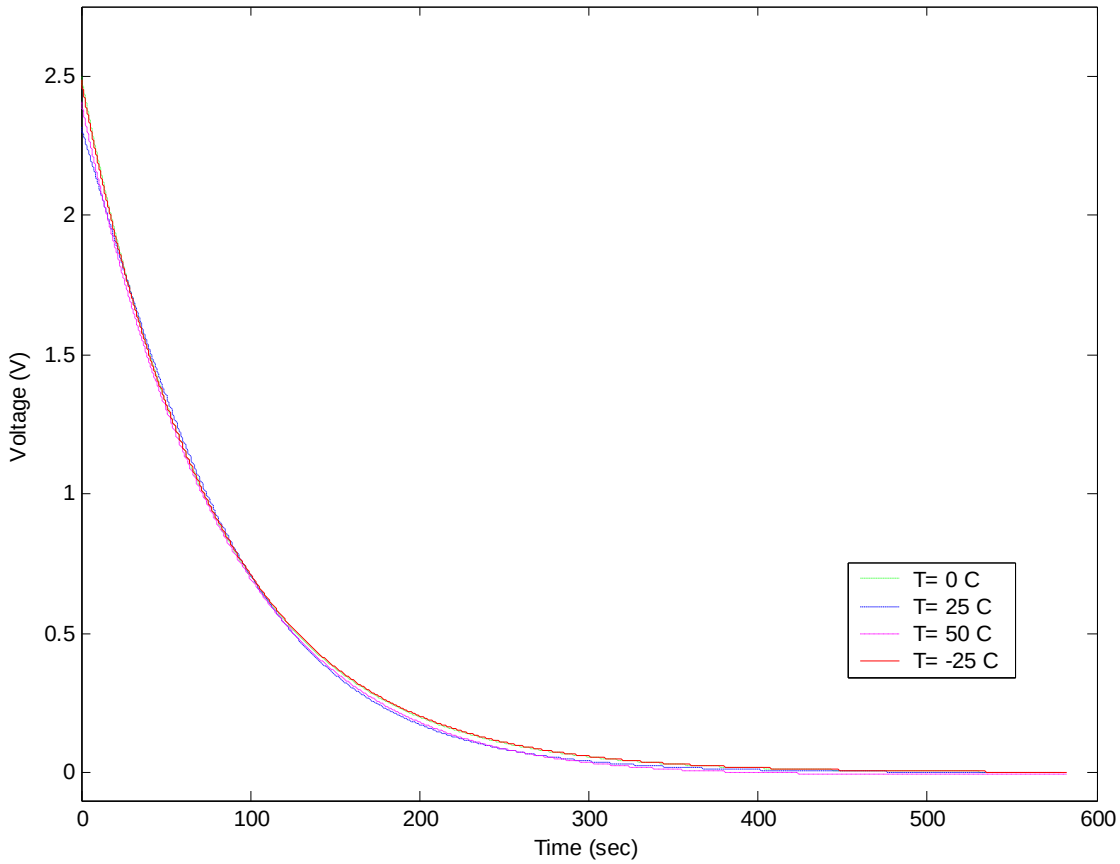

Figure B4.3-3: 60 A Discharge Voltage Best Fit Curves

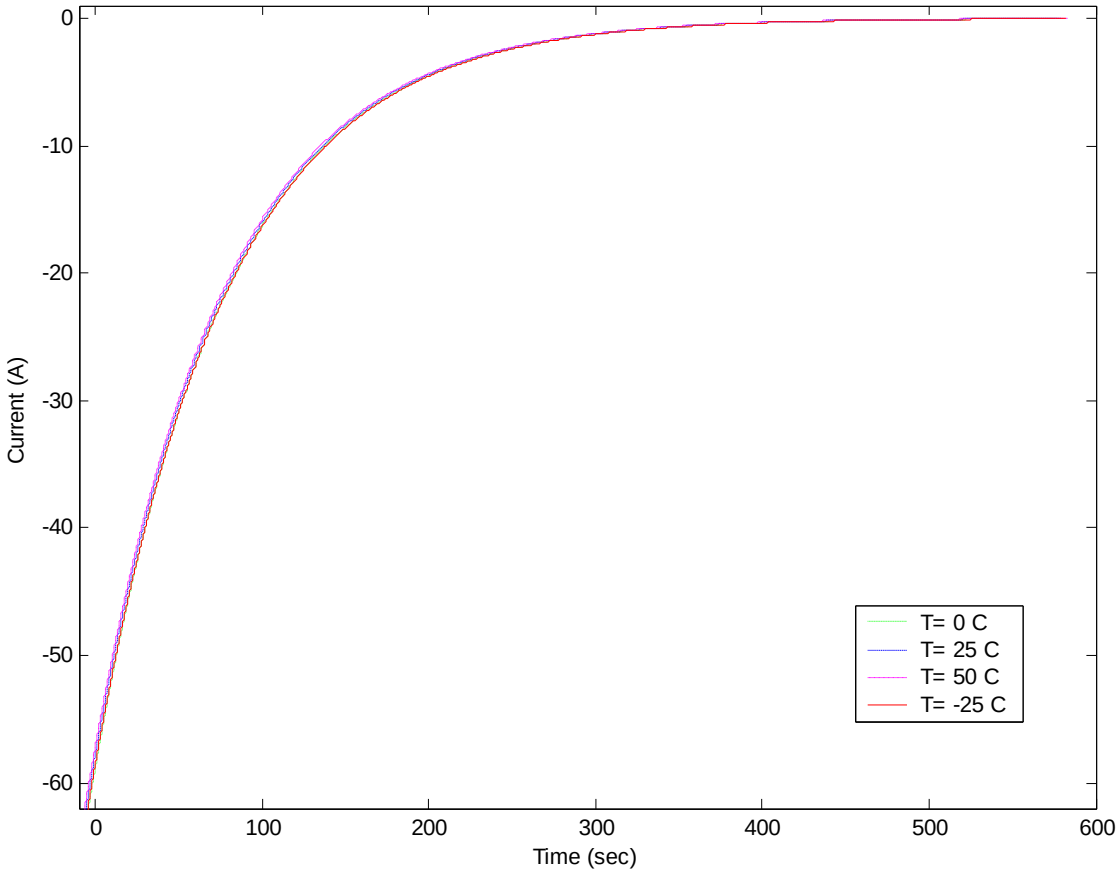

Figure B4.3-4: 60 A Discharge Current Best Fit Curves

Appendix C

Appendix C contains the resistance versus current and resistance versus temperature graphs for the 900 and 1800 F ultracapacitor. In addition, the 900 and 1800 F tables comparing the best fit curve resistance measurements to the calculated resistance using Equations 4.14 and 4.15 are located in this Appendix.

C1. 900 Resistance Graphs and Tables

The 900 F ultracapacitor resistance graphs and comparison tables are located in the following section.

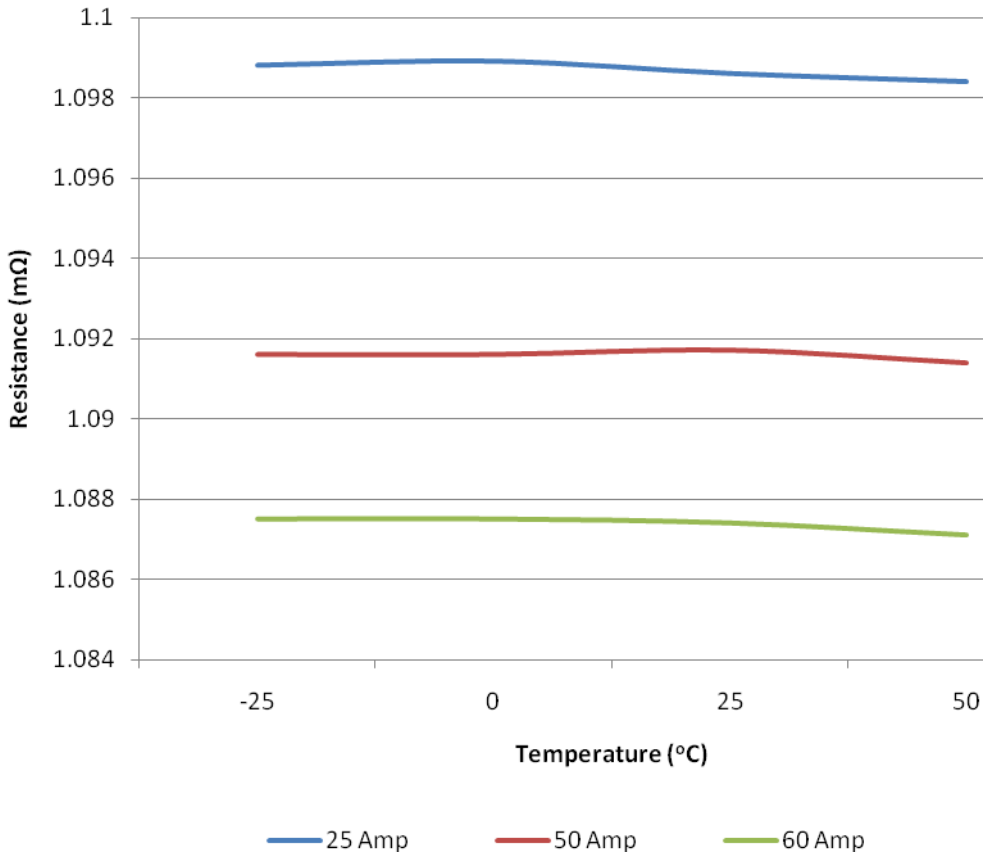

Figure C1-1. 900 F Resistance vs. Temperature

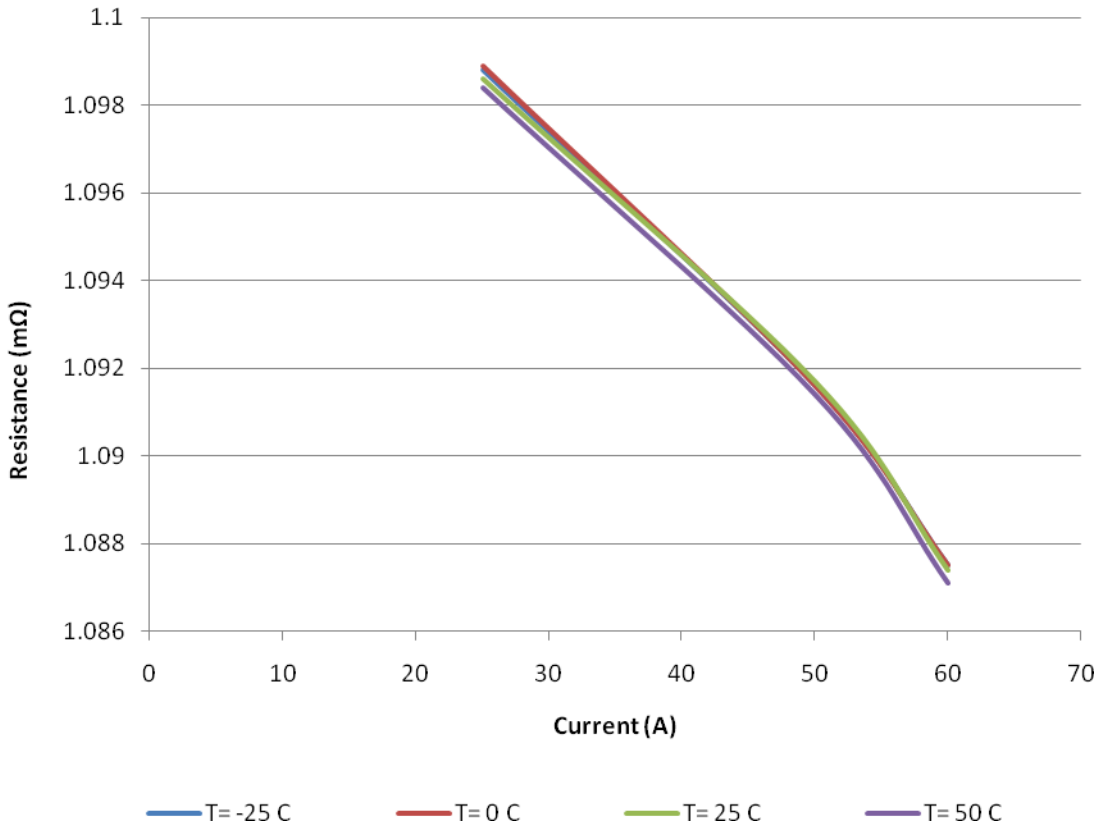

Figure C1-2. 900 F Resistance vs. Current

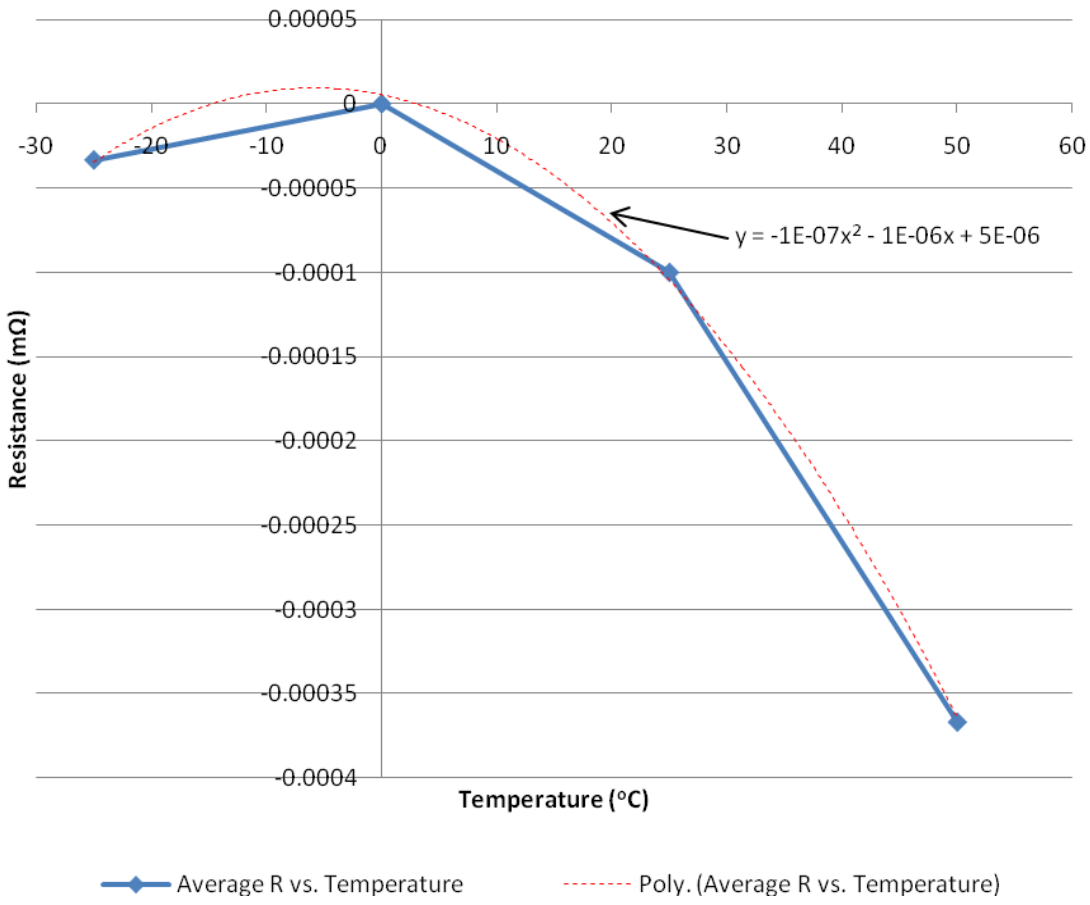

Figure C1-3. 900 F Average Resistance Difference vs. Temperature (0°C is Reference)

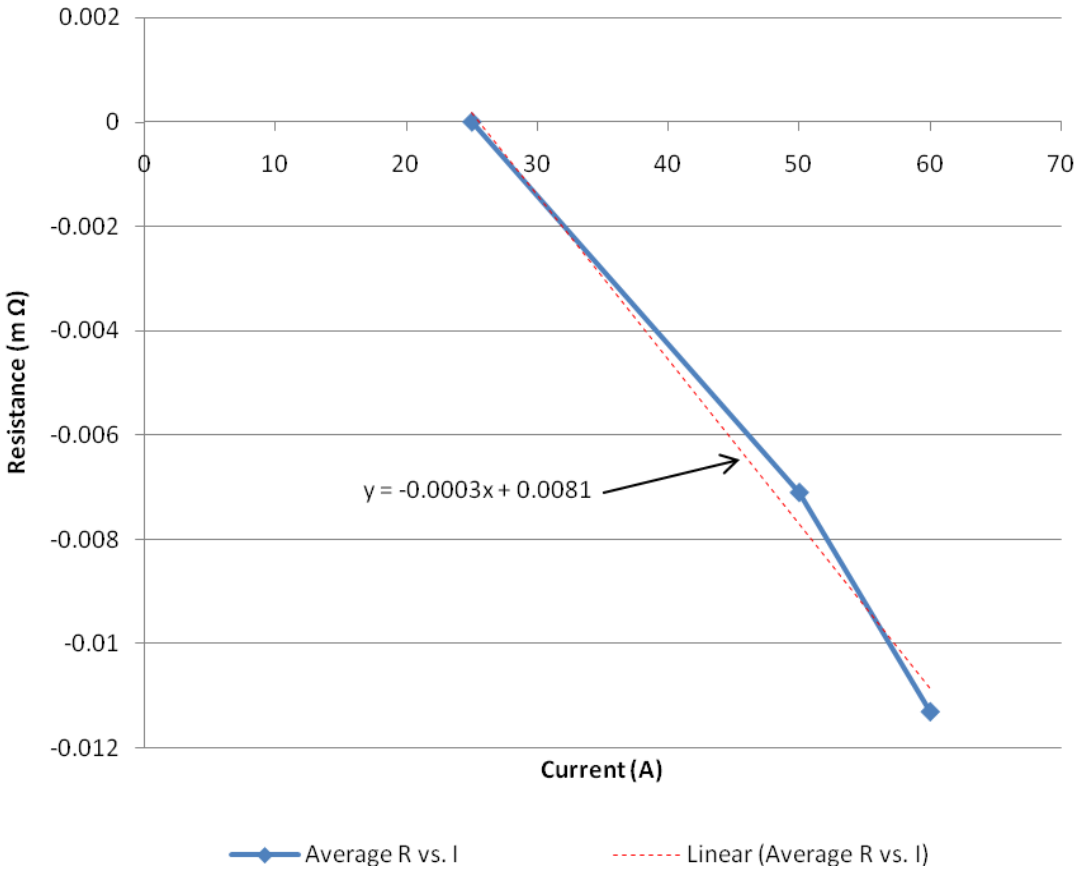

Figure C1-4. 900 F Average Resistance Difference vs. Current (25 A is Reference)

Table C.1-1. 900 F 25 A Resistance Comparison

Temperature	Best Fit Curve	Eq. 4.14	Difference
-25°C	1.0988	1.099036	0.000236
0°C	1.0989	1.099076	0.000175
25°C	1.0986	1.098966	0.000366
50°C	1.0984	1.098706	0.000305

Table C.1-2. 900 F 50 A Resistance Comparison

Temperature	Best Fit Curve	Eq. 4.14	Difference
-25°C	1.0916	1.091151	-0.00045
0°C	1.0916	1.091191	-0.00041
25°C	1.0917	1.091081	-0.00062
50°C	1.0914	1.090821	-0.00058

Table C.1-3. 900 F 60 A Resistance Comparison

Temperature	Best Fit Curve	Eq. 4.14	Difference
-25°C	1.0875	1.087997	0.000497
0°C	1.0875	1.088037	0.000537
25°C	1.0874	1.087927	0.000527
50°C	1.0871	1.087667	0.000567

C2. 1800 Resistance Graphs and Tables

The 1800 F ultracapacitor resistance graphs and resistance comparison tables are located in the following section.

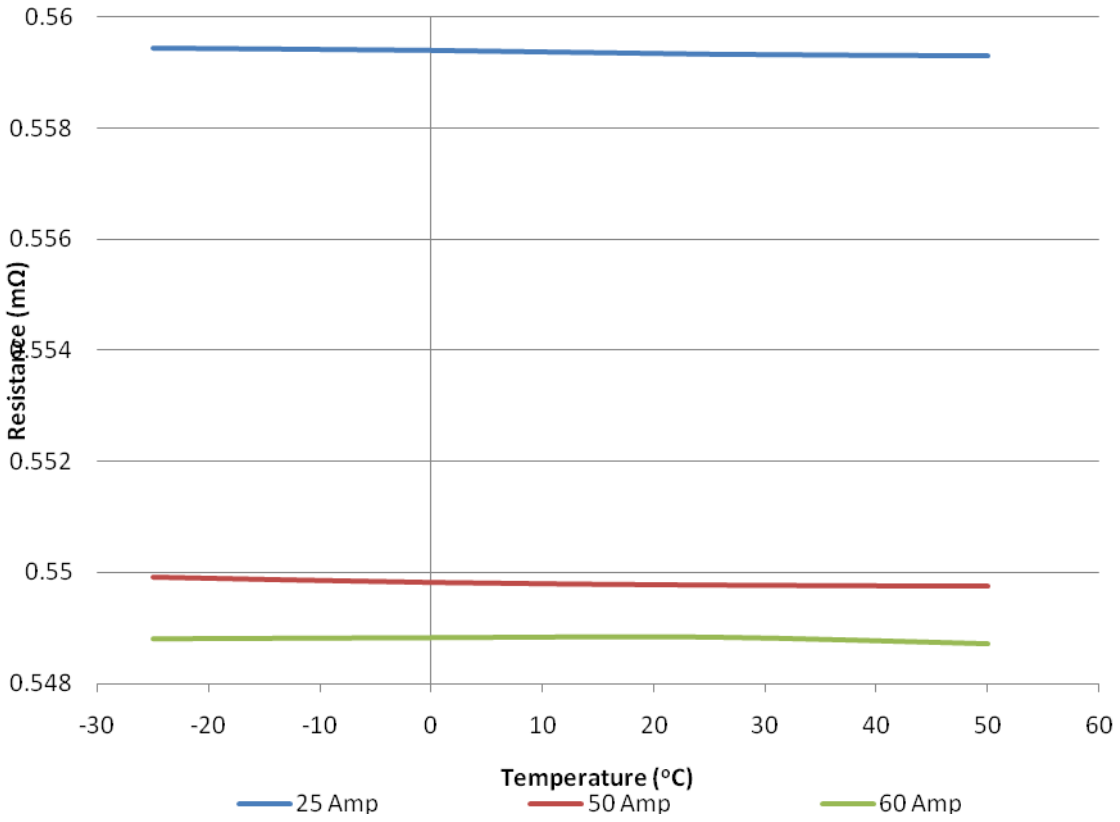

Figure C2-1. 1800 F Resistance vs. Temperature

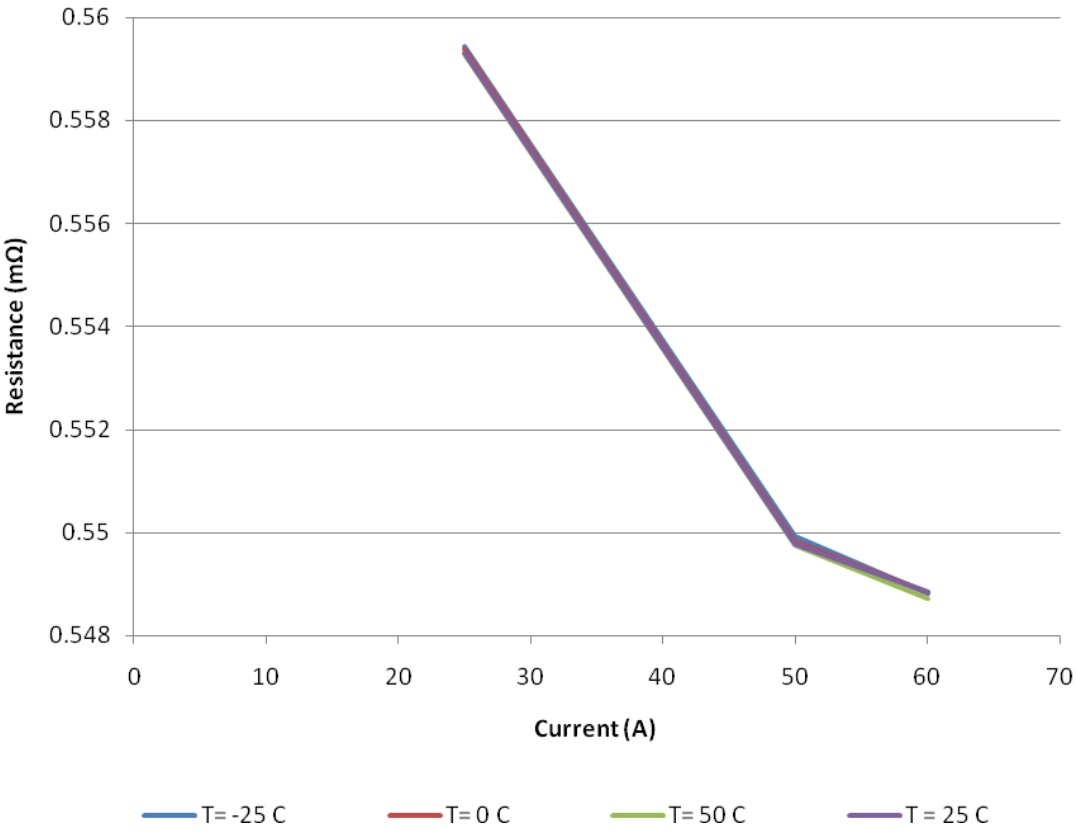

Figure C2-2. 1800 F Resistance vs. Current

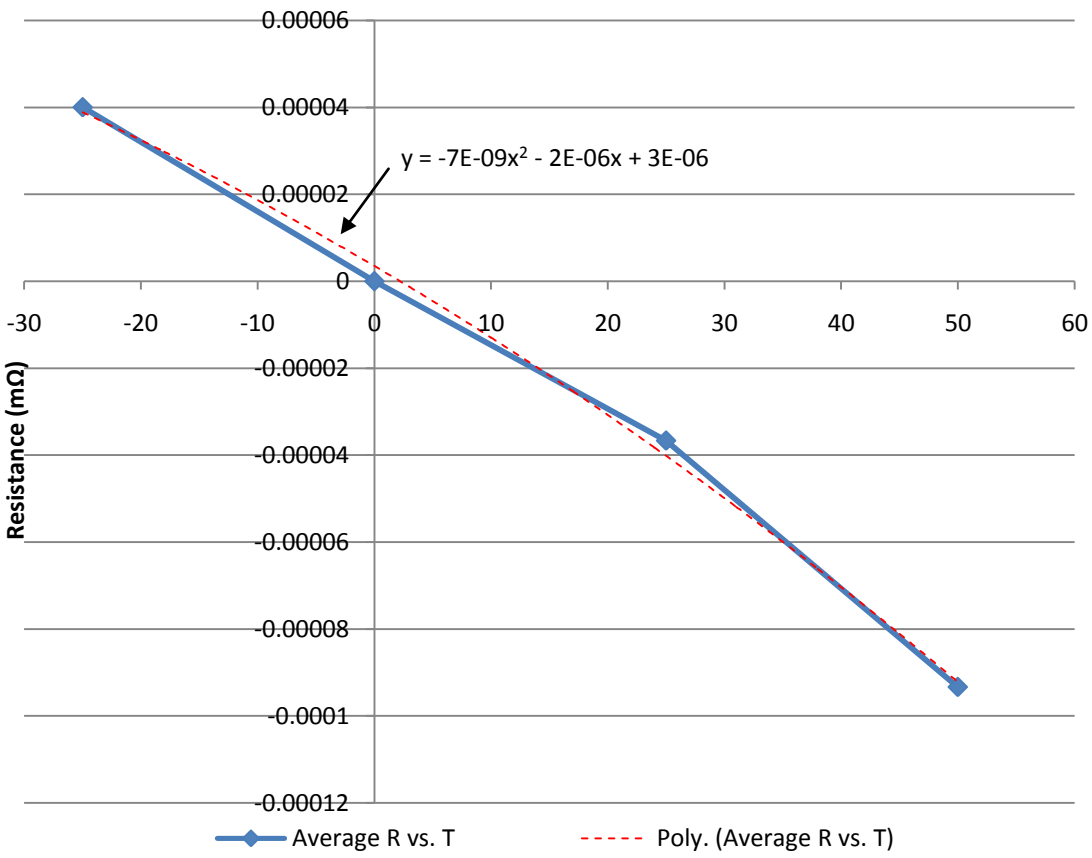

Figure C2-3. 1800 F Average Resistance Difference vs. Temperature (0°C is Reference)

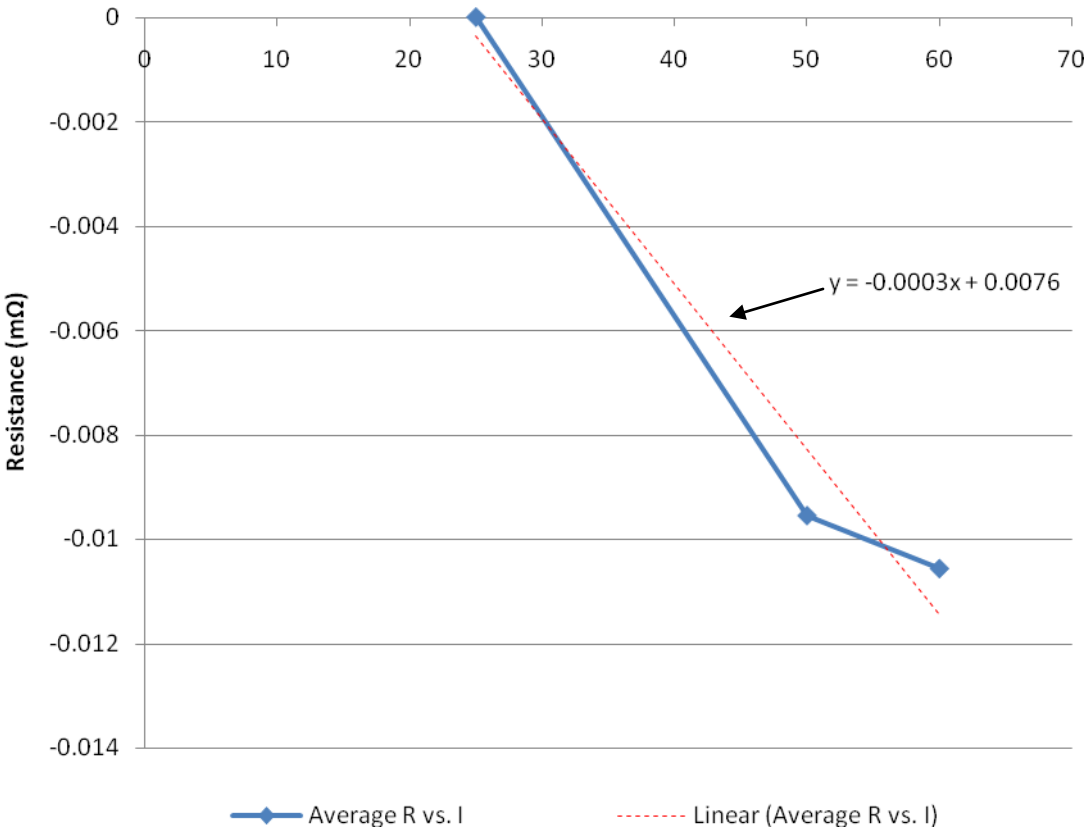

Figure C2-4. 1800 F Average Resistance Difference vs. Current (25 A is Reference)

Table C.2-1. 1800 F 25 A Resistance Comparison

Temperature	Best Fit Curve	Eq. 4.14	Difference
-25°C	0.55943	0.559538625	0.000108625
0°C	0.55939	0.559493	0.000103
25°C	0.55932	0.559438625	0.000118625
50°C	0.55929	0.5593755	8.55E-05

Table C.2-2. 1800 F 50 A Resistance Comparison

Temperature	Best Fit Curve	Eq. 4.14	Difference
-25°C	0.54992	0.552038625	0.002118625
0°C	0.54982	0.551993	0.002173
25°C	0.54977	0.551938625	0.002168625
50°C	0.54975	0.5518755	0.0021255

Table C.2-3. 1800 F 60 A Resistance Comparison

Temperature	Best Fit Curve	Eq. 4.14	Difference
-25°C	0.54881	0.549038625	0.000228625
0°C	0.54883	0.548993	0.000163
25°C	0.54884	0.548938625	9.8625E-05
50°C	0.54872	0.5488755	0.0001555

Vita

Curtis Miller was born in Guymon, Oklahoma. He graduated with from Guymon High School in 1995. He attended Southwestern Oklahoma State University earning a Bachelor of Science in Engineering/Physics in 1999. He attended the University of Tennessee, where he earned a Bachelor of Science in Electrical Engineering in 2003 and a Master of Science in Electrical Engineering in 2008. Currently, he is working as a power systems electrical engineer.